UNIVERSITY OF CALIFORNIA

Los Angeles

Unlocking Mouse Cone Photoreceptors:

Phototransduction and Biophysics

A dissertation submitted in partial satisfaction of the requirements for the degree

Doctor of Philosophy in Molecular Cellular and Integrative Physiology

by

Norianne Theresa Ingram

2019

ABSTRACT OF THE DISSERTATION

Unlocking Mouse Cone Photoreceptors: Phototransduction and Biophysics

by

Norianne Theresa Ingram

Doctor of Philosophy in Molecular Cellular and Integrative Physiology

University of California Los Angeles, 2019

Professor Gordon L. Fain, Co-Chair

Professor Alapakkam P. Sampath, Co-Chair

Genetic engineering in mammals is furthest developed in *Mus musculus* and has facilitated great strides towards understanding the molecular and cellular mechanisms underlying human biology and disease. Despite the advantages afforded through genetic manipulations, studies involving retinal photoreceptors have been largely constrained to rods due to the technical challenges of isolating cones. This dissertation describes the methodology I have developed to reliably identify unlabeled mouse cone somata, and using whole-cell patch clamp, record their conductance and voltage changes in response to diverse stimuli.

I made highly resolved measurements of cone dark current, membrane capacitance, and resting membrane potentials. Photoresponses were recorded with brief and steady-light stimulation protocols, and I characterized parameters describing response sensitivity and kinetics. Wild-type cones showed evidence of lateral electrical coupling to rod photoreceptors (i.e. the rod secondary pathway). The loss of calcium-sensitive proteins affected waveform of the responses to brief and steady-light

stimulation. Notably, when compared to controls, the loss of guanylyl cyclase accelerating proteins caused cones to be more sensitive to a given light stimulus and to reopen fewer light-sensitive channels.

The ability to manipulate the cone membrane potential enabled the biophysical characterization of multiple inner segment ion conductances. Synaptic calcium and the hyperpolarization-activated rectifying conductances were isolated with pharmacology. By combining voltage stimulation with light flashes, I also studied the reversal potential of the light response for the first time in any mammalian species. The inner segment calcium- and calcium-activated anion conductances were significantly large in the mouse cones and had to be blocked in order to isolate the light-sensitive conductance.

Unlike rods, cones must remain active in brighter ambient light. In addition to calcium-dependent adaptation that adjusts the phototransduction machinery, the cone must replenish large fractions of photopigment. We identified a light-driven, non-enzymatic pathway in which all-*trans*-retinal does not even leave the photoreceptor. We show that when bound to a retinyl phosopholipid-complex in the membrane and exposed to blue light, all-*trans*-retinal can be preferential photoconverted back to 11-*cis*-retinal.

All the mechanisms employed to keep cones functional and out of saturation are for naught if well defined synaptic connections are not made properly. We show that cones lacking a synaptic adaptor protein LRIT1 responded to light with normal characteristics. Cone bipolar cells, however, responded to light flashes with altered sensitivities. Thus, visual perception relies not only on high-fidelity encoding of light stimuli, but also on precise circuitry and signal transmission.

The dissertation of Norianne Theresa Ingram is approved.

Gabriel H. Travis

Mark Arthur Frye

Alapakkam P. Sampath, Committee Co-Chair

Gordon L. Fain, Committee Co-Chair

University of California, Los Angeles

2019

This dissertation is dedicated to my family and friends who have believed in me with unwavering faith, to my mentors who have each given gifts of knowledge and guidance, and to all the stars that have lit the way.

TABLE OF CONTENTS

LIST OF FIGURES

LIST OF TABLES

LIST OF ABBREVIATIONS

A	Amplifcation Constant
Ca^{2+}	Calcium
$Ca_{v1.4}$	L-type, Voltage-Gated Calcium Channel 1.4
CBC	Cone Bipolar Cell
cGMP	Cyclic Guanosine Monophosphate
Cl^-	Chloride
CNG	Cylic-Nucleotide Gated (Channels)
Cs-Meth	Cesium Methane Sulfonate
Cx36$^{-/-}$	Genetic KO for Gap Junction Protein, Connexin36
ERG	Electroretinography
E_{rev}	Reversal Potential
$G\alpha_t$	Transducin α-subunit
GC	Guanylyl Cyclase
GCAPs	Guanylyl Cyclase Accelerating Proteins (Isoforms 1 and 2)
GCAPs$^{-/-}$	Genetic KO for GCAPs
GDP	Guanosine Diphosphate
Gnat1$^{-/-}$	Genetic KO of Rod-Specific $G\alpha_t$
GRK1, RK	Rhodopisn Kinase 1
GTP	Guanosine Triphosphate
GTPγS	Guanosine 5'-O-(3-thiotriphosphate), Non-hydrolyzable analog of GTP
$I_{1/2}$	Half-maximal Flash Strength
I_{an}	Inner-Segment Calcium-Activated Anion Current

I_{ca}	Inner-Segment Calcium Current (L-type Channel, $Ca_{v1.4}$)
I_h	Hyperpolarization-activated cationic current (HCN channel)
I_k	Voltage-gate potassium conductance
IPL	Inner Plexiform Layer
IS	Inner Segment
ISR	Isradipine
K^+	Potassium
K-Asp	Potassium Aspartate
KO	Knockout
M	Medium-wavelength opsin, λ_{max} = 508 nm
NFA	Niflumic Acid
Na^+	Sodium
OPL	Outer Plexiform Layer
OS	Outer Segement
PDE	Phosphodiesterase
P*(Rh*)	Pigments (Rhodosins) activated/bleached
$Rv^{-/-}$	Genetic KO for recoverin
R_{max}	Maximum Response
S	Short-wavelength opsin, λ_{max} = 358 nm
TEA	Tetraethylammonium
V_{hold}	Membrane Holding Potential, Command Potential
WT	Wildtype
ϕ	Photons

ρ	M-pigment co-expression ratio
τ_{act}	Time constant for channel activation
τ_{rec}	Time constant for response recovery

ACKNOWLEDGEMENTS

A great many people have made this work possible. Without my mentors, colleagues, collaborators, friends, family, and pets, doors would have remained shut, rocks unturned, and my sanity lost.

First, I thank my advisors Dr. Gordon L. Fain (Gordo) and Dr. Alapakkam P. Sampath (Sam the Man). Both of them saw the scientist I would be before I dared to imagine. They gave me the tools and opportunity to excel, and found just the right amount of freedom and nudgings that I needed to bloom. They are some of the most supportive people I have ever known, and I hope I can continue to make them proud. It is one of the greatest honors in my life to work with them and to be part of their family.

I would like to thank members of the Sampath/Fain group: Dr. Ala Morshedian initially piqued my interest in electrophysiological science and recruited me into Dr. Fain's lab. His zest for life and love of science is something we all must aspire to; Dr. Rikard Frederiksen is a rock and always up for crazy ideas, unusual projects, and shenanigans. I can't wait to see what he does next; Drs. Johan Pahlberg and Katherine E. Fehlhaber taught me how to make the most beautiful retinal slices and to patch clamp mammalian photoreceptors. Johan is an actual rock star, magician, and taught us Finnish curses. Kate became one of my best friends and partner in rainbow-unicorn crimes. I love her dearly; Dr. Mike Woodruff showed me that life and electrophysiology

are all about attitude. Although my time with him was short, the lessons he imparted will ripple through the rest of my life.

I would like to thank various members from the UCLA campus who have supported me and shared incredible wisdoms: Dr. Mark A. Frye's excitement, enthusiasm, and support are un-paralleled. I wish I had that much energy; Dr. Gabe Travis has earnestly asked for and respected my scientific opinion before I thought it worth listening to; Dr. Anthony 'Tony' Friscia trained me to cut up dead bodies, kept me on my toes, and always provided a 'fresh' perspective on life. He *is* punk rock; Dr. Rana R. Khankan introduced me to laboratory science and showed me what pure dedication was. She is a real-life hero, role model, and the real MVP-GOAT; Gabriela Sendek, my Chinchilla, I'm glad we only cut off one of your fingers.

My people outside of science have provided much needed balance: Gwendolyn Rose Pelfini. This woman has saved my life, counseled me, and believed in me like no one else. She even loved me despite that time I ripped the sink off her wall. It was ok. We glued it; I thank my mom, dad, and brothers, especially Jacob Louis Ingram. We fought like feral demons growing-up, but have become pillars in each other's lives like only siblings can.

Further special thanks to: the surliest of gentlemen, Michael Carr; Yesenia Rayos, a true Queen and Savior; Dr. Rachel Crosbie-Watson. She just might be my spirit-animal; Dr. Peter Narins, who embodies my ultimate life goals; Poker-face Dr. James Tidball;

Dr. Patty Phelps, who gave me a chance; Dr. Liz Fraley, an icon of strength and balance; the real heroes of Jules Stein: Susan Ito, Bill Dominguez, and Nick Chiadez; Finally, MoMo', PyePye, and lil' Gigi for unconditional love and deep conversations.

Thanks y'all!

The project in Chapter 4 was done in collaboration with committee member Dr. Gabriel H. Travis who is also at UCLA and part of the Stein Eye Institute. Joanna Kaylor is the first author of the publication in Chapter 4.

The project in Chapter 5 was done in collaboration with Dr. Kirill A. Martemyanov of Scripps Research Institute in Florida. Ignacio Sarria is the first author of the publication in Chapter 5.

The experiments in this dissertation were funded by institution training grants (T32) awarded to MCIP (GM065823; 2013-2015) and Stein Eye Institute (EY007026; 2017-2018) as well as NIH R01-EY001844 (PI Fain).

VITA

PhD Candidate 2013-2019
Molecule, Cellular, and Integrative Physiology PhD Program, UCLA; Los Angeles, CA
Department of Integrative Biology and Physiology
Department of Ophthalmology, Stein Eye Institute
Laboratory of Drs. Gordon L. Fain and Alapakkam P. Sampath

Masters in Science 2011-2013
Integrative Biology and Physiology Masters Program, UCLA; Los Angeles, CA
Department of Integrative Biology and Physiology
Laboratory of Patricia E. Phelps

Bachelor of Science 2007-2011
Physiological Sciences, UCLA; Los Angeles, CA
With minor in English

Selected Publications

Kaylor. J., Xu, T., **Ingram, N.T**., Tsan, A., Hakobyan, H., Fain, G.L, and Travis, G., Blue light regenerates functional visual pigments in mammals through a retinyl-phospholipid intermediate. Nat Commun, 2017. 8(1): p. 16.

Ingram, N.T., A.P. Sampath, and G.L. Fain, Why are rods more sensitive than cones? J Physiol, 2016. 594(19): p. 5415-26.

Ingram, N.T., R.R. Khankan, and P.E. Phelps, Olfactory Ensheathing Cells Express alpha7 Integrin to Mediate Their Migration on Laminin. PLoS One, 2016. 11(4): p. e0153394.

Selected Presentations

Stein Eye Departmental Seminar 2/2019
MCIP Retreat 2/2018
Stein Eye Retreat 10/2017
Poster Presentation and Data Blitz at FASEB: The Biology and Chemistry of Vision 6/2017

Academic and Profession Honors

Dissertation Year Fellowship, UCLA Graduate Division 2018-2019
Stein Eye Pre-doctoral Training Grant, UCLA 2017-2018
Sensory Ecology Course with the Vision Group in Lund, Sweden 2016
Paris Neuroscience Class in Paris, France 2015
MCIP Pre-doctoral Training Grant, UCLA 2013-2015
Distinguished Teaching Assistant award, UCLA IBP 2013
Physiological Science Poster day, 2nd place 2011
UCLA Undergraduate Science Poster Day, Dean's Prize 2011
Valedictorian, Serrano High School, Phelan, California 2007

Other Professional Activities

Co-Instructor for UCLA Extension 2013-2019
Anatomy and Biomechanics special course for the Japanese Federation of Chiropractic Professionals

Association for Research in Vision and Ophthalmology, Student Member	2015-2019
Cabinet Member of Biological Science Counsel	
Treasurer	2014-2017
Departmental Representative	2012-2017
Teaching Assistant for UCLA, IBP	2011-2013

Chapter One:

An Introduction to Vertebrate Photoreceptor Physiology

Overview of the Visual System

Organisms have evolved complex, yet elegant sensory systems that detect changes in external energies. Each species uses specialized adaptations selected for the most relevant information in their environments. Several higher vertebrate species, including primates and birds, rely heavily on sight and have high-resolution, image-forming visual systems. Such animals also dedicate large portions of their brains to interpreting the light information that is collected.

In general, vertebrates have large, camera-type eyes that allow light to enter through a translucent window called the pupil (Fig. 1.1). Light then passes through a lens that focuses it on to a specialized neural tissue called the retina. The retina is typically several hundred micrometers thick and is organized into three distinct layers of somata (Fig. 1.2). The outermost layer contains the cell bodies of specialized neurons called photoreceptors. Vertebrate photoreceptors have developed a morphological specialization called the outer segment. The outer segment is an extension of the primary cilium and consists of stacks of lipid membrane that are packed with light-sensitive photopigments. Once stimulated with light, photoreceptors generate graded electrical signals that are transmitted to the inner nuclear layer containing different types of bipolar and amacrine cells. Between the outer and inner nuclear layers, photoreceptors form additional synaptic contacts with horizontal cells and electrical synapses with neighboring photoreceptors. In the inner nuclear layer, bipolar cells split the light information into parallel channels for processing and transmit signals to the third layer containing the ganglion cells (Masland 2012). Ganglion cells generate action

potentials and extend long axons (via the optic nerve, CNII) from the eye to cerebral structures.

Vertebrate Photoreceptors

Vertebrates have evolved duplex retinas (Schultze 1866). In a duplex retina, image formation is mediated by two classes of light-detecting cells, rods and cones. Rod photoreceptors are highly sensitive to dim light. They reach the physical limit of signal detection by reliably encoding single photons of light (Hecht et al. 1942; Baylor et al. 1979). Cone photoreceptors are specialized for brighter ambient conditions (Normann and Perlman 1979; Burkhardt 1994). When multiple opsin subtypes are expressed, cones act as the spectral detectors for color vision (Marks et al. 1964).

Current theory and evidence suggest that rod photoreceptors evolved from an ancestral ciliary-type cone before vertebrates branched from their last common ancestor (Lamb 1995; Morshedian and Fain 2017). In this process, rods became optimized to signal in dim light and detect single light quanta. To operate near threshold, the rod signal-transduction mechanism is both low-noise and high-gain, and after the rods, downstream circuitry contains linear filters to limit cellular noise (Pahlberg and Sampath 2011). In addition to linear filters, the rod bipolar cells in mouse pool responses from around 20 rods to increase the probability of light detection (Tsukamoto et al. 2001; Field and Rieke 2002). Significant trade offs accompany these optimizations, and compared to cones, rods have slow response kinetics and saturate in relatively dim light (Fig. 1.3B).

As ambient light levels increase, cone phototransduction dominates. With an abundance of photons, less gain is needed for signal detection, and responses occur with faster kinetics (Fig. 1.3B). As a result, temporal resolution is improved, and cones do not saturate even in bright light (Burkhardt 1994; Perlman and Normann 1998). Within multiple subphyla, cones have evolved several times to express distinctive types of opsin that are sensitive to different peak wavelengths. Organisms expressing two or more opsin types can detect color by comparing differential activation of the spectrally defined, downstream channels (Dacey 2000; Breuninger et al. 2011). Thus, cones form the actual physiological substrate for color vision (Marks et al. 1964).

Despite the division of labor, the rod and cone phototransduction machinery is mostly conserved (Fig. 1.3A). Signaling differences, therefore, arise from changes in protein isoform or different expression levels of *conserved* isoforms. Each small adjustment shifts light sensitivity by only a few fold (~2-3), and the cumulative effect results in rods that are approximately 100-fold more sensitive than cones when dark adapted (See Appendix A; Ingram et al. 2016). These collective changes are responsible for the significant differences in response kinetics and adaptation (Fig.1.3B).

Light Detection and Phototransduction

The membrane potentials of dark-adapted rods and cones are depolarized (-35 to -40 mV) compared to typical cortical neurons (-70 mV). In darkness, cyclic-nucleotide gated (CNG) channels located in outer-segment membranes are open (Fig. 1.4). Calcium and sodium flow into the photoreceptor outer segment, depolarizing the cells'

membranes. The electrical circuit is completed as potassium leaves the photoreceptors through channels located in the inner segments. Together these currents are called the 'circulating' or 'dark' currents and set the maximum value of the photoresponse (Baylor et al. 1979).

When a dark-adapted rod photoreceptor is exposed to a brief flash, a high-gain sequence of events can be triggered by the absorption of a single photon. Rhodopsin, the visual pigment in rods, consists of opsin protein with a covalently linked chromophore, 11-*cis*-retinal. The Schiff base linkage of the chromophore to opsin stabilizes the chromophore enough to lower thermal noise to levels necessary to reliably detect single photons (Luo et al. 2011). It also shifts λ_{max} to longer wavelengths (~503 nm in mouse rods). When a photon is absorbed, 11-*cis*-retinal is photoconverted to all-*trans*-retinal. Photoisomerization causes a chain of events that eventually closes the CNG channels.

Activated rhodopsin (Rh*) catalyzes the replacement of GDP on the alpha subunit of the heterotrimetric G protein, transducin ($G\alpha_t$) for GTP (Fu 1995), and $G\alpha_t$–GTP dissociates from its βγ subunits. The gain factor estimates at this step have been contentiously argued and vary between cell type and species. Current evidence suggests that in mouse rods, approximately 15 to 20 $G\alpha_t$ subunits are activated by a single Rh* (Arshavsky and Burns 2014). $G\alpha_t$–GTP disinhibits phosphodiesterase (PDE6 in rods) by interacting with the inhibitory PDEγ subunit. Once activated, PDE6 will begin to hydrolyze cGMP (Fu 1995). A drop in cGMP concentration causes a closure of CNG channels and is recorded as a reduction in inward current (Fig. 1.3B; Hagins et al. 1970; Baylor et al. 1979).

Signal shut off and response recovery are extremely important, as both set the temporal kinetics of the visual system. Because of the gain mechanisms present at every activation step of phototransduction, each step must come to a timely cessation. Rh* is quenched when rhodopsin kinase (RK; GRK1) phosphorylates and a small protein called arrestin binds to the rhodopsin c-terminal. PDE deactivation is speeded by a GTPase accelerating protein (GAP) complex, which quickens the hydrolysis of GTP bound to $G\alpha_t$. As PDE activity returns to basal levels, cGMP concentration increases and reopens CNG channels (Fu 1995).

Phototransduction is similar in cones; however, the gain is lower and response kinetics are faster (Fig. 1.3B). These cumulative changes are necessary to support vision in brighter light conditions.

Light Adaptation

After prolonged light exposure has occurred, photoreceptors begin numerous and profound mechanisms to adapt and remain functional over an extended range of light intensities. Calcium is the key messenger driving light adaptation (Matthews et al. 1988; Nakatani and Yau 1988). Steady-light exposure causes a persistent or sustained closure of CNG channels. A Na^+/Ca^{2+}-K^+ exchanger continues to extrude calcium, causing its internal concentration to fall well below dark-adapted levels. Calcium-sensing proteins in the outer segment detect the decrease in calcium and in turn, mediate the hallmark signs of light adaptation: decreased sensitivity and accelerated response kinetics (Fain 2011).

First, Guanylyl Cyclase Activating Proteins (GCAPs) react to the drop in calcium by increasing the rate of cGMP synthesis by Guanylyl Cyclase (Mendez et al. 2001; Burns et al. 2002). Second, the decrease in calcium causes it to dissociate from another small protein, recoverin. When calcium is high, recoverin slows the phosphorylation rate of the rhodopsin c-terminus by GRK1, extending the lifetime of the Rh* (Makino et al. 2004; Chen et al. 2010; Chen et al. 2012). As calcium concentration falls, GRK1 becomes disinhibited, speeding the rate of rhodopsin phosphorylation, but this has little or no effect on rod adaptation (Morshedian and Fain 2017). Third, CNG channels have binding sites for calcium-calmodulin. The binding of calmodulin to the CNG channels modulates the affinity for the CNG channels to available cGMP (Haynes and Stotz 1997), but also has no effect on adaptation (Chen et al. 2010).

While careful experiments outline this paradigm for mouse rods, few have closely investigated transduction proteins in single mouse cones. When considering conserved calcium-sensing proteins – GCAPs and recoverin – I asked if light-adaptation is controlled similarly in cones and rods. It is possible, if not likely, that interactions with isoform variants affect the photoreceptors at different set points. For example, the PDE subunits are different in rods and cones (Fu and Yau 2007). Interplay between calcium-sensing proteins and these subunits could account for altered operating regimes and different steady-state conditions.

Besides adaptation of the transduction machinery, further mechanisms keep the cone responsive to bright light. To remain responsive in ambient light environments, the cone must not only recover electronically (i.e. reopen CNG channels), but also, the photopigment must be regenerated at a rate that matches or exceeds that of bleaching.

Previous work has identified a primary visual cycle in which all-*trans*-retinal must leave the photoreceptor and be transported to the retinal pigmented epithelium (RPE; Jin et al. 2005). More recently evidence has accumulated for a cone-specific visual cycle. This visual cycle occurs within the Müller glia and produces a pool of 11-*cis*-retinol pigment specifically for cones (Wang and Kefalov 2011).

Chapter 4 proposes a 3rd pathway contributing to photopigment regeneration. We describe how when all-*trans*-retinal is released from opsin, it can condense with phosphatidylethanolamine within the photoreceptor membrane. If exposed to blue light, all-*trans*-retinal can be photoconverted to 11-*cis*-retinal in a highly specific manner (Kaylor et al. 2017). Photopigment regeneration via an association with phospholipids does not require enzymes or retinal to leave the photoreceptor. The discovery of parallel pathways for chromophore regeneration is not surprising as calculations indicated that the rate of pigment regeneration from the RPE alone was not fast enough to supply chromophore for uninterrupted signaling in daylight conditions (Mata et al. 2002).

Physiological Recordings and Model Species: A Brief History

Since the earliest attempts at quantifying visual responses, research on the retina has shifted through multiple technologies along with the use of model organisms. The field is unique in its comparative data with measurements made in species from multiple phyla and subphyla. The outer retina stands alone as being the only area of mammalian neurocircuitry in which all cell types are catalogued (Masland 2012). Stimulus control and robust system read-outs continue to make the visual system a

general model for signal processing and neurocircuitry. Here I give a brief glimpse into the pertinent history and theory leading to this work.

Early psychophysical investigations determined that humans consciously perceive light calculated to activate 5-7 rhodopsins. Stimuli were calibrated such that between 50-150 photons were delivered to the surface of the cornea. After passing through the eye, only 5-14 of those photons fell onto a pool of approximately 500 rod photoreceptors. At this rate, the chances of a single rod absorbing two of those photons were less than 5%, suggesting that human rods are able to detect single photons reliably (Hecht et al. 1942). Experiments with background lights indicated that, together, photoreceptors adapt over 10 log units of light, and that rod-dominant vision smoothly transitions into cone-dominant vision (Barlow 1972; Nelson 1977; Burkhardt 1994).

Tissue and single-cell recordings began in the 1960's when parallel developments in electronics and biomedical science occurred. Hodgkin and Huxley demonstrated that individual cells could generate electrical potentials and currents by controlling when and what charged ions moved across their semi-permeable membranes (Hodgkin and Huxley 1952). Shortly after this, operational amplifiers became commercially available, and neurobiologists no longer had to build their own amplifiers.

Starting with intracellular sharp-electrode recording, photovoltage responses were recorded in fish and amphibian rods and cones (Tomita 1963; Fain and Dowling 1973). The photoreceptors of these species are quite large compared to those in mammals making them easier to manipulate and record from. Despite both being vertebrates, major differences exist in size, temperature, and kinetics of the

photoresponses generated in mammalian and amphibian photoreceptors (Baylor et al. 1979).

In the late 1970s, another technique proved to be highly significant for the study of photoreceptors. Suction-electrode recording utilized the fortuitous polarity of the photoreceptor: experiments showed that all the light-sensitive channels are located in the photoreceptor outer segment (Yau et al. 1977; Baylor et al. 1979). Suction recording provides a relatively noninvasive method for tracking light-induced changes of the outer-segment currents, and it is possible to record from a single cell for over an hour. This technique was first employed on larger amphibian photoreceptors. However, as the 1990's brought the birth of genetic engineering in mice, vision scientists adapted suction-electrode recording to target the smaller mouse rods (Raport et al. 1994).

A huge advancement in cellular physiology came with the introduction of patch-clamp techniques (Neher et al. 1978). Experimenters can 'clamp' the membrane potential, even of small cells, to a specific voltage (i.e. command voltage), and the recorded currents are directly proportional to changes in membrane conductance (Baylor et al. 1979; Baylor and Nunn 1986). This is in contrast to the photocurrents recorded via suction electrode. Because suction-electrode recording does not clamp the membrane potential to a set value, these cells are free to experience changes in membrane potential and subsequent voltage-dependent effects. Shifts in membrane potential directly affects the magnitude of the driving force on conducting ions and may activate voltage-sensitive conductances.

Beyond vision research, voltage-clamp techniques have enabled a careful analysis of G-protein cascades, channel physiology, circuitry analysis, and it continues

to be a powerful tool for neurobiologists. The addition of specific pharmacological blockers can isolate desired current components and detailed biophysical measurements can be made for important ionic channels (major ionic conductances in photoreceptors are described below). Many studies focusing on channel biophysics in photoreceptors utilized cold-blooded vertebrates, and much remains to be measured in both mouse rods and cones.

As the revolution in modern genetics came to the forefront of biomedical research, so too did the mouse to vision research. Making transgenic manipulations in the visual system has additional benefits: 1) many of the protein isoforms expressed are tissue specific and unique to the eye, 2) numerous genetic models show little compensatory changes in the gene expression of other isoforms, and 3) mutations causing degeneration or blindness are not majorly debilitating in mice. While there are exceptions, targeted mutations are generally specific, with few confounding effects.

Single cell recordings of mouse photoreceptors began with suction-electrode recordings when the technique was adapted for photoreceptors with 8-fold smaller outer-segment diameters (salamander vs mouse; Raport el al. 1994; Mendez et al. 2000; Fu and Yau 2007) . Using various lines of transgenic mice, researchers began to explore how the loss or altered expression of signal transduction proteins modulates the photoresponse and cell-viability (Calvert et al. 2000; Mendez et al. 2001; Burns et al. 2002; Makino et al. 2004; Chen et al. 2010).

Despite the power of transgenics, a huge hurdle remained. In the more relevant mammalian model species, cone photoreceptors constitute less than 5% of the total photoreceptor population (Carter-Dawson and LaVail 1979; Curcio et al. 1987; Jeon et

al. 1998). Thus, until the mid-2000s, electrophysiological methods that successfully targeted mammalian cones were limited as compared to rods. The few recordings that were obtained were subject to significant artifacts and/or low signal-to-noise ratios (Nikonov et al. 2005; Sakurai et al. 2011; Asteriti et al. 2014). This is unfortunate since we ourselves are diurnal, and cone physiology is more pertinent to the understanding of human visual experience, than the physiology of rods.

Major Ionic Conductances

After the phototransduction cascade triggers the closure of CNG channels, a photoreceptor undergoes a graded change in current flux. How does this conductance change relate to the membrane voltages that control glutamate release at the synaptic ribbons? Here I will describe the major ion conductances underlying the generation and modulation of graded electrical signals generated by vertebrate photoreceptors. Before my work, most studies characterized the ionic conductances of photoreceptors from cold-blooded animals (Baylor and Nunn 1986; Barnes and Hille 1989; Miller and Korenbrot 1993) or enzymatically-isolated preparations (Yagi and Macleish 1994; Cia et al. 2005). Few have attempted these investigations with *in-situ* preparations of mammalian photoreceptors while maintaining light sensitivity.

Early work demonstrated a cesium-sensitive conductance that increased with hyperpolarization (Fain et al. 1978; Barnes and Hille 1989). Dubbed I_h, this stabilizing, potassium-dominant current speeds the kinetics of the rod photoresponse and produces the ‘nose’ of the photovoltage response (Fain et al. 1978; Schneeweis and Schnapf 1999; Seeliger et al. 2011). Work in salamander quantified the reversal potential of the

rod light response (Baylor and Nunn 1986) as well as several inner-segment conductances including voltage-gated calcium current, calcium-activated anion and potassium currents, and outwardly rectifying potassium conductances (Barnes and Hille 1989). Further studies from fish photoreceptors measured the reversal of the cone light response, assessed a voltage-dependent modulation of the CNG channel (Miller and Korenbrot 1993), and quantified the electrogenic contribution of the Na^+/Ca^{2+}-K^+ exchanger (Brockerhoff et al. 2003).

Reports of mammalian photoreceptor conductances were limited to several studies using enzymatic-dissociation (Yagi and Macleish 1994; Cia et al. 2005). Enzymatic digestion of the retina typically damages the outer segments, and the light response is usually lost. Further, there is evidence that enzymatic dissociation can induce aberrant channel expression (Hestrin and Korenbrot 1987), and results from such experiments should be confirmed with additional methods. A slice preparation was used to study cone photoreceptors in ground squirrel (DeVries 2001); however, the focus of that work was limited to the characterization of the inner-segment calcium-current, and light responses were not investigated.

Cone Pedicles: The First Synapse and The Lateral Network

Cone photoreceptors transmit light responses through various mechanisms located at a specialized synaptic structure called the pedicle (the spherule in rods). The cone pedicle in the mouse retina contains up to 10 ribbon synapses (Kerov et al. 2018), where the cone is able to signal light responses via a decrease in glutamate release. Each ribbon synapse consists of ON-type bipolar cell and horizontal cell processes that

invaginate into the pedicle, directly beneath the vesicle releasing machinery (Raviola and Gilula 1975). Outside of the foveal cones (in applicable species), each cone synapses with multiple types of cone bipolar cells creating separate channels for parallel processing (Masland 2012).

Voltage-gated calcium channels are located within the vicinity of each ribbon release site (Choi et al. 2008). In the dark, sodium and calcium enter through outer-segment CNG channels and depolarize the photoreceptors. When photoreceptors are depolarized, L-type Ca^{2+}-channels located in the spherules and pedicles can maintain a sustained, inward calcium current supporting the continuous release of glutamate-filled vesicles. Upon light exposure photoreceptors hyperpolarize, which decreases the amount of calcium entering the pedicle. With less calcium entering in the vicinity of the synaptic ribbons, fewer vesicles and less glutamate are released.

Also located in the cone pedicle are gap junctions (Raviola and Gilula 1973). Electrical signal spread between neighboring photoreceptors was evident in early works. Voltage traces revealed consistent responses to stimuli activating only a fraction of one rhodopsin per flash, suggestive of a highly-coupled electrical network (Fain 1975). Further studies confirmed the lateral network between neighboring rods and cones and its effects on sensitivity, response kinetics, and signal spread (Fain 1975; Nelson 1977; Schneeweis and Schnapf 1995; Cangiano et al. 2012; Asteriti et al. 2014). Chapter 2 will show that rod signals also spread to cones in mouse, but with transgenic mice lacking photoreceptor gap junctions, it is possible to record isolated cone responses.

Thesis Goals

This thesis explores the molecular and electrical characteristics of mouse cone photoreceptors. I demonstrate the viability and practicality of patch clamping single mouse cones in unlabeled retinal slices. With this ability, I describe in Chapter 2 measurements made in light-responsive cones. Basic measurements include total dark current, membrane capacitance, and resting membrane potentials. These are parameters that have been difficult to obtain in other mammalian species. Because genetic engineering has advanced furthest in mouse compared to any other mammal, I utilized transgenic mouse lines lacking calcium-sensitive proteins to investigate light responses and adaptation.

Chapter 3 describes biophysical measurements of major conductances in mouse cones. Using pharmacology and stimulation protocols, I isolated specific ionic conductances and characterized them. Our methodology maintains photoreceptors with robust light responses, and I am the first to describe the reversal potential for the light-sensitive channel in mammalian photoreceptors.

Cones are optimized to operate with background illumination (Burkhardt 1994). In addition to the adaption occurring in the transduction cascade, bleached photopigment must be regenerated and replaced at adequate rates for the cell to remain responsive to light. In addition to the well known visual cycles carried out in the RPE and Müller glia, Chapter 4 describes a light-driven pathway for the regeneration of photopigment. In this pathway, all-*trans*-retinal can be preferentially converted back to 11-*cis*-retinal when bound to phosopholipid in the photoreceptor membrane and exposed to blue light (λ_{max}

= 450). This third pathway has several advantages: all-*trans*-retinal does not have to leave the photoreceptor, and photoconversion does not require enzymes.

Yet another aspect controlling sensitivity and response kinetics in cone circuitry are feedback mechanisms and connectivity occurring at the first synapse. Chapter 5 describes targeting molecules that are important for correct signal transmission across the first layers of the retina. When the targeting molecule LRIT1 is lost, cone photoreceptors exhibit light responses with normal kinetics and sensitivities. Cone bipolar cells, however, are more sensitive compared to control. These experiments indicate that LRIT1 is an important contributor to the proper synaptic physiology and signal transmission of retinal neurons.

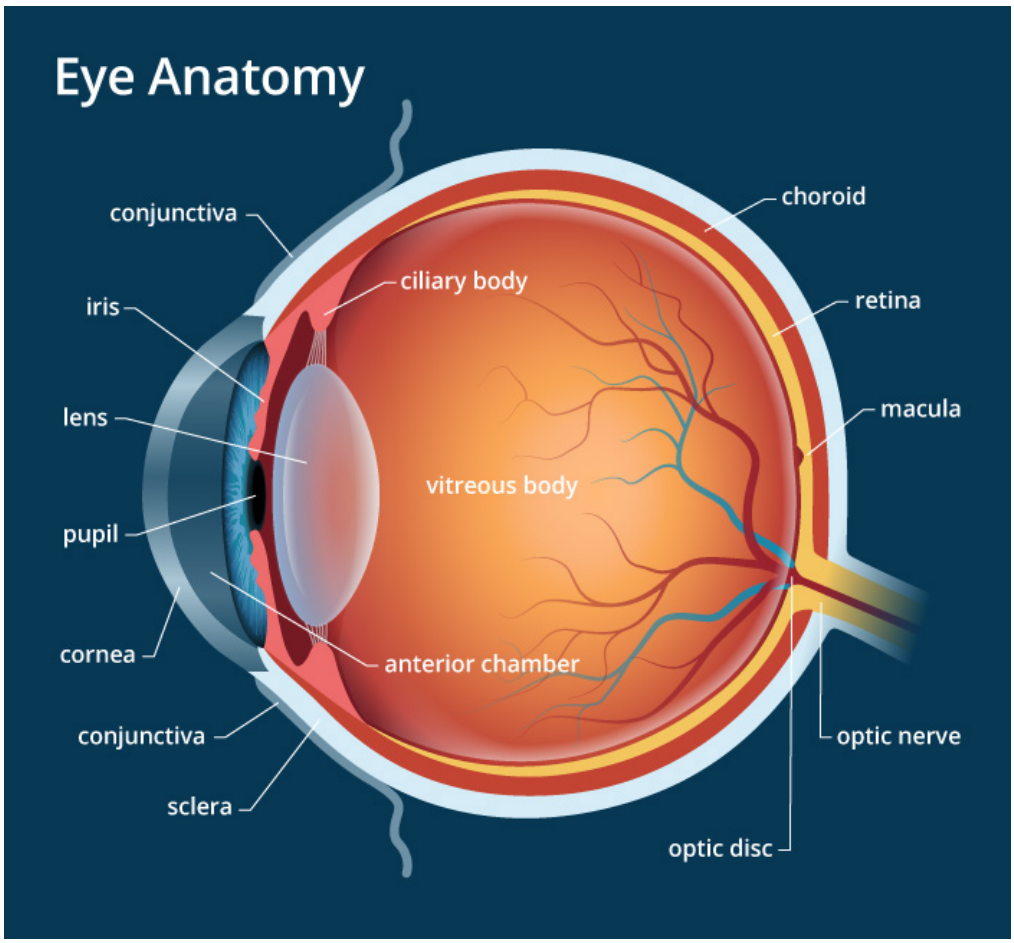

Figure 1.1 The Anatomy of a Camera-Type Eye

Light passes through the translucent cornea, where the pupil acts as an adjustable pinhole. Next, the lens focuses light onto the back retina-lined eye, inverting the visual field in the process. Photon detection occurs in the neural retina located at the back of the eye, and electrical spike responses are transmitted to cerebral structures via the optic nerve. Blood vessels are found primarily in the choroid and the thick sclera provides support and protection for the internal structures.

(https://www.allaboutvision.com/resources/anatomy.htm)

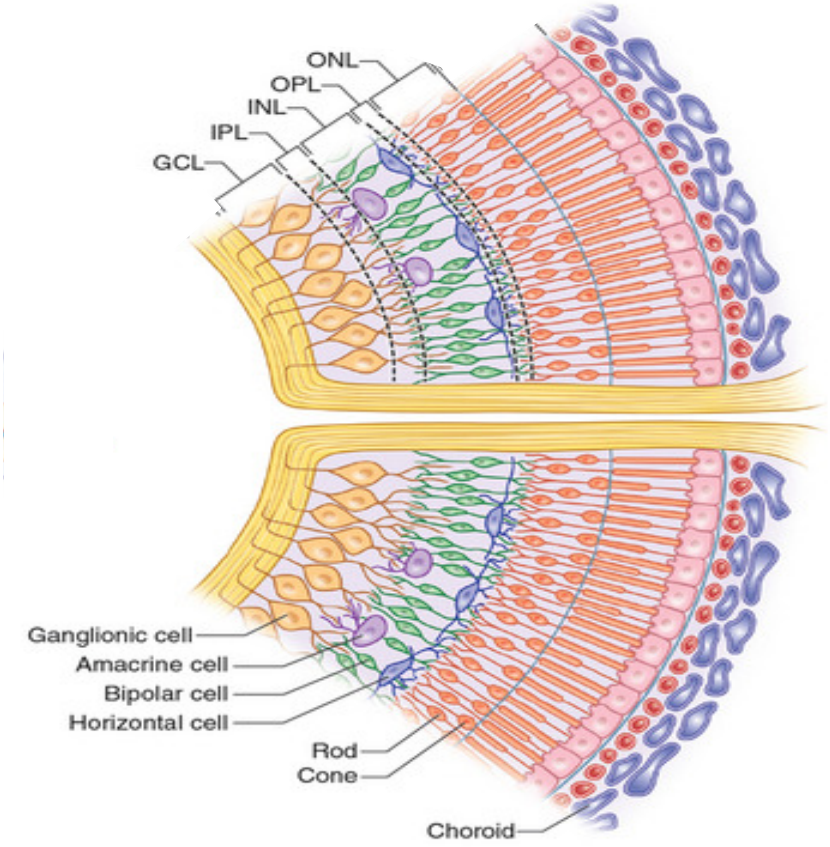

Figure 1.2 Layers of the Neural Retina

The neural retina contains 3 major layers of neuronal somata: the outer nuclear layer (ONL), the inner nuclear layer (INL) and the ganglion cell layer (GCL). Between each layer of somata are extensive contacts between retinal cells. The outer plexiform layer (OPL) connects photoreceptors to bipolar cells. The horizontal cells provide local feedback within the OPL. The inner plexiform layer (IPL) is further subdivided and is the location of signal modulation and transfer between bipolar cells, amacrine cells, and ganglion cells.

(Image adapted from http://www.retinareference.com/anatomy/)

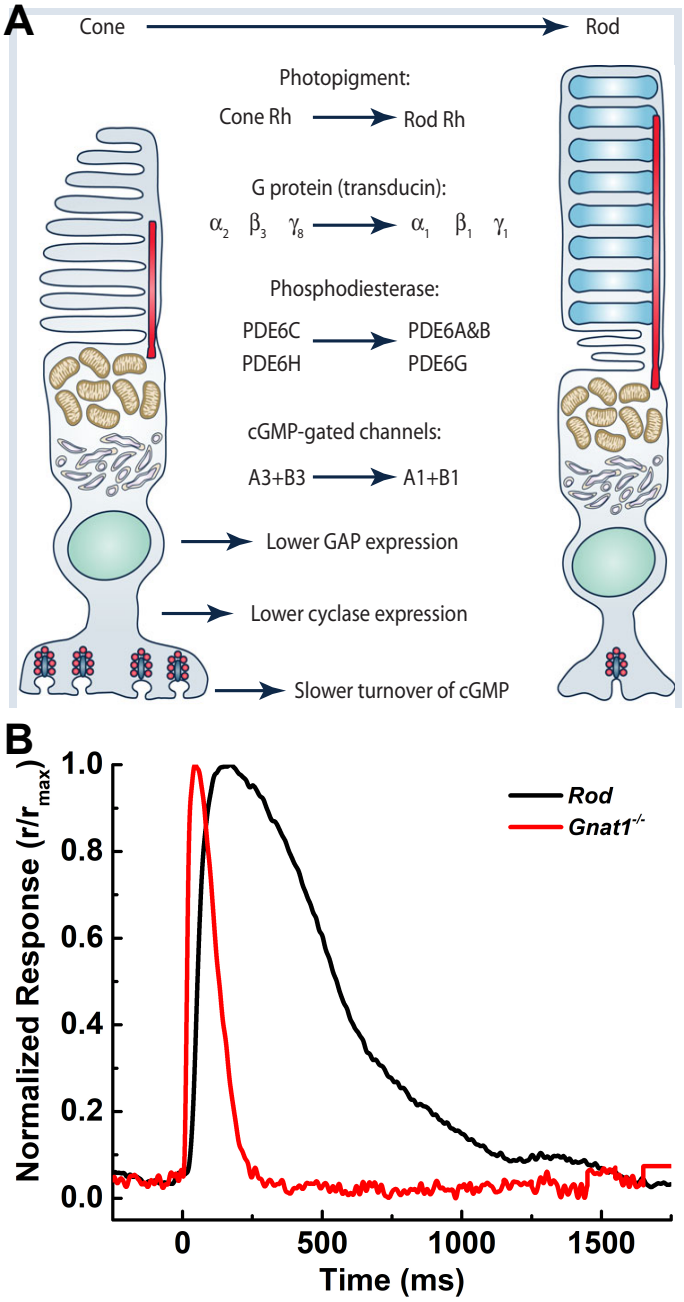

Figure 1.3 Differences Between Rod and Cone Photoreceptors

A) The molecular machinery of phototransduction is largely conserved between ciliary-type photoreceptors. Distinct response characteristics arise from differences in isoforms and expression levels. Originally published in Ingram et al. 2016. B) Normalized, saturating photocurrents from a *Gnat1*$^{-/-}$ cone (red, 3100 P*/flash) and wild-type rod (black 130 Rh*/flash). Photoreceptors were recorded with standard voltage-clamp methods outline in Appendix B.

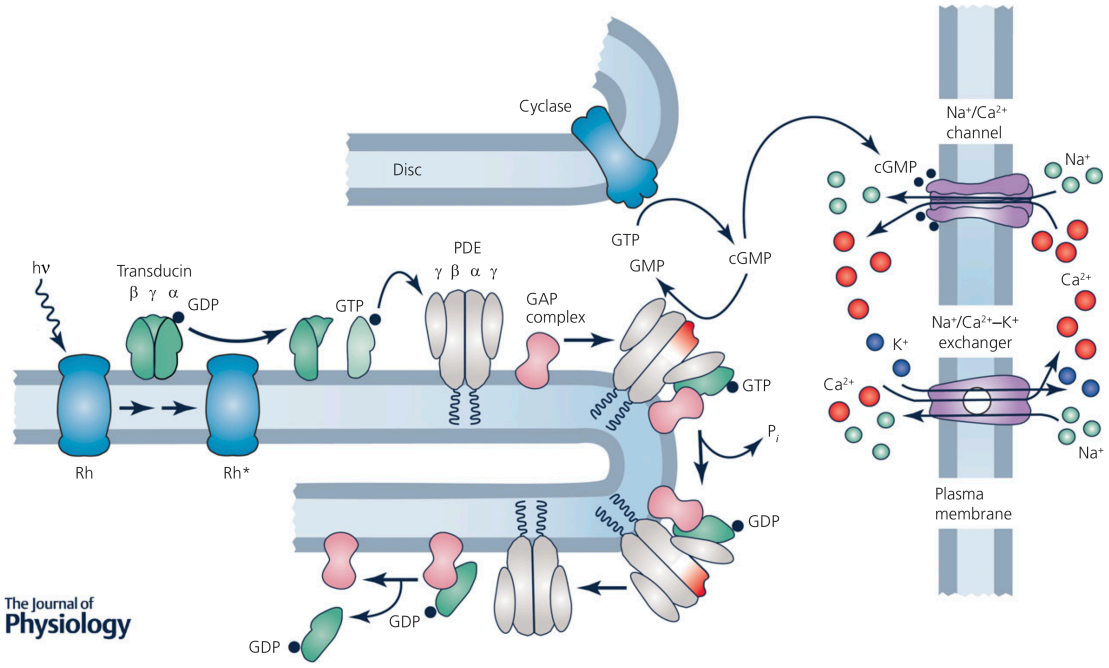

Figure 1.4 The Phototransduction Cascade in Ciliary Photoreceptors

Briefly, in the dark sodium and calcium enter through cyclic nucleotide gated (CNG) channels in the outer segment. A photon of light ($h\nu$) can activate rhodopsin (Rh*), which can then activated the heterotrimetic G-protein transducin (G_t). With GTP bound, the $G\alpha_t$-subunit will activate a phosphodiesterase (PDE), which hydrolyzes cGMP. As cytosolic cGMP concentration drops, CNG channels close and cause the photoreceptor to hyperpolarize. The light response is terminated with rhodopsin inactivation via kinase phosphorylation and PDE shutdown via the hydrolysis of GTP from $G\alpha_t$. The rate of GTP hydrolysis is increased by the GTPase accelerating protein (GAP) complex. After PDE activity decreases, guanylyl cyclase restores the cGMP concentration. Originally published in Fain 2011 and reprinted in Ingram et al. 2016.

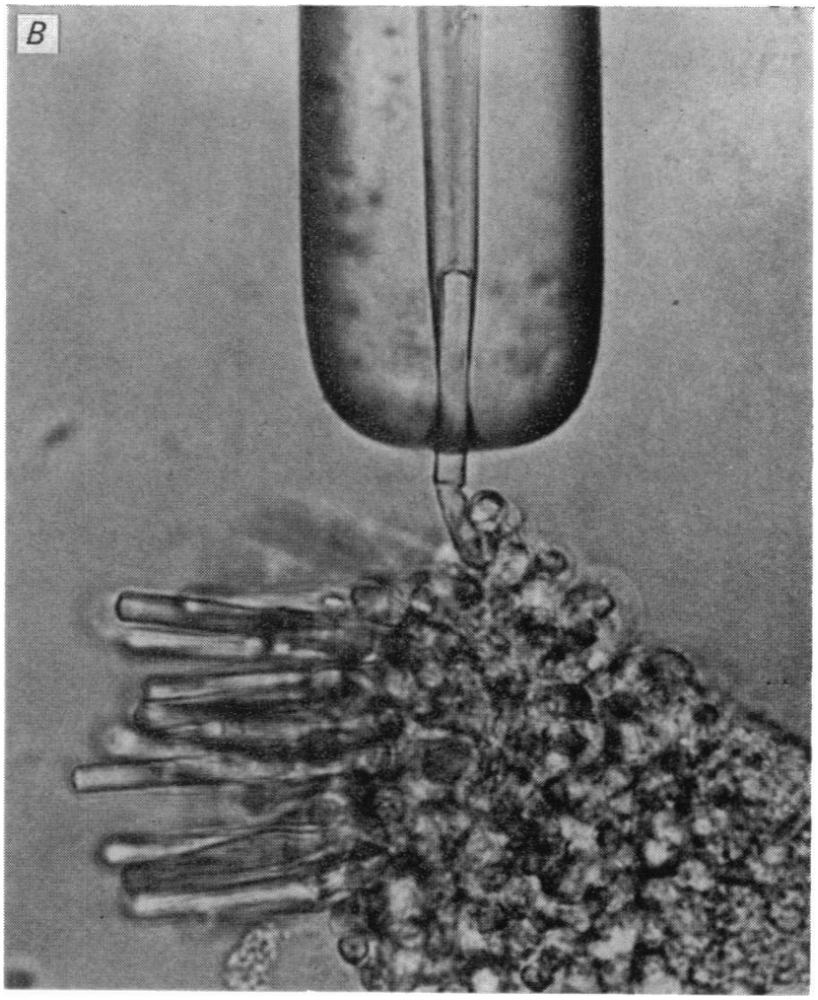

Figure 1.5 Suction-Electrode Recording of a Single Rod Photoreceptor

The outer segment of a single toad photoreceptor is drawn into a suction recording electrode. Light sensitive channels are expressed in the outer segment and changes in standing current can be monitored with suction-electrode recording. Originally published in Baylor et al. 1979.

References

Arshavsky, V. Y. and M. E. Burns (2014). "Current understanding of signal amplification in phototransduction." Cell Logist **4**: e29390.

Asteriti, S., C. Gargini and L. Cangiano (2014). "Mouse rods signal through gap junctions with cones." Elife **3**: e01386.

Barlow, H. B. (1972). Dark and Light Adaptation: Psychophysics. Visual Psychophysics. D. Jameson and L. M. Hurvich. Berlin, Heidelberg, Springer Berlin Heidelberg**:** 1-28.

Barnes, S. and B. Hille (1989). "Ionic channels of the inner segment of tiger salamander cone photoreceptors." J Gen Physiol **94**(4): 719-743.

Baylor, D. A., T. D. Lamb and K. W. Yau (1979). "The membrane current of single rod outer segments." J Physiol **288**: 589-611.

Baylor, D. A., T. D. Lamb and K. W. Yau (1979). "Responses of retinal rods to single photons." J Physiol **288**: 613-634.

Baylor, D. A. and B. J. Nunn (1986). "Electrical properties of the light-sensitive conductance of rods of the salamander Ambystoma tigrinum." J Physiol **371**: 115-145.

Breuninger, T., C. Puller, S. Haverkamp and T. Euler (2011). "Chromatic bipolar cell pathways in the mouse retina." J Neurosci **31**(17): 6504-6517.

Brockerhoff, S. E., F. Rieke, H. R. Matthews, M. R. Taylor, B. Kennedy, I. Ankoudinova, G. A. Niemi, C. L. Tucker, M. Xiao, M. C. Cilluffo, G. L. Fain and J. B. Hurley (2003). "Light stimulates a transducin-independent increase of cytoplasmic Ca2+ and suppression of current in cones from the zebrafish mutant nof." J Neurosci **23**(2): 470-480.

Burkhardt, D. A. (1994). "Light adaptation and photopigment bleaching in cone photoreceptors in situ in the retina of the turtle." J Neurosci **14**(3 Pt 1): 1091-1105.

Burns, M. E., A. Mendez, J. Chen and D. A. Baylor (2002). "Dynamics of cyclic GMP synthesis in retinal rods." Neuron **36**(1): 81-91.

Calvert, P. D., N. V. Krasnoperova, A. L. Lyubarsky, T. Isayama, M. Nicolo, B. Kosaras, G. Wong, K. S. Gannon, R. F. Margolskee, R. L. Sidman, E. N. Pugh, Jr., C. L. Makino and J. Lem (2000). "Phototransduction in transgenic mice after targeted deletion of the rod transducin alpha -subunit." Proc Natl Acad Sci U S A **97**(25): 13913-13918.

Cangiano, L., S. Asteriti, L. Cervetto and C. Gargini (2012). "The photovoltage of rods and cones in the dark-adapted mouse retina." J Physiol **590**(16): 3841-3855.

Carter-Dawson, L. D. and M. M. LaVail (1979). "Rods and cones in the mouse retina. I. Structural analysis using light and electron microscopy." J Comp Neurol **188**(2): 245-262.

Chen, C. K., M. L. Woodruff, F. S. Chen, D. Chen and G. L. Fain (2010). "Background light produces a recoverin-dependent modulation of activated-rhodopsin lifetime in mouse rods." J Neurosci **30**(4): 1213-1220.

Chen, C. K., M. L. Woodruff, F. S. Chen, Y. Chen, M. C. Cilluffo, D. Tranchina and G. L. Fain (2012). "Modulation of mouse rod response decay by rhodopsin kinase and recoverin." J Neurosci **32**(45): 15998-16006.

Chen, J., M. L. Woodruff, T. Wang, F. A. Concepcion, D. Tranchina and G. L. Fain (2010). "Channel modulation and the mechanism of light adaptation in mouse rods." J Neurosci **30**(48): 16232-16240.

Choi, S. Y., S. Jackman, W. B. Thoreson and R. H. Kramer (2008). "Light regulation of Ca2+ in the cone photoreceptor synaptic terminal." Vis Neurosci **25**(5-6): 693-700.

Cia, D., A. Bordais, C. Varela, V. Forster, J. A. Sahel, A. Rendon and S. Picaud (2005). "Voltage-gated channels and calcium homeostasis in mammalian rod photoreceptors." J Neurophysiol **93**(3): 1468-1475.

Curcio, C. A., K. R. Sloan, Jr., O. Packer, A. E. Hendrickson and R. E. Kalina (1987). "Distribution of cones in human and monkey retina: individual variability and radial asymmetry." Science **236**(4801): 579-582.

Dacey, D. M. (2000). "Parallel pathways for spectral coding in primate retina." Annu Rev Neurosci **23**: 743-775.

DeVries, S. H. (2001). "Exocytosed protons feedback to suppress the Ca2+ current in mammalian cone photoreceptors." Neuron **32**(6): 1107-1117.

Fain, G. L. (1975). "Quantum sensitivity of rods in the toad retina." Science **187**(4179): 838-841.

Fain, G. L. (2011). "Adaptation of mammalian photoreceptors to background light: putative role for direct modulation of phosphodiesterase." Mol Neurobiol **44**(3): 374-382.

Fain, G. L. and J. E. Dowling (1973). "Intracellular recordings from single rods and cones in the mudpuppy retina." Science **180**(4091): 1178-1181.

Fain, G. L., F. N. Quandt, B. L. Bastian and H. M. Gerschenfeld (1978). "Contribution of a caesium-sensitive conductance increase to the rod photoresponse." Nature **272**(5652): 466-469.

Field, G. D. and F. Rieke (2002). "Nonlinear signal transfer from mouse rods to bipolar cells and implications for visual sensitivity." Neuron **34**(5): 773-785.

Fu, Y. (1995). Phototransduction in Rods and Cones. Webvision: The Organization of the Retina and Visual System. H. Kolb, E. Fernandez and R. Nelson. Salt Lake City (UT).

Fu, Y. and K. W. Yau (2007). "Phototransduction in mouse rods and cones." Pflugers Arch **454**(5): 805-819.

Hagins, W. A., R. D. Penn and S. Yoshikami (1970). "Dark current and photocurrent in retinal rods." Biophys J **10**(5): 380-412.

Haynes, L. W. and S. C. Stotz (1997). "Modulation of rod, but not cone, cGMP-gated photoreceptor channels by calcium-calmodulin." Vis Neurosci **14**(2): 233-239.

Hecht, S., S. Shlaer and M. H. Pirenne (1942). "Energy, Quanta, and Vision." J Gen Physiol **25**(6): 819-840.

Hestrin, S. and J. I. Korenbrot (1987). "Voltage-activated potassium channels in the plasma membrane of rod outer segments: a possible effect of enzymatic cell dissociation." J Neurosci **7**(10): 3072-3080.

Hodgkin, A. L. and A. F. Huxley (1952). "A quantitative description of membrane current and its application to conduction and excitation in nerve." J Physiol **117**(4): 500-544.

Ingram, N. T., A. P. Sampath and G. L. Fain (2016). "Why are rods more sensitive than cones?" J Physiol **594**(19): 5415-5426.

Jeon, C. J., E. Strettoi and R. H. Masland (1998). "The major cell populations of the mouse retina." J Neurosci **18**(21): 8936-8946.

Jin, M., S. Li, W. N. Moghrabi, H. Sun and G. H. Travis (2005). "Rpe65 is the retinoid isomerase in bovine retinal pigment epithelium." Cell **122**(3): 449-459.

Kaylor, J. J., T. Xu, N. T. Ingram, A. Tsan, H. Hakobyan, G. L. Fain and G. H. Travis (2017). "Blue light regenerates functional visual pigments in mammals through a retinyl-phospholipid intermediate." Nat Commun **8**(1): 16.

Kerov, V., J. G. Laird, M. L. Joiner, S. Knecht, D. Soh, J. Hagen, S. H. Gardner, W. Gutierrez, T. Yoshimatsu, S. Bhattarai, T. Puthussery, N. O. Artemyev, A. V. Drack, R. O. Wong, S. A. Baker and A. Lee (2018). "alpha2delta-4 Is Required for the Molecular and Structural Organization of Rod and Cone Photoreceptor Synapses." J Neurosci **38**(27): 6145-6160.

Lamb, T. D. (1995). Evolution of Phototransduction, Vertebrate Photoreceptors and Retina. Webvision: The Organization of the Retina and Visual System. H. Kolb, E. Fernandez and R. Nelson. Salt Lake City (UT).

Luo, D. G., W. W. Yue, P. Ala-Laurila and K. W. Yau (2011). "Activation of visual pigments by light and heat." Science **332**(6035): 1307-1312.

Makino, C. L., R. L. Dodd, J. Chen, M. E. Burns, A. Roca, M. I. Simon and D. A. Baylor (2004). "Recoverin regulates light-dependent phosphodiesterase activity in retinal rods." J Gen Physiol **123**(6): 729-741.

Marks, W. B., W. H. Dobelle and E. F. Macnichol, Jr. (1964). "Visual Pigments of Single Primate Cones." Science **143**(3611): 1181-1183.

Masland, R. H. (2012). "The neuronal organization of the retina." Neuron **76**(2): 266-280.

Mata, N. L., R. A. Radu, R. C. Clemmons and G. H. Travis (2002). "Isomerization and oxidation of vitamin a in cone-dominant retinas: a novel pathway for visual-pigment regeneration in daylight." Neuron **36**(1): 69-80.

Matthews, H. R., R. L. Murphy, G. L. Fain and T. D. Lamb (1988). "Photoreceptor light adaptation is mediated by cytoplasmic calcium concentration." Nature **334**(6177): 67-69.

Mendez, A., M. E. Burns, A. Roca, J. Lem, L. W. Wu, M. I. Simon, D. A. Baylor and J. Chen (2000). "Rapid and reproducible deactivation of rhodopsin requires multiple phosphorylation sites." Neuron **28**(1): 153-164.

Mendez, A., M. E. Burns, I. Sokal, A. M. Dizhoor, W. Baehr, K. Palczewski, D. A. Baylor and J. Chen (2001). "Role of guanylate cyclase-activating proteins (GCAPs) in setting the flash sensitivity of rod photoreceptors." Proc Natl Acad Sci U S A **98**(17): 9948-9953.

Miller, J. L. and J. I. Korenbrot (1993). "In retinal cones, membrane depolarization in darkness activates the cGMP-dependent conductance. A model of Ca homeostasis and the regulation of guanylate cyclase." J Gen Physiol **101**(6): 933-960.

Morshedian, A. and G. L. Fain (2017). "Light adaptation and the evolution of vertebrate photoreceptors." J Physiol **595**(14): 4947-4960.

Nakatani, K. and K. W. Yau (1988). "Calcium and light adaptation in retinal rods and cones." Nature **334**(6177): 69-71.

Neher, E., B. Sakmann and J. H. Steinbach (1978). "The extracellular patch clamp: a method for resolving currents through individual open channels in biological membranes." Pflugers Arch **375**(2): 219-228.

Nelson, R. (1977). "Cat cones have rod input: a comparison of the response properties of cones and horizontal cell bodies in the retina of the cat." J Comp Neurol **172**(1): 109-135.

Nikonov, S. S., L. L. Daniele, X. Zhu, C. M. Craft, A. Swaroop and E. N. Pugh, Jr. (2005). "Photoreceptors of Nrl -/- mice coexpress functional S- and M-cone opsins having distinct inactivation mechanisms." J Gen Physiol **125**(3): 287-304.

Normann, R. A. and I. Perlman (1979). "The effects of background illumination on the photoresponses of red and green cones." J Physiol **286**: 491-507.

Pahlberg, J. and A. P. Sampath (2011). "Visual threshold is set by linear and nonlinear mechanisms in the retina that mitigate noise: how neural circuits in the retina improve the signal-to-noise ratio of the single-photon response." Bioessays **33**(6): 438-447.

Perlman, I. and R. A. Normann (1998). "Light adaptation and sensitivity controlling mechanisms in vertebrate photoreceptors." Prog Retin Eye Res **17**(4): 523-563.

Raport, C. J., J. Lem, C. Makino, C. K. Chen, C. L. Fitch, A. Hobson, D. Baylor, M. I. Simon and J. B. Hurley (1994). "Downregulation of cGMP phosphodiesterase induced by expression of GTPase-deficient cone transducin in mouse rod photoreceptors." Invest Ophthalmol Vis Sci **35**(7): 2932-2947.

Raviola, E. and N. B. Gilula (1973). "Gap junctions between photoreceptor cells in the vertebrate retina." Proc Natl Acad Sci U S A **70**(6): 1677-1681.

Raviola, E. and N. B. Gilula (1975). "Intramembrane organization of specialized contacts in the outer plexiform layer of the retina. A freeze-fracture study in monkeys and rabbits." J Cell Biol **65**(1): 192-222.

Sakurai, K., J. Chen and V. J. Kefalov (2011). "Role of guanylyl cyclase modulation in mouse cone phototransduction." J Neurosci **31**(22): 7991-8000.

Schneeweis, D. M. and J. L. Schnapf (1995). "Photovoltage of rods and cones in the macaque retina." Science **268**(5213): 1053-1056.

Schneeweis, D. M. and J. L. Schnapf (1999). "The photovoltage of macaque cone photoreceptors: adaptation, noise, and kinetics." J Neurosci **19**(4): 1203-1216.

Schultze, M. (1866). "Zur Anatomie und Physiologie der Retina." Anatomie **2**(1): 175-286.

Seeliger, M. W., A. Brombas, R. Weiler, P. Humphries, G. Knop, N. Tanimoto and F. Muller (2011). "Modulation of rod photoreceptor output by HCN1 channels is essential for regular mesopic cone vision." Nat Commun **2**: 532.

Tomita, T. (1963). "Electrical activity in the vertebrate retina." J Opt Soc Am **53**: 49-57.

Tsukamoto, Y., K. Morigiwa, M. Ueda and P. Sterling (2001). "Microcircuits for night vision in mouse retina." J Neurosci **21**(21): 8616-8623.

Wang, J. S. and V. J. Kefalov (2011). "The cone-specific visual cycle." Prog Retin Eye Res **30**(2): 115-128.

Yagi, T. and P. R. Macleish (1994). "Ionic conductances of monkey solitary cone inner segments." J Neurophysiol **71**(2): 656-665.

Yau, K. W., T. D. Lamb and D. A. Baylor (1977). "Light-induced fluctuations in membrane current of single toad rod outer segments." Nature **269**(5623): 78-80.

Chapter Two:

Mouse Cone Photoresponses and Adaptation

Introduction

Until now, retinal mouse cones have been difficult to target in electrophysiological studies. While the mouse genome is easily manipulated, and genetically-linked reporter systems are commonplace, dark-adapted experimental conditions preclude the use of fluorescent markers to locate sparse cell populations visually. To overcome these difficulties, I developed a preparation relying only on the intrinsic visual cues that could be resolved with infrared illumination. No visible light was used to make slices or identify cone photoreceptors in these experiments. This chapter demonstrates that light-responsive cones can be reliably identified and recorded in a retinal slice preparation.

While other groups have used various approaches to assess mammalian cone photoresponses [Nikonov et al. 2005; Sakurai et al. 2001; Cangiano et al. 2012], each of their methodologies has significant drawbacks and yields artifacts or low signal-to-noise ratios. None of the techniques used prior to this work allowed individual cones to be voltage clamped in whole-cell configuration, and there remained significant gaps in the measurements of basic electrical conductances.

This chapter reports some of the most highly resolved measurements made to date from light-responsive mouse cones. In general, I describe the total dark current, membrane capacitance, and kinetics for a variety of transgenic mice. Chapter 2 shows that rod photocurrents spread to cones through gap junctions (Raviola and Gilula 1973). I then isolated 'pure-cone' photoresponses using *Gnat1*$^{-/-}$ or *Cx36*$^{-/-}$ transgenic mice, which either have electrically silent rods (Calvert et al. 2000) or lack photoreceptor gap junctions (Asteriti et al. 2017).

Next, I investigated the function of calcium-sensitive proteins found in the phototransduction cascade – recoverin (Chen et al. 2010) and the guanylyl cyclase activating proteins (GCAPs; Mendez et al. 2001). These proteins are proposed mediators of light adaptation and are conserved in rods and cones despite these photoreceptors operating at background light intensities that differ by two orders of magnitude (See Appendix A; Ingram et al. 2016). I describe how the loss of these proteins affects the cone photoresponse to brief flashes and to steady presentations of light.

Materials and Methods

Animals

Experiments were performed in accordance with rules and regulations of the NIH guidelines for research animals, as approved by the Institutional Animal Care and Use Committee of the University of California, Los Angeles, USA. See Appendix B for a full description.

Wild-type mice were purchased through Jackson Laboratories (C57BL6). Rod-specific $G\alpha_t$ knockout mice (*Gnat1*$^{-/-}$) were generated by Janice Lem at Tufts University (Calvert et al. 2000) and obtained locally from the laboratory of Dr. Gabriel Travis at UCLA. Jeanie Chen of the University of Southern California provided mice with mutations for calcium-sensitive proteins – GCAPs (*GCAPs*$^{-/-}$) and recoverin (*Rv*$^{-/-}$). They were bred on to the *Gnat1*$^{-/-}$ background to create double knockout (*Gnat1*$^{-/-}$*; Rv*$^{-/-}$ and *Gnat1*$^{-/-}$*; GCAPs*$^{-/-}$) and triple knockout (*Gnat1*$^{-/-}$*; Rv*$^{-/-}$*; GCAPs*$^{-/-}$) lines. Mice lacking the gap junction protein connexin36 (*Cx36*$^{-/-}$) were generated by David Paul from Harvard

University (Deans et al. 2002) and obtained from Sam Wu at Baylor University College of Medicine.

Solutions

I superfused the retinal slices with a bath solution consisting of Ames' media buffered with 1.9 g/L sodium bicarbonate, and slices were cut in Ames'-HEPES solutions. Pipet internal solutions were kept constant throughout these experiments and consisted mainly of potassium aspartate. Full recipes are listed in Appendix B.

Whole Cell Patch Clamp in Retinal Slices

All experiments described used established methods to voltage-clamp mouse cones somata, outlined in Appendix B.

Light Stimuli

Light stimuli were either brief flashes (5 ms) or steady (5 s) presentations of monochromatic light. Monochromatic light was provided by ultra-bright LEDs driven with a linear feedback driver (Opto-LED; Carin Research). LEDs emitting 365 nm and 505 nm light were used to test the spectral sensitivity of individual cells and determine whether each cone expressed S, M, or a mix of opsin types (Applebury et al. 2000). After brief spectral testing, subsequent illuminations were supplied by a 405 nm-emitting LED. 405 nm is approximately the isobestic point of S and M pigments in mouse and stimulates both opsin types with similar efficacy.

Imaging

Individual cones were imaged after the completion of all experimental stimulation protocols. A fluorescent dye (100 μm; Alexa Fluor 750, λ_{max} ~ 750 nm; ThermoFisher) was included in the internal pipet solution and diffused into the target cell during recording. Two types of images were collected. Infrared light was used to capture a wide-field image of the recording site without bleaching significant amounts of visual pigment. Bright red light (X-cite series 120; Excelitas Technologies) was filtered through a Cy7 cube (Nikon) and stimulated the Alexa dye to reveal the single, recorded cone (Fig. 2.1C). Both images were captured with Elements acquisition software (Nikon). Fluorescent images were pseudo-colored in Adobe Photoshop CS6 and merged with the wide field images to demonstrate location and morphology (Fig. 2.1D).

Analyses and Equations

Methods of data analysis and statistical methods are found in Appendix B.

Sensitivity Measurements

To derive sensitivities of response families, normalized photoresponses were plotted against the number of pigment molecules bleached, and data were fit with a Michaelis-Menten relationship:

$$R_x = \frac{I_x}{\left(I_x + I_{\frac{1}{2}}\right)} \quad (2.1)$$

where, R_x is the response at a given intensity, I_x; and $I_{1/2}$ is the intensity required to produce a half maximal response. $I_{1/2}$ was used as a sensitivity measure. Note here that Equation 2.1 is the Hill equation with an exponent equal to 1.

To assess spectral sensitivity and opsin content quickly, I opted to use current-density measurements (pA/P*) of voltage-clamped dim responses. Here, I divided response amplitude by the number of pigment molecules bleached by the flash (P*).

Amplification Constants

Before filtering digitally, I fit the first 1/3 to 1/2 of the rising-phase of each flash response with:

$$R = R_{max}\left(1 - e^{\left(-a\left(t - t_{eff}\right)^2\right)}\right) \quad (2.2)$$

where, R_{max} is the peak photoresponse and t_{eff} (s) is a time delay from stimulus onset to the initiation of the photoresponse. To calculate the amplification constant (*A*) for a specific flash response, the derived parameter *a* was multiplied by 2 and divided by the number of P* activated during the flash.

M-Opsin Co-Expression Ratio

To establish potential differences due to pigment content, I collected test flashes using 505 nm or 365 nm LEDs (Nikonov et al. 2006). For each cone in this data set, I measured respective sensitivities with dim flashes to derive current densities. The sensitivity for an individual cone at 505 nm was divided by the value derived for 365 nm. This gave an M co-expression ratio (ρ; Nikonov et al. 2006), where values greater than 1 are indicative of M-dominant cones, and values less than 1 of S-dominant cones. $I_{1/2}$, *A*, and τ_{rec} were plotted against ρ to determine if there were major differences in response parameters due to pigment content (Fig. 2.4).

Results

Unlabeled Mouse Cones can be Identified in Retinal Slices and Targeted for Whole-Cell Patch-Clamp Recording

I targeted individual cone somata by identifying distinguishable visual cues. Mouse cones are concentrated in the outer-most regions of the outer nuclear layer (ONL) and bear somata that are slightly larger than those of rods (Carter-Dawson and LaVail 1979; Applebury et al. 2000). Using light microscopy and infrared illumination (950 nm), I correctly identified unlabeled cone somata from retinal slices in 90% or more of trials. Cell type was further confirmed through electronic signatures, photosensitivity, and when possible, morphology.

Photosensitivity and membrane capacitance (C_m) were the most robust parameters used to distinguish cones from rods and were measured before other experimental protocols were initiated. C_m measured 2- to 4- fold higher in mouse cones than in rods (7 ± 1 pF vs 3 ± 1 pF, Table 2.1). These numbers are in agreement with early morphological studies that established differences in photoreceptor outer segments (Young 1969). The difference in C_m produced highly distinct waveforms in response to small voltage pulses, and photoreceptor type was easily confirmed.

Differences in rod and cone photosensitivity were determined with a single flash given in the mesopic range (100-200 P*/flash). At this flash strength, rods produced saturating or near-saturating photoresponses (see Fig. 1.3B, black trace), while approximately 20% of the cone's dark current was suppressed (Fig. 2.3A, ~10^2 P*). By measuring C_m and mesopic flash sensitivity, it was possible to identify photoreceptor-type quickly and accurately before carrying out extensive light exposures.

Once identified, cones were stimulated with brief flashes of light that increased in strength. Cones that remained stable after the initial flashes were subjected to a variety of other light protocols until significant bleaching and/or rundown became apparent.

In whole-cell configuration, I recorded dark-adapted photoresponses in both voltage-clamp (Fig. 2.1A) and current-clamp (Fig. 2.1B) modes from the same cone. In voltage-clamp mode, I measured the total dark current to be 20-25 pA. This is similar to the rod dark currents routinely recorded in our lab under similar conditions. In current-clamp mode, resting membrane potentials were typically measured to be between -35 to -40 mV.

When assessing cone morphology, a far-red fluorescent dye (Alexa Fluor 750) was loaded into the recording pipet. Single cones were visualized at the completion of light-stimulation protocols both with infrared and bright red light. Processed images demonstrated distinct cone morphology. Cone somata localized to the outer-most layers of the ONL (Fig. 2.1C and D). The cone outer segments were shorter than those of rods, the somata were larger, and the pedicles extended to the inner portion of the outer plexiform layer (Fig 2.1D).

Characteristics of Wild-type and Genetically Isolated Cone Responses

I was able to target cones of different genetic lines including wild-type strains since it was possible to distinguish cones without any labeling. Cones from wild-type retinas were electrically coupled to rods, albeit to differing degrees (Fig. 2.2A vs Fig. 2.1A; Raviola and Gilula 1973; Schneeweis and Schnapf 1995, 1999; Hornstein et al. 2005; Asteriti et al. 2014, 2017). While some wild-type cones displayed monophasic or

nearly-monophasic waveforms with rapid recovery kinetics (Fig. 2.1A), most had a fast-recovery component, followed by slower component that varied in amplitude (up to 15 pA, typically ~5 pA).

Fig. 2.2A illustrates the typical waveform observed in cones with particularly strong rod input. With adequate recovery time between flashes, the slower rod component was stable and did not increase as was reported in Asteriti et al. 2014. It was possible to preferentially suppress the slow component with dim/mesopic backgrounds (Fig. 2.2A inset). While photoreceptor gap junctions are reported to be under circadian control (Ribelayga et al. 2008; Jin and Ribelayga 2016), I did not detect any correlation between the time that recordings were made and the degree of coupling (data not shown). This result was not surprising, because the wild-type strain used was C57Bl6/J. This strain is reported to under express an important circadian modulator, melatonin (Tosini et al. 2008).

Several lines of evidence indicated that electrical spread from rods was the source of the slower recovery phase. First, the time course of the slow component increased with flash strength (Fig. 2.2A) and was comparable to the time course of rods stimulated with similar flash strengths. Second, the slow component was suppressible with dim background lights (Fig. 2.2A; inset, blue trace), while the fast component was largely unaffected (Schneeweis and Schnapf 1999). Third, the slow component was never observed if the generation or transmission of the rod photoresponse was interrupted by genetic mutations. In *Gnat1*$^{-/-}$ retinas, rod-specific Gα_t is knocked out, yielding electrically silent but otherwise healthy rods (Calvert et al. 2000). *Cx36*$^{-/-}$ cones lack the gap junction protein that forms electrical synapses with neighboring rods

(Asteriti et al. 2017). Cones from *Gnat1*$^{-/-}$ and *Cx36*$^{-/-}$ retinas recovered rapidly from brief flashes with consistently monophasic waveforms (Fig. 2.2B and C). Subsequent experiments utilized G*nat1*$^{-/-}$ and *Cx36*$^{-/-}$ transgenic lines with the goal of measuring isolated cone responses without interference from rod signals.

To assess any differences in sensitivity due to lateral coupling, I measured the photocurrents of all the aforementioned genetic lines by presenting brief flashes (5 ms) of increasing strength. Normalized peak-current responses were plotted against the number of bleached pigment molecules (Fig. 2.3A) and fitted with the Michaelis-Menten relation to derive the value of P* required to produce a half-maximal response ($I_{1/2}$; Table 2.1). $I_{1/2}$ was similar in G*nat1*$^{-/-}$ and *Cx36*$^{-/-}$ cones, with $I_{1/2}$ = 940 ± 110 P* (n = 25) and $I_{1/2}$ = 990 ± 93 P* (n = 30), respectively. The total (rod plus cone) response to flashes from wild-type cones saturated at intensities similar to the values for G*nat1*$^{-/-}$ and *Cx36*$^{-/-}$ cones. Due to coupling, however, wild-type cones responded more robustly to dimmer flashes and for longer durations ($I_{1/2}$ = 470 ± 90 P*; n = 13). Flash sensitivity was measured similarly in several rods for comparison (Fig. 2.3A, black trace; $I_{1/2,rod}$ = 14 ± 2 Rh*; n = 5).

Multiple flash-response parameters were routinely analyzed including the time constant of recovery τ_{rec} (ms), amplification constant *A* (s^{-2}), and the time to peak amplitude (Table 2.1). Rod input to wild-type cones confounds several of these analyses, and data were excluded when appropriate. *A* is a quantification of the rate at which P* activates the transduction cascade (Cobbs and Pugh 1987; Pugh and Lamb 1993). Values of *A* were derived for G*nat1*$^{-/-}$ and *Cx36*$^{-/-}$ cones across the full dynamic range (Fig. 2.3B; Table 2.1). In measurements from G*nat1*$^{-/-}$ cones, *A* decreased slightly

as flash strength increased indicating that the activation of cone $G\alpha_t$ becomes less efficient in brighter light. The same analysis from *Cx36*$^{-/-}$ cone responses yielded fairly constant values of *A* across the majority of the dynamic range.

Mouse cones can express two different types of opsin, S- and M- pigments. To assess pigment content in individual cones, many experiments included test flashes with 365 nm and 505 nm LEDs. For each cone, I produced an M-opsin co-expression ratio (ρ, See Methods) by dividing the flash sensitivity at 505 nm by the 365 nm sensitivity (Nikonov et al. 2006). Because many if not most, mouse cones express both types of pigment (Applebury et al. 2000), and the β-bands of M-pigments are sensitive to UV wavelengths (Govardovskii et al. 2000), ρ measurements across a large population of cones formed a spectrum rather than two distinct population sets (Fig. 2.4).

Parameters $I_{1/2}$, *A*, and τ_{rec} were plotted against ρ to determine if measurable differences in response properties arose due to pigment expression (Fig. 2.4). Few trends were observed. Of note, wild-type cones displayed high sensitivity to 505 nm light, likely because the rhodopsin in rods is maximally sensitive near 505 nm (pink stars). Efforts were made to maintain responses to test flashes at 50% or less of the maximum photocurrent. At these intensities the cone response is proportionately small compared to the rod response, and the rod input affects coupled-cone responses proportionately more. These same cones had the highest values for *A*, again likely due to rod signal spread. Aside from the spectral bias of wild-type cones, most ρ values were centered around 1, supporting the notion that mouse cones largely express both types of opsin (Applebury et al. 2000). From these data I concluded that mouse cones

operate within Rushton's Principle of Univariance, which states that once a photopigment is isomerized, transduction activation and downstream molecular signaling are conserved (Rushton 1972). Subsequently at the S-M isobestic point, 405 nm light activates both opsin types to a similar degree without additional deviations caused by phototransduction. The 405 nm light stimulation was used extensively in these experiments, since it obviated the need for further spectral sorting or subtype identification.

Calcium-Sensitive Proteins in the Phototransduction Cascade Shape the Cone Photocurrent

Next I describe how calcium-sensitive proteins from the phototransduction pathway contribute to the waveform and sensitivity of individual cones. In these experiments, mice with genetic knockouts for recoverin and/or GCAPs were bred on to the *Gnat1*$^{-/-}$ background yielding double knockout (*Gnat1*$^{-/-}$*; Rv*$^{-/-}$ and *Gnat1*$^{-/-}$*; GCAPs*$^{-/-}$) and triple knockout (*Gnat1*$^{-/-}$*; Rv*$^{-/-}$*; GCAPs*$^{-/-}$) lines.

Cones with these genetic backgrounds were first stimulated with brief flashes (Fig. 2.5, left column), followed by presentations of 5 s of steady light (Fig. 2.5, right column). Flash and step responses presented in Fig. 2.5 come from the same cones and derived response parameters are described in Table 2.1 and 2.2. Alterations in the cone flash responses were similar to those reported in rods with similar genetic manipulations (Mendez et al. 2001; Makino et al. 2004), as well as in earlier recordings from cones with suction electrodes (Sakurai et al. 2011; Sakurai et al. 2015).

The loss of GCAPs caused cones to recover more slowly from a given flash of light (Fig. 2.5A vs Fig. 2.5E and G). Concomitantly, the longer response increased integration time, which increased flash sensitivity (Table 2.1). Flash responses of *Gnat1*$^{-/-}$; *Rv*$^{-/-}$ and *Gnat1*$^{-/-}$ cones were remarkably similar. The τ_{rec} and time to peak of *Gnat1*$^{-/-}$; *Rv*$^{-/-}$ cones were only slightly faster than, but within error of, *Gnat1*$^{-/-}$ cones. Additionally, $I_{1/2}$ was marginally higher in *Gnat1*$^{-/-}$; *Rv*$^{-/-}$ cones (Table 2.1). This is in contrast to the loss of recoverin in rods, which produces measurably faster flash responses (Makino et al. 2004; Chen et al. 2010; Chen et al. 2012; Chen et al. 2015; Morshedian et al. 2018).

Previous studies were unable to record photocurrents from individual mouse cones during exposure to continuous light. Data in the right column of Fig. 2.5 show waveforms in steady light. Cones remain responsive even in bright backgrounds. After the initial onset of the steady-light stimulus, there was a strong recovery of photocurrent (Fig. 2.5B and D).

This relaxation could represent the reopening of CNG-gated channels, or it could arise from a positive inward conductance residing in the inner segment. To test whether or not CNG channels were reopening and functional, cones were exposed to bright, steady light (18,000 P*/s) and allowed to come to steady state before additional bright flashes were presented on top of the background (Fig. 2.6C). With sufficiently bright flashes, it was possible to further suppress the photocurrent from steady state close to the initial peak response. These bright flashes never exceeded the initial response, supporting the notion that bright light does cause a temporarily closure of all the CNG channels in cones (circulating current = 0 pA). This background intensity caused a 13-

fold decrease in sensitivity while suppressing less than 60% of the circulating current at steady state (Fig. 2.6B). This is in stark contrast to rods, which remain saturated on these time scales, even with much lower intensity stimulation (75-80% current suppression with 200-1000 Rh*/s from Chen et al. 2010 and Morshedian et al. 2018).

Since prolonged light stimulation causes larger changes in cytosolic calcium concentrations, I examined the contribution of GCAPs and recoverin to shaping the steady-light response of cones. Response recovery was measured by calculating the percent current change from the initial peak response to the steady-state current value (Fig. 2.7A). *Gnat1*$^{-/-}$*; Rv*$^{-/-}$ cones retained a capacity to recover similar to *Gnat1*$^{-/-}$ cones, and both types of cones quickly reopened over 30% of channels until being exposed to the brightest light intensities. Interestingly, *Rv*$^{-/-}$ rods are reported to show less relaxation when exposed to steady light (Morshedian et al. 2018). In contrast, cones with *GCAPs*$^{-/-}$ mutations recovered 20% or less of their dark current. To derive a time constant for this relaxation, current responses were fit with an exponential decay expression (Fig. 2.7B). *Gnat1*$^{-/-}$*; Rv*$^{-/-}$ cones relaxed faster than *Gnat1*$^{-/-}$ cones by approximately 200 ms across the entire dynamic range (Table 2.2). Due to small relaxations and greater noise in *GCAPs*$^{-/-}$ cones, data were difficult to fit. The *GCAPs*$^{-/-}$ responses that could be fit were pooled regardless of whether they were also *Rv*$^{-/-}$. The time constants from *GCAPs*$^{-/-}$ cones were consistently 200 to 300 ms slower than *Gnat1*$^{-/-}$ cones across the majority of their dynamic ranges.

To assess the sensitivity of cones to steady light, $I_{1/2}$ was calculated at two time points. The first measurement used photoresponse amplitudes at the initial peak occurring less than 200 ms after stimulus onset. The second measurement derived

steady state $I_{1/2}$ using the mean current recorded during the last 1 second of the stimulus. When assessing $I_{1/2}$ of initial cone response, mutations affected sensitivities similar to the trends seen with brief flashes (Fig. 2.7C). The *GCAPs*$^{-/-}$ caused increased sensitivity to steady light, which shifted the dynamic range of these cones to lower light intensities. *Gnat1*$^{-/-}$; *Rv*$^{-/-}$ cones were less sensitive to steady light (Table 2.2). Interestingly, the combined loss of GCAPs and recoverin did not counteract the opposing sensitivity changes, and triple-mutant cones remained more sensitive than *Gnat1*$^{-/-}$ cones. Intensity-response relations for the peak responses of *Gnat1*$^{-/-}$ and *Gnat1*$^{-/-}$; *GCAPs*$^{-/-}$ cones were replotted in Fig. 2.7D. The mean steady-state currents were also plotted against the light intensity. The steady-state currents from *Gnat1*$^{-/-}$ cones demonstrate a rightward shift to brighter intensities compared to the peak currents (Fig. 2.7D, black data). This is due to the strong recovery occurring after the stimulus onset. *Gnat1*$^{-/-}$; *GCAPs*$^{-/-}$ cones do not recovery as much circulating current and there is little change between the peak and steady-state current values (Fig. 2.7D, green data).

Discussion

The Power of Patch Clamp

Previously, several attempts were made to characterize the physiological light responses generated by mouse cones. Each of these studies suffers from important experimental limitations. Suction-electrode recording was adapted to record the light responses of single cones in clusters of photoreceptors, but these experiments cannot be done from wild-type animals (Nikonov et al. 2006; Sakurai et al. 2011). Further, the

maximum response amplitudes were small, ranging 5-10 pA, and subject to larger electrical noise. These issues are due to poor pipet seals and significant current leakage. As a result, few studies using suction recording have reached the power needed for statistical significance and require alternate approaches such as the a-wave in isolated, transretinal ERGs.

Transretinal ERGs can yield better signal-to-noise, but data are pooled voltage responses from populations of cells. To record cone population recordings, multiple manipulations are needed. Pharmacology is required to isolate the photoreceptor a-wave from downstream electrical contributions. Again, stimulation of wild-type retinas evokes large rod responses, and *Gnat1*$^{-/-}$ mice are needed to reveal the cone component.

More recently, a lab in Italy began to target the cone pedicles in the outer plexiform layer with perforated patch clamp (Cangiano et al. 2012; Asteriti et al. 2014). Although this procedure does not require *Gnat1*$^{-/-}$ mice, the approach is blind, and perforated patch clamp limits the experimenter to recording only voltage responses. Further, their studies showed unexplained variability. Upon gaining access, the amplitude of the rod signal steadily increased with the duration of recording (Asteriti et al. 2014).

With our methodology, most of these issues are solved. Using whole-cell patch clamp, I was able to record voltage and current responses from the same cell. With a high resistance seal, the entire current response was captured, and electrical noise was greatly reduced. *Gnat1*$^{-/-}$ mice are not required but nevertheless are useful in isolating a pure-cone response. For standard recordings, no pharmacology is required, but drugs

are easily applied if needed (see Chapter 3). There are no systematic or time-dependent artifacts introduced. Recordings are limited by the health of the photoreceptors themselves, the time course of washout, and when applicable, bleaching. Moreover whole-cell recording exploits the principal advantage of voltage clamp. The recorded currents are directly proportional to the change in cone membrane conductance.

Identifying Cones from the Sea of Rods

Using only intrinsic visual cues, I was able to reliably identify cones with over 90% accuracy. The outer nuclear layer in the mouse retina contains approximately 10 rows of photoreceptor nuclei. Cones are concentrated in the outer 3 layers, against the external limiting membrane (Applebury et al. 2000). Due to this concentration, cones occur at a much great frequency than 3% in these regions.

While cone somata are slightly larger than those of rods, the most reliable cue was distinctive patterns seen on the somata. Cones bear a faint stripped and/or spotted pattern. Rod somata present with a smooth gradient and without discrete structures. These differences likely arise from chromatin architecture. Cones are reported to maintain open heterochromatin similar to most neurons in the retina. In contrast, rod chromatin condenses throughout the first month after birth (Solovei et al. 2009). The functional consequences of chromatin condensation in rods remains unclear, but seems to be under control of the key rod transcription factor *nrl* (Hughes et al. 2017).

After locating a suspected cone, the cell was patched at the soma. Immediately after gaining access for whole-cell configuration, rapid voltage pulses were delivered

through the patch pipet to assess the quality of the patch seal, series resistance, and importantly, C_m. I report C_m to be approximately 2- to 3- fold higher in cones. In most vertebrates, the rod outer segment is encapsulated in a single outer membrane, which isolates individual discs from one another and from the extracellular environment (but see Morshedian and Fain 2015). In contrast, the spaces between cone lamellae are continuous with the extracellular space. Thus, the membrane surface area that is subject to capacitive charging and discharging is greater in cones despite shorter outer segment lengths. This parameter alone was robust enough to confirm if the photoreceptor was a rod or a cone.

Gap Junctions and The Rod Secondary Pathway

I have confirmed previous measurements showing that rod responses spread into cone photoreceptors through synaptic-terminal gap junctions. The intensity-response relation in Fig. 2.3 suggests that the electrical coupling to rods has several actions. Not only does this circuit form the entry point at which rod signals can feed into the cone bipolar circuitry, it also boosts the cone response to dim-mesopic stimuli. Approximate spectral testing (Fig. 2.4) indicates that rod coupling biases the cone toward the rod spectral λ_{max} regardless of the pigment expression profile in the cone. This should decrease the mouse's ability to distinguish spectral differences in mesopic light.

I was not able to detect reliable circadian control of gap junctions in my preparations (Jin and Ribelayga 2016; Wong et al. 2018). In addition to C57BL6 mice, several experiments were carried out in the CBA/Ca mouse line. This strain maintains

robust circadian rhythms, unlike C57BL6 mice which are melatonin-deficient (Tosini et al. 2008). Still, I did not see significant correlations between the time of day and the amplitude of rod signal spread. As such, these data were not included in this dissertation. It is possible that the process of slicing the retina disturbs any intact rhythms. Studies focusing on clock gene expression in the retina found a 'culture shock' effect, where by the rhythm of gene expression was reset when tissue was initially harvested (Ruan et al. 2006).

Escaping Saturation and Maintaining Steady-State

While considerable effort has gone into understanding why rods are more sensitive than cones, less work has focused on how cones manage to escape response saturation at bright light intensities. Despite expressing similar or the same transduction proteins, cones can quickly attain a new steady state with a significant number of reopened CNG channels, and rods do not. The reason for this difference is unclear.

A key to this question likely resides in differences controlling calcium flux. Calcium-dependent adaptation accounts for the majority of adaptation occurring in rods and cones (Matthews et al. 1988; Nakatani and Yau 1988). Rods and cones share the same isoforms of GCAPs and recoverin, and both of these proteins bind calcium and together affect GC and PDE rates. From Figs. 2.5 and 2.7, it is clear that GCAP proteins play a significant role in setting the percentage of open CNG channels during a steady-state response. GCAPs directly bind calcium when concentrations are elevated in dark conditions. With steady-light activation, cytosolic calcium concentrations will drop and

GCAPs will act to accelerate the rate of GC. In contrast to rods, cones quickly reopen CNG channels, and calcium levels should begin to rebound in cones faster than in rods.

What actually causes CNG channels to reopen quickly in cones? The PDE isoforms are different and GAP is expressed to a much higher degree in cones than in rods (Cowan et al. 1998; Zhang et al. 2003). Because the maximal amplitude of the photoresponse is set by the number of conducting CNG channels in the dark, R_{max} is measured when $I_{CNG} = 0$. Cone photoresponses easily reach stable R_{max} values (i.e. transient saturation), but quickly recover. Despite rapid recoveries, the rate of cGMP hydrolysis must be great enough to close all the CNG-channels at some point shortly after stimulus onset. Still, Fig. 2.6 demonstrates that the recovery is largely due to functional reopening of CNG channels. If channels are reopening, the enzymatic action of PDE must be slowed to the point that the synthesis of cGMP by GC out paces hydrolysis. Thus, quicker shut-off of cone PDE through isoform modifications or the increased expression of the GAP complex in cones could explain how cones can escape light saturation. Majumder et al. 2015 made similar hypotheses after examining the effects of expressing cone PDE isoforms in rods.

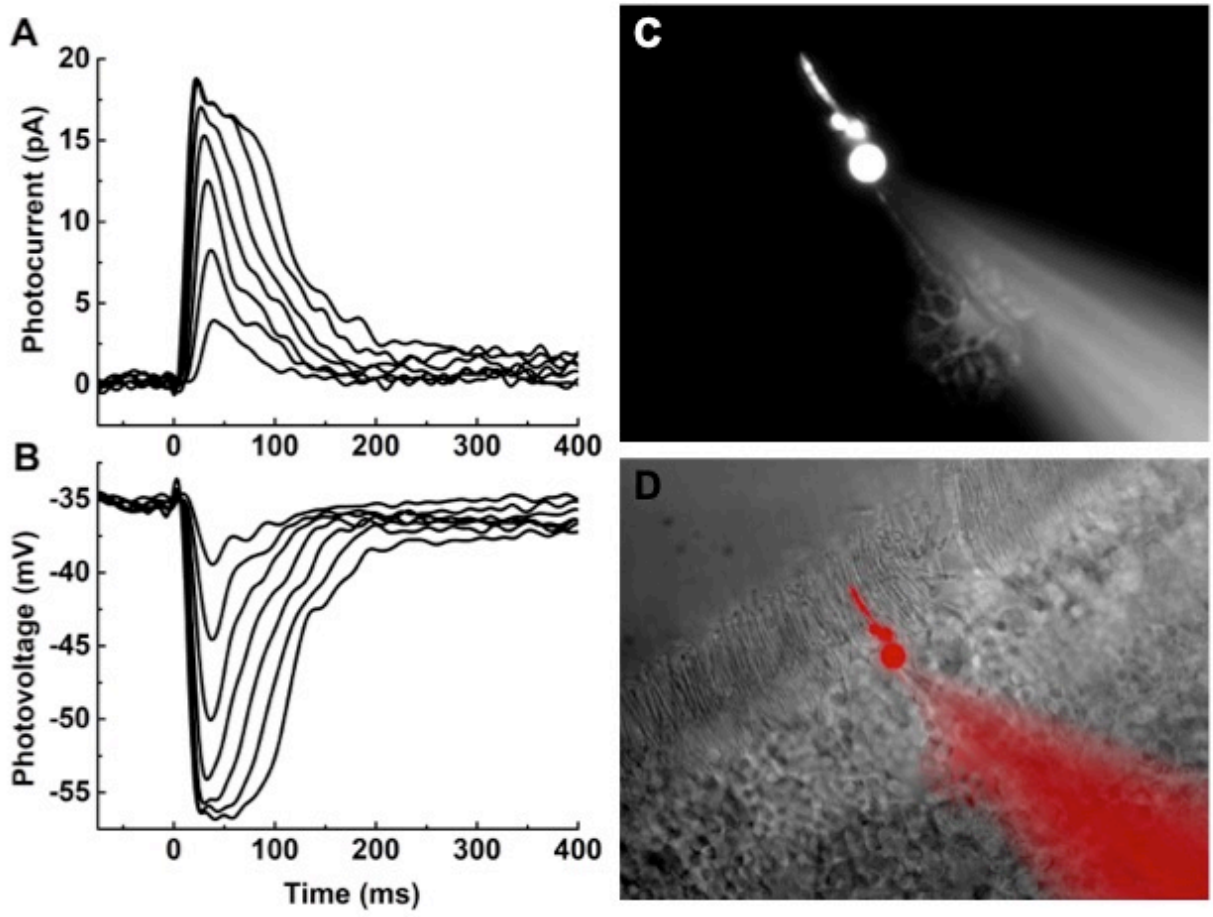

Figure 2.1 Photoresponses of Mouse Cones are Recorded with Whole-cell Patch Clamp

A) Current responses recorded from a wild-type mouse cone with minimal coupling. The cone's soma was voltage clamped and held at -50 mV. Brief flashes of increasing light strength (22-2100 P^*/flash) were presented at time = 0. $I_{1/2}$ = 75 P^*. B) Voltage responses from the same cone as (A), stimulated with the same light flashes. $I_{1/2}$ = 77 P^*. Data traces in (A) and (B) are averages of seven sweeps/flash strength and were filtered digitally during analysis (50 Hz). C) An individual cone visualized with a far-red dye loaded in the recording pipet. D) Merged image of (C, pseudo-colored red) and wide field image of retinal slice

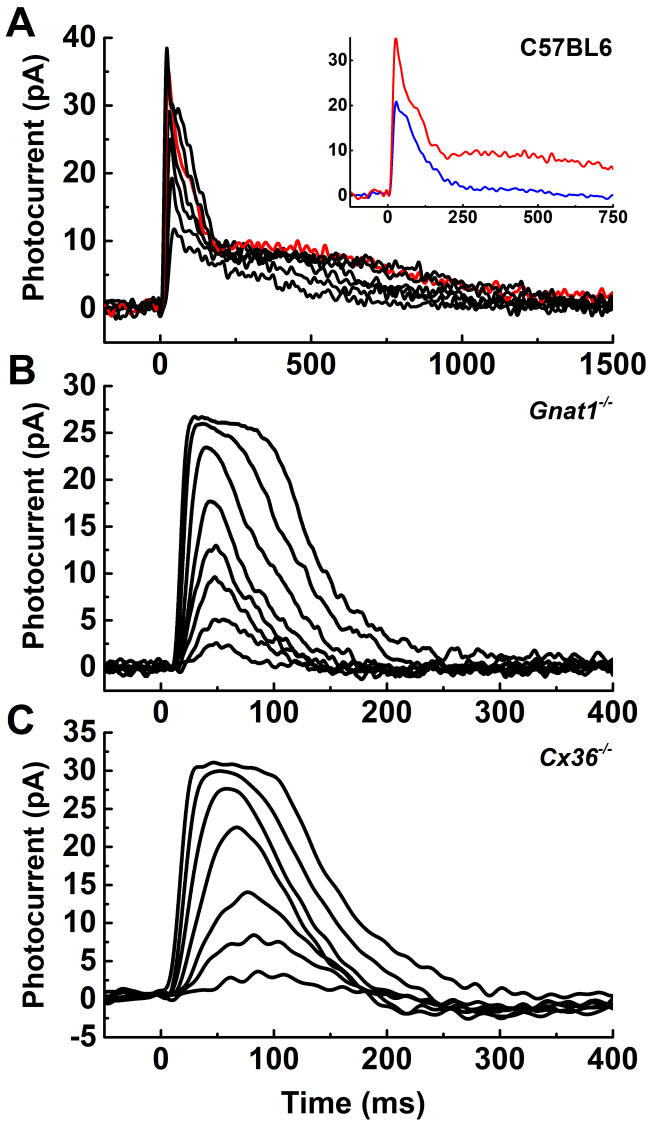

Figure 2.2 The Rod-Secondary Pathway Contributes to Wild-type Cone Photocurrents

Photocurrents were recorded from individual cones of wild-type (A), *Gnat1*$^{-/-}$ (B), and *Cx36*$^{-/-}$ (C) genetic backgrounds. Light strengths ranged from 40 to 6000 P*/flash. A) Wild-type cone with strong rod coupling. Inset: Rod input is suppressed with dim background light. Red trace: dark-adapted response to a flash bleaching 1520 P*. Blue trace: photoresponse to the same flash strength on background light bleaching 9300 Rh*/s (or 3400 M-opsin*/s). B and C) The recovery of photocurrent in *Gnat1*$^{-/-}$ (B) and *Cx36*$^{-/-}$ (C) cones is monophasic, lacking the slower secondary component ('plateau') seen in (A).

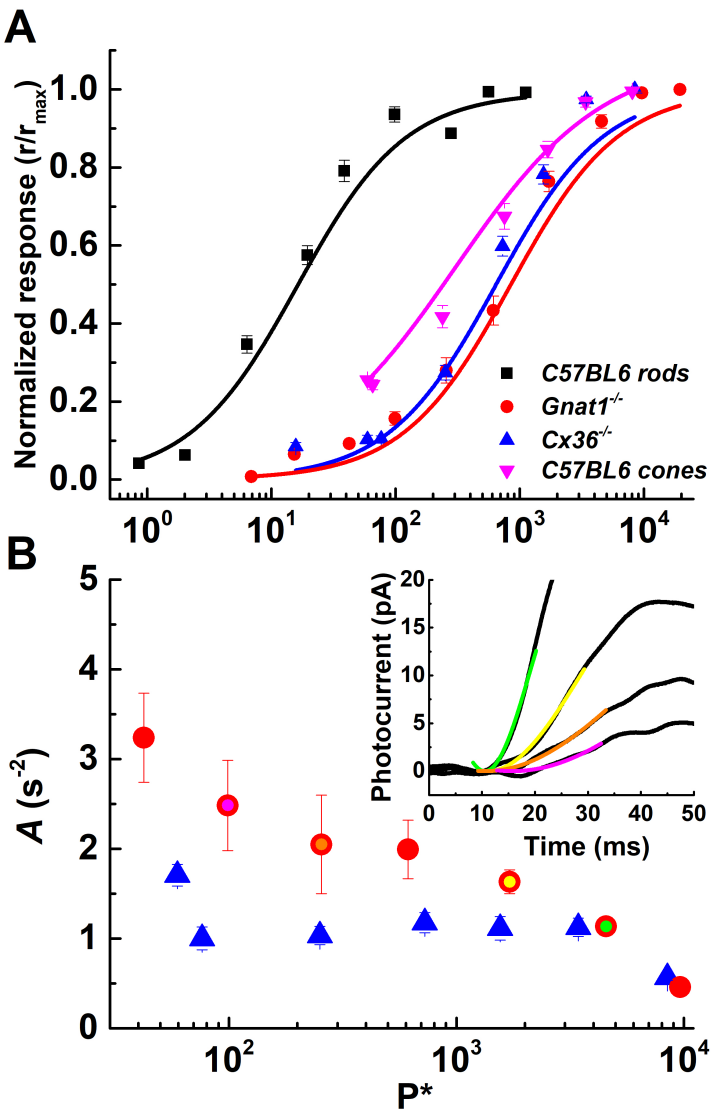

Figure 2.3 Intensity–Response Relationships and Amplification Constants Across the Cone Dynamic Range

A) Normalized photocurrent response (r/r_{max}) is plotted against flash strength (P*/flash) and fit with Equation 2.1. The flash strength producing 50% maximal current response was 14 ± 2 in C57BL6 rods, 940 ± 110 in *Gnat1*$^{-/-}$cones, 990 ± 93 in *Cx36*$^{-/-}$cones, and 470 ± 89 in C57BL6 cones. B) Equation 2.2 was fit to the first 1/3 to 1/2 of the rising phase of each flash response (inset) to derive amplification constants (*A*; s^{-2}). Values of *A* from *Gnat1*$^{-/-}$ and *Cx36*$^{-/-}$cones are plotted against flash strength. Inset: fits to several flashes from the cone in Fig 2.2B. The colors of fit lines are matched to that of the filled *Gnat1*$^{-/-}$ symbols.

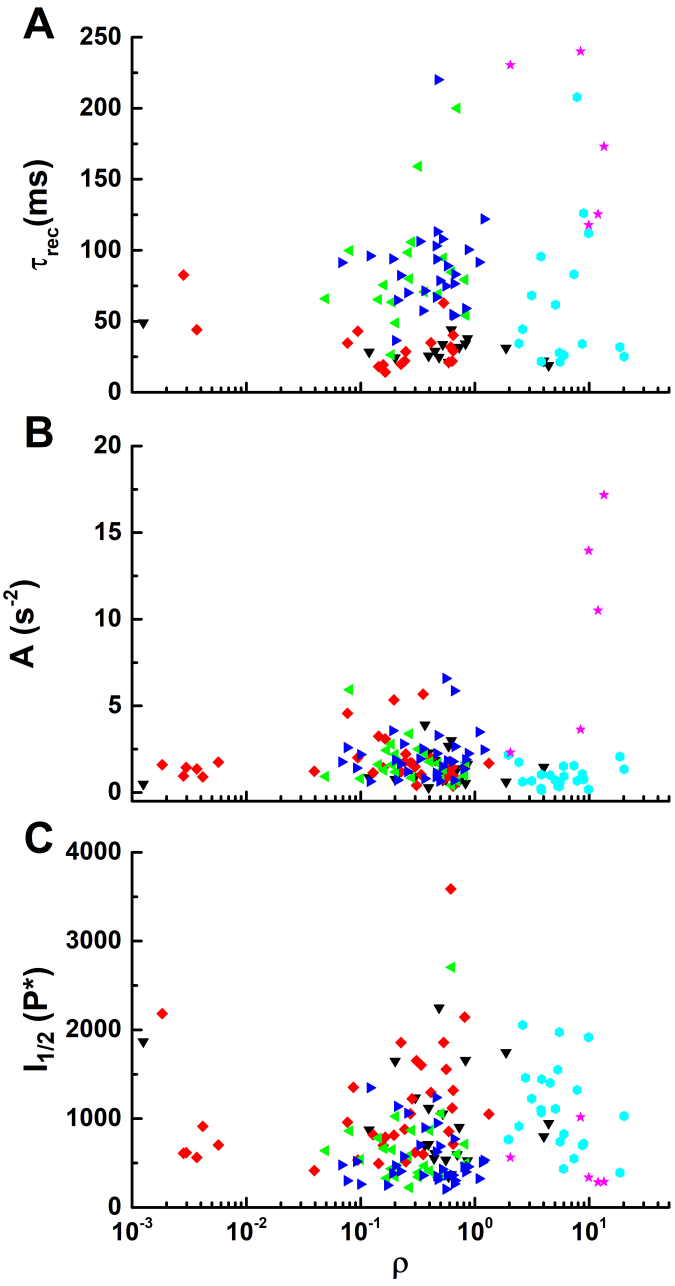

Figure 2.4 Duel Opsin Expression has Little Effect on Response Sensitivity and Kinetics

M-opsin co-expression ratios (ρ; 505/365) were measured in cones from a variety of genetic backgrounds totaling to 142 cones. The response parameters τ_{rec} (A), *A* (B), and $I_{1/2}$ (C), values did not correlate with ρ. Genotypes: black: *Gnat1*$^{-/-}$ cones; red: *Gnat1*$^{-/-}$; *Rv*$^{-/-}$ cones; green: *Gnat1*$^{-/-}$; *GCAPs*$^{-/-}$ cones; blue: *Gnat1*$^{-/-}$; *Rv*$^{-/-}$; *GCAPs*$^{-/-}$ cones; cyan: *Cx36*$^{-/-}$ cones; pink: C57BL6 cones.

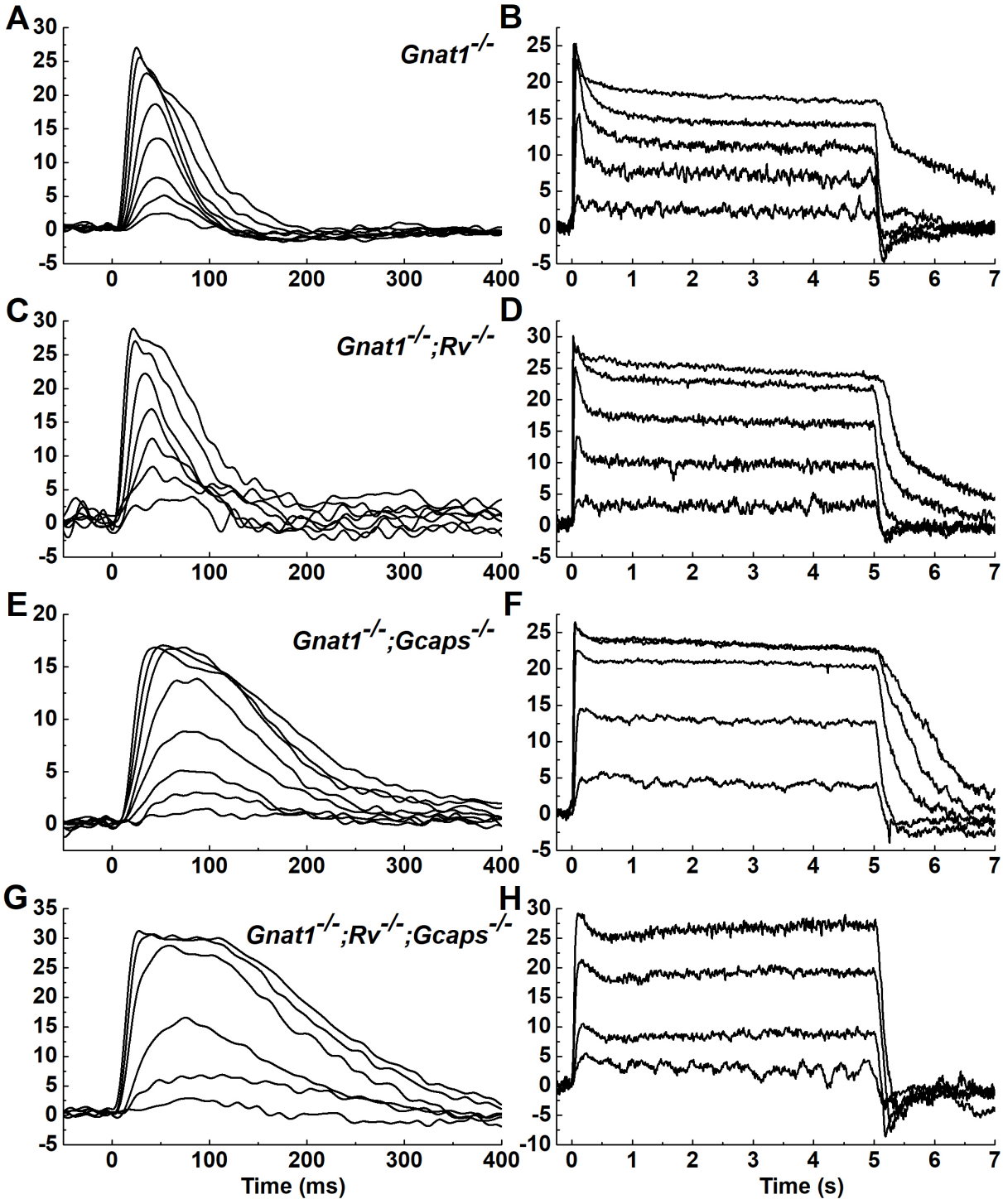
A
B
Gnat1-/-
C
D
Gnat1-/-;Rv-/-
E
F
Gnat1-/-;Gcaps-/-
G
H
Gnat1-/-;Rv-/-;Gcaps-/-
Time (ms)
Time (s)

Figure 2.5 The Calcium-Sensing Proteins of Light Adaptation are Conserved in Rods and Cones.

Photocurrents were recorded from transgenic mouse cones: *Gnat1*$^{-/-}$ (A-B), *Gnat1*$^{-/-}$; *Rv*$^{-/-}$ (C-D), *Gnat1*$^{-/-}$; *Gcaps*$^{-/-}$ (E-F), *Gnat1*$^{-/-}$; *Rv*$^{-/-}$ *Gcaps*$^{-/-}$ (G-H). Stimulus onset was at time = 0 ms. The left column shows current responses from individual, representative cones when exposed to brief flashes of increasing strength (in P*/flash): *Gnat1*$^{-/-}$ 63-15000; *Gnat1*$^{-/-}$; *Rv*$^{-/-}$ 190-39000; *Gnat1*$^{-/-}$; *Gcaps*$^{-/-}$ 76-9400; *Gnat1*$^{-/-}$; *Rv*$^{-/-}$ *Gcaps*$^{-/-}$ 81-7770. Traces are averages of 3-5 traces/flash strength. In the right column, the same cones were stimulated with 5 s of steady light, at increasing intensities (in P*/s): *Gnat1*$^{-/-}$ 3400-1.5x10^{6}; *Gnat1*$^{-/-}$; *Rv*$^{-/-}$ 3700-4.0x10^{6}; *Gnat1*$^{-/-}$; *Gcaps*$^{-/-}$ 4900-1.03 x10^{6}; *Gnat1*$^{-/-}$; *Rv*$^{-/-}$ *Gcaps*$^{-/-}$ 7500-64,000. Each steady-light intensity was presented 2 times in order to limit pigment bleaching.

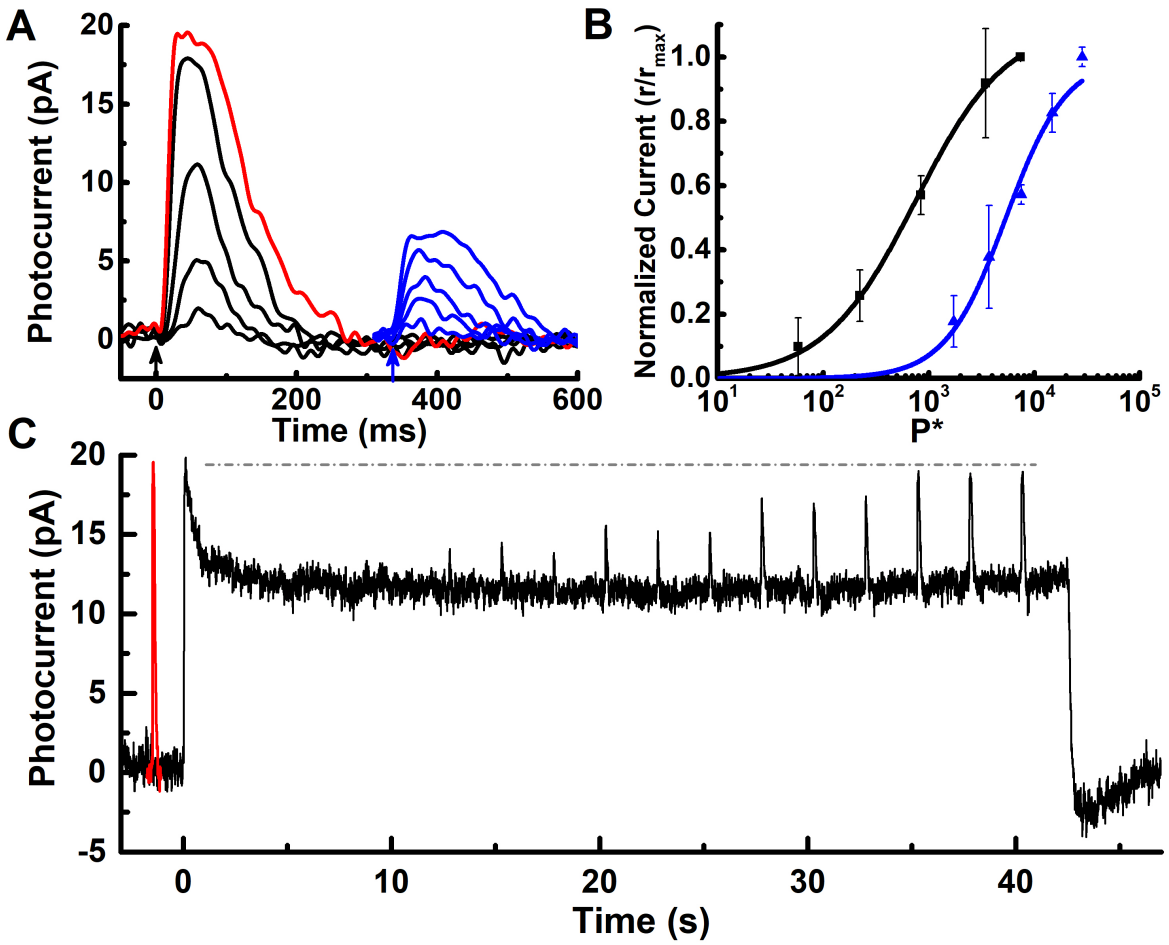

Figure 2.6 Cones Escape Saturation and Reopen CNG Channels in Bright Lights

A) Average photocurrent responses to brief flashes (arrows) were measured in a dark adapted-cone (black + red) and then on a steady background (blue traces, isolated from part C). B) Normalized peak current responses were plotted against flash strength and fit with Equation 2.1. Dark $I_{1/2}$ was determined to be 750 P*. When fitting the light adapted data, the Hill exponent in Equation 2.1 was changed to 1.5 to account for increased steepness. $I_{1/2}$ increased to 5400 ± 440 P*. C) Current response from the same cone as (A) during a 40+ s exposure to steady light (18,000 P*/s). 5 s after the steady light is turned on, flashes of increasing strength are delivered to the cone (1,700 – 29,000 P*/flash). The dashed line illustrates the initial peak current response. The maximal flash response recorded in the dark was replotted in (C) to compare response amplitude and kinetics (red trace). The time scale is the same although it has been shifted along the time-axis.

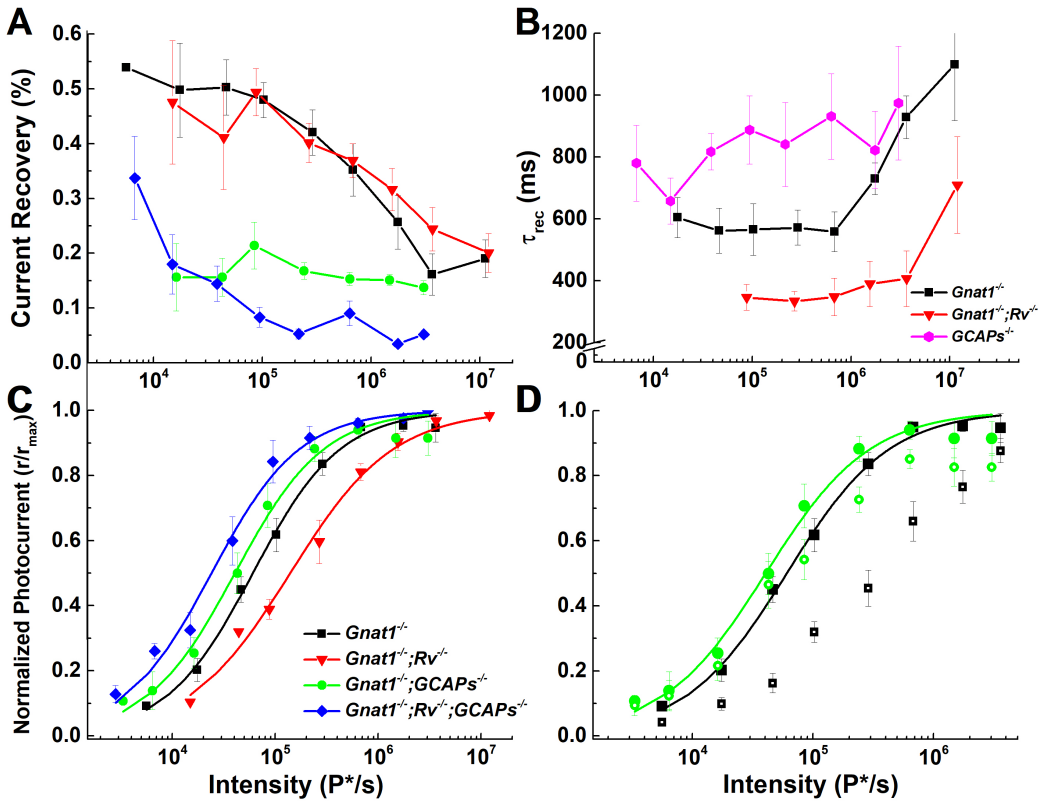

Figure 2.7 Kinetics and Sensitivity Changes Occur when Transduction Proteins are Lost

A) The percentage of current recovery (i.e. channels reopening) was calculated as the difference between the peak and steady-state currents divided by the peak current. *Gnat1*$^{-/-}$ and *Gnat1*$^{-/-}$*; Rv*$^{-/-}$ cones quickly recover a large fraction of their initial dark current (30-50%), before reaching steady state. *GCAPs*$^{-/-}$ cones recovered much less dark current (~20%). B) Time constants for relaxation (τ_{rec}) were derived by fitting the equation for exponential decay to the relaxation after the initial response peak and plotted against intensity. Cones with *Gnat1*$^{-/-}$*; GCAPs*$^{-/-}$ genotypes were similar regardless of whether they were also *Rv*$^{-/-}$ and pooled (pink trace). C) Intensity-response relations for the normalized peak current response was plot against stimulus intensity and fit with Equation 2.1. D) Normalized peak currents from *Gnat1*$^{-/-}$ and *Gnat1*$^{-/-}$*; GCAPs*$^{-/-}$ cones in C) were replotted (solid symbols) with the normalized steady-state currents (open symbols). Steady-state currents generated by *Gnat1*$^{-/-}$ cones were shifted to brighter intensities compared to the peak current responses.

Table 2.1:
Mouse Cone Flash Response Parameters

Genotype	n	R_{max} (pA)	$I_{1/2}$ (P*)	ms to peak	τ_{rec} (ms)	*A* (s^{-2})	R_{in} (MΩ)	C_m (pF)
C57BL6 cones	13	30 ± 2.0	470 ± 89	41 ± 1.9 24 ± 0.6	200 ± 18 155 ± 28	5.3 ± 0.4	850 ± 120	7.5 ± 0.5
C57BL6 rods	5	17 ± 1.6	14 ± 2.4	200 ± 17 140 ± 20	130 ± 23 260 ± 59	4.6 ± 0.3	4000 ± 680	3.6 ± 0.3
Gnat1$^{-/-}$ cones	25	21 ± 0.9	940 ± 110	59 ± 3.2 33 ± 1.9	28 ± 1.9 42 ± 1.9	2.1 ± 0.2	1500 ± 350	6.9 ± 0.6
Cx36$^{-/-}$ cones	30	26 ± 1.3	990 ± 93	79 ± 4.8 50 ± 1.9	64 ± 8.5 61 ± 3.4	1.1 ± 0.1	850 ± 130	7.5 ± 0.3
Gnat1$^{-/-}$;*Rv*$^{-/-}$ cones	36	20 ± 0.9	1100 ± 110	55 ± 4.6 30 ± 2.4	33 ± 3.1 47 ± 2.2	1.7 ± 0.1	773 ± 140	6.2 ± 0.3
Gnat1$^{-/-}$;*GCAPS*$^{-/-}$ cones	30	14 ± 0.9	740 ± 120	79 ± 5.5 43 ± 2.4	125 ± 28 98 ± 6.4	1.8 ± 0.1	1200 ± 310	6.6 ± 0.4
Gnat1$^{-/-}$;*Rv*$^{-/-}$; *GCAPS*$^{-/-}$ cones	34	23 ± 1.4	550 ± 51	67 ± 2.4 42 ± 2.3	94 ± 8.5 110 ± 7.3	2.2 ± 0.1	660 ± 27	6.8 ± 0.2

For parameters that are dependent on light intensity, 2 values are reported corresponding to ~25% (top) and 90% (bottom) of R_{max}. Values are means ± SEM.

Table 2.2:
Mouse Cone Steady-Light Response Parameters

Genotype	n	$R_{max,pk}$ (pA)	$R_{max,ss}$ (pA)	$I_{1/2,pk}$ (P*/s)	ms to peak	τ_{rec} (ms)	*% recovery*
Gnat1$^{-/-}$ cones	9	21 ± 3.2	18 ± 2.5	72,000	140 ± 16	600 ± 57	58 ± 6
				± 13,000	130 ± 18	600 ± 70	40 ± 7
Gnat1$^{-/-}$;*Rv*$^{-/-}$ cones	11	20 ± 1.5	17 ± 1.5	120,000	130 ± 12	370 ± 10	52 ± 7
				± 14,000	75 ± 8	360 ± 61	42 ± 2
Gnat1$^{-/-}$;*GCAPS*$^{-/-}$	10	19 ± 2.3	16 ± 1.8	73,000	170 ± 10	760 ± 79	20 ± 4
cones				± 16,000	130 ± 19	840 ± 93	17 ± 2
Gnat1$^{-/-}$;*Rv*$^{-/-}$;	9	24 ± 2.6	20 ± 2.7	53,000	170 ± 12	570 ± 42	17 ± 4
GCAPS$^{-/-}$cones				± 16,000	160 ± 17	840 ± 140	10 ± 3

$R_{max,pk}$: peak current response, measured less than 200 ms after stimulus on set; $R_{max,ss}$: steady-state current response, averaged from the last 1 second of brightest stimulus; $I_{1/2,peak}$: sensitivity of peak response; For parameters that are dependent on light intensity, 2 values are reported corresponding to ~30% (top) and 80% (bottom) of R_{max}. Values are means ± SEM.

References

Applebury, M. L., M. P. Antoch, L. C. Baxter, L. L. Chun, J. D. Falk, F. Farhangfar, K. Kage, M. G. Krzystolik, L. A. Lyass and J. T. Robbins (2000). "The murine cone photoreceptor: a single cone type expresses both S and M opsins with retinal spatial patterning." Neuron **27**(3): 513-523.

Asteriti, S., C. Gargini and L. Cangiano (2014). "Mouse rods signal through gap junctions with cones." Elife **3**: e01386.

Asteriti, S., C. Gargini and L. Cangiano (2017). "Connexin 36 expression is required for electrical coupling between mouse rods and cones." Vis Neurosci **34**: E006.

Calvert, P. D., N. V. Krasnoperova, A. L. Lyubarsky, T. Isayama, M. Nicolo, B. Kosaras, G. Wong, K. S. Gannon, R. F. Margolskee, R. L. Sidman, E. N. Pugh, Jr., C. L. Makino and J. Lem (2000). "Phototransduction in transgenic mice after targeted deletion of the rod transducin alpha -subunit." Proc Natl Acad Sci U S A **97**(25): 13913-13918.

Cangiano, L., S. Asteriti, L. Cervetto and C. Gargini (2012). "The photovoltage of rods and cones in the dark-adapted mouse retina." J Physiol **590**(16): 3841-3855.

Carter-Dawson, L. D. and M. M. LaVail (1979). "Rods and cones in the mouse retina. I. Structural analysis using light and electron microscopy." J Comp Neurol **188**(2): 245-262.

Chen, C. K., M. L. Woodruff, F. S. Chen, D. Chen and G. L. Fain (2010). "Background light produces a recoverin-dependent modulation of activated-rhodopsin lifetime in mouse rods." J Neurosci **30**(4): 1213-1220.

Chen, C. K., M. L. Woodruff, F. S. Chen, Y. Chen, M. C. Cilluffo, D. Tranchina and G. L. Fain (2012). "Modulation of mouse rod response decay by rhodopsin kinase and recoverin." J Neurosci **32**(45): 15998-16006.

Chen, C. K., M. L. Woodruff and G. L. Fain (2015). "Rhodopsin kinase and recoverin modulate phosphodiesterase during mouse photoreceptor light adaptation." J Gen Physiol **145**(3): 213-224.

Cobbs, W. H. and E. N. Pugh, Jr. (1987). "Kinetics and components of the flash photocurrent of isolated retinal rods of the larval salamander, Ambystoma tigrinum." J Physiol **394**: 529-572.

Cowan, C. W., R. N. Fariss, I. Sokal, K. Palczewski and T. G. Wensel (1998). "High expression levels in cones of RGS9, the predominant GTPase accelerating protein of rods." Proc Natl Acad Sci U S A **95**(9): 5351-5356.

Deans, M. R., B. Volgyi, D. A. Goodenough, S. A. Bloomfield and D. L. Paul (2002). "Connexin36 is essential for transmission of rod-mediated visual signals in the mammalian retina." Neuron **36**(4): 703-712.

Govardovskii, V. I., N. Fyhrquist, T. Reuter, D. G. Kuzmin and K. Donner (2000). "In search of the visual pigment template." Vis Neurosci **17**(4): 509-528.

Hornstein, E. P., J. Verweij, P. H. Li and J. L. Schnapf (2005). "Gap-junctional coupling and absolute sensitivity of photoreceptors in macaque retina." J Neurosci **25**(48): 11201-11209.

Hughes, A. E., J. M. Enright, C. A. Myers, S. Q. Shen and J. C. Corbo (2017). "Cell Type-Specific Epigenomic Analysis Reveals a Uniquely Closed Chromatin Architecture in Mouse Rod Photoreceptors." Sci Rep **7**: 43184.

Ingram, N. T., A. P. Sampath and G. L. Fain (2016). "Why are rods more sensitive than cones?" J Physiol **594**(19): 5415-5426.

Jin, N. G. and C. P. Ribelayga (2016). "Direct Evidence for Daily Plasticity of Electrical Coupling between Rod Photoreceptors in the Mammalian Retina." J Neurosci **36**(1): 178-184.

Majumder, A., J. Pahlberg, H. Muradov, K. K. Boyd, A. P. Sampath and N. O. Artemyev (2015). "Exchange of Cone for Rod Phosphodiesterase 6 Catalytic Subunits in Rod Photoreceptors Mimics in Part Features of Light Adaptation." J Neurosci **35**(24): 9225-9235.

Makino, C. L., R. L. Dodd, J. Chen, M. E. Burns, A. Roca, M. I. Simon and D. A. Baylor (2004). "Recoverin regulates light-dependent phosphodiesterase activity in retinal rods." J Gen Physiol **123**(6): 729-741.

Matthews, H. R., R. L. Murphy, G. L. Fain and T. D. Lamb (1988). "Photoreceptor light adaptation is mediated by cytoplasmic calcium concentration." Nature **334**(6177): 67-69.

Mendez, A., M. E. Burns, I. Sokal, A. M. Dizhoor, W. Baehr, K. Palczewski, D. A. Baylor and J. Chen (2001). "Role of guanylate cyclase-activating proteins (GCAPs) in setting the flash sensitivity of rod photoreceptors." Proc Natl Acad Sci U S A **98**(17): 9948-9953.

Morshedian, A. and G. L. Fain (2015). "Single-photon sensitivity of lamprey rods with cone-like outer segments." Curr Biol **25**(4): 484-487.

Morshedian, A., M. L. Woodruff and G. L. Fain (2018). "Role of recoverin in rod photoreceptor light adaptation." J Physiol **596**(8): 1513-1526.

Nakatani, K. and K. W. Yau (1988). "Calcium and light adaptation in retinal rods and cones." Nature **334**(6177): 69-71.

Nikonov, S. S., L. L. Daniele, X. Zhu, C. M. Craft, A. Swaroop and E. N. Pugh, Jr. (2005). "Photoreceptors of Nrl -/- mice coexpress functional S- and M-cone opsins having distinct inactivation mechanisms." J Gen Physiol **125**(3): 287-304.

Nikonov, S. S., R. Kholodenko, J. Lem and E. N. Pugh, Jr. (2006). "Physiological features of the S- and M-cone photoreceptors of wild-type mice from single-cell recordings." J Gen Physiol **127**(4): 359-374.

Pugh, E. N., Jr. and T. D. Lamb (1993). "Amplification and kinetics of the activation steps in phototransduction." Biochim Biophys Acta **1141**(2-3): 111-149.

Raviola, E. and N. B. Gilula (1973). "Gap junctions between photoreceptor cells in the vertebrate retina." Proc Natl Acad Sci U S A **70**(6): 1677-1681.

Ribelayga, C., Y. Cao and S. C. Mangel (2008). "The circadian clock in the retina controls rod-cone coupling." Neuron **59**(5): 790-801.

Ruan, G. X., D. Q. Zhang, T. Zhou, S. Yamazaki and D. G. McMahon (2006). "Circadian organization of the mammalian retina." Proc Natl Acad Sci U S A **103**(25): 9703-9708.

Rushton, W. A. (1972). "Pigments and signals in colour vision." J Physiol **220**(3): 1P-P.

Sakurai, K., J. Chen and V. J. Kefalov (2011). "Role of guanylyl cyclase modulation in mouse cone phototransduction." J Neurosci **31**(22): 7991-8000.

Sakurai, K., J. Chen, S. C. Khani and V. J. Kefalov (2015). "Regulation of mammalian cone phototransduction by recoverin and rhodopsin kinase." J Biol Chem **290**(14): 9239-9250.

Schneeweis, D. M. and J. L. Schnapf (1995). "Photovoltage of rods and cones in the macaque retina." Science **268**(5213): 1053-1056.

Schneeweis, D. M. and J. L. Schnapf (1999). "The photovoltage of macaque cone photoreceptors: adaptation, noise, and kinetics." J Neurosci **19**(4): 1203-1216.

Solovei, I., M. Kreysing, C. Lanctot, S. Kosem, L. Peichl, T. Cremer, J. Guck and B. Joffe (2009). "Nuclear architecture of rod photoreceptor cells adapts to vision in mammalian evolution." Cell **137**(2): 356-368.

Tosini, G., N. Pozdeyev, K. Sakamoto and P. M. Iuvone (2008). "The circadian clock system in the mammalian retina." Bioessays **30**(7): 624-633.

Wong, J. C. Y., N. J. Smyllie, G. T. Banks, C. A. Pothecary, A. R. Barnard, E. S. Maywood, A. Jagannath, S. Hughes, G. T. J. van der Horst, R. E. MacLaren, M. W. Hankins, M. H. Hastings, P. M. Nolan, R. G. Foster and S. N. Peirson (2018). "Differential roles for cryptochromes in the mammalian retinal clock." FASEB J **32**(8): 4302-4314.

Young, R. W. (1969). "A difference between rods and cones in the renewal of outer segment protein." Invest Ophthalmol **8**(2): 222-231.

Zhang, X., T. G. Wensel and T. W. Kraft (2003). "GTPase regulators and photoresponses in cones of the eastern chipmunk." J Neurosci **23**(4): 1287-1297.

Chapter Three

Ionic Conductances and Biophysics in Mouse Cones

Introduction

Photoreceptors produce graded electrical signals when exposed to light (Baylor and Nunn 1986). Phototransduction causes the closure of CNG-gated channels in outer segments decreasing net inward current flow. This ultimately hyperpolarizes the cells. Multiple conductances in the inner segment are responsible for shaping the photoresponse and mediating the transmission of signals to downstream bipolar cells. To study ion channel biophysics, one must experimentally manipulate membrane potentials as can only be done with voltage clamp. By setting and maintaining command voltages during stimulation protocols, conductance changes are measured directly. The use of specific pharmacological agents allows further isolation and identification of the contribution from different ionic channels. This chapter investigates the major ion conductances in mouse cones and describes how they shape the waveform and reversal potential of the light response.

Major inner segment conductances have been characterized in a variety of vertebrate species. These conductances include: the hyperpolarization-activated conductance, I_h (Fain et al. 1978; Barnes and Hille 1989; Cia et al. 2005), carried through HCN1 channels (Barrow and Wu 2009; Seeliger et al. 2011); voltage-gated calcium current, I_{ca} (Yagi and Macleish 1994; DeVries 2001; Cia et al. 2005) originating from L-type $Ca_{v1.4}$ channels at ribbon synapses; calcium-activated anion and potassium conductances (Barnes and Hille 1989; Yagi and Macleish 1994; Cia et al. 2005); and multiple voltage-gated potassium conductances (Barnes and Hille 1989; Yagi and Macleish 1994; Cia et al. 2005). Additional ionic fluxes through several electrogenic pumps and exchangers contribute to the total measured current (Brockerhoff et al.

2003). Here, I characterize major conductances in mouse cones and probe the role of these conductances in producing the light responses in an unclamped cone.

In addition to measuring inner-segment conductances, our methods provide a further key advantage. Unlike studies that use enzymatic dissociation (Barnes and Hille 1989; Yagi and Macleish 1994; Cia et al. 2005), the slice preparation maintains the structural integrity of the photoreceptor outer segment and perseveres responsitivity to light. I report the first measurements reversing the polarity of the photoresponse in a mammalian species and describe significant effects of I_{ca} within the same voltage range.

Materials and Methods

Animals

Experiments were performed in accordance with rules and regulations of the NIH guidelines for research animals, as approved by the Institutional Animal Care and Use Committee of the University of California, Los Angeles, USA. See Appendix B for full description.

Experiments in Chapter 3 were wholly executed on cones having no contribution from rods. Rod contributions were avoided through the use of rod-specific $G\alpha_t$ knockout mice (*Gnat1*$^{-/-}$), generated by Janice Lem at Tufts University (Calvert et al. 2000) and obtained locally from the laboratory of Dr. Gabriel Travis at UCLA. Additionally, isolated cone photoresponses are recorded from mice lacking the gap junction protein connexin36 (*Cx36*$^{-/-}$). *Cx36*$^{-/-}$ mice were generated by David Paul from Harvard

University (Deans et al. 2002) and obtained from Sam Wu at Baylor College of Medicine.

Solutions

The main perfusion solution was Ames' medium buffered with 1.9 g/L sodium bicarbonate; slices were cut in an Ames'-HEPES solution. When indicated, isradipine (10 μM; ISR; Sigma), niflumic acid (100-250 μM; NFA; Sigma), or tetraethylammonium (25 mM; TEA-Cl; Sigma) were added to Ames' medium to block L-type calcium channels, calcium-activated chloride channels, or potassium conductances, respectively.

The standard internal solution for the filling of recording pipets consisted mainly of potassium aspartate (K-Asp). See Appendix B for a detailed recipe. Where indicated, 2 mM GTPγS (Sigma) was added to the K-Asp internal to constitutively activate $G\alpha_t$ and close CNG-gated channels. In several experiments, the internal solution was changed to a cesium methane sulfonate (Cs-Meth) solution consisting of (in mM): 110 $CsCHSO_3$, 12 TEA-Cl, 10 HEPES, 10 EGTA, 2 QX-314-Br, 11 ATP-Mg, 0.5 GTP-Tris, 0.5 $MgCl_2$, 1 NAD^+, (pH 7.3 with CsOH; 280 ± 1 mOsm). Cs-Meth was used to block potassium conductances including I_h (Fain et al. 1978; Yagi and Macleish 1994). All reported values have been corrected for liquid junction potentials (Neher 1992), which were measured to be approximately -10 mV for K-Asp and Cs-Meth internal solutions.

Whole-Cell Patch Clamp in Retinal Slices

All experiments described here used standard methods established for voltage-clamping mouse cone somata, outlined in Appendix B.

Light Stimuli

All light stimuli in Chapter 3 were 5 ms, monochromatic flashes of 405 nm light. Monochromatic light was provided by ultra-bright LEDs driven with a linear feedback driver (Opto-LED; Carin Research).

Electrical Stimulations

In experiments measuring ionic conductances and reversal potentials (E_{rev}), stimulations were mostly electrical in nature. The E_{rev} of the light response was probed under voltage-clamp conditions. Cones were held at -50 mV and then stepped to a new holding potential (-90 mV to +90 mV, in 20 mV increments) for 4 seconds. While at the new holding potential, cones were generally allowed to stabilize for 2.5 seconds before being stimulated with a 405 nm saturating flash (Baylor and Nunn 1986; Miller and Korenbrot 1993).

Measurements of I_{ca} began by holding cones at a more negative potential (-70 mV). A test pulse was given at -60 mV to use for leak subtraction on a cell-by-cell basis. Finally, depolarizing voltage steps from -50 mV to +40 mV, in 10 mV increments (Yagi and Macleish 1994; Cia et al. 2005) were applied to measure calcium currents.

Activation of I_h was recording by stepping from -50 mV to increasingly hyperpolarized voltage potentials (down to -140 mV), in -10 mV increments (Barnes and

Hille 1989; Yagi and Macleish 1994; Cia et al. 2005). The E_{rev} of I_h was assessed after opening HCN channels with a -120 mV step for 400 ms and then stepping to a depolarized potential (-100 mV to +10 mV) for another 400 ms. The difference in current, 4 ms after applying the depolarizing step and later, after channel relaxation (+250 ms), was calculated and used to determine when current flow reversed polarity (Barnes and Hille 1989; Yagi and Macleish 1994). Blockers were applied as indicated in figure legends.

Analyses and Equations

General Analyses

Data traces were analyzed with custom scripts written in Matlab. Typically, data were baseline subtracted to 0 with linear subtraction.

Leak Subtraction

To perform leak subtraction, an addition small voltage step (from resting potential, ±10 mV; 5-10 sweeps) was quickly measured. During analyses, these sweeps were averaged and multiplied by integer values that matched the incremental difference from the resting potential to the new holding potential (i.e. for a voltage shift of -50 mV to -80 mV, a 10 mV leak step was multiplied by 3). After scaling, the averaged traces were linearly subtracted from the corresponding raw data trace.

Results

Hyperpolarization-Activated Conductance Contributes Little to the Mouse Cone Light Response

My first attempts to record conductance changes after shifting the command potential revealed a prominent inwardly rectifying current at hyperpolarizing potentials (See Fig 3.4A,C and Fig. 3.5A,C,E). I_h was isolated with 25mM TEA and 10 μM ISR added to the bath solution. First, cones were held at -50 mV and then shifted to increasingly hyperpolarized potentials for 400 ms. Leak-subtracted waveforms (Fig. 3.1A) were used to derive an activation time constant. At the potentials measured, the time constant for I_h activation decreased from 25 ms to 10 ms at the most negative hyperpolarizations (Fig. 3.1B). From these data I determined that I_h was highly activated when held at -120 mV and used this potential to study its reversal potential.

To measure the E_{rev} of I_h, the command potential was stepped to -120 mV for 400 ms to activate I_h and was then given a second, depolarizing step (Fig. 3.1C). The difference in current between +4 ms and +250 ms (vertical red lines) after the depolarizing step was calculated and used to assess the magnitude and direction of current flow through HCN1 channels. I_h reversed at approximately -55 ± 2.5 mV (Fig. 3.1D). Using this reversal potential and the Goldman equation, I calculated the Na^+/K^+ permeability ratio to be 0.12 ± 0.01 for the HCN1 channels expressed in mouse cones.

I_h is reported to speed the rod response, and voltage recordings from other species show prominent 'noses' (Fain et al. 1978; Baylor et al. 1979; Schneeweis and Schnapf 1999; Seeliger et al. 2011). I made several attempts to investigate the role of I_h in shaping the cone light response. First, voltage responses to flashes of increasing

strength were recorded in unclamped *Cx36*$^{-/-}$ cones (Fig 3.2A). From these data, the resting membrane potential was measured to be approximately -37 ± 3 mV. Saturating light responses caused a 14-15 mV hyperpolarization with membrane potential peaking around -52 mV. After comparing with the reversal potential of I_h in mouse ($E_{rev,Ih}$ = -55 mV; Fig. 3.1D) to the range of the photovoltage response, I hypothesized that there should be little contribution of I_h while cones are operating in dark-adapted conditions.

To test this hypothesis, hyperpolarizing current was injected into the cone to bias the membrane potential and facilitate the opening of I_h. While hyperpolarizing the cones by ~-20 mV did not cause major changes in the kinetics or waveform of the photoresponse (Fig 3.2C). The voltage response amplitude increased from 8.5 mV to 17 mV (Fig 3.2B), which was explained by a larger driving force on dark-current ions (see below). Small effects on cone response kinetics agree with the findings from Seeliger et al., 2011, who reported nearly normal cone signaling from HCN1-knockout mice recorded with the ERG.

Synaptic Calcium Dynamics and Background Illumination

Both rod and cone photoreceptors are known to express an L-type calcium channel $Ca_{v1.4}$ in their synaptic terminals (Choi et al. 2008). This particular calcium channel can maintain a sustained, slowly inactivating calcium current. To measure the synaptic calcium conductance, depolarizing steps (750 ms) were applied in the presence of NFA (Fig. 3.3A). I_{ca} was activated at low levels around -50 mV and peaked at 55 ± 6 pA between -30 mV and -20 mV (Traces held at -30 mV are highlight red

throughout Chapter 3 figures). These I_{ca} values agree with those measured in other mammalian species (Yagi and Macleish 1994; Cia et al. 2005).

To assess the physiological range over which synaptic calcium operates, we recorded cone light responses to 7.5 s of steady light in current-clamp mode (Fig 3.3B, inset). The resting membrane voltage in the dark, the transient peak, and the steady state membrane potentials were measured across the dynamic range of *Cx36*$^{-/-}$ cones. For this cohort of cones, the resting membrane potential was measured to be -36 ± 1 mV and the maximal voltage response -49 ± 2 mV, similar to values measured with flashes. These voltages fall along the steep leg of calcium channel activation (Fig. 3.3B). Tuning the range of the photoreceptor voltage response to I_{ca} activation allows minor shifts in membrane potential to induce major effects of calcium-channel activation/deactivation. When the membrane potential is approximately at resting values in the dark (V_m = -36 mV) the I_{ca} would be ~60% of its maximum flux. If the pedicle hyperpolarized to the value of the peak voltage response (-49 mV), I_{ca} would decrease to about 10% of the maximum or 15% of the dark levels.

Unlike rods, cones quickly adapt to bright light and remain responsive to additional light stimuli (Fig. 2.6). In these experiments, cone voltage responses typically recovered between 30 and 40% in several seconds (Fig. 3.3B, blue arrows). The traces corresponding to the 3 brightest step intensities maintained a steady-state membrane potential between -39 and -43 mV. These values corresponded to 60 and 80% of the maximum dark I_{ca} value. The calcium current was largely sustained during the 750 ms steps. The I_{ca} evoked by voltage pulses within the physiological voltage range (-40 mV to -10 mV) maintained between 60 to 75% of the initial peak currents. The decrease in

current can at least partly be explained by changes in driving force rather than channel inactivation (see Discussion).

The I_{ca} Shifts the Reversal of the Light Response to Values More Positive than Predicted in Nernst Calculations

Here I investigate the E_{rev} of the light-sensitive channels in mouse. Beginning with *Gnat1*$^{-/-}$ cones, cells were stepped to various command potentials and stimulated with a brief, saturating light flash (Fig. 3.4A and B). In standard solution, the polarity of the photoresponse reversed at holding potentials of +40 mV or greater (Fig. 3.5G). This highly positive E_{rev} contradicts Nernst equation predictions and previous work in lower vertebrates (Baylor and Nunn 1986; Miller and Korenbrot 1993), both of which suggest E_{rev} to be between 0 and +10 mV.

My first hypothesis was that the positive E_{rev} values were due to poor voltage control of the cones. It is possible, if not highly likely, that *Gnat1*$^{-/-}$ cones maintain coupling to neighboring rods and cones. To assess the amount of electrical spread contributing to the light response, I added 2 mM GTPγS to the recording pipet. GTPγS is a non-hydrolyzable analog of GTP and causes light-independent closure of CNG channels within the target cell. If neighboring photoreceptors were substantially contributing to the light response of the patched *Gnat1*$^{-/-}$ cones, light responses should persist even in the presence of GTPγS. I did not, however, detect residual responses while holding the cone at rest or hyperpolarized command potentials, ruling out electrical signal spread (Fig. 3.4C).

The addition of GTPγS did reveal a small, persistent light response while holding at -30 mV, but several pieces of evidence suggest that it was not a direct product of normal phototransduction. First, the voltage step protocols measuring E_{rev} were not initiated until GTPγS was fully incorporated into the transduction cascade, and the cones stopped producing light responses. To accelerate the incorporation of GTPγS and assess any remaining light response, saturating light flashes were applied shortly after gaining access to the clamped cell. Typically, the cone light response was fully suppressed within 10 flashes (20 to 30 s). Second, the GTPγS-light response was voltage-dependent, but it did not show the same voltage-dependence as the $G\alpha_t$-mediated light response. Flashes were delivered over the typical range of voltage steps in Fig. 3.4A. No light response was observed during the -50, -70, or -90 mV holding potentials. If the response in Fig. 3.4D were due to an incomplete closure of CNG channels, the response amplitude should be largest at negative holding potentials. Instead, the GTPγS-light response was the most robust when the membrane potential was held at values that strongly activated I_{ca} (V_m = -30 mV, red traces). Third, the response waveform was anomalous. It was biphasic, starting with a long delay after stimulus onset (~200 ms), and continuing over a much longer duration than the $G\alpha_t$-mediated light response.

These experiments were repeated in *Cx36*$^{-/-}$ cones and the findings were remarkably similar (Fig 3.5), including a highly positive E_{rev} (41 ± 4 mV; Fig. 3.5G, black trace). Again, the addition of 2 mM GTPγS n the recording pipet revealed an atypical light response when cones held at depolarized potentials (Fig 3.5C and D). While the biphasic response was reminiscent of a $G\alpha_t$-insensitive calcium response (Brockerhoff

et al. 2003), the addition on NFA suppressed most of it (Fig 3.5D, red trace), suggesting that the $G\alpha_t$-insensitive photocurrent was largely the result of calcium-activated chloride channels. Despite the GTPγS-light response, signal spread was not detected from neighboring cells in either *Gnat1*$^{-/-}$ or *Cx36*$^{-/-}$ cones, implying that lateral coupling was not the cause of the positive E_{rev}.

A Hidden Interplay Between I_{ca} and Calcium-activated Conductances

Since I_{ca} was strongly activated at the same holding potentials that the light response E_{rev} occurred, I focused on the dynamics of I_{ca} and the calcium-activated chloride conductance during voltage step protocols. To help isolate these conductances, potassium channels were blocked by switching the pipet solution to Cs-Meth internal to block (Fain et al. 1978; Cia et al. 2005). Similar stimulation protocols to those in Fig 3.4 and 3.5 revealed a complicated waveform when cones were depolarized to -30 mV (Fig. 3.6A and B). In standard Ames' solution, the cone experienced dramatic inward and outward conductances changes within the first 1 s of applying a depolarizing command potential. These conductances never fully stabilized over the entire 4 s of the voltage step (Fig. 3.6B).

The addition of 100 to 250 μM of NFA to the bath solution blocked the calcium-activated chloride channels and simplified the response to the -30 mV step (Fig. 3.6C). With NFA washed on, an inward component was still present, but the conductances stabilized after several seconds. The initial inward component was due to an influx of calcium (compare first 750 ms of Fig. 3.6C with Fig. 3.3A, red trace) and was blocked with an L-type calcium channel blocker isradipine (ISR, 10 μM; Fig. 3.6D and E). The

presence of ISR alone was sufficient to block the entire current response generated by stepping the membrane voltage to -30 mV (Fig. 3.6D), and no outward component was observed. These findings further support the hypothesis that the outward conductance component in Fig. 3.6B was generated by calcium-activated chloride channels. The addition of NFA and/or ISR shifted E_{rev} to slightly lower potentials (Fig. 3.6F, from 27 mV to 23 ± 1 mV).

After observing the significant actions of I_{ca} occurring at voltages between the resting and reversal potentials, I again measured E_{rev} with standard internal solution, K-Asp. In this experiment, the bath solution contained 10 μM ISR and 25 mM TEA to block I_{ca} and sustained potassium conductances, respectively (Cia et al. 2005). In these conditions, the E_{rev} decreased almost 30 mV, from +40 mV to +13 mV ± 2 mV (Fig. 3.5 E to G) and was in general agreement with predictions and previous measurements (Baylor and Nunn 1986; Miller and Korenbrot 1993).

The Transient Potassium Conductance is Isolated with I_{ca} Block

The experimental conditions isolating the E_{rev} of the light response enabled the quantification of a transient voltage-activated potassium conductance ($I_{k,fast}$). Blocking I_{ca} revealed the full waveform of $I_{k,fast}$, which began to activate when the holding voltage was stepped to +10 mV. The first 1.5 seconds of the voltage steps from Fig. 3.5E were leak subtracted (Fig. 3.7A). The peak current and time course continued to increase with large depolarizations (Fig. 3.7B). Experiments that included internal cesium blocked $I_{k,fast}$ (Fig. 3.6A).

Discussion

The Effects of Photoreceptor Coupling During Voltage Clamp

Because the photoreceptors form an electrical network with neighboring cells, it raises the question of how well the membrane voltage is maintained at the experimental command voltage. When first measuring the E_{rev} of the light response, I hypothesized that highly positive values could be due to electrical coupling and signal spread. If photoreceptor coupling was responsible for shifting the light response E_{rev}, residual responses should have been detectable even in the presence of GTPγS. Indeed, similar experiments undertaken on coupled cones demonstrate that the lateral spread of rod signals were detectable even after the cone light response has rundown. These rod responses would have complicated measurements of the cone $E_{rev,CNG}$ and also confirm that signal spread would have been detectable if present (data not shown).

If signal spread significantly affected the quality of the voltage clamp on *Gnat1*$^{-/-}$ cones, one would expect the current-voltage relation of *Gnat1*$^{-/-}$ to deviate from that of *Cx36*$^{-/-}$ cones. Instead, cones from both genetic backgrounds produce remarkably similar responses in standard solutions (Fig. 3.5G, blue and black traces). While network effects cannot be completely ruled out for *Gnat1*$^{-/-}$ cones, these effects must have been small. These data are evidence that the membrane potentials of both *Gnat1*$^{-/-}$ and *Cx36*$^{-/-}$ cones were adequately controlled throughout my experiments.

Permeability Ratios

From these data, it was possible to calculate permeability ratios for several ions for multiple channels. First, I considered the permeability of the CNG channels for

potassium. Using the Goldman equation and the measured E_{rev} value of +13 mV, I calculated the permeability ratio of potassium (P_K) through the CNG channel to be 0.5 (K^+/Na^+). Using $P_K = 0.5$ it was possible to estimate the permeability of cesium through the same channel. If we take the measured E_{rev} to be +24 mV when recorded with Cs-Meth internal solution, $P_{Cs} = 0.45$ (Cs^+/Na^+).

Next, I similarly calculated the permeability ratio of sodium (P_{Na}) through the HCN channels. Using the measured E_{rev} of I_h (-55 mV), P_{Na} was 0.12 to 0.13, similar to reported values of 0.13 to 0.15 (Novella Romanelli et al. 2016). Despite the relatively low permeability of HCN channels to sodium, the negative voltage range over which I_h is activated yields a stronger driving force ($V_m - E_x$) for sodium compared to potassium.

A Biophysical Balancing Act: Matching the Photovoltage Response and Transmitter Release

An interesting conundrum arises from my measurements of voltage-dependent conductances. I show that I_h is minimally activated through out the dark-adapted voltage response. The cone photovoltage responses peaked between -50 mV and -55 mV, which are within the immediate vicinity of the E_{rev} of I_h (Fig. 3.1). For the HCN channels to pass net current and contribute to shaping the photovoltage, the cone membrane potential will need to experience further hyperpolarization. This is in contrast to work in rods from lower vertebrates, which describe how channel block with external cesium increased the amplitude of photovoltage response. These studies also highlight the role of I_h in shaping the 'nose' seen in the rod photovoltage response (Fain et al. 1978; Baylor et al. 1979). A more recent study in mice indicated that the loss of HCN1 only

affects cone signaling if the rod secondary pathway is intact (Seeliger et al. 2011). They showed that when HCN1 knockout mice are bred into a *Cx36*$^{-/-}$ background, cone signaling was similar to controls. Together these data suggest that I_h is perhaps crucial to speeding the rod photovoltage response through physiological membrane potentials, but less so for the cone photoresponse.

To further test the functional significance of I_h in shaping cone photoresponses, future experiments will focus on measuring the photovoltage response in mouse cones by applying cesium externally to block I_h, as well as measuring E_{rev} of I_h in mouse rods to assess the possibility of differing set points. Additionaly, I_h might contribute more to the cone impulse response if cones are tested with background illumination. White noise stimuli and background light will be utilized to characterize changes in the impulse transfer function with and without I_h contributions.

With seemingly minimal contribution of I_h to the physiological cone photoresponse, we must ask what role it has in the cone inner segment. I considered I_h in relation to the voltage dependence of I_{ca}. I show that at the peak of the voltage response, I_{ca} is already just 5 pA or 15% of dark values (Fig. 3.3B: if V_m = -35 mV, I_{ca} = ~33 pA). As cones reach the limits of their I_{ca} dynamic range, glutamate release will cease and further hyperpolarization cannot be encoded. However, a strong hyperpolarization below V_m = -55 mV will activate I_h and cause the inward flow of positive ions. Therefore, the purpose of I_h in mammalian cones is likely to stabilize the membrane potential close to the dynamic range of I_{ca} and protect the cones from strong hyperpolarizations that would cause prolonged inhibition of glutamate release.

Calcium Rebound in the Pedicle

Cones and downstream circuitry remain active over an impressive range of bright lights. Some of this ability is mediated through the molecular adaptive processes explored in Chapter 2, whereby cones undergo functional recovery of the light-sensitive channels in the presence of steady light. How does the reopening of CNG channels affect calcium dynamics at the cone pedicle?

I show in Fig. 3.3B that the photovoltage response occurs on the steep leg of the I_{ca} current-voltage relationship. Within this operating range, small shifts in membrane potential have large consequences on the amplitude of I_{ca}. Again, Chapter 2 demonstrated that cones can reach a transient saturation where I_{CNG} = 0 pA, but they then quickly regain ~30% or more of their circulating dark current. This recovery is mirrored in the voltage responses to steady light (Fig. 3.3B, inset). Consequently, synaptic I_{ca} will also undergo a strong but transient suppression (Fig. 3.3B, green arrows) before the cone depolarizes to a new steady-state membrane potential (Fig. 3.3B, blues arrows). Thus, the functional recovery of CNG channels in the cone outer segment leads to a rebound in synaptic I_{ca}. Without a concomitant increase in synaptic I_{ca} as the CNG channels recover, additional light exposure could not produce additional suppression of glutamate release, and the downstream circuitry would remain in saturation.

Darkness or decrements in light intensity are signaled by an increase in glutamate release to bipolar cells. If synaptic calcium channels in photoreceptors were subject to inactivation, it would not be possible to experience darkness as a ‘stable’ perception. My data demonstrates that over 750 ms, the calcium current declines

minimally, and there is no strong inactivation. Again, this is functionally important for photoreceptor physiology since channel inactivation would be perceived as light exposure. Why does the calcium current decline? The small decline, 25-30% of the initial peak current can in part be explained by a change in driving force. After experimentally holding the cones at -70 mV, the calcium concentration in the pedicle is likely to be quite low. With low internal calcium, E_{Ca} is calculated to be highly positive yielding a large driving force to move calcium into the pedicle. With a sustained, depolarizing voltage step, calcium enters the pedicle. Over time, the internal calcium concentration increases and shifts E_{Ca} to lower membrane potentials. Therefore, the driving force slowly decreases and less calcium enters the pedicle as a result. While calcium channel inactivation cannot be completely ruled out, the deceased driving force and explains, at least in part, the decrease in I_{ca} during sustained voltage pulses.

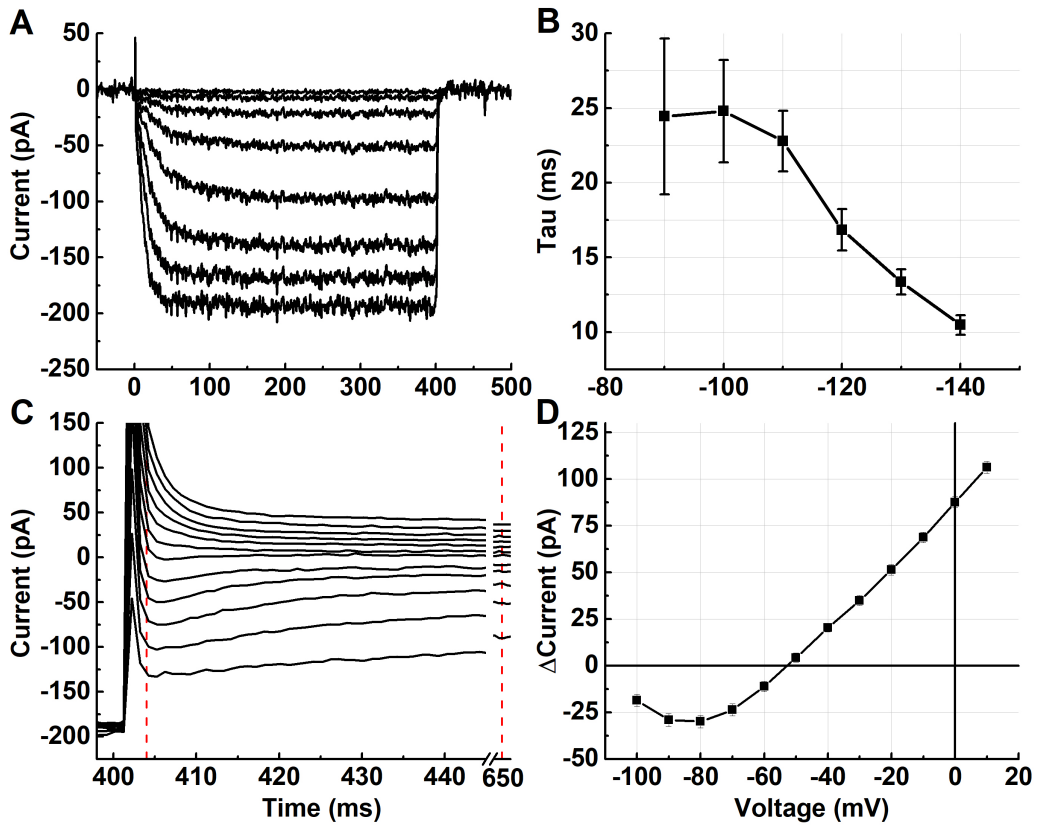

Figure 3.1 The Hyperpolarization-activated Conductance in Mouse Cones

A) Traces are leak-subtracted current responses measure from a representative *Cx36*$^{-/-}$ cone. The cone was held at -50 mV and stepped to hyperpolarizing potentials (-60 to -140 mV, increments of 10 mV) for 400 ms. 25mM TEA and 10 μM ISR were included in the bath solution and pipet solutions were standard K-Asp. B) The currents measured in A) were fit with an exponential expression to derive an activation time constant (τ_{act}). Averaged τ_{act} values are plotted against the holding potential and decrease from 25 ms to 10 ms as hyperpolarization increases. C) The reversal potential of I_h in cones was measured by hyperpolarizing a cone to -120 mV for 400 ms and then depolarizing to different potentials (-100 mV to +30 mV, in increments of 10 mV) for another 400 ms. C) shows the last 2 ms of the first voltage step and the first 45 ms of the second voltage step. Red dashed lines at indicate 4 ms and 250 ms after the second voltage step was applied. The difference in current was calculated at these time points and the averages were plotted against the potential of the second voltage step in D). B) and D) are means ± SEM from 10 different cones

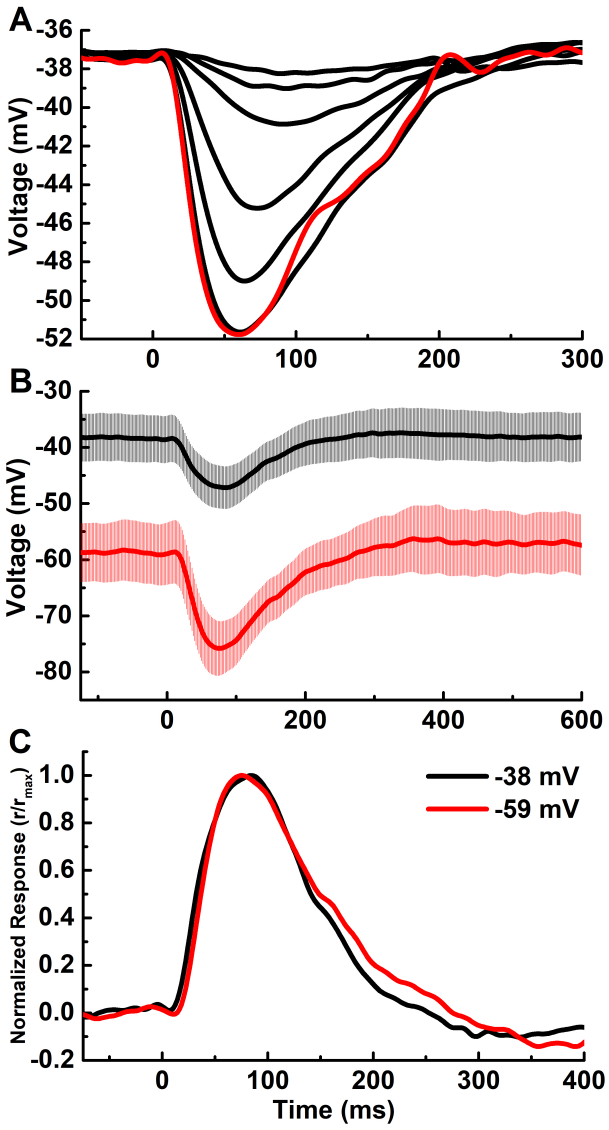

Figure 3.2 Where is I_h?

A) Traces are averaged photovoltage responses from 19 *Cx36*$^{-/-}$ cones recorded in current clamp mode. The resting membrane potential was calculated as -37 mV. B) Cones were stimulated with a flash intensity designed to elicit a half-maximal voltage response during dark, resting conditions (black trace, mean ± SEM). Hyperpolarizing current was then injected to bias the membrane potential to negative potentials before stimulating with the same flash (red trace). Hyperpolarization increases the maximum photovoltage. C) Traces in (B) were normalized and demonstrate that hyperpolarization does not increase response kinetics.

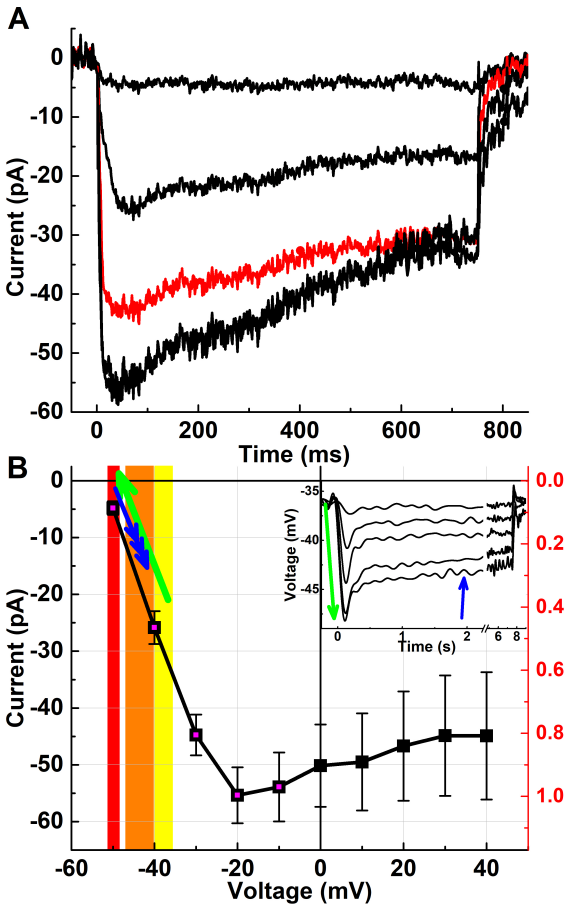

Figure 3.3 Mouse Cones Express a Sustained Calcium Conductance at the Pedicle

Cx36$^{-/-}$ cones were held at -70 mV before stepping the command potential to depolarizing membrane potentials (-50 mV to +40 mV, in 10 mV increments) for 750 ms. 100 µM NFA was perfused throughout the recordings and the pipet solution contained Cs-Meth. A) Leak-subtracted and averaged (n = 8) for calcium currents elicited by -50 mV to -10 mV are plotted. I_{ca} peaked at 55 ± 2.5 pA when cones were depolarized to -20 mV. B) Peak currents (mean ± SEM) at each voltage increment were used to derive the current-voltage relationship of mouse cone I_{ca}. Pink-filled symbols represent the peak currents for the traces in (A). Red axes are values normalized to the peak I_{ca}. Inset: Average voltage responses to 7.5 s of steady light given at increasing intensities. The green arrow represents the voltage changes occurring from rest (yellow range) to the peak voltage response (red range). The blue arrow shows the voltage rebound as the cone escapes saturation in steady light (orange range).

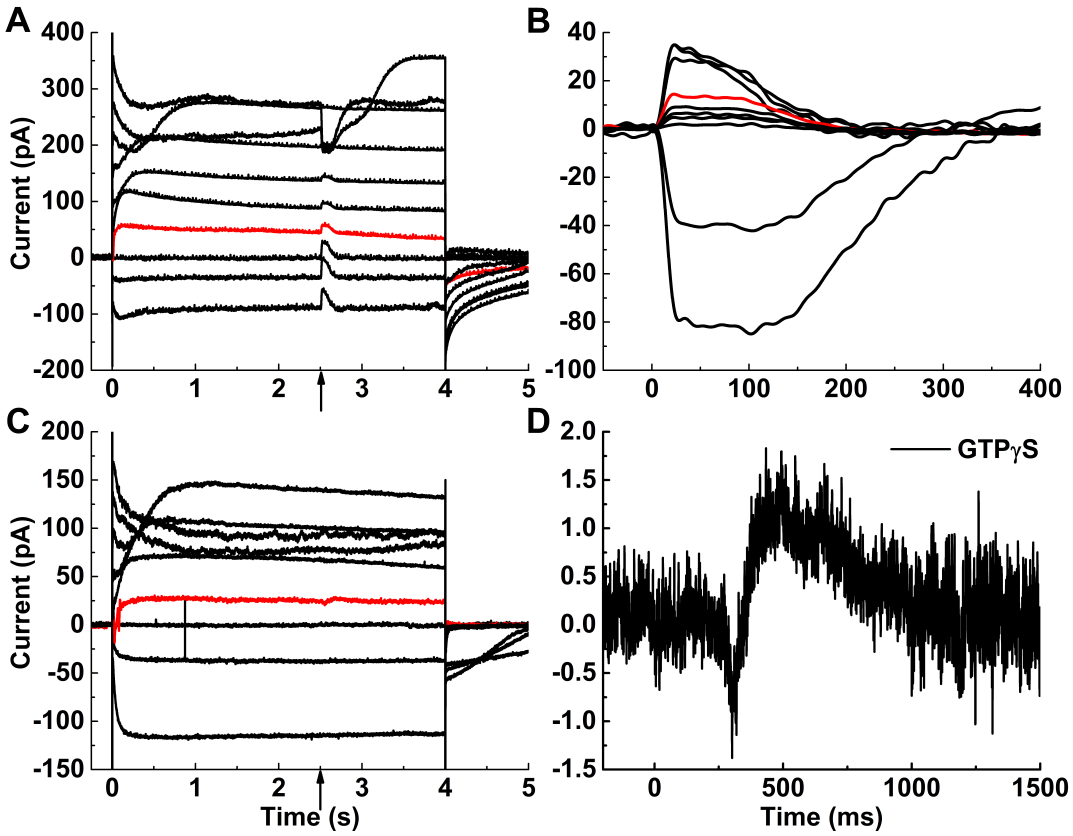

Figure 3.4 The Light Response of *Gnat1*$^{-/-}$ Cones Reverses at Highly Positive Holding Potentials

Gnat1$^{-/-}$ cones were held at V_m = -50 mV. During each trace, V_{hold} was shifted to a new potential (-90 mV to +70 mV, in 20 mV increments). After a delay, a saturating light flash (1.2 x 10^4 P^*/flash, arrows) was delivered to measure peak photocurrent and E_{rev}. Red traces indicate V_{hold} = -30 mV. A and B) Cones were recorded in standard solutions (internal: K-Asp; external: Ames' bicarbonate). B) Photoresponses were baselined and isolated from A. C and D) Transducin-mediated light responses were blocked by adding 2 mM GTPγS to the pipet solution. D) Averaged GTPγS-insensitive photocurrent at V_{hold} = -30 mV (n=6). Light flashes were delivered at t = 0 ms.

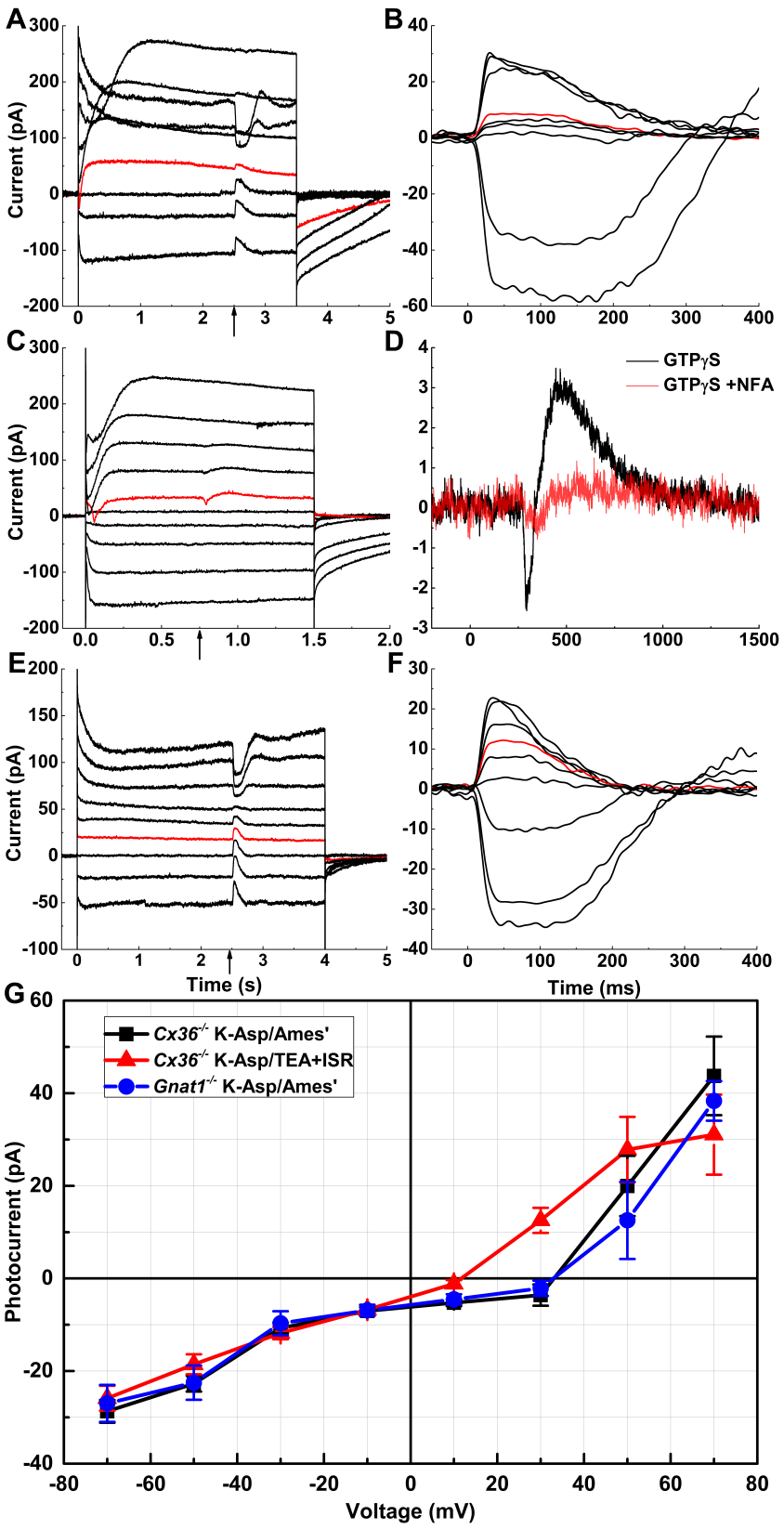
A
B
C
D
E
F
G
Current (pA)
Time (s)
Time (ms)
GTPγS
GTPγS +NFA
Cx36-/- K-Asp/Ames'
Cx36-/- K-Asp/TEA+ISR
Gnat1-/- K-Asp/Ames'
Photocurrent (pA)
Voltage (mV)

Figure 3.5 I_{ca}-activated Conductances Confound Reversal Potentials

Cx36$^{-/-}$ cones were stimulated with the same protocol outlined in Fig. 3.4. A saturating light flash (1.2 x 10^4 P^*/flash, arrows) was delivered to measure peak photocurrent and E_{rev}. Red traces indicate V_{hold} = -30 mV. A and B) Cones were recorded in standard solutions (internal: K-Asp; external: Ames' bicarbonate). B) Photocurrents were baselined and isolated from A). C and D) Transducin-mediated light responses were blocked by adding 2 mM GTPγS to the pipet solution. D) The averaged GTPγS-insensitive photocurrent at V_{hold} = -30 mV (n=14; black trace). Light flashes were delivered at t = 0 ms. Several *Cx36*$^{-/-}$ cones (n=8) were recorded with 100 to 250 μM NFA added to the external solution (red trace). E and F) 25 mM TEA and 10 μM isradipine (ISR) were added to the external solution. The K-Asp internal solution contained no blockers. Light-sensitive current responses are isolated in F). G) Current-voltage relationship of the photocurrent with (red trace) and without (black trace) blockers for I_{ca} and $I_{k,sustained}$. Data from Fig. 3.4 are plotted for comparison (blue trace).

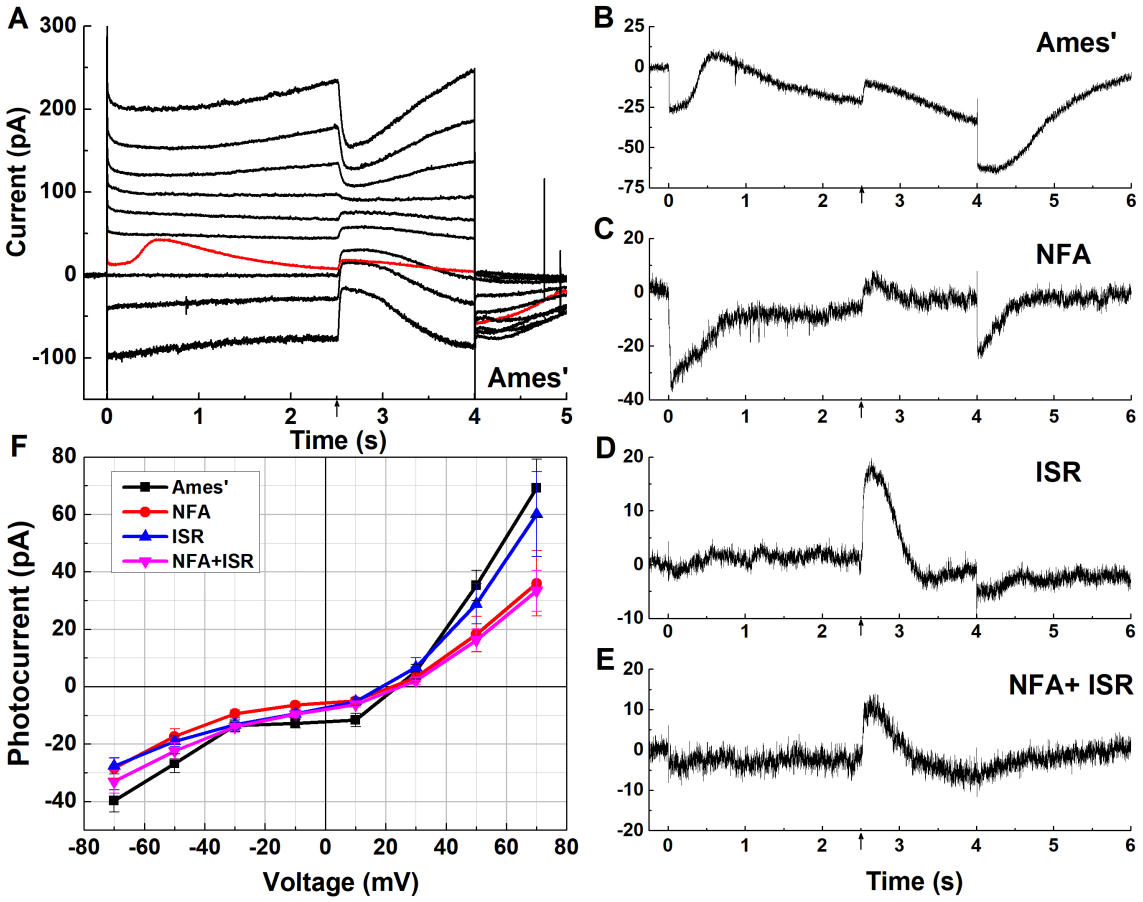

Figure 3.6 Cesium-based Internal Solutions Reveal Large I_{ca} and I_{ca}-activated Conductances in Mouse Cones

Stimulation protocols were similar to those outlined in Figs. 3.4 and 3.5. K-Asp internal solution was exchanged for Cs-Meth and various blockers were added to the external solution as indicated. Arrows represent brief light flashes. A) Current recordings from a representative cone recorded in standard external solution (Ames'; n = 13 total). Red trace indicate V_{hold} = -30 mV. B) The V_{hold} = -30 mV current trace from A) was leak-subtracted. C-E) Similar protocols were repeated on cones with NFA (C; n=13), ISR (D; n=10), or both (E; NFA+ISR; n=8) washed on. F) Current-voltage relationship of the light response in cones recorded with Cs-Meth internal solutions and various external conditions.

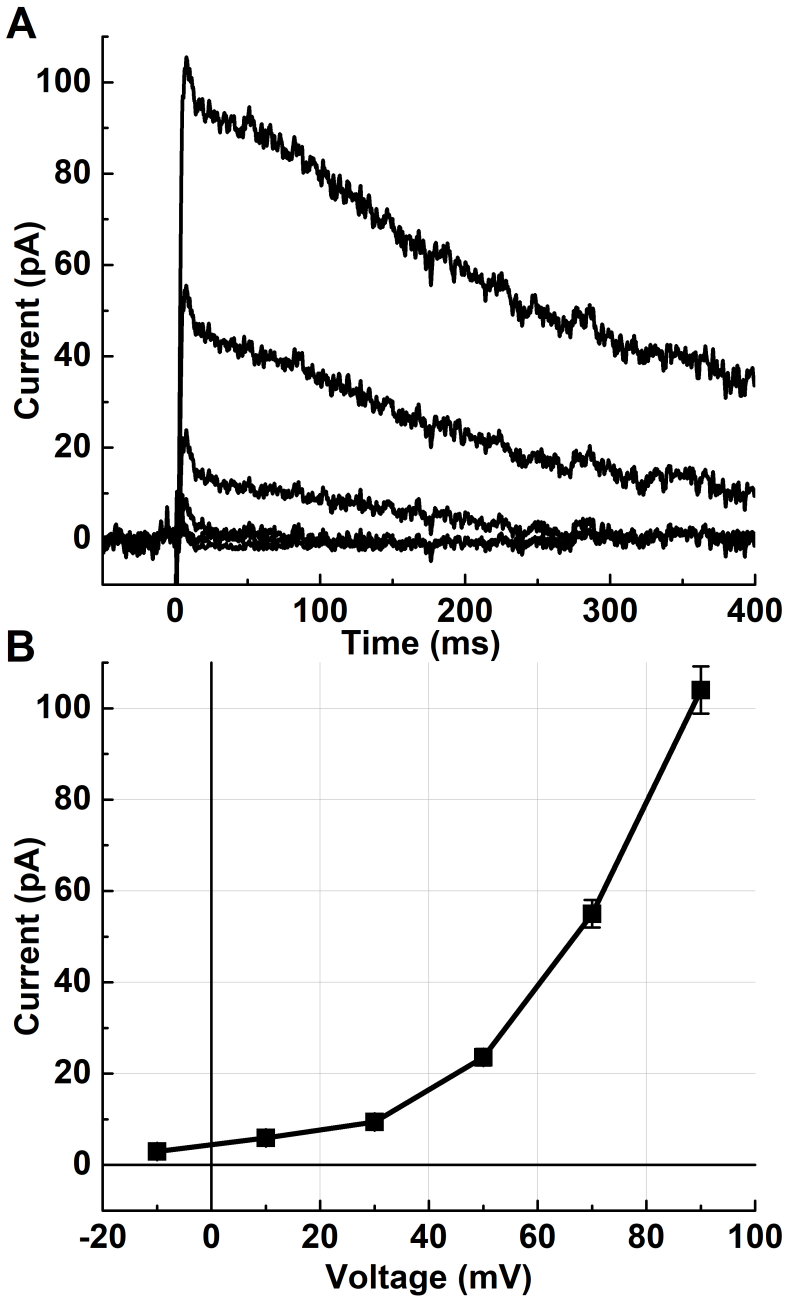

Figure 3.7 A TEA-insensitive Potassium Conductance

A) The first several hundred ms of the current traces were isolated from the records show in Fig. 3.5E. The addition of TEA-Cl and ISR in the bath solution blocks I_{ca} activation during depolarizing steps and reveals a voltage-dependent outward conductance. The first 1.5 s were leak subtracted and the peak conductances were plotted in (B).

References

Barnes, S. and B. Hille (1989). "Ionic channels of the inner segment of tiger salamander cone photoreceptors." J Gen Physiol **94**(4): 719-743.

Barrow, A. J. and S. M. Wu (2009). "Low-conductance HCN1 ion channels augment the frequency response of rod and cone photoreceptors." J Neurosci **29**(18): 5841-5853.

Baylor, D. A., T. D. Lamb and K. W. Yau (1979). "The membrane current of single rod outer segments." J Physiol **288**: 589-611.

Baylor, D. A. and B. J. Nunn (1986). "Electrical properties of the light-sensitive conductance of rods of the salamander Ambystoma tigrinum." J Physiol **371**: 115-145.

Brockerhoff, S. E., F. Rieke, H. R. Matthews, M. R. Taylor, B. Kennedy, I. Ankoudinova, G. A. Niemi, C. L. Tucker, M. Xiao, M. C. Cilluffo, G. L. Fain and J. B. Hurley (2003). "Light stimulates a transducin-independent increase of cytoplasmic Ca2+ and suppression of current in cones from the zebrafish mutant nof." J Neurosci **23**(2): 470-480.

Calvert, P. D., N. V. Krasnoperova, A. L. Lyubarsky, T. Isayama, M. Nicolo, B. Kosaras, G. Wong, K. S. Gannon, R. F. Margolskee, R. L. Sidman, E. N. Pugh, Jr., C. L. Makino and J. Lem (2000). "Phototransduction in transgenic mice after targeted deletion of the rod transducin alpha -subunit." Proc Natl Acad Sci U S A **97**(25): 13913-13918.

Choi, S. Y., S. Jackman, W. B. Thoreson and R. H. Kramer (2008). "Light regulation of Ca2+ in the cone photoreceptor synaptic terminal." Vis Neurosci **25**(5-6): 693-700.

Cia, D., A. Bordais, C. Varela, V. Forster, J. A. Sahel, A. Rendon and S. Picaud (2005). "Voltage-gated channels and calcium homeostasis in mammalian rod photoreceptors." J Neurophysiol **93**(3): 1468-1475.

Deans, M. R., B. Volgyi, D. A. Goodenough, S. A. Bloomfield and D. L. Paul (2002). "Connexin36 is essential for transmission of rod-mediated visual signals in the mammalian retina." Neuron **36**(4): 703-712.

DeVries, S. H. (2001). "Exocytosed protons feedback to suppress the Ca2+ current in mammalian cone photoreceptors." Neuron **32**(6): 1107-1117.

Fain, G. L., F. N. Quandt, B. L. Bastian and H. M. Gerschenfeld (1978). "Contribution of a caesium-sensitive conductance increase to the rod photoresponse." Nature **272**(5652): 466-469.

Miller, J. L. and J. I. Korenbrot (1993). "In retinal cones, membrane depolarization in darkness activates the cGMP-dependent conductance. A model of Ca homeostasis and the regulation of guanylate cyclase." J Gen Physiol **101**(6): 933-960.

Neher, E. (1992). "Correction for liquid junction potentials in patch clamp experiments." Methods Enzymol **207**: 123-131.

Novella Romanelli, M., L. Sartiani, A. Masi, G. Mannaioni, D. Manetti, A. Mugelli and E. Cerbai (2016). "HCN Channels Modulators: The Need for Selectivity." Curr Top Med Chem **16**(16): 1764-1791.

Schneeweis, D. M. and J. L. Schnapf (1999). "The photovoltage of macaque cone photoreceptors: adaptation, noise, and kinetics." J Neurosci **19**(4): 1203-1216.

Seeliger, M. W., A. Brombas, R. Weiler, P. Humphries, G. Knop, N. Tanimoto and F. Muller (2011). "Modulation of rod photoreceptor output by HCN1 channels is essential for regular mesopic cone vision." Nat Commun **2**: 532.

Yagi, T. and P. R. Macleish (1994). "Ionic conductances of monkey solitary cone inner segments." J Neurophysiol **71**(2): 656-665.

Chapter Four

Blue light regenerates functional visual pigments in mammals through a retinyl-phospholipid intermediate

nature COMMUNICATIONS

ARTICLE

DOI: 10.1038/s41467-017-00018-4 OPEN

Blue light regenerates functional visual pigments in mammals through a retinyl-phospholipid intermediate

Joanna J. Kaylor[1], Tongzhou Xu[1,2], Norianne T. Ingram[1,2], Avian Tsan[1], Hayk Hakobyan[1], Gordon L. Fain[1,3] & Gabriel H. Travis[1,4]

The light absorbing chromophore in opsin visual pigments is the protonated Schiff base of 11-*cis*-retinaldehyde (11cRAL). Absorption of a photon isomerizes 11cRAL to all-*trans*-retinaldehyde (atRAL), briefly activating the pigment before it dissociates. Light sensitivity is restored when apo-opsin combines with another 11cRAL to form a new visual pigment. Conversion of atRAL to 11cRAL is carried out by enzyme pathways in neighboring cells. Here we show that blue (450-nm) light converts atRAL specifically to 11cRAL through a retinyl-phospholipid intermediate in photoreceptor membranes. The quantum efficiency of this photoconversion is similar to rhodopsin. Photoreceptor membranes synthesize 11cRAL chromophore faster under blue light than in darkness. Live mice regenerate rhodopsin more rapidly in blue light. Finally, whole retinas and isolated cone cells show increased photosensitivity following exposure to blue light. These results indicate that light contributes to visual-pigment renewal in mammalian rods and cones through a non-enzymatic process involving retinyl-phospholipids.

[1] Jules Stein Eye Institute, University of California Los Angeles School of Medicine, Los Angeles, California 90095, USA. [2] Molecular, Cellular and Integrative Physiology Graduate Program, University of California Los Angeles School of Medicine, Los Angeles, California 90095, USA. [3] Department of Integrative Biology and Physiology, University of California Los Angeles School of Medicine, Los Angeles, California 90095, USA. [4] Department of Biological Chemistry, University of California Los Angeles School of Medicine, Los Angeles, California 90095, USA. Correspondence and requests for materials should be addressed to G.H.T. (email: travis@jsei.ucla.edu)

Light perception in metazoans is mediated by two types of photosensitive cells, rhabdomeric and ciliary photoreceptors. Both contain membranous structures filled with opsin pigments. Ciliary photoreceptors, such as human rods and cones, contain an outer segment (OS) comprising a stack of membranous disks. The first event in light perception is capture of a photon by an opsin pigment. The light-absorbing chromophore in most opsins is 11-*cis*-retinaldehyde (11cRAL) coupled to a lysine residue through a protonated Schiff-base linkage. Absorption of a photon isomerizes the 11cRAL to all-*trans*-retinaldehyde (atRAL), transiently converting the pigment to its active (metarhodopsin II/III) signaling state. In the rhabdomeric photoreceptors of insects, atRAL remains covalently coupled to the opsin following activation. Absorption of a second photon flips the atRAL back to 11cRAL, restoring light sensitivity through photoregeneration[1]. For this reason, rhabdomeric opsins are called bistable pigments. In bright light they flicker between signaling and light-sensitive forms.

The opsin pigments of ciliary photoreceptors decay following photoactivation to yield unliganded apo-opsin and free atRAL[2]. Ciliary opsins are hence called bleaching pigments. Immediately following photon absorption by a ciliary opsin, the resulting metarhodopsin I may absorb a second photon, converting the atRAL back to 11cRAL, and the pigment to its light sensitive state[3, 4]. Thus, during the first millisecond of the rhodopsin cycle, ciliary rhodopsin behaves as a bistable pigment. After deprotonation of the Schiff base with activation of the pigment, photoreversal no longer occurs[5, 6]. Photoreversal therefore contributes negligibly to pigment regeneration in ciliary photoreceptors. Light sensitivity is restored to apo-opsin when it combines with another 11cRAL to form rhodopsin. The conversion of atRAL back to 11cRAL is carried out by multi-step enzyme pathways in cells of the retinal pigment epithelium (RPE)[7] and Müller glial cells in the retina[8, 9, 10]. Thus, rods and cones rely on enzymatic reactions in neighboring cells to synthesize visual chromophore, and appear not to benefit from the faster photoregeneration employed by "lower" metazoan species. For sustained vision in daylight, ciliary photoreceptors must be supplied with fresh 11cRAL at a rate that matches the rate of chromophore consumption through photoisomerization of opsins.

Retinaldehydes are lipophilic with low aqueous solubility[11]. They are present at high concentrations in OS disk membranes, which serve as conduits for 11cRAL and atRAL flowing to and from the opsins. Opsin crystal structures show openings to the ligand-binding cavity between pairs of transmembrane helices[12, 13]. Retinaldehydes are thought to enter and exit the chromophore-binding site of opsin via these openings. In the disk bilayer, retinaldehydes rapidly and reversibly condense with phosphatidylethanolamine (PE) to form the retinyl-lipid, *N*-retinylidene-PE (*N*-ret-PE)[14, 15]. Importantly, it was previously shown that all-*trans*- (at-) *N*-ret-PE undergoes photoisomerization to 11-*cis*- (11c-) *N*-ret-PE in visible light[16], and that 11c-*N*-ret-PE transfers 11cRAL to apo-opsin[14, 17]. Photoregeneration of visual pigments has never been reported in vertebrates. It is currently thought that visual pigments in vertebrate photoreceptors are regenerated exclusively by the enzymatic visual cycles. Here, we show that mammalian photoreceptors possess a mechanism for light-driven regeneration of opsin pigments, employing *N*-ret-PE as a light-sensitive intermediate. This mechanism is distinct from both photoregeneration of bistable opsins in rhabdomeric photoreceptors and the enzymatic visual cycles in RPE and Müller cells of vertebrates.

Results

Photoisomerization of *N*-ret-PE. We synthesized at-*N*-ret-PE and determined its absorbance spectra in acidified or alkalized methanol. The maximum absorption wavelength (λ_{max}) of protonated at-*N*-ret-PE was 450 nm, while the λ_{max} of non-protonated at-*N*-ret-PE was 365 nm (Supplementary Fig. 1). The pK_a of *N*-ret-PE is 6.9[18]. Since the pH near the surface of biological membranes is approximately one pH-unit lower than the surrounding aqueous medium[19], most *N*-ret-PE is protonated in vivo. Non-protonated *N*-ret-PE probably contributes little to chromophore photoregeneration because of its low abundance, and because the optic media blocks transmission of light below 400 nm[20].

We tested whether *N*-ret-PE undergoes at-to-11c photoisomerization in light, as previously observed[16]. To this end, we exposed samples of protonated at-*N*-ret-PE to monochromatic light of wavelengths 325–650 nm for 80 s, each with a photon flux of 0.95 µmol photons/m^2 s. We determined the isomer composition of *N*-ret-PE for each wavelength by reacting the samples with hydroxylamine to form stable retinaldehyde oximes and quantitating by normal-phase liquid chromatography (LC).

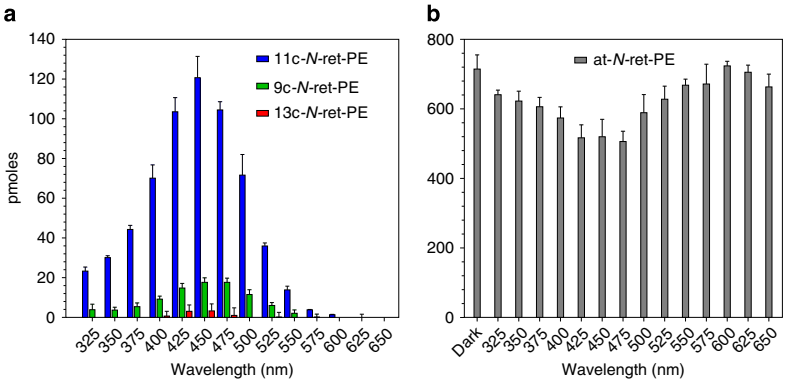

Fig. 1 Action spectrum for photoisomerization of protonated at-*N*-ret-PE. Protonated at-*N*-ret-PE in acidified methanol was incubated in the dark or under monochromatic light of the indicated wavelengths and the same photon flux. **a** Molar composition of 11c-, 9c- and 13c-*N*-ret-PE isomers following the incubation in light. The dark background level of each isomer was subtracted. Note the 37-fold higher level of 11c- versus 13c-*N*-ret-PE in the 450-nm samples. **b** Molar amounts of at-*N*-ret-PE remaining after incubation in the dark or in light of the indicated wavelengths. Data are plotted as mean ± s.d. ($n = 3$)

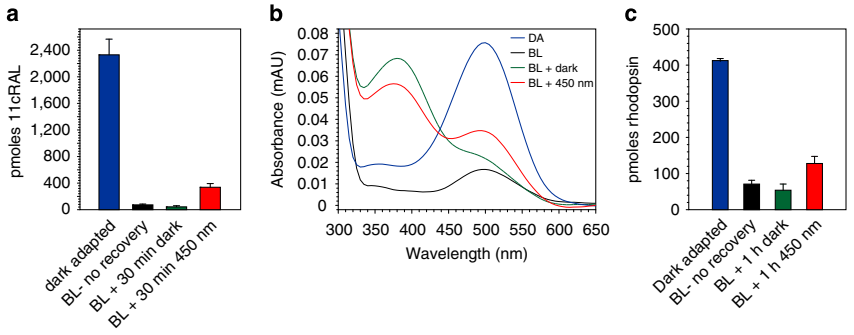

Fig. 2 Light-dependent regeneration of 11cRAL and rhodopsin in bovine OS. Aliquots of rod OS from dark-adapted bovine retinas were analyzed before and after a deep photobleach. After addition of atRAL, the remaining aliquots were incubated in the dark or in 450-nm light at 0.5 W/m^2 for the indicated times. **a** Levels of 11cRAL in dark-adapted (DA), immediate post-bleach (BL—no recovery), post-bleach plus 30 min incubation with atRAL in the dark (BL + 30 min dark), or post-bleach plus 30 min incubation with atRAL in 450-nm light (BL + 30 min 450 nm) OS. Data are plotted as mean ± s.d. ($n = 3$). **b** Representative UV-visible spectra of affinity-purified rhodopsin from bovine OS treated as described in panel **c**. The prominent 360-370-nm shoulders in the rhodopsin spectra from the (BL + 1 h dark) and (BL + 1 h. 450 nm) samples represent the added atRAL. **c** Levels of rhodopsin in bovine OS from dark-adapted bovine eyes (DA), immediately following a photobleach (BL - no recovery), incubated for 1 h in the dark with atRAL following the photobleach (BL + 1 h dark), or incubated for 1 h in 450-nm light with atRAL following the photobleach (BL + 1 h 450 nm). Data are plotted as mean ± s.d. ($n = 3$)

Table 1 Retinaldehydes in N-ret-PE and total retinaldehydes in DA mouse retinas (pmoles per retina)

	11cRAL	atRAL	13cRAL	9cRAL	Combined RALs
Retinaldehydes in *N*-ret-PE	10.0 ± 0.7	18.1 ± 1.3	8.0 ± 0.6	0.9 ± 0.1	37.0 ± 2.7
Total retinaldehydes	454.0 ± 25	72.3 ± 6.1	22.1 ± 3.6	7.9 ± 1.4	556.3 ± 35

We observed dramatic light-dependent conversion of at-*N*-ret-PE to its 11c-isomer (Fig. 1). The action spectrum for synthesis of 11c-*N*-ret-PE was nearly identical to the UV-visible absorbance spectrum of protonated at-*N*-ret-PE, both exhibiting maxima at ~450 nm (Fig. 1 and Supplementary Fig. 1). Light-dependent synthesis of the 9c-isomer and 13c-isomer also exhibited maxima at 450 nm, but were formed in much lower amounts than the 11c-isomer (Fig. 1a). Consistently, at-*N*-ret-PE showed light-dependent depletion, with an inverted action spectrum, also centered at 450 nm (Fig. 1b). To quantitate light-dependent formation of *cis*-isomers, we subtracted the amount of each *cis*-isomer in the dark-incubated samples from that in the 450-nm light-exposed samples (Fig. 1a). This yielded 121 pmol of 11c-, 18 pmol of 9-*cis*- (9c-), and 3.3 pmol of 13-*cis*- (13c-) *N*-ret-PE, balanced by 195 pmol of at-*N*-ret-PE consumed. These pmole values have relative but not absolute meaning. The ratio of 11cRAL to 13cRAL following photoisomerization of *N*-ret-PE was 37:1. Efficient photoconversion of at- to 11c-*N*-ret-PE suggests that *N*-ret-PE in OS may be a source of chromophore for the visual opsins in light-exposed retinas.

Synthesis of rhodopsin by OS membranes exposed to blue light. Next, we tested whether 450-nm light could induce synthesis of 11cRAL in native OS membranes. We prepared rod OS from the retinas of fresh, ex vivo dark-adapted bovine eyes. Equal aliquots of fresh OS membranes were exposed to UV-filtered white light (400-nm cutoff) to bleach the rhodopsin. Following addition of atRAL, one set of OS samples was placed in the dark while a second set was exposed to 450-nm monochromatic light for 30 min. The OS samples were extracted and analyzed for retinoid content by normal-phase LC. The UV-filtered white light photobleached approximately 95% of 11cRAL in the OS samples, indicating that most was in the form of rhodopsin since it was sensitive to visible light (Fig. 2a). OS samples exposed to 450-nm light for 30 min yielded a 7.8-fold increase in total 11cRAL over samples kept in the dark (Fig. 2a). These data suggest that OS membranes support light-driven synthesis of visual chromophore.

To test for light-dependent synthesis of rhodopsin, we again prepared fresh, dark-adapted bovine OS membranes. We divided the OS into samples containing two nmoles of rhodopsin. Some were photobleached by exposure to UV-filtered white light for 45 min while the remaining samples were kept in the dark. Ten nmoles of atRAL substrate was added to the photobleached samples. One set was incubated for 1 h in the dark while the other set was exposed to 450-nm light. We purified opsin protein from the OS samples by immunoaffinity chromatography and quantitated rhodopsin pigment by UV-visible absorbance spectroscopy (Figs 2b and c). The initial exposure to white light bleached 83% of the rhodopsin. No recovery of rhodopsin was observed following 1-h incubation in the dark. This was expected since the required chromophore-regenerating enzymes are not present in OS. In contrast, rhodopsin increased 2.4-fold in OS samples exposed to 450-nm light (Fig. 2c). These data show that free atRAL efficiently combines with PE to form at-*N*-ret-PE, and that following photoisomerization, 11c-*N*-ret-PE efficiently donates 11cRAL to regenerate rhodopsin in OS membranes.

***N*-ret-PE in dark-adapted mouse retinas**. Here we measured *N*-ret-PE in retinas from dark-adapted wild type (strain 129/Sv) mice. We extracted phospholipids from retina homogenates and separated them by reverse-phase LC. Three doublet peaks, all with λ_{max} near 450 nm, eluted between 21 and 38 min (Supplementary Fig. 2a). These peaks likely represent different fatty-acyl forms of *N*-ret-PE. We collected the eluates corresponding to these peaks, reacted the pooled fractions with hydroxylamine to form retinaldehyde oximes, and separated the oximes by normal-phase LC (Supplementary Fig. 2b). This allowed us to quantitate the retinaldehyde isomers of *N*-ret-PE in dark-adapted mouse retinas (Table 1). We also quantitated total

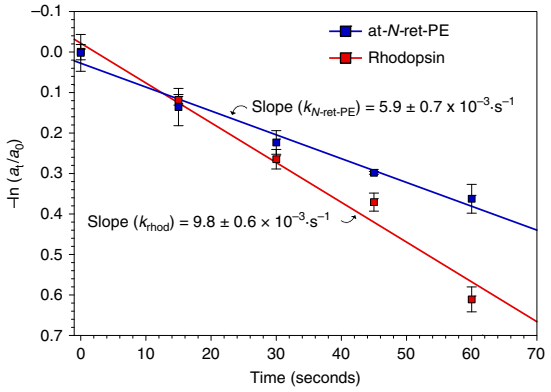

Fig. 3 Kinetics of rhodopsin and *N*-ret-PE photoisomerization. Protonated at-*N*-ret-PE and rhodopsin were exposed to 450-nm or 500-nm monochromatic light respectively at the same photon flux for the indicated times. The initial amounts of at-*N*-ret-PE and rhodopsin are represented by a_0, and the amounts at time *t* by a_t. The first-order rate constant (*k*) is described by: $kt = -\ln(a_t/a_0)$. Here, the slopes of the plots $-\ln(a_t/a_0)$ versus *t* yield the rate constants $k_{(N\text{-ret-PE})}$ and $k_{(rhod)}$. Each data point is shown as the mean ± s.e.m. ($n = 3$). The rate constants are also shown as mean ± s.e.m

retinaldehydes in dark-adapted (DA) 129/Sv mouse retinas (Table 1). Total retinaldehydes, representing mainly rhodopsin, contained predominantly 11cRAL, while *N*-ret-PE contained higher fractions of 13cRAL and atRAL (Table 1) reflecting the much lower thermal stability of *N*-ret-PE versus rhodopsin[21]. By combining the retinaldehyde isomers in *N*-ret-PE, we quantitated total *N*-ret-PE per dark-adapted mouse retina as 37 pmol (Table 1), or approximately 7% of the total retinaldehyde pool.

Quantum efficiency of *N*-Ret-PE. Upon exposure to 450-nm light, at-*N*-ret-PE is specifically converted to 11c-*N*-ret-PE (Fig. 1). Accordingly, we compared the rates of protonated at-*N*-ret-PE disappearance in 450-nm light to rhodopsin disappearance in 500-nm light, both with photon fluxes of 1.0 μmol/m^2 s. We plotted $-\ln(a_t / a_0)$ versus time, where a_t = amount of at-*N*-ret-PE or rhodopsin after illumination for *t* seconds and a_0 = initial amount without illumination ($t = 0$). This plot yielded the first-order rate constants, $k_{N\text{-ret-PE}}$ and k_{rhod} (Fig. 3). We determined the quantum efficiency[22] for *N*-ret-PE ($\Phi_{N\text{-ret-PE}}$) by the relationship shown in Eq. 1, as previously described[23, 24].

$$\Phi_{N-ret-PE} = \frac{\varepsilon_{rhod}}{\varepsilon_{N-ret-PE}} \times \frac{k_{N-ret-PE}}{k_{rhod}} \times \Phi_{rhod} \quad (1)$$

By inserting the molar extinction coefficients ($\mathcal{E}$) for rhodopsin at 500 nm (40,600 M^{-1} cm^{-1})[25] and *N*-ret-PE at 450 nm (31,300 M^{-1} cm^{-1}),[15] and the published quantum efficiency for rhodopsin ($\Phi_{rhod} = 0.65$),[26] we determined that $\Phi_{N\text{-ret-PE}} = 0.51 \pm 0.07$ (mean ± s.e.m.). The quantum efficiencies of rhodopsin and protonated *N*-ret-PE are therefore similar. The quantum efficiencies of cone opsins are similar to that of rhodopsin[27] and hence also to *N*-ret-PE.

Light-stimulated synthesis of chromophore by mouse retinas. Retinal G protein coupled receptor (RGR) opsin is a non-visual opsin in RPE and Müller cells of the retina[28]. Based on its similarity to squid retinochrome, and the phenotype of delayed rhodopsin regeneration in $Rgr^{-/-}$ mutant mice, RGR-opsin was proposed to function as a "reverse" photoisomerase for synthesis of visual chromophore[29]. The λ_{max} of protonated RGR-opsin is 469 nm[30], close to the λ_{max} of protonated *N*-ret-PE. Here we tested whether RGR-opsin contributes to the observed 450-nm light-dependent synthesis of 11cRAL. We prepared retina homogenates from wild type (strain 129/Sv) and $Rgr^{-/-}$ mutant (strain 129/Sv background) mice. After photobleaching the homogenates in UV-filtered (400 nm cutoff) white light, we added all-*trans*-retinol (atROL) substrate and incubated the homogenates in the dark or under 450-nm monochromatic light. Retinaldehydes formed during these incubations were quantitated by normal phase LC. As with bovine OS membranes (Fig. 2), the concentration of 11cRAL was approximately eight-fold higher in wild-type mouse retina homogenates exposed to 450-nm light compared to homogenates kept in the dark (Supplementary Fig. 3a). We observed no light-dependent stimulation of 9cRAL or 13cRAL (Supplementary Figs 3b,c), and the expected light dependent consumption of atRAL (Supplementary Fig. 3d). The high levels of 9cRAL and 13cRAL versus 11cRAL in retinal homogenates kept in the dark (Supplementary Figs 3b–d) is due to thermal isomerization of atRAL during the incubations[9]. Loss of RGR-opsin in $Rgr^{-/-}$ mouse retina homogenates had no effect on light-dependent formation of 11cRAL, in fact levels of 11cRAL were marginally higher in $Rgr^{-/-}$ versus wild-type retina homogenates exposed to 450-nm light (Supplementary Fig. 3a). As with wild-type mouse retinas, levels of 9cRAL and 13cRAL were not increased in $Rgr^{-/-}$ retinas following exposure to 450-nm light (Supplementary Figs 3b,c), while levels of atRAL exhibited a similar compensatory reduction (Supplementary Fig. 3d). These data suggest that RGR-opsin is not responsible for the observed blue light-dependent synthesis of visual chromophore.

Accelerated recovery of rhodopsin in live mice by blue light. To determine whether blue-light stimulates rhodopsin regeneration in vivo, we dark-adapted wild type (129/Sv) mice overnight. The mice were anesthetized and exposed to UV-filtered strobe light to bleach approximately 90% of the rhodopsin. We allowed one group of mice to recover in darkness, exposed another group to 450-nm light, and exposed the third group to 540-nm light, all for 10 min. Photon fluxes were the same for the 450-nm and 540-nm light (1.8 μmol/m^2 s). We chose 540 nm to complement 450 nm because these wavelengths bracket the λ_{max} of rhodopsin (500 nm) and are equally efficient at photoisomerizing rhodopsin. Immediately after the recovery period, we euthanized the mice, collected and homogenized their retinas, and performed immunoaffinity separation to isolate rhodopsin protein. To confirm similar recoveries of affinity purified rhodopsin protein independent of its ligand state, we determined the protein concentration of each supernatant fraction. The concentrations were similar, with a global average of 162 ± 18 μg/ml (s.e.m., $n = 15$). Next, we measured the amounts of functional rhodopsin in the same eluates by measuring the difference in 500-nm absorbance before and after bleaching with a strobe (Figs 4a, b).

Functional rhodopsin approximately doubled in samples from mice allowed to recover in the dark for 10 min versus samples from mice collected immediately following the bleach (Fig. 4b). Mice exposed to 450-nm light during post-bleach recovery showed an additional 1.5-fold increase in percent rhodopsin above the amount in mice that recovered in darkness (Fig. 4b). Finally, retinas from mice exposed to 540-nm light during recovery contained a lower percent of rhodopsin than retinas from mice that either recovered in the dark or were exposed to 450-nm light (Fig. 4b). The difference in rhodopsin levels

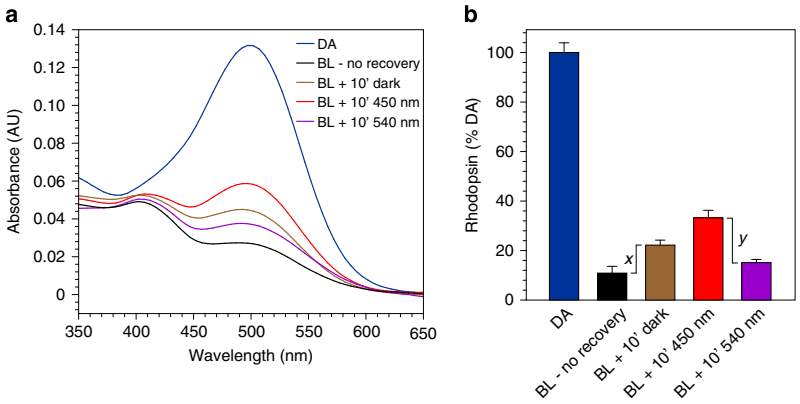

Fig. 4 Light dependent regeneration of rhodopsin in live mice. Wild-type mice were dark adapted overnight and exposed to the following light conditions: dark-adapted (DA); 90% strobe bleach with no recovery time (BL – no recovery); strobe bleach with 10 min recovery in the dark (BL + 10′ dark); strobe bleach with 10 min recovery in 450-nm light (BL + 10′ 450 nm); or strobe bleach with 10 min recovery in 540-nm light (BL + 540 nm). The photon fluxes of the 450-nm and 540-nm light were identical. The mice were euthanized, their retinas collected, and affinity purification of rhodopsin was carried out on the retina homogenates. **a** Representative baseline-normalized UV-Vis spectra of purified rhodopsin from mice exposed to the indicated light conditions. **b** Levels of rhodopsin visual pigment in retinas from mice exposed to the indicated light conditions, expressed as percent of dark-adapted rhodopsin. The value *x* represents the increase in rhodopsin during post-bleach recovery. The value *y* represents the difference in rhodopsin between mice exposed to 450-nm versus 540-nm light during recovery. Error bars show ± s.d. (n = 3)

between mice bleached with no recovery period and mice bleached with 10 min recovery in the dark represents rhodopsin regenerated by the enzymatic visual cycles (*x* in Fig. 4b). The difference in rhodopsin levels between mice that recovered in 450-nm light and mice that recovered in 540-nm light represents rhodopsin regenerated through photoisomerization of *N*-ret-PE (*y* in Fig. 4b). This applies because the 450-nm and 540-nm light photoisomerize rhodopsin with similar efficiency (Fig. 4a), while 540-nm light has little effect on protonated *N*-ret-PE (Fig. 1 and Supplementary Fig. 1). The radiant energies used in this experiment were 0.5 W/m^2 and 0.42 W/m^2 for the 450-nm and 540-nm light, respectively, yielding identical photon fluxes (1.8 µmol photons/m^2 s), similar to the radiant energy in a typical office environment. These results establish that blue-light dependent regeneration of rhodopsin occurs in live mice.

Increased photosensitivity of cones exposed to blue light. Rods comprise > 90% of photoreceptors in retinas from most mammalian species including mice, cattle and humans[31, 32]. Given the small percentage of cones, the blue light-dependent synthesis of 11cRAL observed in bovine OS and mouse retinas (Figs 2, 4) mainly reflects retinyl-lipid photoisomerization in rods. To test if photoisomerization of *N*-ret-PE contributes to regeneration of cone opsins, we made electrical recordings of cone photoresponses before and after bleaching with 450 nm or 560 nm monochromatic light. We chose these two wavelengths because the M-cones are equally sensitive to 450-nm and 560-nm light, while at-*N*-ret-PE is only photoisomerized to 11c-*N*-ret-PE by 450-nm light (Figs 1, 2). To do these experiments, we used a white-light LED and narrow-band interference filters. The absolute intensities at 450 nm and 560 nm (as measured with a calibrated photodiode) were nearly identical at all LED voltages. To demonstrate their equivalence, we measured the response of single M-cones at these two wavelengths as a function of LED intensity (Fig. 5a). Because the maximum amplitude of the current responses varied somewhat from cell to cell, primarily as the result of small differences in the seal of the suction pipette around the cell, we normalized responses (*R*) to maximum response amplitudes (R_{max}) at each of the two wavelengths. After normalization, response amplitudes as a function of flash intensity were nearly identical.

We then recorded photovoltages from M-cone enriched whole dorsal retinas (Fig. 5b) and suction-electrode responses from single M-cones (Fig. 5c). All of our M-cone recordings (including those in Fig. 5a) were made from *Gnat1*$^{-/-}$ mice lacking rod α-transducin, which exhibit normal cone photoresponses but no detectable rod response[33]. We exposed retinas or groups of cells to either 450-nm or 560-nm monochromatic light for 15 sec at the same photon fluxes calculated to bleach 85% of cone M opsin[34, 35], assuming a pigment photosensitivity of 6×10^9 µm^2. After bleaching with either wavelength, M-cones were stimulated at 500 nm, near the λ_{max} of M-cone opsin (508 nm).

The results of these experiments are shown in Fig. 5b for whole-retina recordings and Fig. 5c for suction-electrode recordings. These figures give the value of $I_{½}$ from fits of response amplitudes to the Michaelis–Menten function (see Methods). The value of $I_{½}$ quantifies the amount of light necessary to produce a half-maximal response. Thus the greater the value of $I_{½}$, the more light required to produce a half-maximal response and the lower the sensitivity. Our recordings show that $I_{½}$ was not significantly different in darkness for either whole-retina recordings ($p = 0.357$) or suction-electrode recordings ($p = 0.675$), as would be expected from the results of Fig. 5a. The value of $I_{½}$ increased after both 450-nm and 560-nm bleaches, indicating a drop in sensitivity. The amplitude of this decrease in sensitivity was smaller after the 450-nm bleach compared to the 560-nm bleach by a factor of approximately two. Although we observed small changes in sensitivity with time especially for the 560-nm bleaches, these changes were not significant. We therefore averaged measurements from all the time points, which gave mean $I_{½}$ values for the suction-electrode recordings of $2.6 \pm 0.2 \times 10^4$ after the 450-nm bleach ($n = 75$), and $5.9 \pm 0.9 \times 10^4$ after the 560-nm bleach ($n = 60$). This sensitivity difference was highly significant (Student's *t*, $p < 0.001$). A similar comparison for the whole-retina recordings was also statistically significant (Student's *t*, $p < 0.005$). Thus, with

two different preparations and recording techniques, we observed higher sensitivity in mouse cones after exposure to 450-nm versus 560-nm light. Since M cones were equally sensitive to our 450-nm and 560-nm lights (Fig. 5a), the two illuminations should have produced nearly equal bleaches. The smaller decrease in sensitivity after the 450-nm bleach is consistent with a role for retinyl-lipid photoisomerization in cone pigment regeneration.

Discussion

Rhodopsin and the cone opsin pigments require a continuous supply of visual chromophore to maintain photosensitivity in bright light. One molecule of 11cRAL is required for each photon absorbed. The endergonic conversion of atRAL to 11cRAL is carried out by multi-step enzyme pathways in RPE and Müller cells. Estimates of the maximum turnover rates suggest that the visual cycles cannot keep up with the high rates of rhodopsin and cone-opsin photoisomerization occurring in daylight[36]. Here we demonstrate a non-enzymatic mechanism for visual pigment regeneration involving photoisomerization of retinyl phospholipids in OS disk membranes (Fig. 6).

The OS membranes conduct 11cRAL and atRAL to and from the opsins during light exposure. Both retinaldehyde isomers reversibly condense with PE to form *N*-ret-PE. Protonated at-*N*-ret-PE was converted with remarkable specificity to 11c-*N*-ret-PE by blue light (Fig. 1). As an indication of this specificity, the ratio of 11cRAL to 13cRAL after exposure of at-*N*-ret-PE to 450-nm light was 37:1 (Fig. 1a). In contrast, the ratio of 11cRAL to 13cRAL at thermal equilibrium is 1:240[37]. Therefore, the 11c-isomer was enriched nearly 9000-fold by light over its equilibrium concentration during exposure to 450-nm light. This property of *N*-ret-PE[16] allows it to serve as a source of visual chromophore. The retinoid isomerases, Rpe65 and DES1 of the canonical and non-canonical visual cycles both exhibit much lower 11c-specificity[9, 38]. The difference in free energy between atRAL and 11cRAL is 4.1 kcal/mole[37]. Both Rpe65 and DES1 use hydrolysis of a retinyl ester to drive retinoid isomerization[9, 10, 39]. The actual metabolic cost of retinoid isomerization is 7.5 kcal/mol from hydrolysis of an activated fatty acid. In contrast, the energy of a 450-nm photon is 64 kcal/mol, far more than required to convert at-*N*-ret-PE to 11c-*N*-ret-PE. Regeneration of visual chromophore through retinyl-lipid photoisomerization is a unique example of an energy-requiring metabolic reaction in mammals being powered by visible light.

The membranes of most mammalian cells contain 15–25% PE[40], while OS disk membranes contain 38% PE[15]. The ratio of phospholipids to rhodopsin is 100:1 in OS membranes[41], hence PE is at 38-fold molar excess over rhodopsin. This abundance of PE in OS disks promotes formation of *N*-ret-PE from free retinaldehyde released by rhodopsin, and thereby photoregeneration of visual chromophore. *N*-ret-PE is the translocated substrate for the ABCA4 flippase in OS discs[18]. ABCA4 is the product of the gene affected in recessive Stargardt macular degeneration[42]. Loss of ABCA4 in Stargardt patients and *Abca4*$^{-/-}$ mice causes accumulation of bisretinoids that arise

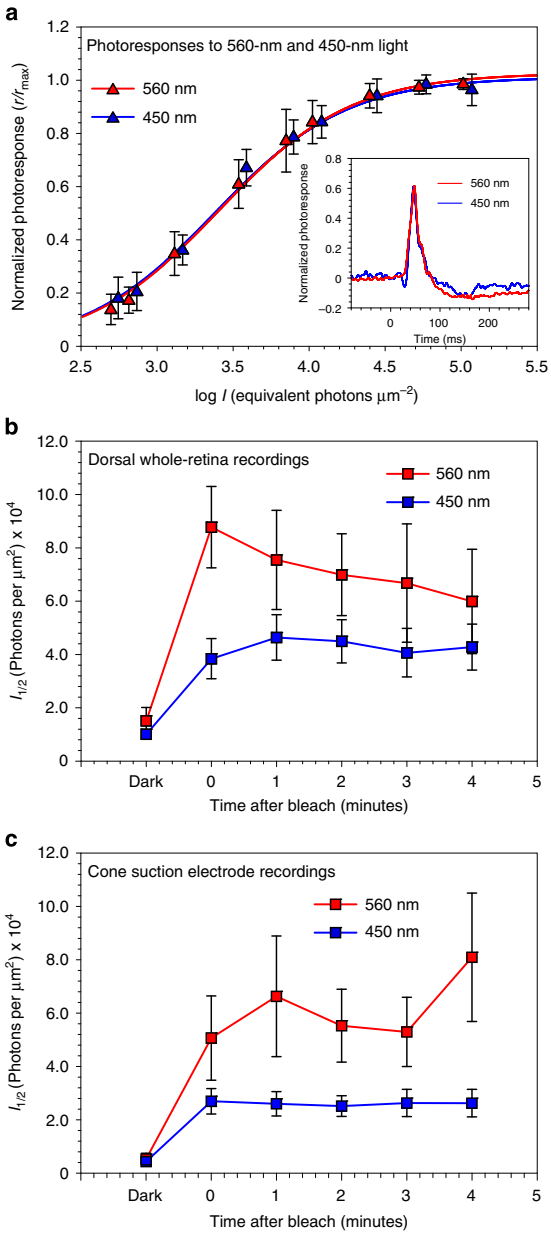

Fig. 5 Photosensitivity in *Gnat1*$^{-/-}$ cones after exposure to 450-nm or 560-nm light. Photoresponses were recorded from M (508-nm) cones in *Gnat1*$^{-/-}$ retinas before and after 15-second exposures to 450-nm or 560-nm light calculated to bleach 85% of the M-cone pigment. **a** Mean suction-electrode responses (±s.e.m.) from dark-adapted M cones as a function of flash intensity to 450-nm ($n = 7$) and 560-nm ($n = 10$) light at the same LED current and flash durations. Peak response amplitudes (r) were separately normalized to maximum peak response amplitudes at saturating light intensities (r_{max}) for the two wavelengths, and intensities were multiplied by 0.6 to give equivalent intensities at the λ_{max} of the M-cone pigment. Curves are Michaelis-Menten equation with values of $I_{1/2}$ of 2410 for 450 nm and 2560 for 560 nm (in equivalent photons µm^{-2}). Inset: mean responses to 450-nm and 560-nm light of flashes 2.5 ms in duration at intensities of approximately 3600 equivalent photons µm^{-2}. **b**,**c** Mean M-cone responses (±s.e.m.) before and after bleaching 85% of the cone visual pigment from **b** whole dorsal *Gnat1*$^{-/-}$ retinas from five mice and **c** suction-electrode recordings from single *Gnat1*$^{-/-}$ cones ($n = 14$ for 450-nm bleach, $n = 12$ for 560-nm bleach). Bleaching was performed with the same 450-nm and 560-nm light sources used in **a**. Cones and whole retinas were stimulated before and after the photobleach with three 500-nm flash intensities spanning the range of cone responses from small to nearly saturating. Mean response amplitudes were used to estimate the intensity required to produce a half-maximal response from fits to the Michaelis-Menten equation

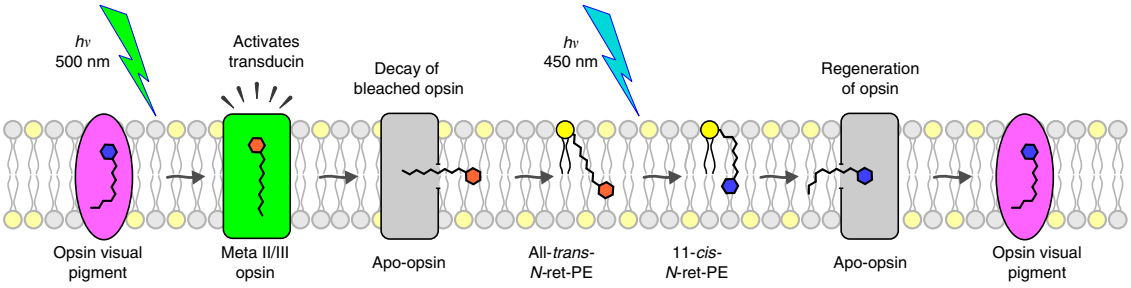

Fig. 6 Retinyl-lipid photoregeneration of opsins in rod or cone OS. The results presented here suggest the existence of a light-driven mechanism to regenerate visual pigments in rod and cone OS through photoisomerization of retinyl-lipids. This diagram shows the phospholipid bilayer of a rod OS disk. Rhodopsin absorbs a 500-nm photon (*hv*) that photoisomerizes its 11cRAL chromophore to atRAL, converting the pigment to its active metarhodopsin II/III (meta II/III) state. After a brief signaling period, the bleached opsin decays, releasing free atRAL into the bilayer. The atRAL reversibly condenses with PE (yellow circles) to form at-*N*-ret-PE. Protonated at-*N*-ret-PE is converted specifically to 11c-*N*-ret-PE upon absorption of a 450-nm photon. Spontaneous hydrolysis of 11c-*N*-ret-PE yields free 11cRAL, which irreversibly combines with unliganded apo-opsin to form a new rhodopsin pigment. A similar process occurs in cone OS to regenerate cone opsin pigments

through delayed clearance and secondary condensation of *N*-ret-PE with another retinaldehyde[43, 44]. We quantitated *N*-ret-PE in dark-adapted mouse retinas by comparing retinaldehydes contained in *N*-ret-PE to total retinaldehydes, which are mostly 11cRAL in rhodopsin (Supplementary Figs 2a,b and Table 1). *N*-ret-PE comprised ~7% of total retinaldehydes in a dark-adapted retina. 11cRAL not associated with rhodopsin undergoes thermal isomerization to its lower-energy isomers in the dark. This is exemplified by the higher fraction of atRAL and 13cRAL in *N*-ret-PE versus total retina following overnight dark adaptation (Table 1). Within the OS, any 11cRAL that thermally isomerizes to atRAL or 13cRAL would be quickly restored to the 11c-configuration through photoisomerization of *N*-ret-PE. Thus, 11c-*N*-ret-PE represents a protected and readily available pool of visual chromophore in photoreceptor OS.

While rods are single-photon detectors with a photoresponse that saturates in bright light, cones are less sensitive, providing color vision in bright light with a photoresponse that never saturates. Accordingly, cones seem better suited than rods to benefit from chromophore photoregeneration. We employed two experimental systems to test whether photoisomerization of *N*-ret-PE contributes to cone opsin regeneration. First, we recorded cone photovoltages from whole dorsal retinas of *Gnat1*$^{-/-}$ mice. We observed approximately two-fold greater sensitivity of M cones in the explants following exposure to 450-nm versus 560-nm light at the same photon flux (Fig. 5b). We also performed suction recording from isolated M-cone photoreceptors. Here again, we observed approximately two-fold greater sensitivity following a photobleach with 450-nm versus 560-nm light (Fig. 5c). These differences in cone photosensitivity are consistent with the higher levels of rhodopsin in mouse retinas following in vivo exposure to 450-nm versus 540-nm light (Fig. 4b). Hence, cones as well as rods appear to use photoisomerization of retinyl-lipids to regenerate visual pigments.

Although we used 450-nm light to uncover *N*-ret-PE photoisomerization, monochromatic light is not required for retinyl-lipid photoregeneration. In fact, white light is far more effective at photoisomerizing *N*-ret-PE than narrow-band 450-nm light, as indicated by the broad absorbance spectrum of protonated *N*-ret-PE (Supplementary Fig. 1). Given their overlapping spectra (Supplementary Fig. 1 and Fig. 4a), photoisomerization of *N*-ret-PE and bleaching of rhodopsin occur simultaneously in natural light. The rate of rhodopsin bleaching was slightly faster than the rate of *N*-ret-PE photoisomerization (Fig. 3), consistent with the observation that light exposure causes net depletion of visual pigments in retina membranes. Photoisomerization of *N*-ret-PE is therefore in the "kinetic shadow" of rhodopsin bleaching and difficult to observe.

The bleach/recovery experiment in mice (Fig. 4) allowed us to compare contributions of the enzymatic visual cycles to retinyl-lipid photoregeneration. Rhodopsin increased above its immediate post-bleach levels during the 10-min recovery period in the dark (Fig. 4b). This increase, shown by x in Fig. 4b, is due to the chromophore-synthesis activities of the enzymatic visual cycles. Significantly higher rhodopsin levels were seen in retinas from mice that recovered under 450-nm light, while lower rhodopsin levels were seen in retinas from mice that recovered under 540-nm light (Fig. 4b). Rhodopsin was bleached to the same extent by the 450-nm and 540-nm lights, while only 450-nm light significantly photoisomerized *N*-ret-PE (Fig. 1 and Supplementary Fig. 1). Accordingly, three factors affected rhodopsin levels in retinas from mice that recovered under 450-nm light: (i) the enzymatic visual cycles, (ii) photoisomerization of rhodopsin and (iii) photoisomerization of *N*-ret-PE; while only two factors affected rhodopsin levels in samples from mice that recovered under 540-nm light: (i) the enzymatic visual cycles and (ii) photoisomerization of rhodopsin. The contribution of *N*-ret-PE photoisomerization to rhodopsin regeneration is therefore represented by the difference in rhodopsin levels between samples that recovered under 450-nm and 540-nm light (y in Fig. 4b). Since $y > x$, photoisomerization of *N*-ret-PE contributed more to rhodopsin regeneration than did the enzymatic visual cycles under these light conditions.

The cone suction-recording experiment provided additional information about the contribution of retinyl-lipid photoisomerization to opsin pigment levels. Using the relationships in Eq. 3 and 4 (Methods), we estimated that cones exposed to 450-nm light behaved as if they contained approximately 15% more pigment than cones exposed to 560-nm light, suggesting a 15% contribution of *N*-ret-PE photoisomerization to cone opsin regeneration under these conditions. In nature, the contribution of retinyl-lipid photoisomerization to opsin pigment regeneration probably increases with intensifying ambient light. Retinyl-lipid photoregeneration may be required for sustained vision in daylight.

Methods

Animal use and care statement. This study was carried out in accordance with recommendations in the guide for the care and use of laboratory animals of the National Institutes of Health, and the Association for Research in Vision and

Ophthalmology Statement for the use of animals in ophthalmic and vision research. The animal use protocol was approved by the University of California, Los Angeles Animal Research Committee (permit number: A3196-01). Euthanasia was performed by cervical dislocation on deeply anesthetized (xylazine 10 mg/kg and ketamine 100 mg/kg) mice. All steps were taken to minimize pain and distress in the mice.

Synthesis and purification of at-N-Ret-PE. All reactions were performed under dim red light. We synthesized at-*N*-ret-PE according to published methods[45] with modifications. Briefly, atRAL (Sigma-Aldrich) was mixed with 5.6 mg 1-oleoyl-2-hydroxy-*sn*-glycero-3-phosphoethanolamine (18:1 lyso PE, Avanti Polar Lipids) in three ml of a solution containing six volumes of methanol (Fisher Scientific), 12 volumes of chloroform (Sigma-Aldrich) and one volume of triethylamine (Sigma-Aldrich). The solution was incubated at room temperature for 1 h with gentle mixing in the dark. Three ml of one-M hydrochloric acid (EM Science) was added and the mixture was centrifuged at 3500 × *g* for 5 min. The lower organic phase (chloroform) containing at-*N*-ret-PE was collected and the upper phase was extracted again with 2 ml chloroform. The pooled extracts were further rinsed with 3 ml of one-M hydrochloric acid, and the final chloroform extracts were dried under a stream of nitrogen and dissolved in acidified methanol (20-µl trifluoroacetic acid (TFA) per liter methanol). The at-*N*-ret-PE was purified in its protonated form by reverse-phase LC (see below) with an elution time of approximately 14 min. By this method, free atRAL eluted at approximately 10 min.

Action spectrum of at-N-Ret-PE. Ten µM at-*N*-ret-PE was dissolved in acidified methanol (20 µl TFA per liter) to maintain the protonated state. Its concentration was determined by absorption at 450 nm using a Shimadzu UV-2401PC UV-Vis spectrophotometer and a molar extinction coefficient of 31,300 $M^{-1}cm^{-1}$ [15]. Triplicate samples were placed into quartz 10 mm cuvettes (SCC) covered in black paper with only the front side exposed to light. The samples were either kept in the dark or illuminated with monochromatic light at wavelengths of 325 to 650 nm with 25-nm increments at room temperature for 80 s. The monochromatic light was generated by a custom monochromator (Newport Instruments) with a xenon arc lamp. The light intensities were measured with a spectroradiometer (Black-comet CXR-SR-50, StellarNet Inc.) and adjusted (from 0.35 W/m^2 at 325 nm to 0.18 W/m^2 at 650 nm) such that each wavelength delivered a photon flux of 0.95 µmol photons/(m^2 s). Two hundred µl from each sample were analyzed by normal-phase LC.

Normal-phase LC analysis of retinoids. Retinoids were treated with 20–25 µl 5% sodium dodecyl sulfate (SDS) (for samples of at-*N*-ret-PE in methanol, SDS was not added) and 50 µl brine. To quantitate retinaldehydes in *N*-ret-PE and opsin pigments, retinaldehyde oximes were generated by addition of hydroxylamine hydrochloride (200–500 µl of 2 M solution, pH 7.0) (Sigma). The samples were mixed by vortexing and incubated at room temperature for 15 min. 2 ml of methanol were added and the samples were extracted twice with 2 ml hexane as previously described[9]. The identity of each eluted peak was established by comparing the spectra and elution times with those of authentic retinoid standards. Sample peaks were quantitated by comparing peak areas to calibration curves established with retinoid standards. Peak areas for the corresponding *syn*-oximes and *anti*-oximes were summed to quantitate each retinaldehyde isomer.

Determination of the decay constants. Bovine rod OS were purified by published methods[46] and used as the source of rhodopsin. Purified rod OS were dissolved in 20 mM sodium phosphate (Fisher Scientific) buffer pH 7.2 with 100 mM sodium chloride (Fisher Scientific), 2.5% sucrose (Fisher Scientific) and 2% CHAPS (Calbiochem), and diluted to an absorbance of 0.22 AU at 500 nm (the λ_{max} of rhodopsin). Purified protonated at-*N*-ret-PE was diluted in acidified methanol to yield an absorbance of 0.22 AU at 450 nm (the λ_{max} of at-*N*-ret-PE). Triplicate aliquots of purified rod OS were exposed to 500-nm monochromatic light at 0.25 W/m^2 (1.0 µmol photons/m^2 s) at room temperature for 0, 15, 30, 45, and 60 s. Triplicate aliquots of protonated *N*-ret-PE were exposed to 450-nm monochromatic light at 0.28 W/m^2 (1.0 µmol photons/m^2 s) and otherwise treated identically as the rhodopsin samples. Two hundred µl from each sample were removed and analyzed for retinoid content by normal-phase LC. The amount of rhodopsin at each time point was determined by quantitation of 11cRAL.

Reverse-phase LC of phospholipids. Phospholipid extraction was performed with modifications to a previously published protocol[47]. All extractions were performed under dim red light. Retina homogenates from 8-week-old strain 129/Sv mice or bovine OS were extracted by the addition of 3 ml of 1:2 (vol/vol) mixture of chloroform (Sigma) and acidified methanol (Fisher) (one L methanol + 8 µl trifluroacetic acid (Sigma)) followed by brief vortexing and incubation on ice for 10 min. Next, 1.3 ml of 0.3 M NaCl were added and the samples extracted twice into one ml chloroform with centrifugation at 1750 × g for 10 min at 10 °C to separate phases. The pooled chloroform layers were transferred to 16 × 100 mm borosilicate glass test tubes and evaporated to dryness under a stream of nitrogen. Samples were dissolved in 100 µl of acidified methanol and analyzed by reverse-phase LC[48] on an Agilent 1100 series chromatograph equipped with a photodiode-array detector using an Phenomenex Primeshere C18-HC 110 A column (250 × 4.6 mm) and a 15–0% water gradient in acidified methanol (8 µl TFA/L methanol) at a flow rate of 1.0 (gradient) to 2.4 (isocratic) ml per min. Spectra (190–550 nm) were acquired for all eluted peaks. The identity of each eluted peak was established by comparing the spectra and elution times with those of authentic retinoid and *N*-ret-PE standards. Sample peaks were quantitated by peak area.

Mice and genotyping. All mice were reared in cyclic light. The 129/Sv wild-type control mice were purchased from Taconic Biosciences, Inc. Retinal G protein-coupled receptor knockout (*Rgr*$^{-/-}$) mice[29] were generously provided by Henry Fong, genotyping protocols and strain background information were reported previously[49]. *Gnat1*$^{-/-}$ mice lacking rod α-transduc in[33] were generously provided by Janis Lem. All mice were genotyped to exclude the *rd8* and *rpe65* L450M mutations. The primers for each genotyping: *rd8*, F: 5′GGTGACCAATCTGTTG ACAATCC, R: 5′GCCCCATTTGCACACTGATGAC; *rpe65* codon 450, F: 5′CCTTTGAATTTCCTCAAATCAATTA, R: 5′TTCCAGAGCATCTGGTTGAG.

Rhodopsin purification from mouse retinas. Retinas from 8-week-old wild-type (strain 129/Sv) mice were dissected under dim red light and homogenized in a glass to glass tissue grinder (Kontes) in solubilization buffer (40 mM Tris (Fisher) pH 7.2, 1% CHAPS (Fisher), and 0.1 mg/ml PMSF (Sigma)). The homogenates were spun at 17,000 × g for 15 min at 4 °C to pellet cell debris. Collected supernatants were added to 100 µl agarose beads coupled to the 1D4 antibody against rhodopsin (PureCube Rho1D4 Agarose), washed with solubilization buffer, and incubated overnight with agitation at 4 °C. Beads were combined with elution buffer (40 mM Tris pH 7.2, 1% CHAPS, 200 µM 1D4 peptide (Cube Biotech)) for 1 h at room temperature. The beads were then pelleted by centrifugation (3000 RPM for 5 min, Eppendorf 5415D centrifuge) and the rhodopsin-containing supernatants were collected. Rhodopsin was quantified spectrophotometrically at 500 nm (Shimadzu UV-2401PC UV-Vis spectrophotometer) using the molar extinction coefficient of 40,600 $M^{-1}cm^{-1}$ [25].

Rhodopsin purification from bovine rod OS. Bovine rod OS were prepared from the eyes of freshly slaughtered cattle using published procedures[46]. Purified OS in 50 µl aliquots containing 2-nmoles rhodopsin were prepared in triplicate for each light condition. OS samples for rhodopsin regenerative studies were bleached on ice (12,000 lux for 45 min with a halogen lamp) to remove endogenous retinoids. The OS were supplemented with 50 µM atRAL in dimethyl sulfoxide and diluted to 200 µl with pH 6.0 phosphate-citrate buffer containing 0.1 mg/ml PMSF. Samples were incubated overnight at 4.0 °C with gentle agitation. The following day, samples were incubated at 37 °C for 30 or 60 min with gentle agitation in the dark or under 450-nm monochromatic light (20-nm bandwidth) at 0.5 W/m^2. Samples incubated for 30 min were extracted and analyzed for retinoid content by normal-phase LC to measure production of 11cRAL. Rhodopsin was purified from samples incubated for 1 h using Rho 1D4-agarose (Cube Biotech) as described above. Absorbance spectra were acquired for all samples using a Shimadzu UV-2401PC UV-Vis spectrophotometer. Difference spectra were acquired after bleaching the samples in the same cuvette with a Novatron strobe light (3 × 1500 W). The difference spectra were normalized to the baseline (A_{650}) and protein content (A_{280}). Additional OS samples (dark and 450-nm light-treated) were examined for *N*-ret-PE content by reverse-phase LC, as described above. Peaks identified as *N*-ret-PE by their absorbance spectra were collected, reacted with hydroxylamine to form retinaldehyde oximes, and re-analyzed by normal-phase LC to determine the retinaldehyde content of *N*-ret-PEs.

Photoisomerization in retina homogenates from mice. Eight to 10-week-old wild type (strain 129/Sv) and *Rgr*$^{-/-}$ (129/Sv background) mice were euthanized and their eyes collected. Retinas from mice of each genotype were pooled and disrupted by glass/glass homogenization (Kontes) in 6.0 ml 40 mM Tris buffer pH 7.2. The homogenates were extensively bleached (20,000 lux from a xenon arc lamp with a 400-nm UV cutoff filter for 45 min) to destroy endogenous retinoids. Protein concentrations were determined (Pierce BCA Protein Assay Kit, Thermofisher) and used for normalization of pre- and post-bleach retinoid content. Photoisomerization assays were performed on similar homogenate samples in 500 µl reactions with addition of 5% BSA, 25 µM all-*trans*-retinol, and 500 µM $NADP^+$ (all from Sigma). Samples were placed in cuvettes and agitated in the dark or during exposure to 450-nm light (10-nm bandwidth with an irradiance of 0.2 W/m^2) for 25 min at 37 °C. Retinoids were extracted from samples and analyzed by normal-phase LC, as described above.

Blue-light dependent regeneration of rhodopsin in live mice. Triplicate sets of 8-week-old wild type (129/Sv) mice were dark adapted overnight. All mice were anesthetized as described above and their pupils dilated with one drop of 1.5% tropicamide and 2.5 % phenylephrine. Three sets of six mice were kept in the dark for the dark-adapted (DA) rhodopsin determinations (90 mice total). The remaining mice were bleached by exposure to ten 1500-W flashes of a Novatron strobe. We observed no change in the thickness of any retina layer by optical coherence

tomography at one and 7 days post-exposure, indicating that the strobe light caused no retinal damage in mice. Immediately post-bleach, three sets of six mice were euthanized, their retinas collected (12 retinas per sample) and homogenized, as described above. The remaining nine sets of six mice were exposed for 10 min to one of three different light conditions: (i) darkness, (ii) 450-nm light, or (iii) 540-nm light. Both "monochromatic" light sources had a 10-nm bandwidth. The irradiances on the corneal surfaces were 0.5 W/m^2 for the 450-nm light and 0.42 W/m^2 for 540-nm light, to yield identical photon fluxes of 1.8 µmol photons/m^2 s. Immediately following the 10-min recovery periods, the mice were euthanized in the dark, their retinas dissected (12 retinas per sample) and homogenized, as described above. Rhodopsin was purified from mouse retina homogenates by immunoaffinity chromatography, also as described above. After purification, rhodopsin was quantitated by difference spectra analysis. The purified rhodopsin samples were also analyzed for 11cRAL and atRAL content by normal-phase LC.

Whole-retina and cone-suction recordings from mouse cones. *Gnat1*$^{-/-}$ mice (8-week-old) reared under cyclic light were dark-adapted overnight then euthanized. Their eyes were marked with a cauterization tool at the ventral pole, enucleated, and only the dorsal retina, which contains predominantly middle-wavelength sensitive (M) cones[50], was collected. The dorsal retinas were isolated from the RPE and perfused with Ames solution (Sigma) containing an additional 1.9 g/l $NaHCO_3$ and bubbled with 95% O_2 / 5% CO_2. For whole-retina recordings of cone responses, dorsal retinas were placed photoreceptors up on Whatman Anodisc filter membranes (Sigma) in a custom built recording chamber. Retinas were isolated and perfused with 2 mM aspartic acid and 40 µM DL-AP4 (Tocris, Bristol, UK) on the photoreceptor side and 2 mM aspartic acid and 1 mM barium chloride (Sigma) on the ganglion-cell surface. Photovoltages were measured with a DP-311 differential amplifier (Warner Instruments, Hamden, CT). For suction recordings, retinas were sliced into pieces and recordings were made from individual cone inner segments[51]. Both preparations were stimulated with an LED optical system (Cairn Research, Faversham, UK) coupled to an inverted microscope. Test flashes were delivered with a 505-nm LED through a 500-nm interference filter. Cones were bleached with either 450-nm or 560-nm illumination from a white-light LED and interference filters at 450 nm and 560 nm. The intensities of the test and bleaching lights were calibrated with a photodiode (United Detector Technology, San Diego, CA). The intensities of the 450-nm and 560-nm illuminations from the LED were nearly the same at the same diode currents, and M-cones were equally sensitive to these two wavelengths at the same diode intensities and flash durations (see Fig. 5a). Recordings were filtered with an 8-pole Bessel filter and sampled at 100 Hz. Data were displayed and analyzed with PCLAMP (Molecular Devices, Sunnyvale, CA) and Origin plotting software (OriginLabs, Cambridge, MA).

Estimation of sensitivity. Sensitivities for Fig. 5b and c were estimated by measuring responses to two dim light intensities and to a nearly saturating bright light. The test-flash intensities were (photons µm^{-2}) 2840, 9690, 200,000 before bleaches and 19,000, 43,200, 200,000 following bleaches for Fig. 5b (whole retina); and 2200, 3500, and 66,600 before bleaches and 6900, 15,500, and 66,600 after bleaches for one series of experiments, and 650, 5,410, and 95,000 before the bleaches and 9200, 40,500, and 220,000 after bleaches for a second series for Fig. 5c (suction-electrode recordings). At each intensity, 10 flashes were given at 1-s intervals for the dim flashes, or every 1.5 s for the nearly saturating flashes, and response amplitudes were averaged. The determinations at 0 min were begun 10 sec after the bleach; recovery of photoresponse and maximum response amplitude was virtually complete after 10 s, even for these large bleaches[52]. Determinations at 1–4 min were begun one to 4 min after the bleach. Each determination took a total of about 40 s. Sensitivities were then determined by fitting each series of three mean response amplitudes to the Michaelis–Menten equation (Eq. 2),

$$r = r_{\max}\frac{I}{I + I_{1/2}} \quad (2)$$

where r is response amplitude in pA, $r_{\max}$ is the maximum value of r, I is intensity in 500-nm photons µm^{-2}, and $I_{1/2}$ is a constant equal to the intensity of the flash producing a half-maximal response. The Michaelis–Menten relation predicts that responses at dim light intensities ($I \ll I_{1/2}$) are directly proportional to light intensity, with a proportionality constant equal to $r_{\max}/I_{1/2}$. This proportionality constant gives the response per unit light intensity at dim light intensities in the linear range of the Michaelis–Menten relation and is therefore equal to the sensitivity of the photoreceptor. Sensitivity is thus inversely related to $I_{1/2}$, and plotting the value of $I_{1/2}$ is therefore a meaningful and appropriate way to display differences in cone sensitivity provided there are no changes in $r_{\max}$. In Fig. 5 we therefore show the changes in the value of $I_{1/2}$ after the 450-nm and 560-nm bleaches. There were no significant changes in $r_{\max}$.

Estimation of cone pigment regenerated from N-Ret-PE. Previous experiments have shown that photoreceptor desensitization after strong bleaches is the result of two mechanisms: (i) the decrease in quantum catch produced by the decrease in concentration of unbleached pigment, and (ii) adaptation produced by activation of the cascade by bleached pigment[53, 54, 55]. These two mechanisms sum to produce a decrease in sensitivity that is well described by the equation (Eq. 3)

$$\frac{S_F}{S_F^D} = \frac{1 - F}{1 + kF} \quad (3)$$

where S_F is the sensitivity of the photoreceptor, S_F^D is the sensitivity in darkness, F is the fraction bleached, and k is a constant, equal to 34–35 for mouse rods[56] but 8.6 for salamander cones[53].

Although no similar measurements have been made for bleached mouse cones, we can estimate the value of k from our data if we assume that, following the 560-nm bleach, no pigment regeneration occurred. We need first to use the values of $I_{1/2}$ before and after bleaching to estimate S_F/S_F^D. We observe that the Michaelis–Menten equation (Eq. 2) provides an adequate description of the responses of cones to increasing flash intensity (Fig. 5a); and that for dim flash intensities ($I \ll I_{1/2}$), the amplitude of the response (and therefore the sensitivity of the cone) is inversely proportional to $I_{1/2}$. Therefore, we can estimate S_F^D as 2560/59,000 or 0.043 after the 560-nm bleach, and 2410/26,000 or 0.093 after the 450-nm bleach.

Now, if no pigment regeneration had occurred after the 560-nm bleach, $F = 0.85$ and we can solve equation in Eq. 3 for k and obtain a value of 2.9, considerably lower than for salamander cones. We now insert this value into Eq. 3 and solve for the fraction bleached (Eq. 4).

$$F = \frac{1 - \frac{S_F}{S_F^D}}{1 + k\frac{S_F}{S_F^D}} \quad (4)$$

If k is 2.9 and, after the 450-nm bleach, S_F/S_F^D is 0.093, then F is 0.71 instead of 0.85. The cones are behaving as if the 450-nm light had produced approximately 15% less bleached pigment than the 560-nm bleach, presumably because of retinyl-lipid photoisomerization. We note that if we have underestimated the value of k, and it is in fact larger and nearer to that for salamander cones or mouse rods, the value of F from Eq. 4 would have been smaller and the amount of pigment regenerated through *N*-ret-PE photoisomerization even larger.

Reproducibility and statistical analysis of mouse studies. No power studies were performed on mouse experiments. No experimental animals were excluded from analysis. No randomization or blinding was used in the mouse studies. Statistical significance (p-values) were determined either with a two-tailed Welch's t-test or Student's t. p-values of less than 0.05 were considered significant.

Data availability. All data generated and analyzed during this study are included in this published article and its Supplementary Information files, and available from the corresponding author upon request.

Received: 28 December 2016 Accepted: 15 February 2017
Published online: 04 May 2017

References

1. Montell, C. *Drosophila* visual transduction. *Trends. Neurosci.* **35**, 356–363 (2012).
2. Ebrey, T. & Koutalos, Y. Vertebrate photoreceptors. *Prog. Retin. Eye Res.* **20**, 49–94 (2001).
3. Williams, T. P. Photoreversal of rhodopsin bleaching. *J. Gen. Physiol.* **47**, 679–689 (1964).
4. Grimm, C., Reme, C. E., Rol, P. O. & Williams, T. P. Blue light's effects on rhodopsin: photoreversal of bleaching in living rat eyes. *Invest Ophthalmol. Vis. Sci.* **41**, 3984–3990 (2000).
5. Arnis, S. & Hofmann, K. P. Photoregeneration of bovine rhodopsin from its signaling state. *Biochemistry* **34**, 9333–9340 (1995).
6. Furutani, Y., Kandori, H. & Shichida, Y. Structural changes in lumirhodopsin and metarhodopsin I studied by their photoreactions at 77 K. *Biochemistry* **42**, 8494–8500 (2003).
7. Wright, C. B., Redmond, T. M. & Nickerson, J. M. A history of the classical visual cycle. *Prog. Mol. Biol. Transl. Sci.* **134**, 433–448 (2015).
8. Wang, J. S. & Kefalov, V. J. The cone-specific visual cycle. *Prog. Retin. Eye. Res.* **30**, 115–128 (2011).
9. Kaylor, J. J. *et al.* Identification of DES1 as a vitamin a isomerase in Muller glial cells of the retina. *Nat. Chem. Biol.* **9**, 30–36 (2013).
10. Kaylor, J. J. *et al.* Identification of the 11-*cis*-specific retinyl-ester synthase in retinal Muller cells as multifunctional *O*-acyltransferase (MFAT). *Proc. Natl. Acad. Sci. USA* **111**, 7302–7307 (2014).
11. Szuts, E. Z. & Harosi, F. I. Solubility of retinoids in water. *Arch. Biochem. Biophys.* **287**, 297–304 (1991).
12. Hildebrand, P. W. *et al.* A ligand channel through the G protein coupled receptor opsin. *PLoS ONE* **4**, e4382 (2009).
13. Wang, T. & Duan, Y. Retinal release from opsin in molecular dynamics simulations. *J. Mol. Recognit.* **24**, 350–358 (2011).

14. Poincelot, R. P., Millar, P. G., Kimbel, R. L. Jr. & Abrahamson, E. W. Lipid to protein chromophore transfer in the photolysis of visual pigments. *Nature* **221**, 256–257 (1969).
15. Anderson, R. E. & Maude, M. B. Phospholipids of bovine outer segments. *Biochemistry* **9**, 3624–3628 (1970).
16. Shichi, H. & Somers, R. L. Possible involvement of retinylidene phospholipid in photoisomerization of all-*trans*-retinal to 11-*cis*-retinal. *J. Biol. Chem.* **249**, 6570–6577 (1974).
17. Kimbel, R. L. Jr., Poincelot, R. P. & Abramhamson, E. W. Chromophore transfer from lipid to protein in bovine rhodopsin. *Biochemistry* **9**, 1817–1820 (1970).
18. Quazi, F., Lenevich, S. & Molday, R. S. ABCA4 is an N-retinylidene-phosphatidylethanolamine and phosphatidylethanolamine importer. *Nat. Commun.* **3**, 925 (2012).
19. Tsui, F. C., Ojcius, D. M. & Hubbell, W. L. The intrinsic pKa values for phosphatidylserine and phosphatidylethanolamine in phosphatidylcholine host bilayers. *Biophys. J.* **49**, 459–468 (1986).
20. Boettner, E. A. & Wolter, J. R. Transmission of the ocular media. *Invest. Ophthalmol. Vis. Sci.* **1**, 776–783 (1962).
21. Groenendijk, G. W., Jacobs, C. W., Bonting, S. L. & Daemen, F. J. Dark isomerization of retinals in the presence of phosphatidylethanolamine. *Eur. J. Biochem.* **106**, 119–128 (1980).
22. Dartnall, H. J. The photosensitivities of visual pigments in the presence of hydroxylamine. *Vis. Res.* **8**, 339–358 (1968).
23. Saari, J. C. & Bredberg, D. L. Photochemistry and stereoselectivity of cellular retinaldehyde-binding protein from bovine retina. *J. Biol. Chem.* **262**, 7618–7622 (1987).
24. Hao, W. S. & Fong, H. K. W. The endogenous chromophore of retinal G protein-coupled receptor opsin from the pigment epithelium. *J. Biol. Chem.* **274**, 6085–6090 (1999).
25. Wald, G. & Brown, P. K. The molar extinction of rhodopsin. *J. Gen. Physiol.* **37**, 189–200 (1953).
26. Kim, J. E., Tauber, M. J. & Mathies, R. A. Wavelength dependent *cis-trans* isomerization in vision. *Biochemistry* **40**, 13774–13778 (2001).
27. Okano, T., Fukada, Y., Shichida, Y. & Yoshizawa, T. Photosensitivities of iodopsin and rhodopsins. *Photochem. Photobiol.* **56**, 995–1001 (1992).
28. Pandey, S., Blanks, J. C., Spee, C., Jiang, M. & Fong, H. K. Cytoplasmic retinal localization of an evolutionary homolog of the visual pigments. *Exp. Eye. Res.* **58**, 605–613 (1994).
29. Chen, P. *et al.* A photic visual cycle of rhodopsin regeneration is dependent on Rgr. *Nat. Genet.* **28**, 256–260 (2001).
30. Hao, W. & Fong, H. K. Blue and ultraviolet light-absorbing opsin from the retinal pigment epithelium. *Biochemistry* **35**, 6251–6256 (1996).
31. Krebs W. & Krebs I. P. in *The Structure of the Eye* (eds Hollyfield, J. G.) (Elsevier Biomedical, Amsterdam, Netherlands, 1982).
32. Carter-Dawson, L. D. & LaVail, M. M. Rods and cones in the mouse retina. I. Structural analysis using light and electron microscopy. *J. Comp. Neurol.* **188**, 245–262 (1979).
33. Calvert, P. D. *et al.* Phototransduction in transgenic mice after targeted deletion of the rod transducin alpha-subunit. *Proc. Natl. Acad. Sci. USA* **97**, 13913–13918 (2000).
34. Woodruff, M. L., Lem, J. & Fain, G. L. Early receptor current of wild-type and transducin knockout mice: photosensitivity and light-induced Ca^{2+}release. *J. Physiol.* **557**, 821–828 (2004).
35. Nymark, S., Frederiksen, R., Woodruff, M. L., Cornwall, M. C. & Fain, G. L. Bleaching of mouse rods: microspectrophotometry and suction-electrode recording. *J. Physiol.* **590**, 2353–2364 (2012).
36. Mata, N. L., Radu, R. A., Clemmons, R. & Travis, G. H. Isomerization and oxidation of vitamin a in cone-dominant retinas. A novel pathway for visual-pigment regeneration in daylight. *Neuron* **36**, 69–80 (2002).
37. Rando, R. R. & Chang, A. Studies on the catalyzed interconversion of vitamin A derivatives. *J. Am. Chem. Soc.* **105**, 2879–2882 (1983).
38. Redmond, T. M., Poliakov, E., Kuo, S., Chander, P. & Gentleman, S. RPE65, visual cycle retinol isomerase, is not inherently 11-*cis*-specific: support for a carbocation mechanism of retinol isomerization. *J. Biol. Chem.* **285**, 1919–1927 (2010).
39. Deigner, P. S., Law, W. C., Canada, F. J. & Rando, R. R. Membranes as the energy source in the endergonic transformation of vitamin A to 11-*cis*-retinol. *Science* **244**, 968–971 (1989).
40. Vance, J. E. Phospholipid synthesis and transport in mammalian cells. *Traffic* **16**, 1–18 (2015).
41. Shichi, H. & Shelton, E. Assessment of physiological integrity of sonicated retinal rod membranes. *J. Supramol. Struct.* **2**, 7–16 (1974).
42. Allikmets, R. *et al.* A photoreceptor cell-specific ATP-binding transporter gene (*ABCR*) is mutated in recessive Stargardt macular dystrophy. *Nat. Genet.* **15**, 236–246 (1997).
43. Weng, J. *et al.* Insights into the function of Rim protein in photoreceptors and etiology of Stargardt's disease from the phenotype in *abcr* knockout mice. *Cell* **98**, 13–23 (1999).
44. Mata, N. L., Weng, J. & Travis, G. H. Biosynthesis of a major lipofuscin fluorophore in mice and humans with ABCR-mediated retinal and macular degeneration. *Proc. Natl. Acad. Sci. USA* **97**, 7154–7159 (2000).
45. Ahn, J., Wong, J. T. & Molday, R. S. The effect of lipid environment and retinoids on the ATPase activity of ABCR, the photoreceptor ABC transporter responsible for Stargardt macular dystrophy. *J. Biol. Chem.* **275**, 20399–20405 (2000).
46. Pentia, D. C., Hosier, S., Collupy, R. A., Valeriani, B. A. & Cote, R. H. Purification of PDE6 isozymes from mammalian retina. *Methods. Mol. Biol.* **307**, 125–140 (2005).
47. Bligh, D. G. & Dyer, W. J. A rapid method for total lipid extraction and purification. *Can. J. Biochem. Physiol.* **37**, 911–917 (1959).
48. Parish, C. A., Hashimoto, M., Nakanishi, K., Dillon, J. & Sparrow, J. Isolation and one-step preparation of A2E and iso-A2E, fluorophores from human retinal pigment epithelium. *Proc. Natl. Acad. Sci. USA* **95**, 14609–14613 (1998).
49. Radu, R. A. *et al.* Retinal pigment epithelium-retinal G protein receptor-opsin mediates light-dependent translocation of all-*trans*-retinyl esters for synthesis of visual chromophore in retinal pigment epithelial cells. *J. Biol. Chem.* **283**, 19730–19738 (2008).
50. Szel, A. *et al.* Unique topographic separation of two spectral classes of cones in the mouse retina. *J. Comp. Neurol.* **325**, 327–342 (1992).
51. Nikonov, S. S. *et al.* Jr. Photoreceptors of $Nrl^{-/-}$ mice coexpress functional S- and M-cone opsins having distinct inactivation mechanisms. *J. Gen. Physiol.* **125**, 287–304 (2005).
52. Nikonov, S. S., Kholodenko, R., Lem, J. & Pugh, E. N. Jr. Physiological features of the S- and M-cone photoreceptors of wild-type mice from single-cell recordings. *J. Gen. Physiol.* **127**, 359–374 (2006).
53. Jones, G. J., Fein, A., MacNichol, E. F. Jr. & Cornwall, M. C. Visual pigment bleaching in isolated salamander retinal cones. Microspectrophotometry and light adaptation. *J. Gen. Physiol.* **102**, 483–502 (1993).
54. Cornwall, M. C. & Fain, G. L. Bleached pigment activates transduction in isolated rods of the salamander retina. *J. Physiol.* **480**, 261–279 (1994).
55. Jones, G. J., Cornwall, M. C. & Fain, G. L. Equivalence of background and bleaching desensitization in isolated rod photoreceptors of the larval tiger salamander. *J. Gen. Physiol.* **108**, 333–340 (1996).
56. Fan, J., Woodruff, M. L., Cilluffo, M. C., Crouch, R. K. & Fain, G. L. Opsin activation of transduction in the rods of dark-reared *Rpe65* knockout mice. *J. Physiol.* **568**, 83–95 (2005).

Acknowledgements

This work was supported by NIH R01 Grants EY011713, EY024379 (G.H.T.) and EY0001844 (G.L.F.), the Charles Kenneth Endowed Professorship (G.H.T.), the National Eye Institute Core Grant P30EY00331, and a Research to Prevent Blindness Unrestricted Grant to the Jules Stein Eye Institute. T.X. was supported in part by a China Scholarship Council scholarship. We thank Wayne Hubbell and Alapakkam Sampath for helpful discussions. We also thank Roxana Radu, Tamara Lenis and Jeremy Cook for their useful comments on the manuscript. Finally, we thank Nicholas Bischoff for his technical assistance.

Author contributions

J.J.K. designed and performed the experiments on bovine OS, mouse retinas, and live mice. T.X. designed and performed experiments on photoisomerization of *N*-ret-PE in solution and the quantum efficiency determination. N.T.I. helped design and performed whole-retina and suction-electrode cone recording experiments. A.T. performed experiments on OS and in live mice. H.H. performed experiments on OS and mouse retinas. G. L.F. helped design the experiments in Fig. 5, analyzed data from whole-retina and suction-electrode cone recording experiments, and wrote this section of the manuscript. G.H.T. conceptualized the study, analyzed the data, and wrote the manuscript.

Additional information

Supplementary Information accompanies this paper at doi:10.1038/s41467-017-00018-4.

Competing interests: The authors declare no competing financial interests.

Reprints and permission information is available online at http://npg.nature.com/reprintsandpermissions/

Publisher's note: Springer Nature remains neutral with regard to jurisdictional claims in published maps and institutional affiliations.

SUPPLEMENTARY INFORMATION

SUPPLEMENTARY FIGURES

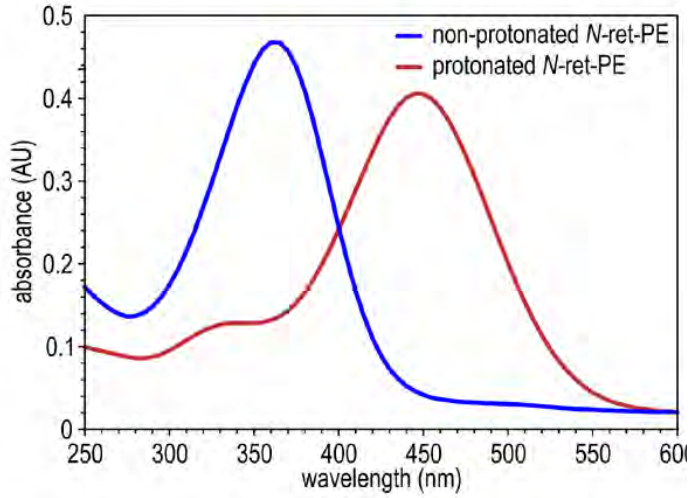

Supplementary Figure 1. Absorbance spectra of protonated and non-protonated *N*-ret-PE. Absorbance spectra for synthetic *N*-ret-PE were acquired in acidified (red curve) or alkalinized (blue curve) methanol. The λ_{max} is 450 nm for protonated- and 365 nm for non-protonated-*N*-ret-PE.

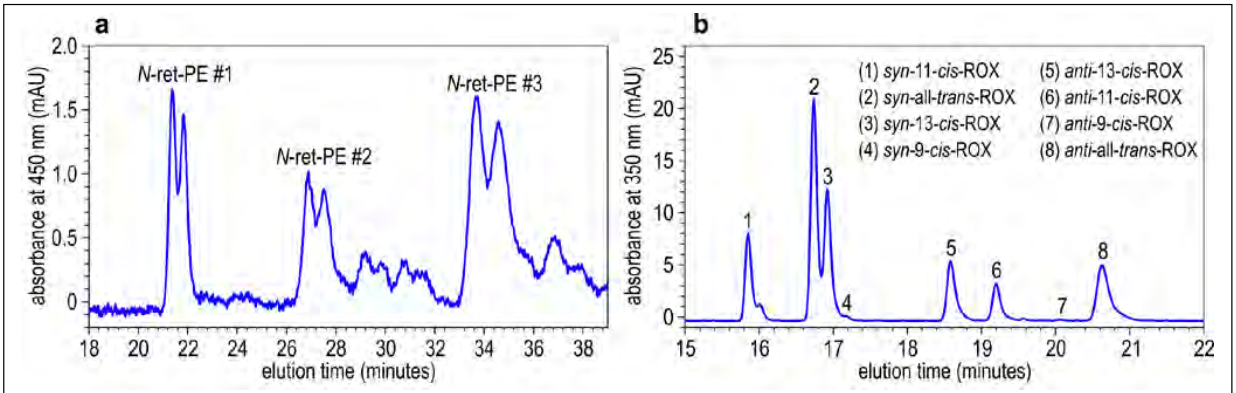

Supplementary Figure 2. Quantitation of *N*-ret-PE and constituent retinaldehydes in dark-adapted mouse retinas. (a) Reverse-phase chromatogram. Phospholipids were extracted from dark-adapted mouse retinas and separated by reverse-phase LC. An excerpt of the chromatogram is shown here. Three doublet peaks were identified with λ_{max} = 450 nm (*N*-ret-PE #1, *N*-ret-PE #2 and *N*-ret-PE #3), representing different fatty-acyl forms. Fractions containing these peaks were collected and pooled. **(b)** Normal-phase chromatogram. The pooled *N*-ret-PE sample was reacted with hydroxylamine to form retinaldehyde oximes, which were separated by normal-phase LC. An excerpt of the chromatogram containing the retinaldehyde oximes is shown. The *syn*- and *anti*-oximes of the four retinaldehyde isomers found are identified in the inset. Retinaldehyde levels are shown in Table 1.

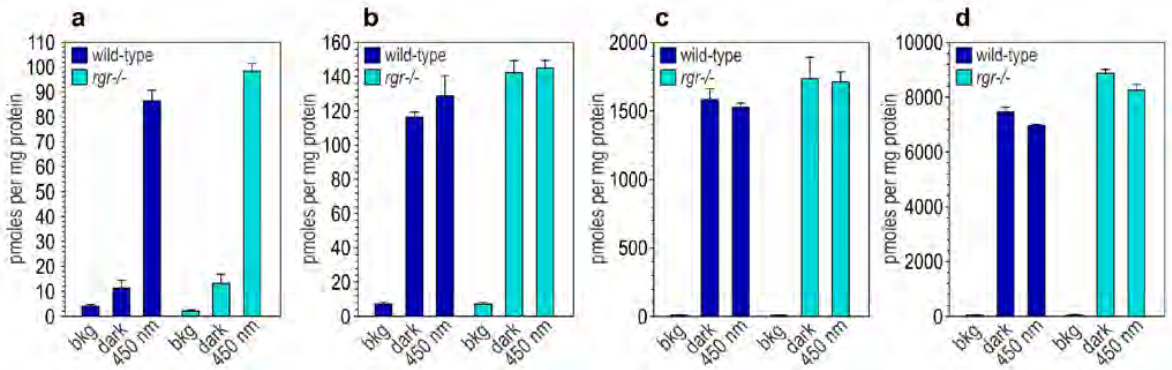

Supplementary Figure 3. Blue-light dependent synthesis of 11cRAL by wild type and *Rgr-/-* mouse retinas. Homogenates of retinas from wild type and *Rgr-/-* mice were photobleached to remove endogenous retinoids and incubated with atROL in the dark or during exposure to 450-nm light. Homogenates then were extracted into hexane and analyzed by normal phase LC. The retinaldehyde isomers: **(A)** 11cRAL, **(B)** 9cRAL, **(C)** 13cRAL, and **(D)** atRAL are shown as pmoles per mg protein in retinas immediately post-bleach (bkg), following incubation in the dark (dark), and following incubation in 450-nm light (450 nm). The dark and 450-nm light exposed samples were incubated with at-retinol. Error bars show mean ± S.D. (n=4). Note the approximately eight-fold higher 11cRAL in wild type and *Rgr-/-* retina homogenates incubated in 450-nm light versus darkness. Also note the similar levels of 11cRAL in wild type and *Rgr-/-* homogenates incubated in 450-nm light.

Chapter Five

LRIT1 Modulates Adaptive Changes in Synaptic Communication of Cone Photoreceptor

Article

Cell Reports

LRIT1 Modulates Adaptive Changes in Synaptic Communication of Cone Photoreceptors

Graphical Abstract

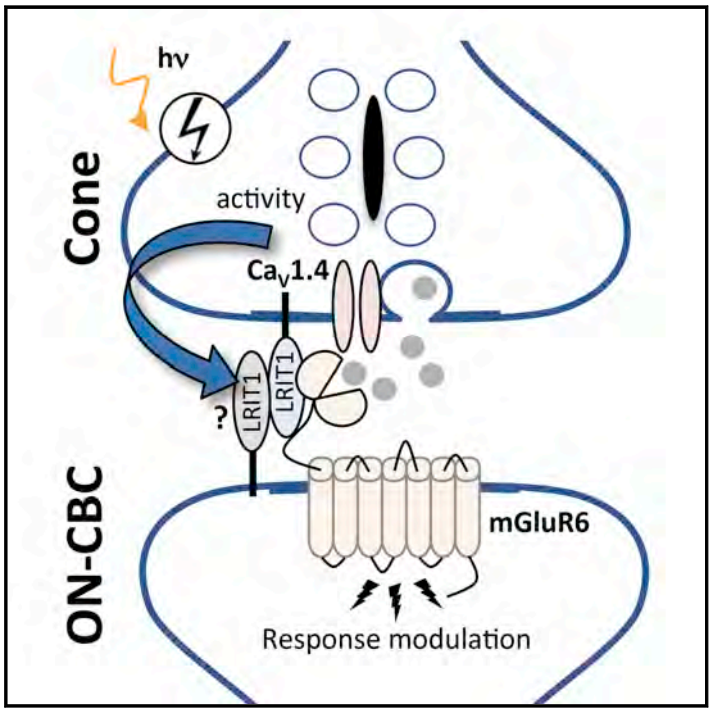

Highlights

- LRIT1 is identified as a binding partner of mGluR6 complex in the retina
- LRIT1 accumulates at photoreceptor synapses in an activity-dependent manner
- Deletion of LRIT1 in mice increases the sensitivity of cone synaptic transmission
- Loss of LRIT1 impairs light adaptation of cone synapses and daylight vision

Authors

Ignacio Sarria, Yan Cao, Yuchen Wang, ..., Vladimir J. Kefalov, Alapakkam P. Sampath, Kirill A. Martemyanov

Correspondence

kirill@scripps.edu

In Brief

Sarria et al. show LRIT1 accumulates at photoreceptors synapses. It forms a complex with a key receptor involved in processing neurotransmitter output of photoreceptors. They show that this protein plays an essential role in synaptic communication of cone photoreceptors and impacts daylight vision.

Sarria et al., 2018, Cell Reports *22*, 3562–3573
March 27, 2018
https://doi.org/10.1016/j.celrep.2018.03.008

CellPress

OPEN ACCESS
CellPress

Cell Reports
Article

LRIT1 Modulates Adaptive Changes in Synaptic Communication of Cone Photoreceptors

Ignacio Sarria,[1,5] Yan Cao,[1,5] Yuchen Wang,[1,5] Norianne T. Ingram,[2] Cesare Orlandi,[1] Naomi Kamasawa,[3] Alexander V. Kolesnikov,[4] Johan Pahlberg,[2] Vladimir J. Kefalov,[4] Alapakkam P. Sampath,[2] and Kirill A. Martemyanov[1,6,*]
[1]Department of Neuroscience, The Scripps Research Institute, Jupiter, FL 33458, USA
[2]Department of Ophthalmology, Stein Eye Institute, UCLA School of Medicine, Los Angeles, CA 90095, USA
[3]Electron Microscopy Core Facility, Max Planck Florida Institute, Jupiter, FL 33458, USA
[4]Department of Ophthalmology and Visual Sciences, Washington University School of Medicine, St. Louis, MO 63110, USA
[5]These authors contributed equally
[6]Lead Contact
*Correspondence: kirill@scripps.edu
https://doi.org/10.1016/j.celrep.2018.03.008

SUMMARY

Cone photoreceptors scale dynamically the sensitivity of responses to maintain responsiveness across wide range of changes in luminance. Synaptic changes contribute to this adaptation, but how this process is coordinated at the molecular level is poorly understood. Here, we report that a cell adhesion-like molecule, LRIT1, is enriched selectively at cone photoreceptor synapses where it engages in a *trans*-synaptic interaction with mGluR6, the principal receptor in postsynaptic ON-bipolar cells. The levels of LRIT1 are regulated by the neurotransmitter release apparatus that controls photoreceptor output. Knockout of LRIT1 in mice increases the sensitivity of cone synaptic signaling while impairing its ability to adapt to background light without overtly influencing the morphology or molecular composition of photoreceptor synapses. Accordingly, mice lacking LRIT1 show visual deficits under conditions requiring temporally challenging discrimination of visual signals in steady background light. These observations reveal molecular mechanisms involved in scaling synaptic communication in the retina.

INTRODUCTION

In the vertebrate retina, the rod and cone photoreceptors respond to incident light by modulating their membrane potential. This signal is transmitted to their bipolar cells and eventually to higher visual centers that enable our complex visual experience. Rods and cones subdivide the range of the visual system by mediating light reception in different regimes of intensity (Ingram et al., 2016; Pugh and Lamb, 2000; Yau and Hardie, 2009). Rods are exquisitely sensitive and are capable of detecting single photon absorptions, yet their responses are relatively slow and their dynamic range is limited. In contrast, cones are less sensitive, but faster, cover a wider range of light intensities, and are more resistant to saturation than rods (Burkhardt, 1994; Matthews et al., 1990; Nikonov et al., 2006). Furthermore, cones normally operate under daylight conditions where light intensities vary over a wide range, requiring them to adjust dynamically the sensitivity of their responses (Korenbrot, 2012; Soo et al., 2008; Stockman et al., 2006).

Photoreceptors use a variety of mechanisms to modulate their gain to maintain responsiveness as light intensities vary (Govardovskii et al., 2000; Morshedian and Fain, 2017; Pugh et al., 1999); one critical control point is at their synapse with bipolar cells (Wu, 1994). Light hyperpolarizes the photoreceptor membrane potential, which biases voltage-gated $Ca_V1.4$ Ca^{2+} channels in their axonal terminals toward the closed state, thereby reducing Ca^{2+} influx and glutamate release (Heidelberger et al., 2005; Joiner and Lee, 2015). Modulating neurotransmitter release through a combination of intrinsic mechanisms that control the release machinery (Thoreson et al., 2004; Yang and Wu, 1997) as well as through the negative feedback from the downstream neurons (Kramer and Davenport, 2015; Vroman et al., 2013) has been established as a powerful means for adjusting the gain of the photoreceptor synaptic output. However, the molecular mechanisms underlying this process, particularly as it varies between rods and cones, remain controversial and poorly understood. Even less clear is how photoreceptors coordinate the gain of the synaptic transmission with their dedicated postsynaptic bipolar cells, which are responsible for decoding photoreceptor signals.

In postsynaptic bipolar cell dendrites, the reduction in glutamate release is detected by two classes of bipolar cells; the OFF type neurons (OFF-BCs) that predominantly contact cones in the mammalian retina and utilize ionotropic glutamate receptors to preserve the hyperpolarizing photoreceptor light response, and the ON type (ON-BCs) that use metabotropic mGluR6 receptors to generate a depolarizing response that inverts the sign of the photoreceptor response. We now appreciate that there are at least 8 subtypes of ON-BCs showing functional specialization and selectivity in establishing contacts with either rods or cones (Euler et al., 2014; Hoon et al., 2014).

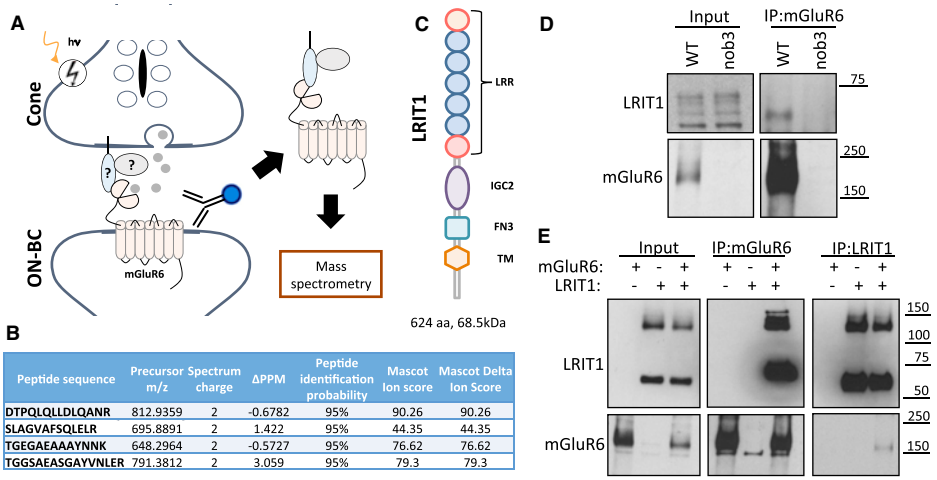

B

Peptide sequence	Precursor m/z	Spectrum charge	ΔPPM	Peptide identification probability	Mascot Ion score	Mascot Delta Ion Score
DTPQLQLLDLQANR	812.9359	2	-0.6782	95%	90.26	90.26
SLAGVAFSQLELR	695.8891	2	1.422	95%	44.35	44.35
TGEGAEAAAYNNK	648.2964	2	-0.5727	95%	76.62	76.62
TGGSAEASGAYVNLER	791.3812	2	3.059	95%	79.3	79.3

Figure 1. Identification of LRIT1 as mGluR6 Binding Partner

(A) Schematic of the affinity purification strategy for the identification of the mGluR6 binding partners of mGluR6 at photoreceptor synapses. Specific anti-mGluR6 antibodies were used for the immunoprecipitation from membrane fractions of the retina and the eluates were subjected to mass-spectrometry.

(B) Peptides matching to LRIT1 sequences identified in the mass-spectrometric experiments. Characteristics and parameters used for defining the sequences are shown.

(C) Domain organization of LRIT1. LRR, leucine reach repeat; IGC2, type 2 IgG-like domain; FN3, fibronectin type 3 domain; TM, transmembrane segment.

(D) Verification of mGluR6 interaction with LRIT1 by co-immunoprecipitation from retina lysates. Anti-mGluR6 antibodies were used for the immunoprecipitation (IP) and the presence of LRTI1 and mGluR6 in the IP eluates was detected by western blotting. Retinas lacking mGluR6 (nob3) were used as a specificity control.

(E) Characterization of mGluR6-LRIT1 interaction in transfected HEK293T cells. Both forward and reverse immunoprecipitation experiments using anti-LRIT1 and mGluR6 antibodies were conducted following expression of the indicated constructs and the proteins were detected by western blotting.

The core of the postsynaptic mGluR6 pathway that activates ON-BCs includes the heterotrimeric G protein $G\alpha_o\beta3\gamma13$, which in turn gates the effector ion channel TRPM1 (Martemyanov and Sampath, 2017; Morgans et al., 2010; Vardi et al., 2002). This signaling cascade is coordinated additionally by a host of proteins with critical roles in enabling synaptic transmission including regulator of G protein signaling (RGS) proteins, the orphan receptor GPR179, and leucine-rich repeat (LRR) proteins NYX and LRIT3, scaffolded together in a macromolecular complex (Gregg et al., 2014; Martemyanov and Sampath, 2017; Zeitz et al., 2015).

Recent findings suggest that the postsynaptic cascade of ON-BCs is further engaged in contacts with the photoreceptor presynaptic release apparatus (Cao et al., 2015; Tummala et al., 2016; Wang et al., 2017). For example, the mGluR6 is directly recruited by the rod-specific molecule ELFN1 to the $Ca_V1.4$ channel complex, an interaction that is crucial for the physical assembly of rod synapses and the transmission of rod signals to rod ON-BCs (Cao et al., 2015; Wang et al., 2017). No analogous interactions have yet been reported for the cone synapses. In addition, how these interactions influence the functional properties of synapses is not understood at any metabotropic synapse. Here, we report the identification of a leucine-rich repeat (LRR) protein, LRIT1, at photoreceptor synapses that binds *trans*-synaptically to mGluR6 and facilitates synaptic adaptations of cone photoreceptors upon changes in luminance.

RESULTS

Identification of LRIT1 As a Component of mGluR6 Complex

We have previously reported a screen for the mGluR6 binding partners by immunoprecipitation with specific anti-mGluR6 antibodies followed by mass-spectrometric identification of co-purified proteins present in the eluates. In this study, we focused on candidate cell-surface molecules with potential roles in cone synaptic function (Figure 1A). In this screen, we found 4 peptides with high identification confidence that map to the sequence of the transmembrane protein, LRIT1 (Figure 1B). This protein features multiple extracellular modules including leucine-rich repeats (LRR) and IgG-like and fibronectin type III domains (Figure 1C) and belongs to the extended family of cell-adhesion like proteins (de Wit and Ghosh, 2016). To validate the specificity of the interaction, we conducted mGluR6 immunoprecipitation from wild-type mouse retinas while in parallel using retinas from nob3 mice, lacking mGluR6. When probing blots with our anti-LRIT1 antibodies, we found a single band corresponding to the predicted size of LRIT1 protein in the eluates of wild-type but not *nob3* retinas, confirming the specificity of LRIT1-mGluR6 interaction in native retinas (Figure 1D). We then probed the binding in the reconstituted system. For this, HEK293 cells were co-transfected with various combinations of mGluR6 and LRIT1 followed by reciprocal immunoprecipitation experiments. Again, we detected the robust and specific

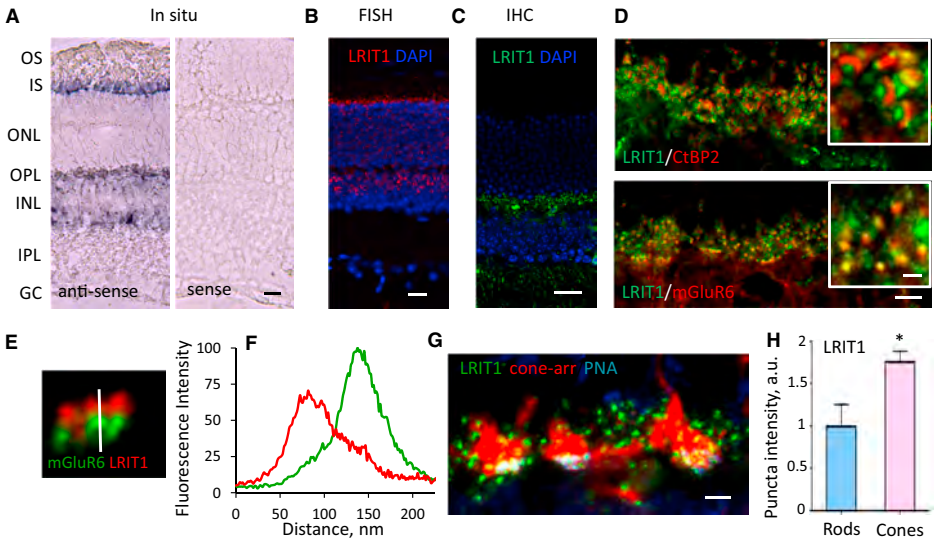

Figure 2. Characterization of LRIT1 Expression and Localization in the Retina

(A) Traditional *in situ* hybridization for LRIT1 detection. Anti-sense or sense (negative control) probes derived from the LRIT1 sequence were used to probe retina cross-sections. Specific signal is revealed in both photoreceptor and bipolar cell layers. Scale bar, 25 μm.

(B) High-resolution fluorescence *in situ* hybridization for *Lrit1* expression. Specific signal is detected in individual photoreceptors and bipolar cells. Scale bar, 20 μm.

(C) Immunohistochemical detection of LRIT1 protein expression by staining retina cross-sections with anti-LRIT1 antibodies. The signal is confined to the outer plexiform layer (OPL). Scale bar, 20 μm.

(D) Localization of LRIT1 at photoreceptor synapses revealed by co-immunostaining with pre-synaptic marker CtBP2 and postsynaptic marker mGluR6. Scale bar, 5 μm. Insets show higher magnification, scale bar, 1 μm.

(E) High magnification for LRIT1 localization in synaptic puncta relative to mGluR6 by co-immunostaining of retina cross-section with the indicated antibodies. Vertical bar shows the scan line.

(F) Quantification of LRIT1 distribution across synaptic puncta relative to mGluR6 determined by scanning fluorescence intensity along the line in (E).

(G) Localization of LRIT1 in synapses of rod and cone photoreceptors. Cone pedicles were labeled by cone arrestin staining (red) along with the cone-specific active zone marker PNA used to determine selective localization of LRIT1 in cone synapses. Puncta outside of PNA/b-arrestin mask were considered to be rod synapses. Scale bar, 2.5 μm.

(H) Quantification of LRIT1 content in rod and cone synapses by determining fluorescence intensities in respective puncta identified as in (G). Two sections from each retina, two retinas per genotype; *$p < 0.05$; t test.

pull down of LRIT1 when mGluR6 was immunoprecipitated and reciprocally mGluR6 upon LRIT1 immunoprecipitation (Figure 1E). Together, these findings establish LRIT1 as a binding partner of mGluR6.

LRIT1 Is a Synaptic Protein Expressed in Both Photoreceptors and ON-BCs

We studied further LRIT1 expression and localization in the mouse retina. First, we performed *in situ* hybridization with anti-sense probes complementary to *Lrit1* mRNA and detected signals in layers occupied by photoreceptors and bipolar cells (Figure 2A). The signal was absent when the sense probe was used, demonstrating the specificity of hybridization. This result was confirmed by using a higher resolution and sensitivity *in situ* hybridization approach with fluorescence probes, where again we found *Lrit1* mRNA to be present in both photoreceptors and bipolar cells (Figure 2B). Next, we probed the localization of LRIT1 in retinal cross-sections by immunohistochemistry using anti-LRIT1 antibodies. These studies revealed the nearly exclusive presence of LRIT1 in the outer plexiform layer (OPL) that contains photoreceptor-to-bipolar cell synapses (Figure 2C). Detailed examination of the OPL showed that LRIT1 immunoreactivity is confined to characteristic puncta in close apposition to both the photoreceptor synaptic ribbons, as judged by co-staining with CtBP2 (Ribeye), and dendritic tips of ON-BCs, identified by co-staining with mGluR6 (Figure 2D). Higher power analysis followed by fluorescence line-scan intensity showed only partial overlap of LRIT1 with mGluR6, consistent with the presence of the LRIT1 in the synaptic cleft (Figures 2E and 2F). We further examined the cell-type specificity of LRIT1 expression and found it to be present at synapses of both rod and cone photoreceptors (Figure 2G). Quantitative analysis revealed its enrichment in the active zones of cone axonal terminals compared to rods suggesting that it might play a more prominent role in cone synaptic connectivity and/or function (Figure 2H). Overall, these data indicate that LRIT1 is produced by both rod and cone

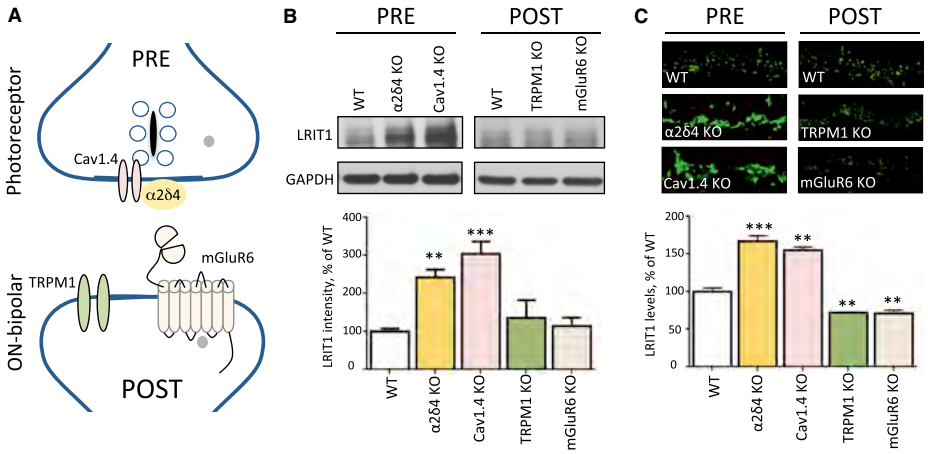

Figure 3. LRIT1 Synaptic Content Is Regulated by Changes in Presynaptic Release Apparatus

(A) Scheme of the molecular organization of the photoreceptor synapse. Knockout mice lacking pre- and post-synaptic players depicted on the scheme were analyzed in the experiments.

(B) Analysis of LRIT1 protein expression by western blotting in total lysates prepared from retinas of the respective mouse strains. Retinas from 3–5 mice for each genotype were used for the quantification of the LRIT1 band intensities and the values were normalized to WT. **p < 0.01, ***p < 0.001; t test.

(C) Analysis of LRIT1 synaptic targeting by immunohistochemical staining of retina cross-sections of knockout mouse retinas as indicated. OPL regions are shown. Scale bar, 10 μm. The intensity of LRIT1 signal in the OPL was quantified and normalized to WT values. Two sections from each retina, two retinas per genotype; **p < 0.01, ***p < 0.001; t test.

photoreceptors and ON-bipolar cells and is transported to the synapse where it is prominently present in the cone synaptic cleft.

Synaptic LRIT1 Content Is Modulated by Changes in Photoreceptor Activity

To assess the contribution of pre- and post-synaptic compartments to LRIT1 expression and localization, we examined several mouse models with deletions in key components of the photoreceptor pre-synaptic release machinery or the post-synaptic signaling complex in ON-BCs (Figure 3A). Analysis of LRIT1 expression in the retinas by western blotting revealed that the elimination of either the neurotransmitter receptor mGluR6, or the ON-BC effector channel TRPM1 has no effect on LRIT1 expression. In contrast, the knockout of $Ca_V1.4$ or α2δ4, which mediates the coupling of light-induced changes in membrane potential to glutamate release and synapse morphogenesis, respectively, results in a dramatic elevation of LRIT1 expression (Figure 3B). We further examined LRIT1 modulation at synapses by immunohistochemical staining of retinal cross-sections with anti-LRIT1 antibodies (Figure 3C). The results revealed a massive induction of LRIT1 content that occurs specifically at synapses where it is accumulated following deletion of pre-synaptic components: $Ca_V1.4$ and α2δ4. In contrast, the deletion of the postsynaptic mGluR6 or TRPM1 resulted only in a minor downregulation of LRIT1 in the OPL. These findings suggest that LRIT1 expression and synaptic accumulation is inversely dependent on the neurotransmitter release orchestrated by the $Ca_V1.4$ complex.

Elimination of LRIT1 Does Not Affect Structural or Molecular Architecture of Photoreceptor Synapses

To determine the role of LRIT1 in the retina, we obtained *Lrit1* knockout mice (*Lrit1*$^{-/-}$). In this line, the *Lrit1* allele is disrupted by placing a LacZ-Stop trap cassette immediately downstream of the first coding exon, thereby preventing translation of most of the *Lrit1* sequence (Figure 4A). Indeed, western blotting of whole retina lysates showed elimination of a specific band corresponding to LRIT1, indicating a complete ablation of LRIT1 protein (Figure 4B). Consistent with its transmembrane nature, the LRIT1 band was eliminated in knockout retinas and was concentrated in the membrane fraction while not present in the cytosol. In contrast, the major contaminating band was extracted in the soluble fraction, further confirming the specificity of assigning LRIT1 immunoreactivity (Figure S3). Immunohistochemical analysis showed elimination of immunostaining in the outer plexiform layer (OPL), additionally confirming the specificity of the antibodies (Figure 4C).

We found that deletion of LRIT1 did not affect overall morphology of the retina, its viability, or its laminar organization up to 3 months of age (Figures 4C and S1). Western blotting of *Lrit1*$^{-/-}$ retina lysates revealed no significant changes in the expression of key components of synaptic signaling between photoreceptors and ON-BCs. Furthermore, we found no changes in synaptic targeting of molecules involved in synaptic transmission (mGluR6, GPR179, $Ca_V1.4$, α2δ4) or the formation/maintenance of rod and cone synapses (ELFN1, LRIT3, connexin 36) (Figures 4E and S4). Detailed quantitative examination showed no changes in levels of mGluR6 in apposition to

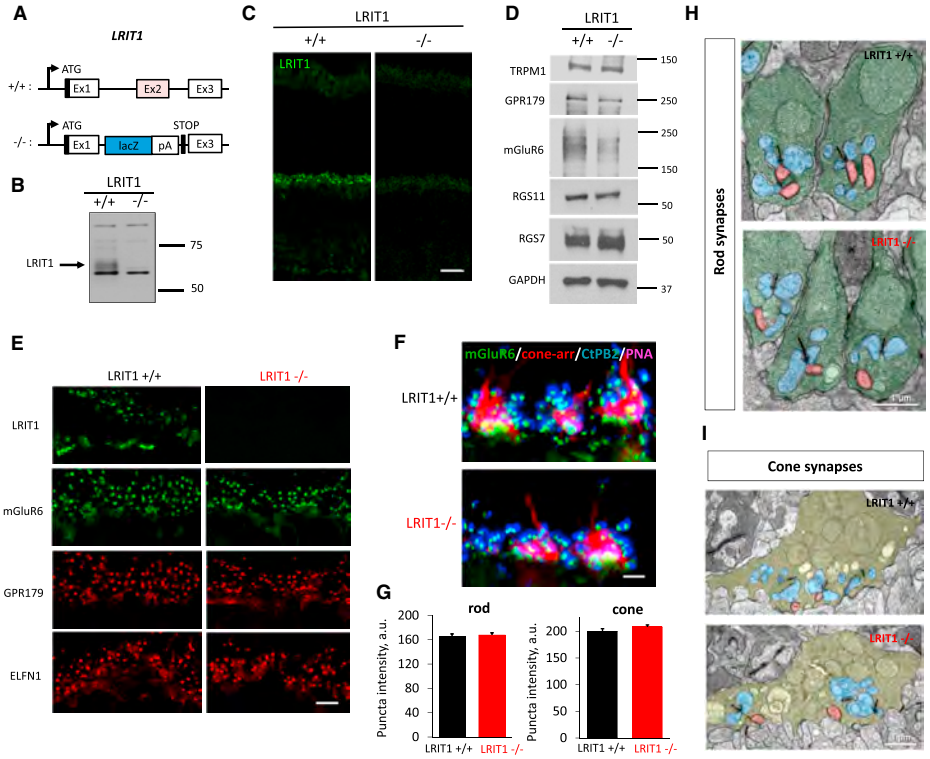

Figure 4. Generation and Characterization of Lrit1 Knockout Mice

(A) Scheme for targeting *Lrit1* gene. The deletion strategy included elimination of the critical coding exon 2 and introduction of the premature stop-codon preceding exon 3.

(B) Analysis of LRIT1 expression in wild-type and *Lrit1* knockout (−/−) mouse retinas by western blotting.

(C) Analysis of LRIT1 localization in wild-type and *Lrit1* knockout (−/−) mouse retinas by immunohistochemical staining of retina cross-sections, scale bar, 20 μm.

(D) Analysis of expression of proteins present in photoreceptor synapses by western blotting comparing wild-type and *Lrit1* knockout (−/−) mouse retinas.

(E) Analysis of distribution of proteins present in photoreceptor synapses by immunohistochemical staining of retina cross-sections of wild-type and *Lrit1* knockout (−/−) mouse retinas. OPL regions are shown, scale bar, 5 μm.

(F) Analysis of mGluR6 content in rod and cone synapses by immunohistochemistry. Staining with cone arrestin was used to define cone terminals and with PNA to identify active zones in the cone axons. Scale bar, 2.5 μm.

(G) Quantification of changes in mGluR6 staining in rod and cone synapses in the retinas of wild-type and *Lrit1* knockout (−/−) mice.

(H) Analysis of rod synapse morphology by electron microscopy. Rod terminals are labeled in green, horizontal cell processes in blue and ON-bipolar dendrites in red.

(I) Analysis of cone synapse morphology by electron microscopy. Cone terminals are labeled in pale green, horizontal cell processes in blue and bipolar dendrites in red.

active zones in rod or cone synaptic terminals (Figures 4F and 4G).

We further studied the fine synaptic morphology by transmission electron microscopy and found no obvious evidence for structural abnormalities. Rod spherules in *Lrit1*$^{-/-}$ retinas displayed normal shape and contained the expected elements, including the synaptic ribbon and the invaginating processes of horizontal cells and rod ON-BCs in direct apposition to synaptic ribbon (Figure 4H). Similarly, cone pedicles contained multiple ribbons and displayed clearly identifiable contacts with both horizontal cells and ON-BCs (Figure 4I). We thus conclude that deletion of LRIT1 had no major effect on the structural or molecular architecture of photoreceptor synapses.

Ablation of LRIT1 Causes Selective Deficits In Background Adaptation Of Cone Synaptic Signaling

We sought to determine a functional role for LRIT1 in light reception. Probing light-evoked responses of dark-adapted mice by electroretinography (ERG) revealed that *Lrit1*$^{-/-}$ mice displayed a normal ERG waveform; a-wave and b-wave components were indistinguishable from wild-type littermates under both scotopic (Figure 5A) and photopic (Figure 5B) light regimes that activate

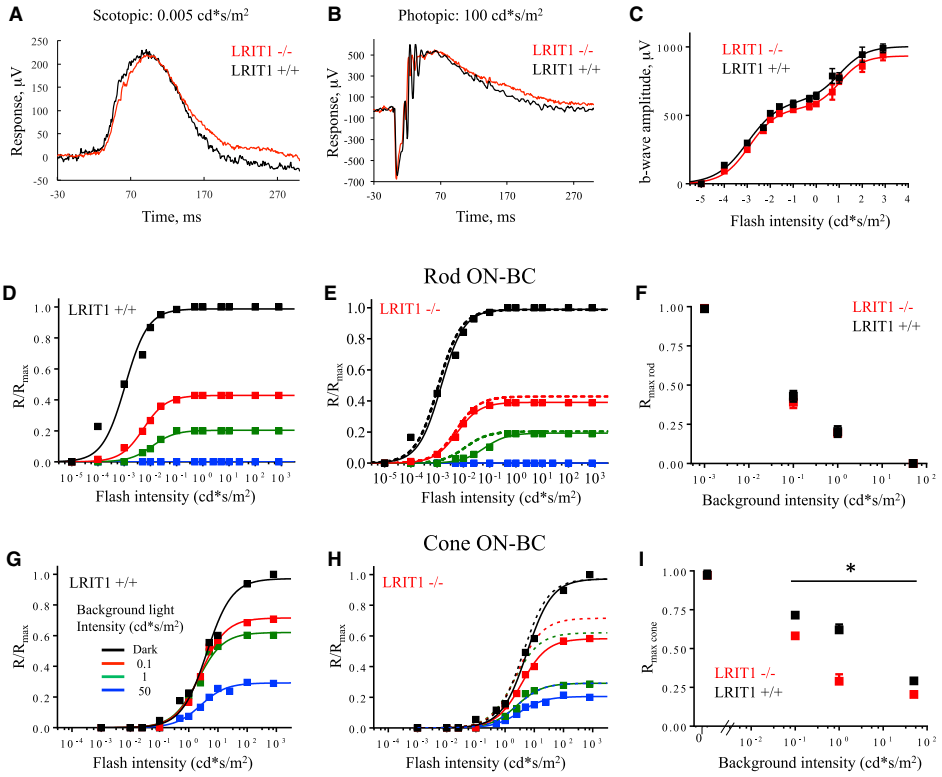

Figure 5. Analysis of LRIT1 Knockout by Electroretinography

(A) Representative electroretinography (ERG) waveform recorded from dark-adapted mice in response to scotopic flash of light.

(B) Representative ERG waveform recorded from dark-adapted mice in response to photopic flash of light.

(C) Light-dependence profile of b-wave amplitudes. 4–6 mice were used for each genotype.

(D) Rod-driven component of the b-wave across light intensities recorded in wild-type mice under dark-adapted conditions and various levels of background light. The first phase of the response at scotopic light intensities in (C) is shown.

(E) Rod-driven component of the b-wave across light intensities recorded in *Lrit1* knockout mice under dark-adapted conditions and various levels of background light. Dashed lines represent superimposed fits from WT in (D).

(F) Normalized changes in maximal amplitude of the rod-driven b-wave as a function of background light intensity recorded in both genotypes.

(G) Cone-driven component of the b-wave across light intensities recorded in wild-type mice under dark-adapted conditions and various levels of background light. The second phase of the response at photopic light intensities in (C) is shown.

(H) Cone-driven component of the b-wave across light intensities recorded in *Lrit1* knockout mice under dark-adapted conditions and various levels of background light. Dashed lines represent superimposed fits from wild-type mice in (G).

(I) Normalized changes in maximal amplitude of the cone-driven b-wave as a function of background light intensity recorded in both genotypes.

rods and cones, respectively. Quantitative analysis revealed no changes in the maximal ERG b-wave amplitude in either the rod or cone-driven components (Figure 5C), indicating no gross abnormality in synaptic transmission to ON-BCs in dark-adapted mice. Single-cell recordings from rod ON-BCs and cone photoreceptor corroborated this observation. Voltage clamp (V_m = −60 mV) recordings from *Lrit1*$^{-/-}$ and wild-type rod ON-BCs confirm the normal sensitivity of rod phototransduction and synaptic processing (Figure S2; Table S1). Furthermore, voltage clamp (V_m = −40 mV) recordings directly from cone photoreceptors revealed a robust maximum photocurrent with similar sensitivities and time courses in *Lrit1*$^{-/-}$ and *Lrit1*$^{+/+}$ retinas (Figure S2). We also observed no significant differences in the waveform or amplitudes of oscillatory potentials between the genotypes across the range of photopic light flashes, suggesting that LRIT1 ablation does not grossly affect processing of the visual signal by the inner retinal circuitry (Figure S5).

Next, we evaluated the role of LRIT1 in modulating the sensitivity of photoreceptor to ON-BC signaling during light adaptation. Consistent with previous reports, we found that increasing background light intensity reduced b-wave amplitudes elicited by both scotopic and photopic flashes. In the scotopic light intensity range, we observed no differences between genotypes over the range of background intensities (Figures 5D–5F),

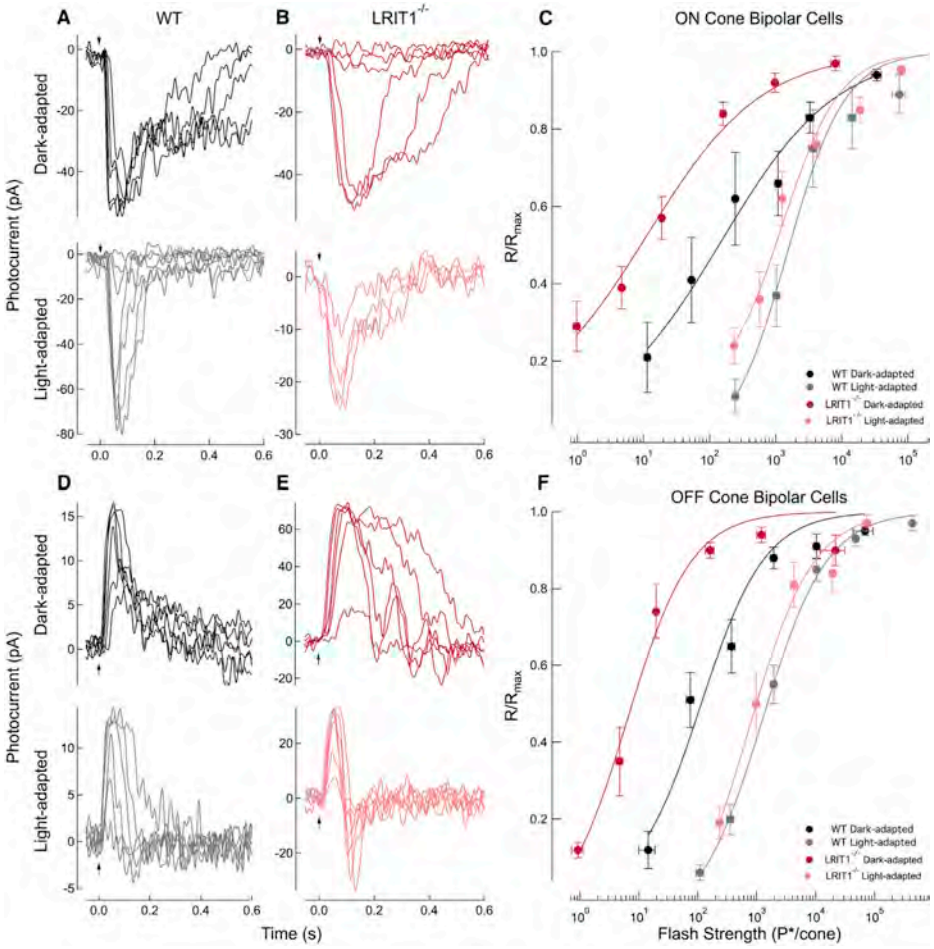

Figure 6. Analysis of Cone-to-BC Synaptic Transmission

(A) Whole-cell voltage clamp recordings (V_m = −60 mV) were made from wild-type ON-BCs in retinal slices. Flash families were collected in the dark-adapted state and following the presentation of a background light that generated 2,100 P*/cone/s, where P* is an estimated number of activated cone pigments. The dark-adapted flash family was collected during the presentation of 10-ms flashes delivering 38, 69, 160, 560, and 2,000 P*/cone, whereas the family collected during the presentation of background light delivered 160, 560, 2,000, 7,700, 33,000, 160,000, and 560,000 P*/cone. Top and bottom panels are recordings made in sequence from the same cell. In light adaptation experiments, retinas were exposed to light for 2 min before recording.

(B) Whole-cell voltage clamp recordings (V_m = −60 mV) from *Lrit1*$^{-/-}$ ON-BCs. Flash families again were collected in the dark-adapted state and following the presentation of a background light that generated 2,100 P*/cone/s. The dark-adapted flash family was collected for 10-ms flashes delivering 0.7, 2.5, 9.5, 38, 130, and 560 P*/flash, whereas families collected during the presentation of background light generated 270, 1,100, 2,000, and 3,000 P*/flash. Top and bottom panels are recordings made in sequence from the same cell.

(C) Response-intensity relationships for the dark-adapted and light-adapted WT and *Lrit1*$^{-/-}$ ON-BC flash families. Population data were averaged across flash strengths and fit with a Hill Curve with an exponent of 0.5 for the dark-adapted families and 1.0 for the light-adapted families. The half-maximal flash strength ($I_{1/2}$) for the fit was 150 P*/cone and 1,500 P*/cone for WT ON-BCs in the dark- and light-adapted states, respectively, a 10-fold shift. The half-maximal flash strength ($I_{1/2}$) for the fit was 11 P*/cone and 1,300 P*/cone for *Lrit1*$^{-/-}$ ON-BCs in the dark- and light-adapted states, respectively, a 120-fold shift.

(D) Whole-cell voltage clamp recordings (V_m = −60 mV) were made from WT OFF-BCs in retinal slices. Flash families were collected in the dark-adapted state and following the presentation of a background light that generated 2,100 P*/cone/s. The dark-adapted flash family was collected during the presentation of 10-ms flashes delivering 37, 69, 560, 2,000, 7,700, and 33,000 P*/cone, whereas the family collected during the presentation of background light delivered 160, 560, 2,000, 33,000, 160,000, and 560,000 P*/cone. Top and bottom panels are recordings made in sequence from the same cell.

(E) Whole-cell voltage clamp recordings (V_m = −60 mV) from *Lrit1*$^{-/-}$ OFF-BCs. Flash families again were collected in the dark-adapted state and following the presentation of a background light that generated 2,100 P*/cone/s. The dark-adapted flash family was collected for 10-ms flashes delivering 7.0, 24, 40, 78, 640,

(legend continued on next page)

thought to drive solely rod-mediated responses. In contrast, when a rod-suppressing background was delivered, the cone-mediated b-waves displayed reduced amplitudes in *Lrit1*$^{-/-}$ mice compared to their *Lrit1*$^{+/+}$ littermates (Figures 5G–5I). Together, these observations suggest that elimination of LRIT1 impairs light adaptation for cone-driven signals in ON-BCs, resulting in a more pronounced suppression of the ON-BC response amplitude by background light.

LRIT1 Controls the Sensitivity of Synaptic Transmission to Cone Bipolar Cells

To determine the mechanistic basis for the selectively impaired photopic ERG b-wave in background light, we measured the light-evoked responses of cone BCs in retinal slices. Recordings were made without a consideration of cone bipolar cell subtype, but appeared consistent across subtypes. Surprisingly, dark-adapted responses from *Lrit1*$^{-/-}$ cone ON-BCs were ~10-fold more sensitive than their wild-type (WT) counterparts (Figures 6A and 6B), as determined based on the flash strength that yields a half-maximal response. Interestingly, ~10-fold increased sensitivity was also observed in dark-adapted responses from *Lrit1*$^{-/-}$ cone OFF-BCs (Figures 6D and 6E), suggesting a common presynaptic origin of LRIT1 influence. Because the light intensities used to generate the flash families for *Lrit1*$^{-/-}$ BCs activate rods only, but rod ON-BC responses remain unchanged compared to WT cells (Figure S2; Table S1), these data suggest that the absence of LRIT1 influences specifically synaptic communication between cones and cone BCs.

We probed further the mechanism underlying observed reduction of ERG b-wave amplitude by background light that suggests reduced capacity of *Lrit1*$^{-/-}$ retinas for light adaptation. In the presence of a rod-suppressing background light delivering 2,100 P*/cone/s, flash families for cone ON- and OFF-BCs of both genotypes displayed a similar half-maximal flash strength (Figures 6A–6C; Table S1). Thus, the background light desensitized the *Lrit1*$^{-/-}$ cone BCs to a much greater extent than wild-type cone BCs, effectively diminishing their difference in sensitivity. It should be stressed that response families recorded in background light were from the same cone BCs that the dark-adapted data were collected from, permitting formal analysis of the changes in sensitivity induced by background. When maximum response amplitude in this background light was considered, we additionally found that *Lrit1*$^{-/-}$ ON-BCs displayed reduced amplitudes compared to their wild-type counterparts (Figures 6A and 6B; Table S1).

Thus, in addition to confirming deficits in light adaptation seen by ERG analysis, single-cell recordings further revealed an additional phenotype: increased dark-adapted sensitivity of ON an OFF cone BC light responses. This effect was not evident from the *en masse* analysis of neuronal responses to light by ERG likely due to large contributions by rod ON-BC activity, which effectively mask cone CB differences.

LRIT1 Is Needed for Achieving High Temporal Resolution of Visual Discrimination

To further assess the functional role of diminished light adaptation in *Lrit1*$^{-/-}$ retinas, we measured the capacity for the b-wave to track flickering light stimuli in the photopic light regime. Given the diminished cone-driven responses under background illumination, we tested processing of cone-derived signals in a flicker ERG paradigm that assesses mostly cone-mediated responses upon repeated stimulation, yet not fully eliminating rod contributions (Figure 7A). We found that under the conditions of this continuing light challenge, the *Lrit1* knockouts exhibited substantially reduced b-wave amplitudes consistent with deficits in background adaptation (Figures 7A and 7B). No genotype differences in the a-wave components of the flicker ERG were found, indicating normal rod and cone function (Figure 7C) and suggesting that the reduction in the b-wave is associated with changes in synaptic transmission to ON-BCs.

To understand the contribution of these observed adaptation deficits to vision, we evaluated behavior sensitivity in the optokinetic reflex (OKR) task on a steady light background (Figure 7D). Consistent with the reduction in the b-wave at the high-frequency stimulation, *Lrit1*$^{-/-}$ mice showed reduced visual acuity (i.e., spatial resolution of stimuli presented at high temporal frequency) (Figure 7E). However, we found no significant differences in the ability of *Lrit1*$^{-/-}$ mice to discriminate changes in contrast at any of the speed settings as compared to their wild-type littermates (Figure 7F). These observations suggest that loss of LRIT1 selectively compromises photopic visual acuity in a temporally challenging environment.

DISCUSSION

The diversity of the neuronal cell types is thought to underlie the unique properties of individual circuits that collectively specialize to perform a vast range of computations enabling complex behaviors (Lodato and Arlotta, 2015; Zeng and Sanes, 2017). Such design requires not only specificity in wiring between distinct cell classes, but also that emergent properties are matched for the demands of the circuit (Bargmann and Marder, 2013; de Wit and Ghosh, 2016). Here, we provide support for the functional specialization of synaptic contacts for cone photoreceptor, but not rods. We propose that cones selectively rely on an adhesion molecule, LRIT1, for controlling scaling of their synaptic output (Figure 7G). Specifically, we found that LRIT1 is recruited to the active zones of both rod and cone photoreceptors where it is found in complexes involving the postsynaptic neurotransmitter receptor, mGluR6, on ON-BC dendrites. The

and 2,300 P*/flash, whereas families collected during the presentation of background light generated 310, 640, 1,200, 2,300, 5,400, 12,000, and 55,000 P*/flash. Top and bottom panels are recordings made in sequence from the same cell.

(F) Response-intensity relationships for the dark-adapted and light-adapted WT and *Lrit1*$^{-/-}$ OFF-BC flash families. Population data were averaged across flash strengths and fit with a Hill Curve with an exponent of 0.8 for the dark-adapted and light-adapted families. The half-maximal flash strength ($I_{1/2}$) for the fit was 110 P*/cone and 1,300 P*/cone for WT OFF-BCs in the dark- and light-adapted states, respectively, a 12-fold shift. The half-maximal flash strength ($I_{1/2}$) for the fit was 6.3 P*/cone and 740 P*/cone for *Lrit1*$^{-/-}$ OFF-BCs in the dark- and light-adapted states, respectively, a 120-fold shift.

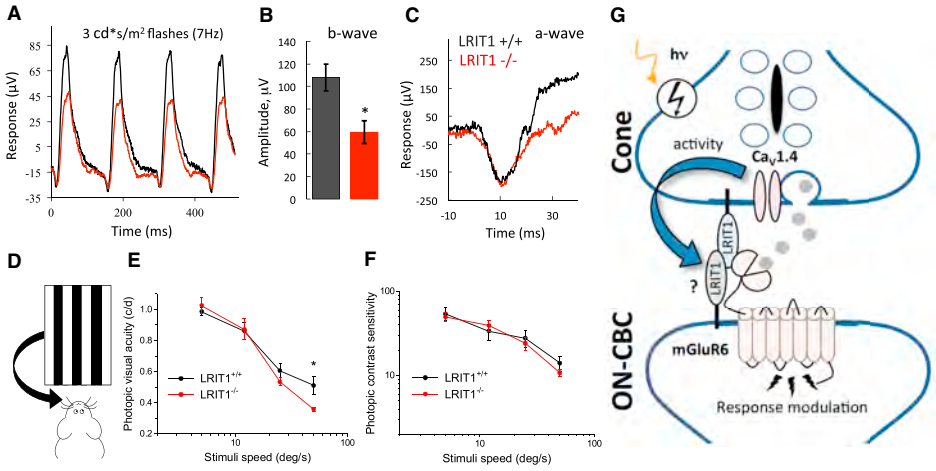

Figure 7. Visual Deficits in Mice Lacking LRIT1

(A) Representative flicker ERG traces in response to trains of stimulation delivered at 7 Hz frequency.

(B) Quantification of b-wave amplitude changes recorded in flicker ERG protocol. *$p < 0.05$, t test, 4–6 mice per genotype.

(C) Analysis of the a-wave recorded under flicker ERG protocol.

(D) Scheme of the optokinetic reflex testing principle to assess visual function in mice. The ability of mice to track virtually moving grids with varying contrast, spatial, and temporal properties is recorded.

(E) Dependence of photopic visual acuity on stimulation speed in the ORK test under 100% contrast of gratings. Deficits in photopic (light background of 1.1 cd s/m^2) contrast sensitivity of *Lrit1* knockout mice are apparent only at highest stimuli speed of 50°/s (error bars are SEM; t test: *$p < 0.05$, n = 5–6).

(F) Dependence of photopic contrast sensitivity on stimulation speed in the ORK test under constant light background of 1.1 cd/m^2 (error bars are SEM; t test: *$p < 0.05$, n = 5–6).

(G) Schematic representation of proposed role of LRIT1 in synaptic communication of cones. LRIT1 is expressed predominantly in cones and could also be present in cone BC with a possibility of forming *trans*-synaptic dimers given its capacity for heteromerization. It further interacts with postsynaptic mGluR6 receptor and presynaptic release apparatus containing Ca$_V$1.4 complex to adjust neurotransmitter signaling at the synapse in response to light adaptation scaling synaptic transmission of cones. Changes in photoreceptor synaptic activity modulate LRIT1 levels further contributing to adaptation.

deletion of LRIT1 did not affect the physical synapse assembly or molecular composition of synapses, yet it fundamentally changed their properties. Although LRIT1 is expressed in both rods and cones, we only detected effects at cone synapses. Remarkably, we found that knockout of LRIT1 increased the gain of synaptic transmission to ON and OFF bipolar cells, converting the sensitivity of cone ON-BCs to the range of rod ON-BCs. At the behavioral level, loss of LRIT1 compromised temporal aspects of photopic vision, although the exact mechanisms by which LRIT1 contributes to visual acuity remain to be established.

Despite the well documented role played by LRR proteins in synaptic structure (de Wit et al., 2011; Yogev and Shen, 2014), their influence on the functional aspects of signaling at metabotropic synapses have not been observed previously. We found that the augmentation of absolute sensitivity in cone BCs came at a price of reducing the ability of this synapse to adapt to continuous light exposure, thus limiting the operating range for transmitting signals. A key property of the cone system is the ability to operate over a wide range of background light, which they achieve by scaling their responsiveness with an increase in stimulation. Our findings demonstrate that LRIT1 is one of the molecular factors operating in cones that allow such adaptation at the level of controlling synaptic gain.

How can LRIT1 influence light sensitivity and synaptic scaling? Mechanistically, we think LRIT1 may exert its effects by several mechanisms, which are not necessarily mutually exclusive but remain to be established. We believe that the similar effects on the sensitivities of both ON and OFF CBs suggest that LRIT1 may act in photoreceptors to influence the presynaptic machinery that sets the rate of glutamate release. In line with this idea, we documented that the expression of LRIT1 is inversely dependent on the expression of the Ca$_V$1.4 channel complex. Interestingly, we found that neither targeting nor accumulation levels of Ca$_V$1.4 and α2δ4 was affected by LRIT1 elimination (Figure S4), suggesting that LRIT1 may influence glutamate release through fine-tuning the activity of the pre-synaptic calcium channel or other components of the release apparatus. Although we did not detect by EM any overt morphological changes precipitated by LRIT1 loss, some effects may also involve subtle structural changes in the synaptic cleft, including those related to positioning of active zone elements in relation to glutamate receptors that influence the efficiency of synaptic transmission.

Furthermore, physical interactions of LRIT1 with the principal neurotransmitter receptor mGluR6 may change the receptor signaling properties, perhaps by influencing the range of its responsiveness to glutamate. Such changes might affect the magnitude of the postsynaptic depolarization mediated by the

downstream TRPM1 channel. These mechanisms may be further integrated together via *trans*-synaptic LRIT1 homomerization, suggested by the ability of LRIT1 to form dimers (Gomi et al., 2000). Although our *in situ* hybridization data indicate that LRIT1 messenger RNA is indeed present in both photoreceptors and bipolar neurons, the postsynaptic accumulation of LRIT1 in the dendritic tips of bipolar neurons is less certain at the protein level. Further experimentation will be required to establish the relevance of this dimerization model. LRIT1 can also have an additional role in regulating rod-cone coupling. Although we showed no significant change in connexin 36 content induced by LRIT1 loss, it is still possible that LRIT1 regulates cone ON-BCs sensitivity by suppressing rod-to-cone coupling through changes in gap junction efficiency rather than the connexin36 expression. Ultimately, a combination of these mechanisms is likely shaping LRIT1's function and establishing their relative contributions will be an exciting future direction.

The discovery of LRIT1 as a key player in synaptic function of cones adds to a growing list of cell adhesion-like molecules that shape photoreceptor synapses. Interestingly, the expression of LRIT1 in photoreceptors was noted earlier (Gomi et al., 2000); however, it was reported to be localized to photoreceptor outer segments. We show clearly that LRIT1 is a synapse-specific protein located at both pre- and post-synaptic side of photoreceptor synapses using antibodies that we have validated against the *Lrit1*$^{-/-}$ retina. The closest homolog of LRIT1 is LRIT3, another photoreceptor synaptic protein expressed by ON-bipolar neurons (Zeitz et al., 2013). LRIT3 is indispensable for the synaptic transmission for photoreceptor signals, as its inactivation in mice and humans leads to complete disruption of both rod and cone synaptic signaling (Neuillé et al., 2014, 2015; Qian et al., 2015). Additionally, LRIT3 appears to play a role in the morphogenesis of cone synaptic contacts with ON-BCs (Neuillé et al., 2015). The relationship between LRIT1 and LRIT3 is unclear but based on their similarity in domain composition, ~40% sequence identity and propensity of LRIT1 to dimerize, it seems possible that both molecules may work together to orchestrate molecularly similar processes.

In addition, two other leucine-rich repeat proteins with similar organization are present at the photoreceptor synapses. Rods specifically express the cell adhesion molecule ELFN1, which like LRIT1 forms complexes with mGluR6 and plays an essential role in physical assembly of the rod to rod ON-BC connections (Cao et al., 2015). Both rods and cones also rely on nyctalopin (NYX), which does not appear to be involved in synapse assembly but rather in photoreceptor synaptic signaling. NYX is expressed in both rod and cone ON-BCs where it was shown to play a role for the synaptic localization of the effector channel, TRPM1 (Cao et al., 2011; Pearring et al., 2011). Thus, it appears that photoreceptor synapses utilize a host of LRR molecules, possibly interwoven together, to coordinate synaptic assembly with synaptic function. Intriguingly, the cell adhesion molecules in this organization are further integrated with the components of the GPCR signaling cascade, pointing to higher level scaffolding and integration of morphogenic factors with the synaptic transmission machinery. Deciphering the molecular logic of this synaptic code at photoreceptor synapses will inform more generally how metabotropic synapses are specified and regulated.

EXPERIMENTAL PROCEDURES

Detailed methods including reagents, mice strains, antibodies, procedures for western blotting, *in situ* hybridization, electroretinography (ERG), single-cell recordings, optokinetic testing (OKR) of vision in mice, immunoprecipitation, cell culture, appear in the Supplemental Experimental Procedures. When appropriate, statistical analyses were performed by employing Student's t test with sample size of more than 3 independent biological replicates (mice), and the data are reported together with SEM values.

Mice

Embryonic stem cell line with the *Lrit1*-targeted allele (Lrit1tm1a(EUCOMM)Hmgu) was obtained from EUCOMM (project 115689) and intended modifications described in the Results section were verified by sequencing and long range PCR. All studies involving mice were carried out in accordance with the NIH guidelines and were granted formal approval by the Institutional Animal Care and Use Committees.

Antibodies and Western Blotting

The generation of the most antibodies was described previously. Rabbit anti-LRIT1 antibodies were generated against mouse recombinant LRIT1 (aa 549–624). Rabbit anti-LRIT3 CT antibody was generated against human recombinant LRIT3 (aa 604–679).

Whole retinas were removed from mice and lysed by sonication in ice-cold PBS supplemented with 150 mM NaCl, 1% Triton X-100, and Complete protease inhibitor tablets (Roche). Following sonication, lysates were cleared by centrifugation, subjected to 12.5% SDS/PAGE. Protein bands were transferred onto PVDF membranes and probed with antibodies.

Cell Culture and Transfection

HEK293T cells were obtained from Clontech and cultured at 37°C and 5% CO_2 in DMEM supplemented with antibiotics, 10% FBS. HEK293T cells were transfected at ~70% confluency using Lipofectamine LTX (Invitrogen) according to the protocol of the manufacturer. The cells were harvested processed for co-immunoprecipitation.

Fluorescence *In Situ* Hybridization

The mRNA expression was evaluated with ViewRNATM 2-plex *In Situ* Hybridization Assay (Panomics, Santa Clara, CA) using the following probes: *Lrit1* (NM_146245.2; Cat# VB1-17470). 12-μm sections were post-fixed in 4% paraformaldehyde for 10 min, washed, and incubated with the probes.

Immunohistochemistry

Dissected eyecups were fixed for 15 min in 4% paraformaldehyde, cryoprotected with 30% sucrose in PBS for 2 hr at room temperature, and embedded in optimal cutting temperature medium. 12-μm frozen sections were obtained and blocked in PT1 (PBS with 0.1% Triton X-100 and 10% donkey serum) for 1 hr then incubated with primary antibody in PT2 (PBS with 0.1% Triton X-100 and 2% donkey serum) for at least 1 hr. After four washes with PBS with 0.1% Triton, sections were incubated with fluorophore-conjugated secondary antibodies in PT2 for 1 hr. After four washes, sections were mounted in Fluoromount (Sigma).

Electroretinography

Electroretinograms were recorded by using the UTA system and a Big-Shot Ganzfeld (LKC Technologies). Mice (~4–8 weeks old) were dark-adapted (≥6 hr) and prepared for recordings using a red dim light. ERG signals were sampled at 1 kHz and recorded with 0.3-Hz low-frequency and 300-Hz high-frequency cut-offs.

Single-Cell Recordings

Light-evoked responses from photoreceptors and bipolar cells were recorded retinal slices using methods described previously (Okawa et al., 2010). Briefly,

mice were dark-adapted overnight and euthanized according to protocols approved by the University of California, Los Angeles Animal Research Committee (Protocol 14-005-11). Slices were superfused with bicarbonate-buffered Ames media (equilibrated with 5% CO_2/95% O_2) heated to 35°C–37°C, visualized under infrared illumination, and stimulated with a blue light-emitting diode (λ_{max} ~405 nm). Light-evoked responses were measured using patch electrodes in voltage-clamp mode.

Evaluation of Mouse Vision by Optokinetic Reflex Test

Photopic contrast sensitivity of mice was evaluated from optomotor responses using a two-alternative forced-choice protocol, as previously described (Kolesnikov et al., 2011; Umino et al., 2008).

SUPPLEMENTAL INFORMATION

Supplemental Information includes Supplemental Experimental Procedures, five figures, and one table and can be found with this article online at https://doi.org/10.1016/j.celrep.2018.03.008.

ACKNOWLEDGMENTS

We thank Ms. Natalia Martemyanova for performing genetic crosses needed to obtain mice utilized in these studies. This work was supported by NIH grants EY018139, MH105482, DA026405 (to K.A.M.), EY028033 (to K.A.M. and A.P.S.), EY026675 (to V.J.K.), and EY019312 (to V.J.K.) and unrestricted grants from Research to Prevent Blindness to the Departments of Ophthalmology at UCLA and Washington University.

AUTHOR CONTRIBUTIONS

I.S., Y.C., and Y.W. conducted most of the cell biological and biochemical experiments. I.S. and Y.W. performed ERG and analyzed the data. C.O. performed cell biological experiments and analyzed the data. N.T.I. and J.P. performed single-cell recordings. N.K. performed EM experiments and analyzed the data. A.V.K. and V.J.K. performed OKR evaluation of mouse vision and analyzed the data. A.P.S. designed electrophysiological experiments and analyzed the data. K.A.M. designed the study, analyzed the data, and wrote the paper. All authors contributed to writing and editing the manuscript.

DECLARATION OF INTERESTS

The authors declare no competing interests.

Received: December 20, 2017
Revised: February 10, 2018
Accepted: February 28, 2018
Published: March 27, 2018

REFERENCES

Bargmann, C.I., and Marder, E. (2013). From the connectome to brain function. Nat. Methods *10*, 483–490.

Burkhardt, D.A. (1994). Light adaptation and photopigment bleaching in cone photoreceptors in situ in the retina of the turtle. J. Neurosci. *14*, 1091–1105.

Cao, Y., Posokhova, E., and Martemyanov, K.A. (2011). TRPM1 forms complexes with nyctalopin in vivo and accumulates in postsynaptic compartment of ON-bipolar neurons in mGluR6-dependent manner. J. Neurosci. *31*, 11521–11526.

Cao, Y., Sarria, I., Fehlhaber, K.E., Kamasawa, N., Orlandi, C., James, K.N., Hazen, J.L., Gardner, M.R., Farzan, M., Lee, A., et al. (2015). Mechanism for Selective Synaptic Wiring of Rod Photoreceptors into the Retinal Circuitry and Its Role in Vision. Neuron *87*, 1248–1260.

de Wit, J., and Ghosh, A. (2016). Specification of synaptic connectivity by cell surface interactions. Nat. Rev. Neurosci. *17*, 22–35.

de Wit, J., Hong, W., Luo, L., and Ghosh, A. (2011). Role of leucine-rich repeat proteins in the development and function of neural circuits. Annu. Rev. Cell Dev. Biol. *27*, 697–729.

Euler, T., Haverkamp, S., Schubert, T., and Baden, T. (2014). Retinal bipolar cells: elementary building blocks of vision. Nat. Rev. Neurosci. *15*, 507–519.

Gomi, F., Imaizumi, K., Yoneda, T., Taniguchi, M., Mori, Y., Miyoshi, K., Hitomi, J., Fujikado, T., Tano, Y., and Tohyama, M. (2000). Molecular cloning of a novel membrane glycoprotein, pal, specifically expressed in photoreceptor cells of the retina and containing leucine-rich repeat. J. Neurosci. *20*, 3206–3213.

Govardovskii, V.I., Calvert, P.D., and Arshavsky, V.Y. (2000). Photoreceptor light adaptation. Untangling desensitization and sensitization. J. Gen. Physiol. *116*, 791–794.

Gregg, R.G., Ray, T.A., Hasan, N., McCall, M.A., and Peachey, N.S. (2014). Interdependence among members of the mGluR6 G-protein mediated signaplex of retinal depolarizing bipolar cells. In G Protein Signaling Mechanisms in the Retina, A.P. Sampath and K. Martemyanov, eds. (Springer), pp. 67–79.

Heidelberger, R., Thoreson, W.B., and Witkovsky, P. (2005). Synaptic transmission at retinal ribbon synapses. Prog. Retin. Eye Res. *24*, 682–720.

Hoon, M., Okawa, H., Della Santina, L., and Wong, R.O. (2014). Functional architecture of the retina: development and disease. Prog. Retin. Eye Res. *42*, 44–84.

Ingram, N.T., Sampath, A.P., and Fain, G.L. (2016). Why are rods more sensitive than cones? J. Physiol. *594*, 5415–5426.

Joiner, M.L., and Lee, A. (2015). Voltage-gated Cav1 channels in disorders of vision and hearing. Curr. Mol. Pharmacol. *8*, 143–148.

Kolesnikov, A.V., Rikimaru, L., Hennig, A.K., Lukasiewicz, P.D., Fliesler, S.J., Govardovskii, V.I., Kefalov, V.J., and Kisselev, O.G. (2011). G-protein beta-gamma-complex is crucial for efficient signal amplification in vision. J. Neurosci. *31*, 8067–8077.

Korenbrot, J.I. (2012). Speed, sensitivity, and stability of the light response in rod and cone photoreceptors: facts and models. Prog. Retin. Eye Res. *31*, 442–466.

Kramer, R.H., and Davenport, C.M. (2015). Lateral inhibition in the vertebrate retina: the case of the missing neurotransmitter. PLoS Biol. *13*, e1002322.

Lodato, S., and Arlotta, P. (2015). Generating neuronal diversity in the mammalian cerebral cortex. Annu. Rev. Cell Dev. Biol. *31*, 699–720.

Martemyanov, K.A., and Sampath, A.P. (2017). The transduction cascade in retinal ON-bipolar cells: signal processing and disease. Annu. Rev. Vis. Sci. *3*, 25–51.

Matthews, H.R., Fain, G.L., Murphy, R.L.W., and Lamb, T.D. (1990). Light adaptation in cone photoreceptors of the salamander: a role for cytoplasmic calcium. J. Physiol. *420*, 447–469.

Morgans, C.W., Brown, R.L., and Duvoisin, R.M. (2010). TRPM1: the endpoint of the mGluR6 signal transduction cascade in retinal ON-bipolar cells. BioEssays *32*, 609–614.

Morshedian, A., and Fain, G.L. (2017). Light adaptation and the evolution of vertebrate photoreceptors. J. Physiol. *595*, 4947–4960.

Neuillé, M., El Shamieh, S., Orhan, E., Michiels, C., Antonio, A., Lancelot, M.E., Condroyer, C., Bujakowska, K., Poch, O., Sahel, J.A., et al. (2014). Lrit3 deficient mouse (nob6): a novel model of complete congenital stationary night blindness (cCSNB). PLoS ONE *9*, e90342.

Neuillé, M., Morgans, C.W., Cao, Y., Orhan, E., Michiels, C., Sahel, J.A., Audo, I., Duvoisin, R.M., Martemyanov, K.A., and Zeitz, C. (2015). LRIT3 is essential to localize TRPM1 to the dendritic tips of depolarizing bipolar cells and may play a role in cone synapse formation. Eur. J. Neurosci. *42*, 1966–1975.

Nikonov, S.S., Kholodenko, R., Lem, J., and Pugh, E.N., Jr. (2006). Physiological features of the S- and M-cone photoreceptors of wild-type mice from single-cell recordings. J. Gen. Physiol. *127*, 359–374.

Okawa, H., Miyagishima, K.J., Arman, A.C., Hurley, J.B., Field, G.D., and Sampath, A.P. (2010). Optimal processing of photoreceptor signals is required to maximize behavioural sensitivity. J. Physiol. *588*, 1947–1960.

Pearring, J.N., Bojang, P., Jr., Shen, Y., Koike, C., Furukawa, T., Nawy, S., and Gregg, R.G. (2011). A role for nyctalopin, a small leucine-rich repeat protein, in localizing the TRP melastatin 1 channel to retinal depolarizing bipolar cell dendrites. J. Neurosci. *31*, 10060–10066.

Pugh, E.N., Jr., Nikonov, S., and Lamb, T.D. (1999). Molecular mechanisms of vertebrate photoreceptor light adaptation. Curr. Opin. Neurobiol. *9*, 410–418.

Pugh, E.N., Jr., and Lamb, T.D. (2000). Phototransduction in Vertebrate Rods and Cones: Molecular Mechanisms of Amplification, Recovery and Light Adaptation (Amsterdam: Elsevier).

Qian, H., Ji, R., Gregg, R.G., and Peachey, N.S. (2015). Identification of a new mutant allele, Grm6(nob7), for complete congenital stationary night blindness. Vis. Neurosci. *32*, E004.

Soo, F.S., Detwiler, P.B., and Rieke, F. (2008). Light adaptation in salamander L-cone photoreceptors. J. Neurosci. *28*, 1331–1342.

Stockman, A., Langendörfer, M., Smithson, H.E., and Sharpe, L.T. (2006). Human cone light adaptation: from behavioral measurements to molecular mechanisms. J. Vis. *6*, 1194–1213.

Thoreson, W.B., Rabl, K., Townes-Anderson, E., and Heidelberger, R. (2004). A highly Ca2+-sensitive pool of vesicles contributes to linearity at the rod photoreceptor ribbon synapse. Neuron *42*, 595–605.

Tummala, S.R., Dhingra, A., Fina, M.E., Li, J.J., Ramakrishnan, H., and Vardi, N. (2016). Lack of mGluR6-related cascade elements leads to retrograde trans-synaptic effects on rod photoreceptor synapses via matrix-associated proteins. Eur. J. Neurosci. *43*, 1509–1522.

Umino, Y., Solessio, E., and Barlow, R.B. (2008). Speed, spatial, and temporal tuning of rod and cone vision in mouse. J. Neurosci. *28*, 189–198.

Vardi, N., Dhingra, A., Zhang, L., Lyubarsky, A., Wang, T.L., and Morigiwa, K. (2002). Neurochemical organization of the first visual synapse. Keio J. Med. *51*, 154–164.

Vroman, R., Klaassen, L.J., and Kamermans, M. (2013). Ephaptic communication in the vertebrate retina. Front. Hum. Neurosci. *7*, 612.

Wang, Y., Fehlhaber, K.E., Sarria, I., Cao, Y., Ingram, N.T., Guerrero-Given, D., Throesch, B., Baldwin, K., Kamasawa, N., Ohtsuka, T., et al. (2017). The auxiliary calcium channel subunit alpha2delta4 is required for axonal elaboration, synaptic transmission, and wiring of rod photoreceptors. Neuron *93*, 1359–1374.

Wu, S.M. (1994). Synaptic transmission in the outer retina. Annu. Rev. Physiol. *56*, 141–168.

Yang, X.L., and Wu, S.M. (1997). Response sensitivity and voltage gain of the rod- and cone-bipolar cell synapses in dark-adapted tiger salamander retina. J. Neurophysiol. *78*, 2662–2673.

Yau, K.W., and Hardie, R.C. (2009). Phototransduction motifs and variations. Cell *139*, 246–264.

Yogev, S., and Shen, K. (2014). Cellular and molecular mechanisms of synaptic specificity. Annu. Rev. Cell Dev. Biol. *30*, 417–437.

Zeitz, C., Jacobson, S.G., Hamel, C.P., Bujakowska, K., Neuillé, M., Orhan, E., Zanlonghi, X., Lancelot, M.E., Michiels, C., Schwartz, S.B., et al.; Congenital Stationary Night Blindness Consortium (2013). Whole-exome sequencing identifies LRIT3 mutations as a cause of autosomal-recessive complete congenital stationary night blindness. Am. J. Hum. Genet. *92*, 67–75.

Zeitz, C., Robson, A.G., and Audo, I. (2015). Congenital stationary night blindness: an analysis and update of genotype-phenotype correlations and pathogenic mechanisms. Prog. Retin. Eye Res. *45*, 58–110.

Zeng, H., and Sanes, J.R. (2017). Neuronal cell-type classification: challenges, opportunities and the path forward. Nat. Rev. Neurosci. *18*, 530–546.

SUPPLEMENTAL INFORMATION

Supplemental Figures and Tables

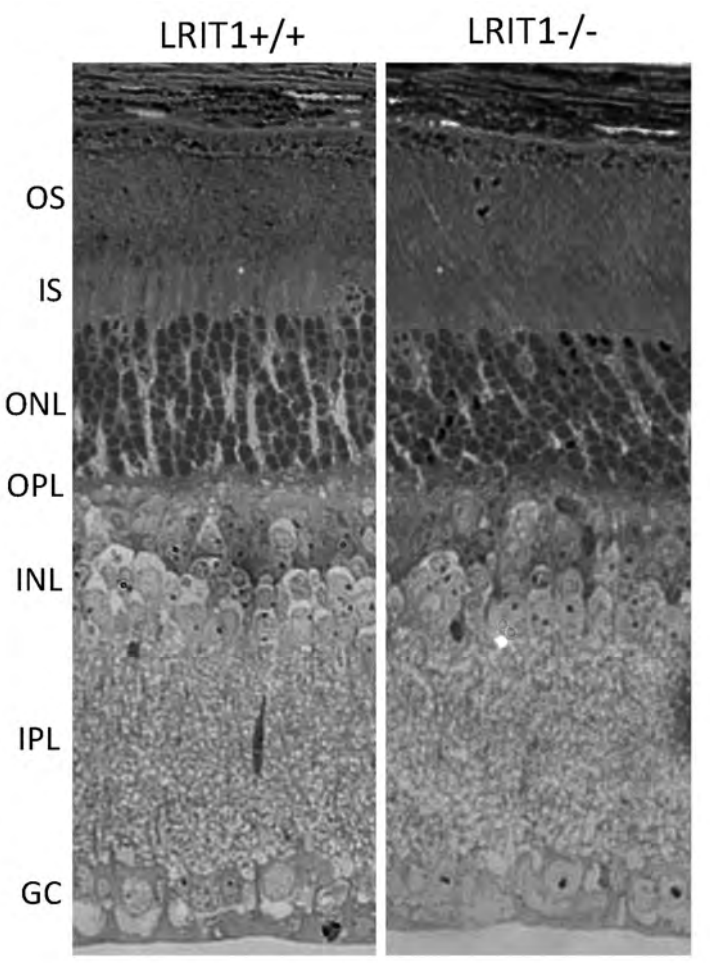

Figure S1. Related to Figure 4. Normal retina morphology in *Lrit1*$^{-/-}$ mice.

Analysis of the retina morphology by toluidine blue staining of ultra-thin (0.2 μm) retina cross-sections

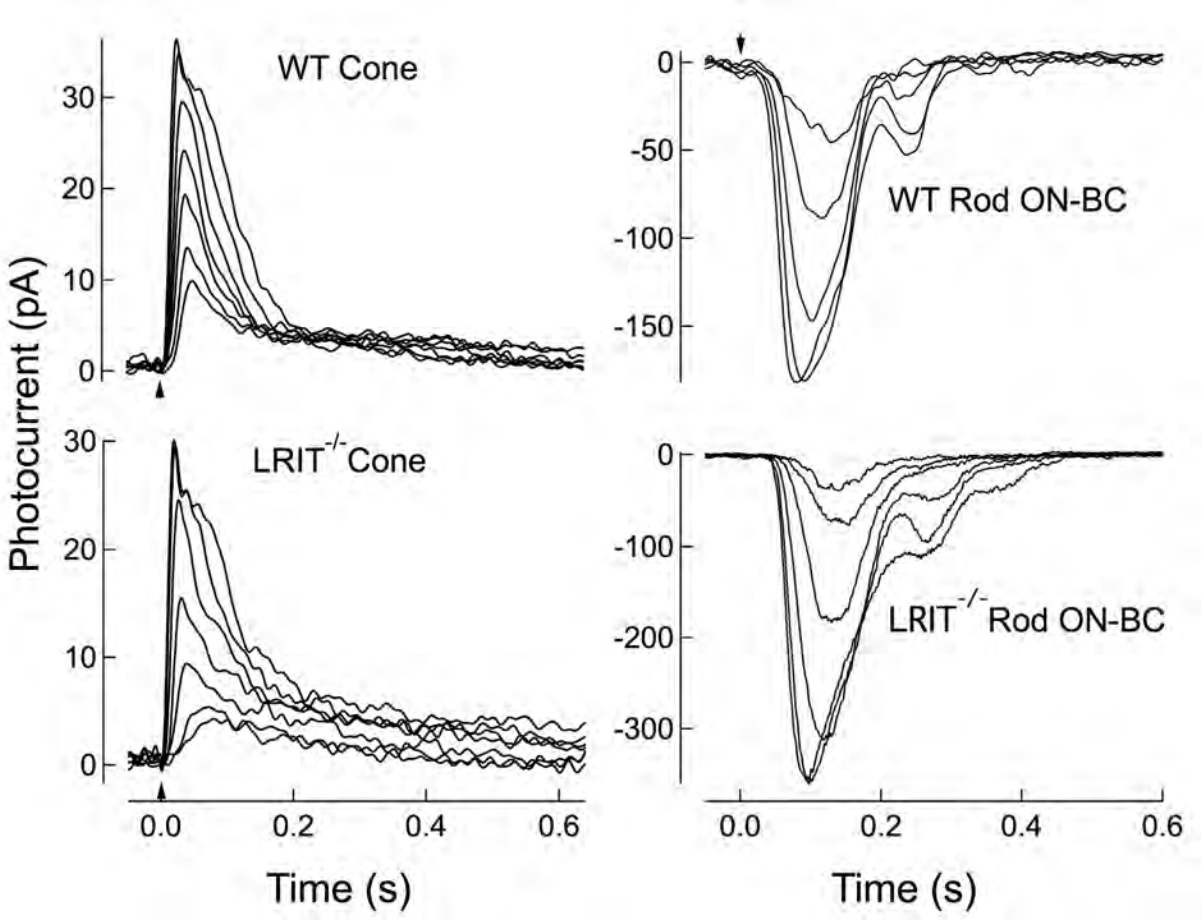

Figure S2. Related to Figure 6. Normal cone photoreceptor and rod ON-BC responses in *Lrit1*$^{-/-}$ mice.

Voltage-clamp (V_m = -40 mV) recordings from WT and *Lrit1*$^{-/-}$ cones. WT responses were evoked by 10ms flashes generating 350, 720, 1,400, 2,600, 4,500, 14,000, and 31,000 P*. *Lrit1*$^{-/-}$ responses were evoked by 10 ms flashes generating 70, 160, 560, 2,000, 7,700, 33,000, and 76,000 P*. Voltage-clamp (V_m = -60 mV) recordings from WT and *Lrit1*$^{-/-}$ rod ON-BCs. WT response were evoked by 10 ms flashes generating 1.5, 2.8, 6.6, 11, and 23 activated rhodopsins (R*). *Lrit1*$^{-/-}$ response were evoked by 10 ms flashes generating 1.2, 3.5, 5.9, 8.3, 13, and 20 R*.

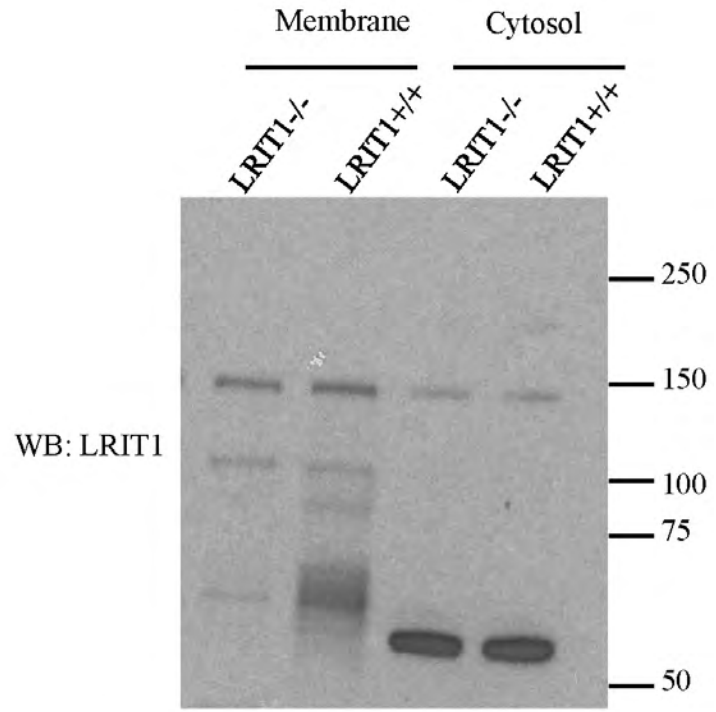

Figure S3. Related to Figure 4. Specific immunoreactive band for LRIT1 is associated with membranes

Western blotting analysis of LRIT1 using whole retina lysate from both wild-type (*Lrit1*$^{+/+}$) and *Lrit1*$^{-/-}$ mice after membrane fractionation. Equal amount of total protein from both cytosolic and membrane portion of each genotype was loaded and analyzed by western blot using specific LRIT1 antibody. Note that the intense band around 60kD detected by this antibody showed in cytosolic portion but not in membrane portion in both genotypes confirming its non-specificity.

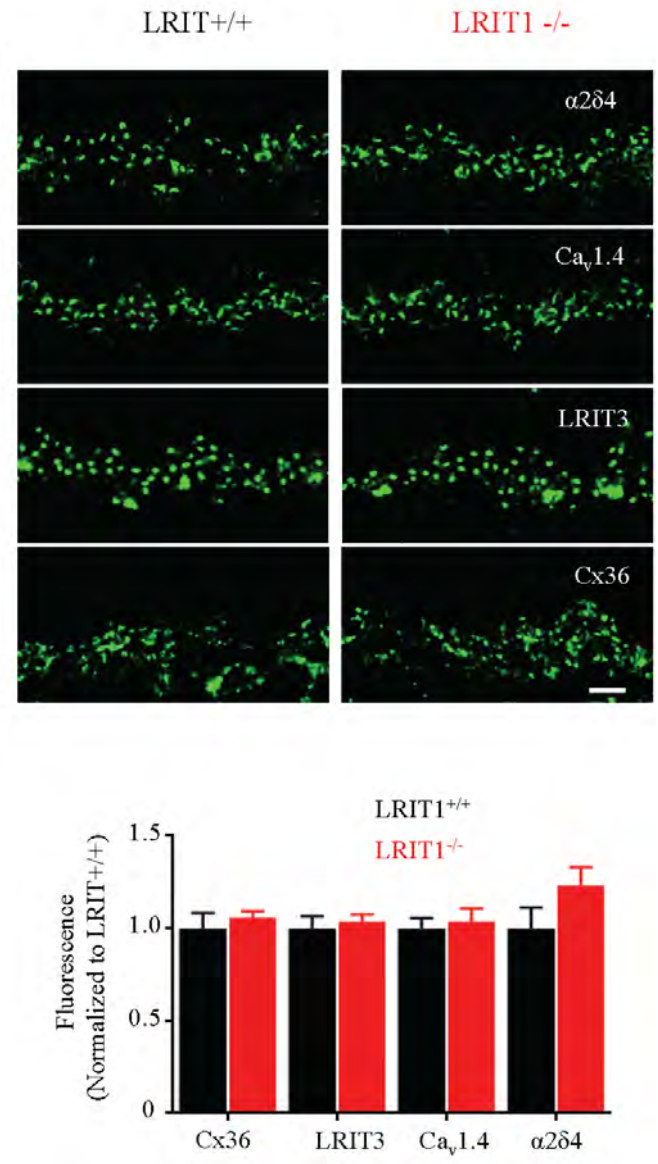

Figure S4. Related to Figure 4. The effect of *Lrit1* knockout on content of key synaptic proteins.

A, Representative confocal pictures of retina cross-sections from wild type (*Lrit1*$^{+/+}$) and LRIT1 knockout (*Lrit1*$^{-/-}$) mice stained with specific antibodies against different synaptic molecules as indicated. Scale bar: 20μm). OPL regions are shown. **B,** Quantification of the immunofluorescence intensities of synaptic molecules examined in panel A. Mean values were normalized to *Lrit1*$^{+/+}$ controls and plotted with corresponding SEMs.

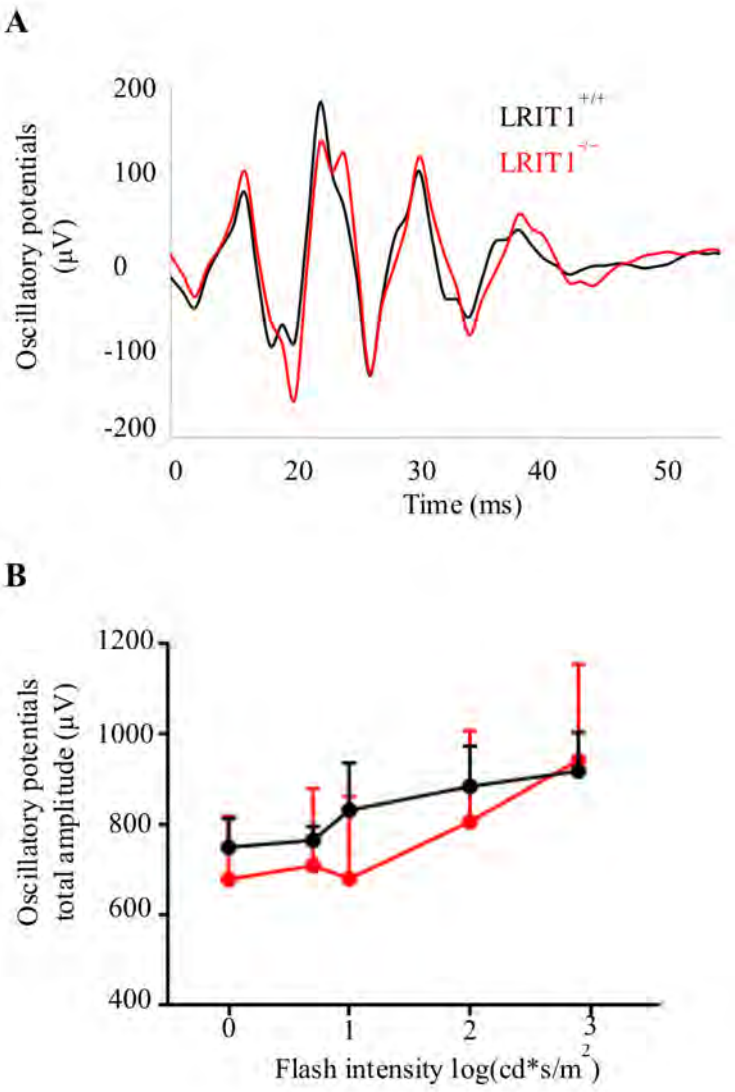

Figure S5. Related to Figure 5. Analysis of the oscillatory potentials of ERG recording.
A, Representative ERG traces of oscillatory potential components measured from dark-adapted mice stimulated with 100 cd/m^2 light. **B,** Statistical analysis of the oscillatory potential amplitudes at different intensities of light stimuli in *Lrit1*$^{+/+}$ and *Lrit1*$^{-/-}$ mice (Mean values and SEM were shown, multiple t-test, N=3 for *Lrit1*$^{+/+}$ and N=5 for *Lrit1*$^{-/-}$).

Table S1: Related to Figure 6. Response Characteristics of Photoreceptors and Bipolar Cells.

Cell Type		V_m (mV)	$I_{1/2}$ (P*/cone)	R_{max} (pA)
Cone Photoreceptor	WT	-37 ± 2.1 (13)	1800 ± 270 (20)	22 ± 1.9 (20)
	Lrit1$^{-/-}$	-33 ± 1.5 (7)	2600 ± 340 (8)	29 ± 1.4 (8)
Rod ON-BC** Dark-adapted	WT	-	4.8 ± 2.7 (2)	220 ± 41 (2)
	Lrit1$^{-/-}$	-	5.0 + 0.3 (5)	220 ± 51 (5)
Cone ON-BC Dark-adapted	WT	-	480 ± 92 (7)	70 ± 7.3 (7)
	Lrit1$^{-/-}$	-	28 ± 2.0 (22)	31 ± 1.0 (22)
Cone ON-BC 210 P*/cone/sec	WT	-	4700 ± 1600 (5)	48 ± 4.5 (5)*
	Lrit1$^{-/-}$	-	5000 ± 530 (14)	14 ± 0.88 (14)*
Cone OFF-BC Dark-adapted	WT	-	220 ± 110 (7)	34 ± 11 (7)
	Lrit1$^{-/-}$	-	9.5 ± 3.0 (7)	45 ± 10 (7)
Cone OFF-BC 210 P*/cone/sec	WT	-	1100 ± 320 (7)	26 ± 5.7 (7)
	Lrit1$^{-/-}$	-	1500 ± 560 (7)	27 ± 6 (7)

Data from (n) individual cells were first fit, then averaged. Response characteristics are documented as mean ± SEM (n)

* Denotes $p<0.05$ based on a paired student's t-test

** Note that rod ON-BC values for sensitivity are calculated in R*/rod

Supplemental Experimental Procedures

Mice

ES cell line with the *Lrit1* targeted allele (Lrit1tm1a(EUCOMM)Hmgu was obtained from EUCOMM (project 115689) and intended modifications described in the Results section were verified by sequencing and long range PCR. The ES cell line was used to generate chimeric mice by blastocyst injection at the Mouse Genetics core at the Scripps Research Institute. Resulting progeny was crossed with C57BL6 strain to establish germline transmission and the F1 mice were further crossed with the germline Cre- expressor strain B6.FVB-TgN(EIIa-Cre)C5379Lmgd (Jackson) to achieve elimination of exon 2 by LoxP recombination. The resulting constitutive *Lrit1* heterozygous knockout mice were inbred to produce -/- and +/+ littermates used in the study. Mice of both sexes were used in the experiments during daytime. Mice used in the study were 1–3 months old, and were maintained on a diurnal 12 h light/dark cycle. Procedures involving mice strictly followed NIH guidelines and were approved by the Institutional Animal Care and Use Committees at Scripps Florida, Washington University and the University of California, Los Angeles.

DNA constructs

Full-length cDNAs encoding human mGluR6 was purchased from Missouri S&T cDNA Resource Center (Cat# GRM6000000). Full-length cDNA encoding mouse *Lrit1* was purchased from Open Biosystems (Clone ID: 5401567). The C-terminal c-myc tagged mouse full length *Lrit1*, NT-LRIT1 (aa 1-527) were amplified from mouse *Lrit1* cDNA clone then sub-cloned into a pcDNA3.1/V5-His-TOPO (Invitrogen) expression vector according to manufacturer's specifications.

Antibodies and Western Blotting

The generation of the following antibodies was described previously: sheep anti-RGS11 (Cao et al., 2008), sheep anti-TRPM1 (Cao et al., 2011). Rabbit anti-RGS7 (7RC1), was a generous gift from William Simonds (NINDDK/NIH), and the guinea pig anti-mGluR6 antibody was a gift from Dr. Takahisa Furukawa (Osaka University). Rabbit anti-Cav1.4 antibody was a generous gift from Dr. Amy Lee (University of Iowa). Rabbit anti-LRIT1 antibodies were generated against mouse recombinant LRIT1 (aa 549-624). Rabbit

anti-LRIT3 CT antibody was generated against human recombinant LRIT3 (aa 604-679). Rabbit anti-ELFN1 (NTR) and rabbit anti-ELFN1 (CTR) antibodies were generated against synthetic peptides of mouse ELFN1 (aa 305-320 and aa 530-547, respectively). Mouse anti-PKCα (ab11723; Abcam), mouse anti-CtBP2 (612044; BD Biosciences), mouse anti-Connexin36 (Clone 8F6.2, Millipore Bioscience Research Reagents, MAB3045), rabbit anti-α2δ4 (Aviva, OAAF04451) and mouse anti-GAPDH (Millipore; MAB374) were purchased.

Whole retinas were removed from mice and lysed by sonication in ice-cold PBS supplemented with 150 mM NaCl, 1% Triton X-100, and Complete protease inhibitor tablets (Roche). Lysates were cleared by centrifugation at 20,800 × *g* for 15 min at 4 °C. Total protein concentration in the supernatant was measured by using BCA Protein Assay Kit (Pierce). Supernatants were added with SDS sample buffer (pH 6.8) containing 8 M urea and were subjected to 12.5% SDS/PAGE. Protein bands were transferred onto PVDF membranes, subjected to Western blot analysis by using HRP-conjugated secondary antibodies, and detected by using ECL West Pico system (Pierce). Signals were captured on film and scanned by densitometer. For quantification, band intensities were determined by using NIH ImageJ software. Integrated intensity of GAPDH was used for data normalization.

Membrane fractionation was done as described in “Preparative immunoprecipitation of mGluR6 complexes” section.

Preparative immunoprecipitation of mGluR6 complexes from mouse retina and mass- spectrometry

Retinas were removed from mice and lysed by sonication in ice-cold PBS supplemented with 150 mM NaCl and Complete protease inhibitor tablets (Roche). After 30-minute centrifugation at 100,000 x g, 4 °C, the pellet was resuspended in ice-cold PBS IP buffer supplemented with 150 mM NaCl, 1% Triton X-100, and Complete protease inhibitor tablets (Roche). The membrane fraction was obtained by 30-minute incubation at 4 °C, and cleared by 30-minute centrifugation at 100,000 x g, 4 ° C, then subjected to immunoprecipitation as previously described (Cao et al., 2015). The beads were washed three times with ice-cold IP buffer. Proteins were eluted with 50 µL SDS sample buffer (62 mM Tris, 10% glycerol, 2% SDS, and 5% β-mercaptoethanol), entered SDS-PAGE by applying ~150 mV for 15-20 minutes. Gels were fixed with using 5% acetic acid in 50% methanol, stained by NOVEX colloidal blue (Invitrogen). Stained areas

were cut out, digested with trypsin (Promega), and alkylated as described previously (Shevchenko et al., 2006). The resulting peptide mixtures were desalted, resolved by high-pressure liquid chromatography, and analyzed using LTQ-Orbitrap XL mass spectrometer, as described previously (Posokhova et al., 2011).

Cell culture and transfection

HEK293T cells were obtained from Clontech and cultured at 37°C and 5% CO in 2

DMEM supplemented with antibiotics, 10% FBS. HEK293T cells were transfected at ~70% confluency using Lipofectamine LTX (Invitrogen) according to the protocol of the manufacturer. The cells were harvested and preceded to co-immunoprecipitation.

Immunoprecipitation

Cells or retina were lysed in ice-cold PBS IP buffer by sonication followed by centrifugation at 14,000 x g for 15 minutes. The supernatant was incubated with 20 µl of 50% protein G slurry (GE Healthcare) and 5 µg antibodies on a rocker at 4°C for 1 hour. After three washes with IP buffer, proteins were eluted from beads with 50 µl of SDS sample buffer. Proteins retained by the beads were analyzed with SDS-PAGE, followed by Western blotting using HRP conjugated secondary antibodies and an ECL West Pico (Thermo Scientific) detection system. Signals were captured on film and scanned by densitometer.

In situ hybridization

Eyeballs were dissected out and put into 4 % paraformaldehyde for 15 minutes. After incubated in 30% sucrose overnight, 12-µm retina sections were moved to OCT and cut using a Leica CM3050 S cryostat, rinsed in PBS and incubated for 90 minutes in hybridization solution (50% deionized formamide, 5X SSC, 5X Denhardt's solution, 500 µg/ml yeast tRNA, 500µg/ml sonicated salmon sperm DNA) at 50 °C. Each section was incubated overnight with hybridization solution at 55 °C containing the Dig-labeled riboprobes. On the second day, each section was washed three times with 0.5X SSC and 30% formamide at 55 °C for 10 minutes, followed by additional three-time washes with PBS at room temperature. The sections were incubated with blocking buffer (10% goat serum, 0.15M NaCl, 0.1M Tris-Cl pH7.5) for 1 hour at room temperature, followed by incubation with anti-dig-AP conjugate (1:500 in blocking buffer) overnight at 4 °C. After three 10-minute washes with washing buffer (0.15M NaCl, 0.1M Tris-Cl pH7.5),

the endogenous peroxidase was inactivated with buffer Developer Buffer (0.5 mg/mL levamisole, 100mM Tris-HCl pH 10, 50mM MgCl2, 100mM NaCl) for 5 minutes. The color was detected by incubation with Developer Buffer with 0.45 µl/mL NBT and 3.5 µl/mL BCIP for 30 minutes. Then the reaction was terminated by TE (pH8). The sections were mounted and images were acquired using an optical microscope (Leica DM IL LED).

Fluorescence *in situ* hybridization

The mRNA expression was evaluated with ViewRNATM 2-plex In Situ Hybridization

Assay (Panomics, Santa Clara, CA) using the following probes: *Lrit1* (NM_146245.2; Cat# VB1-17470). The whole eye bulb was extracted, embedded in OCT and flash frozen in liquid nitrogen. 12 µm sections were cut using a Leica CM3050 S cryostat, rapidly post-fixed in 4% paraformaldehyde for 10 minutes, washed twice in phosphate buffered saline (PBS) and incubated for 2h in pre-hybridization mix (50% deionized formamide, 5X SSC, 5X Denhardt's solution, 250 µg/ml yeast tRNA, 500µg/ml sonicated salmon sperm DNA) at room temperature. Each section was incubated overnight with Panomics hybridization solution (using an incubator set to 40oC, no CO_2 and humidity higher than 85%) containing the QuantiGene ViewRNA probe set diluted 1:50 in Probe Set Diluent QT. On the second day, the retina sections were processed according to manufacturer's instructions provided with the ViewRNA ISH Tissue Assay Kit (QVT0012). Briefly, sections were successively incubated with PreAmplifier Mix QT, Amplifier Mix QT, Label Probe 1-AP (1:1000), AP-Enhancer Solution and Fast Red Substrate. Finally, the nuclei were counterstained with DAPI and mounted using Fluoromont-G (SouthernBiotech). Confocal images were generated at The Light Microscopy Facility, the Max Planck Florida Institute, using a LSM 780 Zeiss confocal microscope. Image acquisition and processing were accomplished using ZEN 2011 (64 bit) software (Carl Zeiss) with only minor manipulations of the images setting the fluorescence intensity in non-saturating conditions and maintaining similar parameters for each acquired image

Immunohistochemistry

Dissected eyecups were fixed for 15 min in 4% paraformaldehyde, cryoprotected with 30% sucrose in PBS for 2 h at room temperature, and embedded in optimal cutting temperature medium. Twelve-micrometer frozen sections were obtained and blocked in

PT1 (PBS with 0.1% Triton X-100 and 10% donkey serum) for 1 h, then incubated with primary antibody in PT2 (PBS with 0.1% Triton X-100 and 2% donkey serum) for at least 1 h. After four washes with PBS with 0.1% Triton, sections were incubated with fluorophore-conjugated secondary antibodies in PT2 for 1 h. After four washes, sections were mounted in Fluoromount (Sigma). For LRIT3 and α2δ4 staining, antigen retrieval was done by incubating slides in basic antigen retrieval reagent (R&D system) preheated to ~80 degree for 5 min before blocking. Images were taken with a Leica SP800 or Zeiss LSM 880 confocal microscope. Quantitative analysis of LRIT1, mGluR6, GPR179, and ELFN1 immunofluorescence from confocal images was performed using Leica software or Zen Blue 2 analysis software. Sections were double stained with for marker protein mGluR6, which localizes at the synaptic puncta of ON-BC and was used as a mask to define synapses. The fluorescence intensity within synaptic puncta was analyzed using constant puncta-encircling area, which tightly surrounded the contours of each puncta. A line of 1-1.5 μm (white bar) was drawn through the center of the distinct mGluR6-positive synapses and the distribution of the fluorescence intensity along this line was scanned to generate the traces. Mean fluorescent intensity (measured in pixels) was averaged from ~10-20 individual and randomly selected mGluR6-positive puncta per imaged section. For LRIT1 immunofluorescence in different animal models and different synaptic molecules staining the entire OPL was first selected using hand drawn tool in Zen Blue and the mean immunofluorescent intensity within OPL was calculated by the software. The mean fluorescent intensity of two to three sections per retina, and two to three retinas per genotype were used for final quantification and comparison. Imaging parameters were the same for all sections and retinas.

Electroretinography (ERG)

Electroretinograms were recorded by using the UTA system and a Big-Shot Ganzfeld (LKC Technologies). Mice (~ 4-8 weeks old) were dark-adapted (≥6 h) and prepared for recordings using a red dim light. Mice were anesthetized with an i.p. injection of ketamine and xylazine mixture containing 100 and 10 mg/kg, respectively. All procedures were approved by the Institutional Animal Care and Use committee at the Scripps Florida Research Institute. Recordings were obtained from the right eye only, and the pupil was dilated with 2.5% phenylephrine hydrochloride (Bausch & Lomb), followed by the application of 0.5% methylcellulose. Recordings were performed with a gold loop electrode supplemented with contact lenses to keep the eyes immersed in

solution. The reference electrode was a stainless steel needle electrode placed subcutaneously in the neck area. The mouse body temperature was maintained at 37 °C by using a heating pad controlled by ATC 1000 temperature controller (World Precision Instruments). ERG signals were sampled at 1 kHz and recorded with 0.3-Hz low-frequency and 300-Hz high-frequency cut-offs. Full field white flashes were produced by a set of LEDs (duration < 5 ms) for flash strengths ≤ 2.5 cd*s/m^2 or by a Xenon light source for flashes > 2.5 cd*s/m^2 (flash duration < 5 ms). ERG responses were elicited by a series of flashes ranging from 1× 10^{-5} to 800 cd*s/m^2 in 10-fold increments. Ten trials were averaged for responses evoked by flashes up to 0.1 cd*s/m^2, and three trials were averaged for responses evoked by 0.5 and 1 cd*s/m^2 flashes. Single flash responses were recorded for brighter stimuli. To allow for recovery, interval times between single flashes were as follows: 5 s for 1× 10^{-5} to 0.1 cd*s/m^2, 30 s for 0.5 and 1 cd*s/m^2, 60 s for 5 and 10 cd*s/m^2, and 180 s for 100 and 800 cd*s/m^2 flashes. Light backgrounds of 50, 1, and 0.1 cd/m^2 were administered for 5 minutes for recording partially saturated rod- and cone-only ERGs. At rod saturating (cone-only) backgrounds, ten trials were averaged at an interval recovery time of 1 second between flashes.

ERG traces were analyzed using the EM LKC Technologies software and Microsoft Excel. The b-wave amplitude was calculated from the bottom of the a-wave response to the peak of the b-wave. The data points from the b-wave stimulus–response curves were fitted by Equation 1 using the least-square fitting method in GraphPad Prism6.

(1) $R=R_{max,r}*I/(I + I_{0.5,\ r}) + R_{max,c}*I/(I + I_{0.5,c})$

The first term of this equation describes rod-mediated responses (r), and the second term accounts primarily for responses that were cone mediated (usually at flash intensities ≥1 cd*s/m^2 for dark-adapted mice; index c). $R_{max,r}$ and $R_{max,c}$ are maximal response amplitudes, and $I_{0.5,r}$ and $I_{0.5,c}$ are the half-maximal flash intensities. Stimulus responses of retina cells increase in proportion to stimulus strength and then saturate, this is appropriately described by the hyperbolic curves of this function.

The oscillatory potential traces were generated by transforming the original ERG traces using the built-in Oscillatory Potential Analysis function in EM LKC Technologies software which also calculated the amplitude of oscillatory potential.

For the flicker ERG response test, 10 trials were averaged from 3cd*s/m^2 flashes at a delivery rate of 7 Hz.

Electron Microscopy

Eyes were enucleated, cleaned of extra-ocular tissue, and pre-fixed for 15 min in cacodylate-buffered half-Karnovsky's fixative containing 2mM calcium chloride. Then the eyecups were hemisected along the vertical meridian and fixed overnight in the same fixative. The specimens were rinsed with cacodylate buffer and postfixed in 2% osmium tetroxide in buffer for 1 hour, then gradually dehydrated in an increasing ethanol and acetone series (30– 100%), and embedded in Durcupan ACM resin (Electron Microscopy Sciences, PA). Blocks were cut with 70-nm-thickness, and were stained with 3% lead citrate. Sections were examined in a Tecnai G2 spirit BioTwin (FEI) transmission electron microscope at 80 or 100 kV accelerating voltage. Images were captured with a Veleta CCD camera (Olympus) operated by TIA software (FEI).

Single cell recordings from cones and bipolar cells, and light calibrations

Light-evoked responses from photoreceptors and bipolar cells were recorded retinal slices using methods described previously (Okawa et al., 2010). Briefly, mice were dark-adapted overnight and euthanized according to protocols approved by the University of California, Los Angeles Animal Research Committee (Protocol 14-005-11). Eyes were enucleated under infrared light, retinas were isolated, and 200-µm thick slices were cut with a vibrating microtome. Slices were superfused with bicarbonate-buffered Ames' media (equilibrated with 5% CO_2/95% O_2) heated to 35-37^oC, visualized under infrared illumination, and were stimulated with a blue light- emitting diode (λ_{max} ~ 405nm).

Light-evoked responses were measured using patch electrodes in voltage-clamp mode (V_m = -40 mV for photoreceptor cells, V_m = -60 mV for bipolar cells), using an electrode internal solution consisting of (in mM): 125 K-aspartate, 10 KCl, 10 HEPES, 5 N-methyl-glucamine/HEDTA, 0.5 CaCl2, 1 ATP-Mg, and 0.2 GTP-Mg; pH was adjusted to 7.3 with N- methyl-glucamine hydroxide, and osmolarity was adjusted to 280 mOsm. Patch clamp recordings from cones additionally included 1 mM NADPH in the internal solution, which prevented response rundown. Light-evoked responses were sampled 10 kHz and filtered at 300 Hz with an 8-pole Bessel filter (Frequency Devices, Ottawa, IL). Data was further decimated and filtered offline at 50 Hz in Matlab (Mathworks, Natick, MA).

Recordings were made during experiments on WT and *Lrit1*$^{-/-}$ from cone photoreceptors, rod ON-BCs, and cone ON-BCs in retinal slices. The experimenter was blinded to the genotype of the animal until the recorded data was analyzed. We distinguished between bipolar cell types based on the polarity and time course of the response in conjunction with the cell's morphology. Recorded cells were visualized following their patch dialysis with a fluorophore (Alexa-750; Life Technologies) added to the electrode internal solution, allowing visualization in the far red without significant visual pigment bleaching. The responses of cones, and rod and cone ON-BCs were recorded from the same slices, and were typically adjacent to one another.

Light stimulation consisted of 10ms flashes of light that varied in strength from those yielding a just discernable response to those that generate a maximal response. Flash strengths are reported in activated cone pigment molecules (or P*/cone) at 405 nm, near the isosbestic point for S-cone and M-cone spectral sensitivities. To derive P*/cone, collecting areas were calculated from quantal responses at 405 nm recorded from control rods to derive the R*/rod. To calculate P*/cone, we adjusted this value for the difference in the volume of the cone vs. rod outer segment (cone/rod: $14\mu m^3/38\mu m^3$), which were then used to scale for the cone collecting area.

Evaluation of mouse vision by optokinetic reflex (OKR) test

Photopic contrast sensitivity of mice was evaluated from optomotor responses using a two- alternative forced-choice protocol, as previously described (Kolesnikov et al., 2011; Umino et al., 2008). Briefly, a mouse was placed on a pedestal surrounded by four computer monitors and observed from above using a camera. Mice responded to visual stimuli (sine-wave vertical gratings presented on the computer monitors using staircase paradigm and invisible to the experimenter), by reflexively rotating their head in either clockwise or counterclockwise direction. By looking at the very tip of animal's nose on a zoomed video view (140%), the observer registered the direction of optomotor responses and the computer determined the correctness of the choice (Prusky et al., 2004). In contrast to previous work (Kolesnikov et al., 2011; Umino et al., 2008), the duration of each trial was not strictly limited to 5 s, and the trial started only when the mouse was in a stable position on the pedestal, which could take up to several minutes. Photopic visual acuity was estimated as the threshold for spatial frequency of the stimuli at 100% contrast. Photopic contrast sensitivity was defined as the inverse of contrast threshold values which were obtained at fixed background luminance of monitors (1.1

cd m^{-2} at the mouse eye level, as attenuated by neutral density film filters that formed a cylinder around the animal), over a range of various stimuli speeds (Sp), from 5 to 50 deg/s. Spatial frequency (Fs) of stimuli was kept constant at its optimal value of 0.128 cyc/deg, for a range of corresponding temporal frequencies (Ft = Sp*Fs) from 0.64 to 6.4 Hz (Umino et al., 2008). All data were analyzed using independent two-tailed Student *t*-test, with accepted significance level of $p < 0.05$.

Supplemental References

Cao, Y., Posokhova, E., and Martemyanov, K.A. (2011). TRPM1 forms complexes with nyctalopin in vivo and accumulates in postsynaptic compartment of ON-bipolar neurons in mGluR6-dependent manner. J Neurosci *31*, 11521-11526.

Cao, Y., Sarria, I., Fehlhaber, K.E., Kamasawa, N., Orlandi, C., James, K.N., Hazen, J.L., Gardner, M.R., Farzan, M., Lee, A.*, et al.* (2015). Mechanism for Selective Synaptic Wiring of Rod Photoreceptors into the Retinal Circuitry and Its Role in Vision. Neuron *87*, 1248-1260. Cao, Y., Song, H., Okawa, H., Sampath, A.P., Sokolov, M., and Martemyanov, K.A. (2008). Targeting of RGS7/Gbeta5 to the dendritic tips of ON-bipolar cells is independent of its association with membrane anchor R7BP. J Neurosci *28*, 10443-10449.

Kolesnikov, A.V., Rikimaru, L., Hennig, A.K., Lukasiewicz, P.D., Fliesler, S.J., Govardovskii, V.I., Kefalov, V.J., and Kisselev, O.G. (2011). G-protein betagamma-complex is crucial for efficient signal amplification in vision. J Neurosci *31*, 8067-8077. Okawa, H., Miyagishima, K.J., Arman, A.C., Hurley, J.B., Field, G.D., and Sampath, A.P. (2010). Optimal processing of photoreceptor signals is required to maximize behavioural sensitivity. J Physiol *588*, 1947-1960.

Posokhova, E., Song, H., Belcastro, M., Higgins, L., Bigley, L.R., Michaud, N.A., Martemyanov, K.A., and Sokolov, M. (2011). Disruption of the Chaperonin containing TCP-1 function affects protein networks essential for rod outer segment morphogenesis and survival. Mol Cell Proteomics *10*, M110 000570. Prusky, G.T., Alam, N.M., Beekman, S., and Douglas, R.M. (2004). Rapid quantification of adult and developing mouse spatial vision using a virtual optomotor system. Invest Ophthalmol Vis Sci *45*, 4611-4616.

Shevchenko, A., Tomas, H., Havlis, J., Olsen, J.V., and Mann, M. (2006). In-gel digestion for mass spectrometric characterization of proteins and proteomes. Nature protocols *1*, 2856-2860. Umino, Y., Solessio, E., and Barlow, R.B. (2008). Speed, spatial, and temporal tuning of rod and cone vision in mouse. J Neurosci *28*, 189-198.

Appendix A

Why are rods more sensitive than cones?

JPn Neuroscience
The Journal of Physiology

J Physiol 594.19 (2016) pp 5415–5426

TOPICAL REVIEW

Why are rods more sensitive than cones?

Norianne T. Ingram[1], Alapakkam P. Sampath[2] and Gordon L. Fain[1,2]

[1]*Department of Integrative Biology and Physiology, University of California, Los Angeles, CA 90095–7239, USA*
[2]*Department of Ophthalmology and Jules Stein Eye Institute, University of California, Los Angeles, CA 90095–7000, USA*

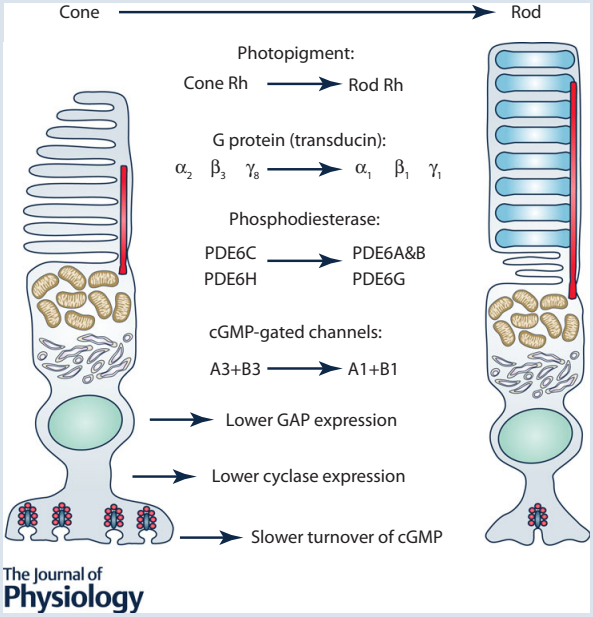

Abstract One hundred and fifty years ago Max Schultze first proposed the duplex theory of vision, that vertebrate eyes have two types of photoreceptor cells with differing sensitivity: rods for dim light and cones for bright light and colour detection. We now know that this division is fundamental not only to the photoreceptors themselves but to the whole of retinal and visual processing. But why are rods more sensitive, and how did the duplex retina first evolve? Cells resembling cones are very old, first appearing among cnidarians; the emergence of rods was a key step in the evolution of the vertebrate eye. Many transduction proteins have different isoforms in rods and cones, and others are expressed at different levels. Moreover rods and cones

Gordon L. Fain is Distinguished Professor of Integrative Biology/Physiology and of Ophthalmology at the University of California Los Angeles (UCLA) and a member of the Jules Stein Eye Institute. His laboratory works on the physiology of vertebrate photoreceptors. **Norianne Ingram** is a graduate student in the Molecular, Cellular, and Integrative Physiology Program at UCLA and is presently doing her thesis on cone photoreceptors and retinal signal processing. **Alapakkam P. Sampath** is Professor of Ophthalmology at UCLA and a member of the Jules Stein Eye Institute. His laboratory works on vertebrate photoreceptor physiology and signal integration in vertebrate retina.

DOI: 10.1113/JP272556

have a different anatomy, with only rods containing membranous discs enclosed by the plasma membrane. These differences must be responsible for the difference in absolute sensitivity, but which are essential? Recent research particularly expressing cone proteins in rods or changing the level of expression seem to show that many of the molecular differences in the activation and decay of the response may have each made a small contribution as evolution proceeded stepwise with incremental increases in sensitivity. Rod outer-segment discs were not essential and developed after single-photon detection. These experiments collectively provide a new understanding of the two kinds of photoreceptors and help to explain how gene duplication and the formation of rod-specific proteins produced the duplex retina, which has remained remarkably constant in physiology from amphibians to man.

(Received 1 April 2016; accepted after revision 16 May 2016; first published online 24 May 2016)
Corresponding author G. L. Fain: 2129 Terasaki Life Sciences, 610 Charles E Young East, University of California, Los Angeles, Los Angeles, CA 90095–7239, USA. Email: gfain@ucla.edu

Abstract figure legend Rods evolved from cones or their progenitors through the emergence of distinct isoforms and altered expression levels of proteins required for transducing light into an electrical signal. These changes must collectively explain why rods are more sensitive.

Abbreviations *A*, activation constant; cGMP, cyclic guanosine monophosphate; CNG, cyclic-nucleotide gated; GAP, GTPase-accelerating protein; GC, guanylyl cyclase; GCAP, guanylyl cyclase-activating protein; GRK, G-protein receptor kinase; hν, light (photon); mG, mouse 508 nm cone rhodopsin; mS, mouse 360 nm cone rhodopsin; PDE6, phosphodiesterase 6; PDE6*, light-activated phosphodiesterase 6; Rh*, light-activated rhodopsin or metaII; Tα, α subunit of photoreceptor G protein; WT, wild-type.

Introduction

In 2016 we celebrate the 150th anniversary of the groundbreaking article of Max Schultze (1866), who first proposed that rod and cone photoreceptors have different functions. Schultze noticed that retinas of nocturnal animals tend to have a larger proportion of cells with rod-shaped outer segments (Fig. 1*A*), and that diurnal animals have greater numbers of cells with outer segments tapering like cones (Fig. 1*B*). He then proposed the *duplex* theory of vision: that rods mediate perception in dim light and cones are specialized for bright light and colour vision. We now know that his division of visual detection into two systems is fundamental not only to the properties of photoreceptors but also to the connections these cells make with other neurons and to the whole of retinal and visual processing (Masland, 2012).

Since the publication of Schultze's paper, we have wondered why rod vision is more sensitive. The first intracellular recordings showed that most of the sensitivity difference is inherent in the photoreceptors themselves: single rods are more sensitive than single cones (Fain & Dowling, 1973). Soon afterward, biochemists and molecular biologists discovered that the two photoreceptors have many of the same kinds of proteins and detect light in a similar way. Cones are much older than rods: from the sequences of a very large number of vertebrate photopigments, we can infer that gene duplication produced all of the different kinds of cone pigments before the evolution of rod pigments (Nickle & Robinson, 2007; Shichida & Matsuyama, 2009). Along with the pigment came the many other molecular and anatomical differences between the two kinds of cells, with the result that rods are able to integrate incoming light over a longer period and operate at the theoretical limit of single-photon detection, whereas cones are less sensitive but exhibit adaptive properties that allow them to detect luminance changes and motion when the photon flux is less limiting. These differences in physiology must ultimately derive from differences in the mechanism of transduction in the two kinds of photoreceptors.

Recent experiments are beginning to clarify these differences. Some of the most interesting observations have been made from the combined efforts of molecular biologists and physiologists inserting cone genes into mouse rods. These experiments along with more traditional observations by biochemists and single-cell physiologists are gradually clarifying the roles of different proteins in rod sensitivity. Our initial expectation had been that one particular alteration might dramatically change the properties of the photoreceptor. Instead we have discovered what we should have suspected all along, that evolution proceeded by making small changes in many transduction proteins, incrementally increasing sensitivity to produce the rods and cones that emerged as long as 500 million years ago. Although the present state of research leaves many questions unanswered, we can now begin to see how rods became more sensitive.

Mechanism of transduction: rod/cone protein isoforms

Both rods and cones detect light according to the same basic scheme (Fig. 2). They use similar photopigments, which were once given distinct names but are now usually called rod or cone opsin or rhodopsin. The absorption of light produces a change in the pigment conformation to an intermediate called metaII or Rh*, which triggers a G-protein cascade (for an overview, see for example Fain, 2014). The heterotrimeric G proteins of rods and cones (called transducins) are different: rods express α1, β1 and γ1, whereas cones express α2, β3 and γ8 (Sakmar & Khorana, 1988; Kubo *et al.* 1991; Ong *et al.* 1995; Deng *et al.* 2009). The G protein binds to Rh*, and exchange of GTP for GDP on the transducin α subunit (Tα) produces the active form Tα•GTP.

Tα•GTP binds to the photoreceptor effector enzyme, which is phosphodiesterase 6 (PDE6). This protein has four subunits, two catalytic and two inhibitory. The catalytic subunits are slightly different from one another in rods and are called PDE6α and PDE6β (or PDE6A and PDE6B), whereas the two in cones are the same and called PDE6α' (or PDE6C). Each PDE tetramer also has two inhibitory subunits, one for each catalytic subunit, which have somewhat different sequences in the two types of photoreceptors and are called rod or cone PDE6γ, or PDEG (in rods) and PDEH (in cones). Activated PDE6 hydrolyses cGMP, which acts as the second messenger of the cascade by binding to cGMP-gated channels. The channels are tetramers again with different protein subunits called CNGA1 and CNGB1 in rods and CNGA3 and CNGB3 in cones (see Kaupp & Seifert, 2002; Zhong *et al.* 2002; Shuart *et al.* 2011).

Based on this general scheme, the activation of a single rhodopsin molecule is amplified across these stages to lead ultimately to the destruction of as many as one million cGMP molecules per Rh* in rods (Yee & Liebman, 1978). This reduction in cGMP concentration across vertebrate species is sufficient to reduce the cGMP-gated current by more than its intrinsic noise in darkness (Baylor *et al.* 1979, 1984; Nakatani *et al.* 1991). The natural question to ask then is, can the lower sensitivity of cones be the result purely of reduced amplification within these steps? Let us suppose that rod and cone responses were to *inactivate* at the same rate. A reduced rate of *activation* would then cause cone responses to reach smaller peak amplitudes and might account entirely for the difference in sensitivity. But do rod and cone responses inactivate at the same rate? Not even close! In every vertebrate species from lamprey (Morshedian & Fain, 2015; Asteriti *et al*, 2015) to mouse (see Fig. 3), the rate is much faster in cones, and this difference must also contribute to the reduced cone sensitivity.

The rate of inactivation is determined by the rates at which Rh*, transducin and PDE return to their basal

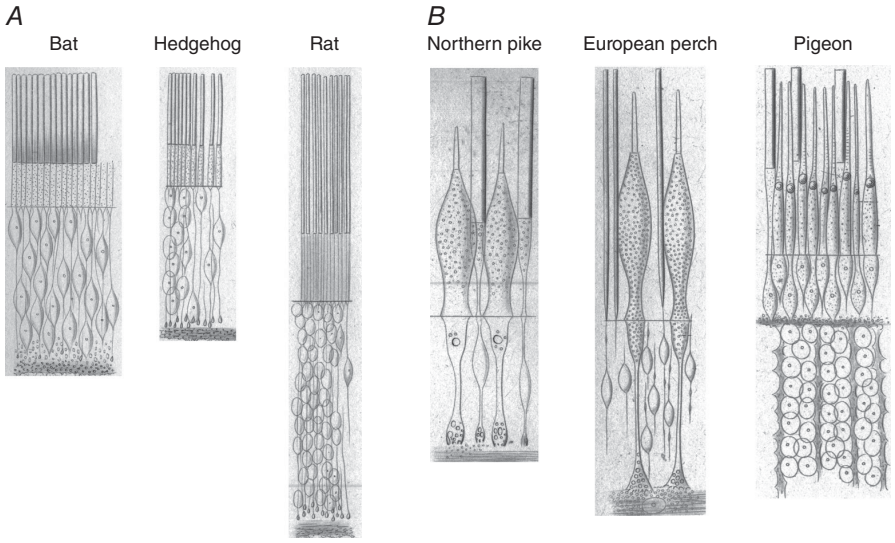

Figure 1. Rods and cones in nocturnal and diurnal animals
Drawings from Schultze's original paper (1866) of photoreceptors from nocturnal animals (*A*) and diurnal animals (*B*), magnification approximately 350–400 times. Schultze claimed that the bat retina lacked even a trace of cones, but in rat he noticed occasional gaps (*Lücken*) which he speculated could possibly correspond to cones, as we now know to be true. Fish and pigeon on the other hand have many easily observable cones in addition to rods. Schultze commented that these observations 'would seem to indicate that rods are more advantageous than cones for quantitative light perception', but that 'cones would seem to be the nerve end-organs for colour perception'.

conformations and the cGMP concentration goes back to its dark level. Rh* is silenced like other G-protein receptors by phosphorylation and binding of arrestin. Rods and cones can have two different G-protein receptor kinases, GRK1 in rods and GRK1 and/or GRK7 in cones, but rodents, including mice, have only GRK1 in both kinds of photoreceptors. Rods in mice have arrestin-1 and cones both arrestin-1 and arrestin-4, though arrestin-1 is by far the predominant species in both kinds of photoreceptors (Nikonov *et al.* 2008).

Activated transducin and phosphodiesterase are extinguished as in other G-protein cascades by hydrolysis of Tα•GTP to Tα•GDP with the assistance of PDEγ and three GTPase-accelerating proteins (GAPs): RGS9-1, Gβ5 and the R9AP-1 binding protein (see Arshavsky & Wensel, 2013). These proteins are required to speed PDE deactivation into the functional range of tens to hundreds of milliseconds, compared to the seconds or tens of seconds required in their absence (Hollinger & Hepler, 2002). Although these GAP complex proteins are the same in rods and cones, expression is significantly higher in cones (Cowan *et al.* 1998; Zhang *et al.* 2003), a point we return to later.

The cGMP concentration is restored by guanylyl cyclase (GC), which in photoreceptors is a member of the membrane guanylyl cyclase family (Potter, 2011). There are two cyclases in mammalian photoreceptors called retGC1 (or GC-E) and retGC2 (or GC-F); in mouse, rods have mostly retGC1 with some retGC2, whereas cones have only retGC1 (Wen *et al.* 2014). This difference is unlikely to be physiologically significant because when the gene for retGC2 is deleted there is little effect on rod sensitivity or response waveform (Baehr *et al.* 2007). The rate of cyclase activity is controlled by small molecular weight Ca^{2+}-binding proteins called guanylyl cyclase-activating proteins or GCAPs. There are again two in mouse, GCAP1 and GCAP2, with somewhat different sensitivities for divalent ion binding (Dizhoor *et al.* 2010); rods express both GCAPs but cones mostly express GCAP1 (Dizhoor *et al.* 1995; Xu *et al.* 2013; Boye *et al.* 2015).

The differences in transduction proteins for rods and cones are summarized in Table 1. Rods and cones also display differences in anatomy: the photopigment in rods is contained almost entirely within the membrane of intracellular discs, whereas cone outer segments are formed from infoldings of the plasma membrane. We have long wondered whether this difference in anatomy might hold the key to the difference in sensitivity, but we now know the answer. Nature did the experiment for us: the rods and cones of lamprey have an identical morphology, which is like that of cones (see for example Dickson & Graves, 1979), but lamprey rods are nearly as sensitive as mouse rods and about 70 times more sensitive than lamprey cones (Morshedian & Fain, 2015; Asteriti *et al.* 2015). The discs of

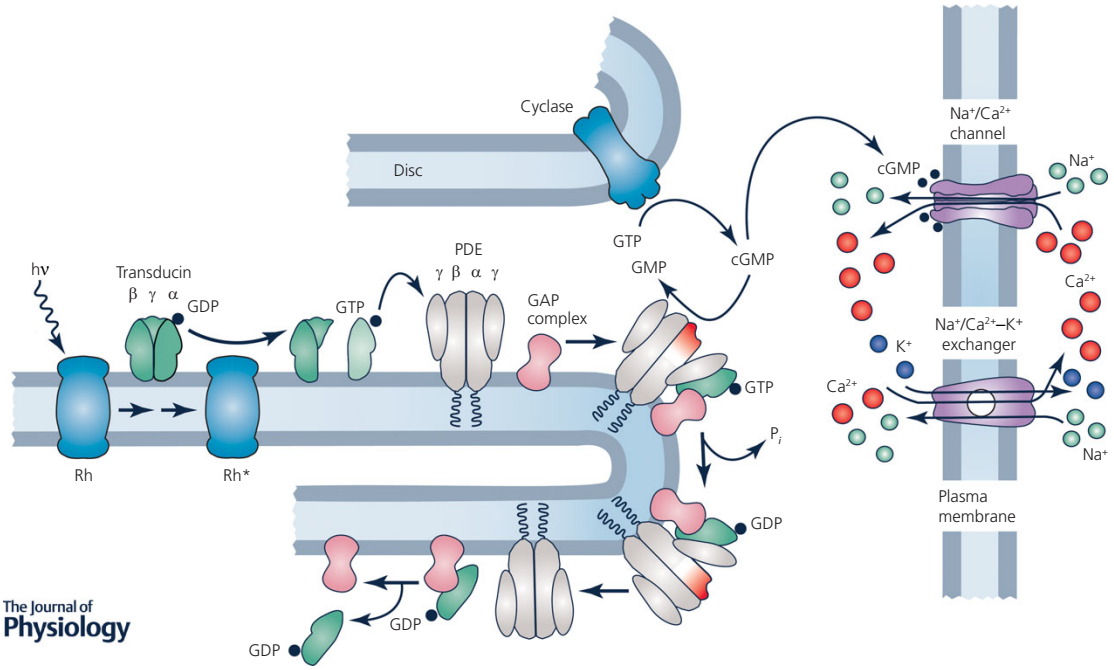

Figure 2. Phototransduction in vertebrate photoreceptors
Redrawn and printed with permission from Fain *et al.* (2010).

rods do not seem to be essential for high sensitivity vision (see also Ma *et al.* 2001) but may instead have evolved to allow more efficient renewal of outer segment membrane (Morshedian & Fain, 2015).

Activation of transduction

Although rods are universally more sensitive than cones, the value of the sensitivity difference varies among vertebrates, ranging from 25-fold in mudpuppy (Fain & Dowling, 1973) to 1000-fold between red-sensitive cones and rods in carp (Tachibanaki *et al.* 2001). In our examination of the cause of this sensitivity difference, we will take as our example the mouse, because many of the most recent experiments have utilized transgenic mice. In Fig. 3*A* and *B*, we show mean responses of mouse rods and cones recorded with suction electrodes. Rod responses decay much more slowly than cone responses (note ten-fold difference in the scale of the abscissa) and are typically about twice as large; after normalizing response amplitudes to their maximum values, rods are a little more than 100 times more sensitive than cones (Fig. 3*C*), as previously reported (see for example Nikonov *et al.* 2006). Part of this difference is the result of the larger volume of the rod outer segment, which increases the probability of absorption of a photon by pigment molecules. We can, however, correct for these differences by calculating the percentage decrease in photocurrent per photon absorbed. Calculations of this kind give about 0.2–0.25% per Rh* for cones (Nikonov *et al.* 2006; Sakurai *et al.* 2011; Cao *et al.* 2014) and 5% for rods (Sampath *et al.* 2005; see Reingruber *et al.* 2015). The resulting factor of between 20 and 30 is the difference in sensitivity produced by the transduction cascade.

One reason rods are more sensitive is that early events in the transduction cascade have greater gain and close channels more rapidly, as alluded to previously. As a consequence, rod responses rise more quickly per photon absorbed; with everything else being equal, rod responses would reach a commensurately larger peak amplitude for the same intensity of stimulus. Following the theoretical treatment of Pugh and Lamb (1993, 2000), we can use the rising phases to calculate values of an amplification constant *A* (see Fig. 4*A* and legend), equal to the product of (1) the rate of formation of light-activated PDE6* by the photopigment, (2) the rate of decline of cGMP

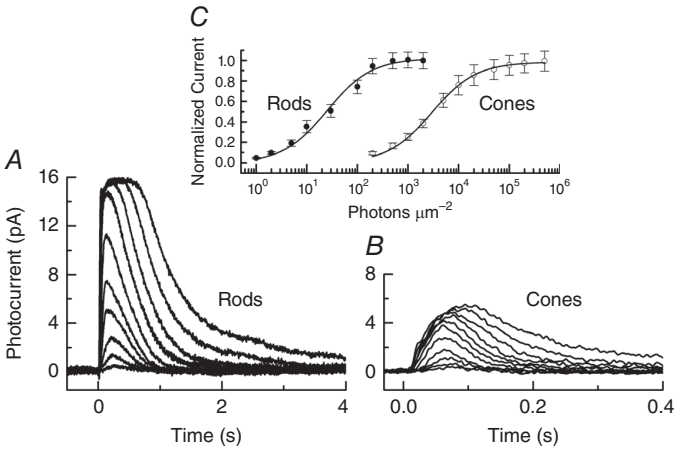

Figure 3. Responses of mouse rods and cones
A, mean responses of 11 WT mouse rods to 20 ms flashes of 500 nm illumination from 0.5 to 2000 photons μm^{-2}. *B*, mean responses of 18 mouse M (508 nm) cones to 20 ms flashes of 500 nm illumination from 200 to 500,000 photons μm^{-2}. Responses in *A* and *B* were filtered with an 8-pole Bessel filter with a low-pass filter setting of 75 Hz. *C*, mean peak amplitudes (with SEM) of responses of mouse rods (•) and mouse cones (○) to 20 ms flashes of 500 nm illumination, normalized to maximum response and plotted as a function of flash intensity. Curves give best-fitting Michaelis–Menten equation with flash intensities at half-maximal amplitude of 25.3 (for rods) and 2960 (for cones) photons μm^{-2}. All recordings were made from C57BL/6 mice from Jackson Laboratory (Bar Harbor, ME, USA), dark adapted for at least 4 h and usually overnight. All experiments were performed on mice of either sex in accordance with the rules and regulations of the NIH guidelines for research animals, as approved by the institutional animal care and use committee (IACUC) of the University of California, Los Angeles. Animals were kept in cyclic 12 h/12 h on/off lighting in approved cages and supplied with ample food and water. Animals in all experiments were killed before tissue extraction by approved procedures, usually CO_2 inhalation or decerebration. Recordings were made at 37°C in Ames solution. Light intensities are given as photons effective at the lambda max of the rod or cone pigment calculated by convolving the spectrum of the stimulating beam with the rod or cone photopigment absorption curves.

Table 1. Photoreceptor transduction protein isoforms in mouse rods and cones

	Rod	Cone
Photopigment	Rod opsin (or rhodopsin)	Cone opsin (or rhodopsin)
G protein (transducin)	α1, β1 and γ1	α2, β3 and γ8
Phosphodiesterase 6	PDE6A and PDE6B	PDE6C
	Rod PDE6γ (PDE6G)	Cone PDE6γ (PDE6H)
cGMP-gated channels	CNGA1 and CNGB1	CNGA3 and CNGB3
Rhodopsin kinase	GRK1	GRK1
Arrestin	Arrestin-1	Arrestin-1 and arrestin-4
GAPs	RGS9-1, Gβ5 and R9AP-1	RGS9-1, Gβ5 and R9AP-1
Guanylyl cyclase	retGC1 and retGC2	retGC1
GCAPs	GCAP1 and GCAP2	GCAP1
Na^+/Ca^{2+}–K^+ exchanger	NCKX1	NCKX2 and NCKX4

concentration per PDE6* molecule, and (3) the Hill coefficient of binding of cGMP to the channels. The value of *A* is somewhat dependent on the frequency response of the recording (Chen *et al.* 2010*b*) but is at least 2–3 times larger in rods than in cones (see Pugh & Lamb, 1993; Nikonov *et al.* 2006; Cao *et al.* 2014). This difference must be produced by the collective properties of the proteins responsible for activation. Since the Hill coefficient of rod and cone cGMP-gated channels is nearly the same (Picones & Korenbrot, 1992; see Kaupp & Seifert, 2002), we can focus our attention on the photopigments, G proteins and PDE6s, which, as we have seen, all have different isoforms in rods and cones.

One way to test the role of these proteins is by exogenous expression of cone proteins in rods or rod proteins in cones. Gene incorporation is easier for rods because there is only one rod photopigment in mouse with a reliable and widely used promoter, and rods are more convenient for physiology; so most experiments have put cone genes into rods. There is one complication: the value of *A* depends upon the rate of change of the cGMP concentration which is inversely proportional to cytoplasmic volume, because the larger the volume, the smaller the change in concentration per activated enzyme. Since mouse rods are about 2.5 times larger in volume than mouse cones, *A* would be 2.5 times smaller in rods even if the properties of all of the proteins were the same. To account for the *greater* value of *A* actually recorded from rods, activation would need to proceed at a rate at least 5–10 times faster (Nikonov *et al.* 2006). That is, if we could express the cone variants of all the activation proteins in a rod, activation should be at least something like 5–10 times slower. No one has yet expressed all of the proteins together, but many attempts have been made to express them one by one.

We begin with the photopigments. Sakurai and colleagues (2007) inserted the mouse 508 nm cone pigment gene (*mG*) in place of mouse rhodopsin. They found that *mG/mG* rods were about a factor of 3–4 less sensitive than wild-type (WT) rods and gave smaller values for the activation constant *A*, but *mG/mG* rods expressed considerably less pigment and transducin, had smaller outer segments, and showed signs of degeneration. Clearer perhaps were experiments expressing the mG pigment on a background of mutant E112Q rod rhodopsin (Sakurai *et al.* 2007), whose peak absorbance is shifted into the blue so that rod and cone pigments in mG/Rh^{EQ} rods can be stimulated selectively. The cone mG pigment produced a response per Rh* only about a third as large as the rod E112Q rhodopsin.

In a similar study, Shi and colleagues (2007) expressed the mouse short wavelength-sensitive (360 nm) pigment (mS) in mouse rods and recorded from homozygous *mS/mS* rods lacking rod rhodopsin as well as from heterozygous photoreceptors expressing both the mS pigment and rod rhodopsin. Although the single-photon response of *mS/mS* rods was smaller than in WT rods, confirming the study of Sakurai *et al.* (2007), recordings from heterozygotes expressing both the mS cone and WT rod pigments and selectively stimulated with short- and long-wavelength light showed no differences in sensitivity or response waveform. The two pigments seemed to produce nearly identical responses when expressed in the same rod.

Fu and colleagues (2008) then expressed the human long-wavelength pigment in mouse rods. Responses to the rod and cone pigments were indistinguishable in sensitivity and waveform. The cone pigment produced greater dark noise as also in the experiments of Sakurai *et al.* (2007; but see Shi *et al.* 2007), perhaps as a result of the lower stability of cone pigments generally (Rieke & Baylor, 2000; Sampath & Baylor, 2002; Kefalov *et al.* 2003; Kefalov *et al.* 2005; but see Angueyra & Rieke, 2013). This increase in noise was, however, not large enough to affect photoreceptor sensitivity. In conclusion, cone pigments expressed in rods either have no effect on sensitivity or reduce it by as much as a factor of 2–3.

The first experiments expressing transducin used a viral vector approach to inject the rod or cone Tα gene into

a mouse line that lacked both rod and cone transducins (Deng *et al.* 2009). Only a small fraction of the rods had any light response, probably reflecting the variability in expression level. From the few cells that could be recorded, there was no marked difference between cells expressing rod Tα and those expressing cone Tα. Since, however, the sensitivity of the rod is heavily dependent on transducin expression level (Sokolov *et al.* 2002), which was not (and could not) be measured for individual cells with this technique, the results were inconclusive.

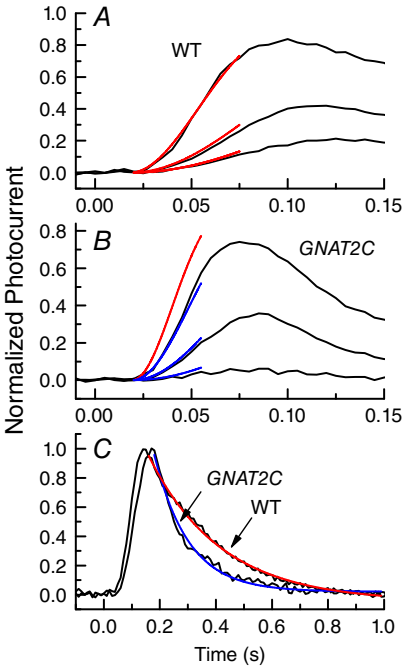

Figure 4. Differences in rate of activation and decay of WT and *GNAT2C* rods
A, black traces are mean initial time courses of responses of 16 WT rods to 10 ms flashes at intensities of 8.6, 21 and 79 photons μm^{-2}, after filtering with an 8-pole Bessel filter with a low-pass filter setting of 70 Hz. Responses have been normalized to the peak amplitude of the response. Red traces are fits to the data of the function $\frac{r}{r_{max}} = 1 - \exp[-\frac{1}{2}IA(t - t_{eff})^2]$ where r/r_{max} is the normalized flash response, I is the flash intensity in photoisomerizations, A is the amplification constant, t is time, and t_{eff} is the effective delay time of transduction (Pugh & Lamb, 1993), with the same mean values of A of 20.5 s^{-2} and t_{eff} of 18 ms at all three intensities. *B*, black traces are mean initial time courses of responses recorded and normalized as in *A* but of 14 *GNAT2C* rods to 10 ms flashes at intensities of 21, 79 and 227 photons μm^{-2}. Blue traces are fits to the data with an A of 10.2 s^{-2} and t_{eff} of 19.3 ms. Single red curve gives prediction for brightest intensity with WT rod value of A (20.5 s^{-2}). The value of A is about two times smaller in *GNAT2C* rods. *C*, mean small-amplitude responses of 21 WT rods and 9 *GNAT2C* rods to flashes of intensities 17 photons μm^{-2} (WT) and 79 photons μm^{-2} (*GNAT2C*). Responses have been normalized rod by rod to the peak amplitude of the response to compare waveforms of response decay. Responses have been fitted with single exponentials of 258 ms (red trace, WT) and 122 ms (blue trace, *GNAT2C*). Responses of *GNAT2C* rods decay significantly more rapidly. (Panels *A*–*C* reprinted with permission from Chen *et al.* 2010*b*).

Chen *et al.* (2010*b*) used a more traditional transgenic approach to express cone transducin in *Gnat1−/−* mice lacking rod transducin. They were fortunate to isolate a *GNAT2C* line in which the level of cone transducin was nearly the same as the WT rod transducin level. Sensitivity in *GNAT2C* rods was reduced by a factor of about 3, and the amplification constant A was about a factor of 2 smaller. This effect on amplification can be seen in Fig. 4*A* and *B*, which shows that the initial phase of the WT response rises more rapidly than that of *GNAT2C* rods.

Mao and colleagues (2013) then did a similar experiment also using a transgenic approach but with a different result. Rods in their mice expressed less cone Tα than *GNAT2C* rods and were less sensitive than WT rods, but the decrease in sensitivity seemed to depend only upon the expression level of the transducin and not upon the properties of cone Tα. They concluded that the species of transducin has no effect on the sensitivity difference between rods and cones. Thus incorporation of cone Tα in rods either has no effect on sensitivity or decreases it by as much as a factor of 3. No attempts have been made to express cone β3 or γ8 in place of rod β1 or γ1.

Two groups have attempted to express cone PDE6C in rods. Deng *et al.* (2013) injected viral vectors containing the *PDE6C* gene into the eyes of *rd10* mice, a line that is deficient in rod PDE6 but does not lack it entirely. Rods with cone PDE6C were surprisingly about twice as sensitive as those with the rod PDE6 proteins and showed a slower time course of decay. This anomalous result may have been produced by an unphysiological level of expression of PDE6, which again could not be measured. A clearer result was obtained by Majumder and colleagues (2015), who used a transgenic approach and were able to compare rod and cone PDE6 at the same expression level. Rods with cone PDE6C had a higher PDE6 basal activity and a single-photon response between 1.5 and 2 times smaller than WT rods, with a more rapid time course of decay (Fig. 5*A*). No attempt has been made to substitute cone PDE6γ for rod PDE6γ. This experiment could be revealing in view of Muradov *et al.* (2007), who showed that lamprey rods and cones have the same catalytic PDE6 subunits but different γ subunits. In conclusion, substitution of cone PDE6 for rod PDE6 either has no effect or decreases sensitivity by about a factor of two.

In summary, activation in mouse cones is at least 2- to 3-fold slower than activation in mouse rods. Taking outer segment volumes into account, we would predict that expression of cone pigment, cone transducin and cone PDE into a rod should together decrease the rate of activation by at least a factor of 5 with a commensurate decrease in sensitivity. Experiments expressing cone isoforms have, however, given conflicting results, with some

showing a 2- to 3-fold difference and some none at all. There are three possibilities: either papers showing significant differences are at least partially correct, or cone isoforms have to be expressed together (for example cone pigment with cone transducin), or other proteins (such as PDEγ or G-protein β and γ) also have a role. One conclusion, however, seems clear: the contribution of any one isoform is individually small, such that no one protein by itself is responsible for the entire difference in activation or sensitivity between the two kinds of photoreceptors.

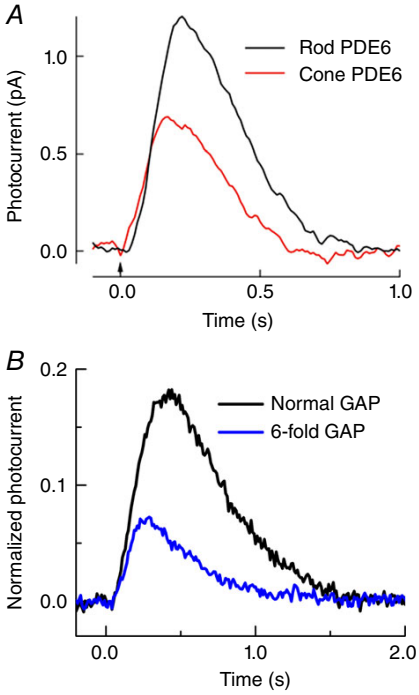

Figure 5. Single-photon responses of mouse rods with altered transduction proteins
A, derived average single-photon responses from control rods (black; rod PDE6) and cone-PDE6C-expressing rods (red; cone PDE6) (redrawn and reprinted with permission from Majumder *et al.* 2015). *B*, superimposed single-photon responses of WT mouse rods and of R9AP95 rods with six times the normal expression of GAP proteins (Chen *et al.* 2010*a*). Responses were plotted as a fraction of the peak current of the rod, effectively giving the fraction of channels closed per photon. Recordings were made from animals on a *GCAPs−/−* background to remove the effects of cyclase modulation on response amplitude and waveform (Gross *et al.* 2012). All experiments were performed on pigmented mice of either sex in accordance with the rules and regulations of the NIH guidelines for research animals, as approved by the institutional animal care and use committees (IACUCs) of the Virginia Commonwealth University and the University of California, Los Angeles. Animals were kept in cyclic 12 h/12 h on/off lighting in approved cages and supplied with ample food and water. Animals in all experiments were killed before tissue extraction by approved procedures, usually CO_2 inhalation or decerebration. Rods were perfused at 37°C with Dulbecco's modified Eagle's medium (Sigma Chemical, St Louis, MO, USA), supplemented with 15 mM $NaHCO_3$, 2 mM sodium succinate, 0.5 mM sodium glutamate, 2 mM sodium gluconate, and 5 mM NaCl, bubbled with 95% O_2–5% CO_2 (pH 7.4). Unless otherwise indicated, data were filtered at 35 Hz (8 pole, Bessel) and sampled at 100 Hz. (M. L. Woodruff, C. K. Chen & G. L. Fain, unpublished data).

Inactivation

If the response per Rh* is 20–30 times smaller in mouse cones than in mouse rods and activation accounts for only part of this difference, the remainder must emerge from mechanisms of inactivation. The records in Fig. 3 show that rods decay much more slowly than cones and integrate incoming photons over a longer time period. This difference in decay could in theory be produced by any of the reactions terminating the response.

We begin with extinction of Rh*. Rods and cones in mouse both phosphorylate photopigment with the same GRK1 kinase with no marked difference in antibody labelling and presumably expression (Lyubarsky *et al.* 2000; Weiss *et al.* 2001). Moreover both rods and cones use arrestin-1 with the small amount of arrestin-4 in cones unlikely to affect the rate of Rh* decay (Nikonov *et al.* 2008). The mean lifetime of Rh* in rods is probably as short as 40–45 ms (see Burns & Pugh, 2011), which is already so short that it is difficult to understand how even two or three serines or threonines could be phosphorylated and arrestin bind in so little time (Gurevich *et al.* 2011). If phosphorylation is faster in cones as Tachibanaki and colleagues have argued (2005), it is probably not much faster at least in mouse, whose rods and cones both express GRK1 at a similar level. More likely suspects for the slower rate of rod inactivation may be differences in the rates of decay of light-activated PDE6* and restoration of cGMP concentration by the cyclase.

Decay of PDE6* is produced by hydrolysis of Tα•GTP to Tα•GDP and rebinding of the PDE6γ inhibitory subunits to the PDE catalytic subunits. The rate of hydrolysis of Tα•GTP may be affected by the particular isoforms of transducin and PDE6: both cone transducin and cone PDE6C expressed in rods have been reported to produce responses that decay more rapidly than WT rod responses (see Figs 4*C* and 5*A*). The rate of hydrolysis may also be affected by the GAP proteins which, as we have said, are the same in rods and cones but are more abundantly expressed in cones at perhaps a 10-fold higher concentration (Cowan *et al.* 1998; Zhang *et al.* 2003). This difference in expression could have a significant effect on sensitivity. In Fig. 5*B*, we compare single-photon responses from rods with the normal GAP level and mutant *R9AP95* rods in which the GAP proteins are 6-fold over-expressed (Chen *et al.* 2010*a*). This experiment was done on a *GCAPs−/−* background to obviate any effect of cyclase feedback on response waveform or amplitude (Gross *et al.*

2012). Rods with over-expressed GAPs are about a factor of 2–3 less sensitive and decay more rapidly.

There are two ways guanylyl cyclase could produce a difference in the rate of cGMP synthesis between rods and cones and alter sensitivity. Both rods and cones in mouse use the same retGC1 cyclase, but the expression level is likely to be higher in cones. Staining with a retGC1 antibody is brighter in cones than in rods (Dizhoor *et al.* 1994), and unpublished measurements on retinas lacking the neural retina leucine zipper (Nrl) transcription factor (Mears *et al.* 2001), where all photoreceptors are cone-like, indicate that mouse cones may have something like 2–3 times more retGC1 than rods (A. Dizhoor, personal communication). Cone PDE6 expression may also be greater than rod but probably by no more than a factor of 1.5 (Zhang *et al.* 2003; Lobanova *et al.* 2010); however, cone PDE6 has a higher basal activity (Majumder *et al.* 2015). Together the cyclase and PDE6 would produce a higher rate of cGMP turnover in darkness, which in salamander has actually been measured and is about 3-fold greater in cones than in rods (Cornwall & Fain, 1994; Cornwall *et al.* 1995). This increase in turnover rate would produce both an increase in the rate of response decay and a decrease in sensitivity (Rieke & Baylor, 1996; Nikonov *et al.* 2000; Fain *et al.* 2001). Measurements in salamander indicate that if turnover in a rod were increased by a factor of 3, sensitivity would be reduced by about a factor of about 2 (Cornwall & Fain, 1994; Nikonov *et al.* 2000).

The rate of cGMP synthesis is also controlled by GCAP proteins, which in turn are regulated by the outer-segment Ca^{2+} concentration. Although the GCAPs themselves are similar in rods and cones, the change in Ca^{2+} concentration is considerably faster in cones, at least in salamander (Sampath *et al.* 1999). Rods and cones express different isoforms of the Na^+/Ca^{2+}–K^+ exchanger (Lytton, 2007; Vinberg *et al.* 2015) and may have different concentrations or isoforms of Ca^{2+} buffers. This accelerated decline in Ca^{2+} would produce a more rapid modulation of the GCAPs and faster activation of the cyclase, which could in theory decrease cone sensitivity. This notion has, however, been tested by deleting the genes for the GCAP proteins, which increases sensitivity by about the same factor of 3 in both rods (M. L. Woodruff & G. L. Fain, unpublished observations; Gross *et al.* 2012) and cones (Sakurai *et al.* 2011). These observations indicate that GCAP-mediated feedback makes little contribution to the sensitivity difference (however, see Wen *et al.* 2014). A similar conclusion emerges from comparison of salamander rod and cone responses under conditions that suppress changes in outer-segment Ca^{2+} (Matthews *et al.* 1988, 1990; Nakatani & Yau, 1988, 1989).

In conclusion, the rate of inactivation of transduction is slower in rods than in cones, with the major effects apparently produced by the species of transducin and PDE6, the expression level of cyclase, PDE6 basal activity, and the expression level of the GAP proteins. Each of these differences seems, however, to make a relatively small contribution, and once again no single change predominates.

We have based our conclusions on results from mouse, but it is possible and even likely that additional adaptations are present in other species that contribute to the difference in rod and cone inactivation. Fish are of particular interest, because the difference in rod and cone sensitivity can be much larger than in mouse (Tachibanaki *et al.* 2001). Kawamura's laboratory has shown that fish cones have a very high rate of pigment phosphorylation by GRK7 (Tachibanaki *et al.* 2005), an enzyme highly expressed in fish but not present in mouse (Liu *et al.* 2005). Moreover carp also show a much higher rate of cGMP synthesis in cones than in rods, and therefore a higher cGMP turnover rate (Takemoto *et al.* 2009). These changes would collectively cause photoresponses from carp cones to be smaller and faster (Tachibanaki *et al.* 2005;Liu *et al.* 2005; Takemoto *et al.* 2009). In addition, Rebrik and Korenbrot have identified a Ca^{2+}-binding protein present in fish cones but not fish rods that reduces the affinity of cyclic nucleotide-gated ion (CNG) channels for cGMP in high $[Ca^{2+}]_i$, a protein they first called CNG-modulin (Rebrik *et al.* 2012), but later identified as echinoderm microtubule-associated protein-like 1 (EML-1, Korenbrot *et al.* 2013). Knockdown of this protein in zebrafish produced a 5-fold increase in cone sensitivity (Korenbrot *et al.* 2013), presumably by slowing the rate at which CNG channels open following illumination. This protein has not as yet been identified in mammalian cones.

Why are rods more sensitive?

The key step in the formation of the duplex retina of vertebrates was the evolution of more sensitive rods to accompany cones, so that the entire range of light intensities could be encoded by the photoreceptors. Molecular and biochemical studies tell us that rods and cones have many of the same transduction proteins but use different isoforms probably arising by gene duplication (see Table 1); in some cases they use the same isoform but at a different level of expression. No one change accounts for the difference in absolute sensitivity between rods and cones. Instead, each of the differences we have described seems to have produced a small increase in the rate of activation or prolongation of response decay, conferring an incremental advantage to the organism.

Accumulated changes in a large number of proteins eventually produced a sensitivity great enough in the rod to allow it to operate in dim light, with cones remaining for enhanced temporal resolution when photon flux is no longer limiting. These changes also have

implications for the dynamic properties of rods and cones, namely their ability to adapt to increasing light intensity. While we have not discussed these mechanisms in this review, the fundamental tradeoff between sensitivity and dynamic range between rods and cones will also depend upon differences in their transduction mechanisms. The properties of the two receptor types form the basis of our duplex visual system, whose fundamental nature was first proposed by Schultze 150 years ago.

References

Angueyra JM & Rieke F (2013). Origin and effect of phototransduction noise in primate cone photoreceptors. *Nat Neurosci* **16**, 1692–1700.

Arshavsky VY & Wensel TG (2013). Timing is everything: GTPase regulation in phototransduction. *Invest Ophthalmol Vis Sci* **54**, 7725–7733.

Asteriti S, Grillner S & Cangiano L (2015). A Cambrian origin for vertebrate rods. *Elife* **4**, e07166.

Baehr W, Karan S, Maeda T, Luo DG, Li S, Bronson JD, Watt CB, Yau KW, Frederick JM & Palczewski K (2007). The function of guanylate cyclase 1 and guanylate cyclase 2 in rod and cone photoreceptors. *J Biol Chem* **282**, 8837–8847.

Baylor DA, Lamb TD & Yau KW (1979). Responses of retinal rods to single photons. *J Physiol* **288**, 613–634.

Baylor DA, Nunn BJ & Schnapf JL (1984). The photocurrent, noise and spectral sensitivity of rods of the monkey *Macaca fascicularis*. *J Physiol* **357**, 575–607.

Boye SL, Peterson JJ, Choudhury S, Min SH, Ruan Q, McCullough KT, Zhang Z, Olshevskaya EV, Peshenko IV, Hauswirth WW, Ding XQ, Dizhoor AM & Boye SE (2015). Gene therapy fully restores vision to the all-cone $Nrl^{-/-}$ $Gucy2e^{-/-}$ mouse model of Leber congenital amaurosis-1. *Hum Gene Ther* **26**, 575–592.

Burns ME & Pugh EN Jr (2011). Lessons from photoreceptors: turning off G-protein signaling in living cells. *Physiology (Bethesda)* **25**, 72–84.

Cao LH, Luo DG & Yau KW (2014). Light responses of primate and other mammalian cones. *Proc Natl Acad Sci USA* **111**, 2752–2757.

Chen CK, Woodruff ML, Chen FS, Chen D & Fain GL (2010*a*). Background light produces a recoverin-dependent modulation of activated-rhodopsin lifetime in mouse rods. *J Neurosci* **30**, 1213–1220.

Chen CK, Woodruff ML, Chen FS, Shim H, Cilluffo MC & Fain G (2010*b*). Replacing the rod with the cone transducin α subunit decreases sensitivity and accelerates response decay. *J Physiol* **588**, 3231–3241.

Cornwall MC & Fain GL (1994). Bleached pigment activates transduction in isolated rods of the salamander retina. *J Physiol* **480**, 261–279.

Cornwall MC, Matthews HR, Crouch RK & Fain GL (1995). Bleached pigment activates transduction in salamander cones. *J Gen Physiol* **106**, 543–557.

Cowan CW, Fariss RN, Sokal I, Palczewski K & Wensel TG (1998). High expression levels in cones of RGS9, the predominant GTPase accelerating protein of rods. *Proc Natl Acad Sci USA* **95**, 5351–5356.

Deng WT, Sakurai K, Kolandaivelu S, Kolesnikov AV, Dinculescu A, Li J, Zhu P, Liu X, Pang J, Chiodo VA, Boye SL, Chang B, Ramamurthy V, Kefalov VJ & Hauswirth WW (2013). Cone phosphodiesterase-6α' restores rod function and confers distinct physiological properties in the rod phosphodiesterase-6β-deficient *rd10* mouse. *J Neurosci* **33**, 11745–11753.

Deng WT, Sakurai K, Liu J, Dinculescu A, Li J, Pang J, Min SH, Chiodo VA, Boye SL, Chang B, Kefalov VJ & Hauswirth WW (2009). Functional interchangeability of rod and cone transducin α-subunits. *Proc Natl Acad Sci USA* **106**, 17681–17686.

Dickson DH & Graves DA (1979). Fine structure of the lamprey photoreceptors and retinal pigment epithelium (*Petromyzon marinus* L.). *Exp Eye Res* **29**, 45–60.

Dizhoor AM, Lowe DG, Olshevskaya EV, Laura RP & Hurley JB (1994). The human photoreceptor membrane guanylyl cyclase, RetGC, is present in outer segments and is regulated by calcium and a soluble activator. *Neuron* **12**, 1345–1352.

Dizhoor AM, Olshevskaya EV, Henzel WJ, Wong SC, Stults JT, Ankoudinova I & Hurley JB (1995). Cloning, sequencing, and expression of a 24-kDa Ca^{2+}-binding protein activating photoreceptor guanylyl cyclase. *J Biol Chem* **270**, 25200–25206.

Dizhoor AM, Olshevskaya EV & Peshenko IV (2010). Mg^{2+}/Ca^{2+} cation binding cycle of guanylyl cyclase activating proteins (GCAPs): role in regulation of photoreceptor guanylyl cyclase. *Mol Cell Biochem* **334**, 117–124.

Fain GL (2014). *Molecular and Cellular Physiology of Neurons*, 2nd edn. Harvard University Press, Cambridge, MA, USA.

Fain GL & Dowling JE (1973). Intracellular recordings from single rods and cones in the mudpuppy retina. *Science* **180**, 1178–1181.

Fain GL, Hardie R & Laughlin SB (2010). Phototransduction and the evolution of photoreceptors. *Curr Biol* **20**, R114–124.

Fain GL, Matthews HR, Cornwall MC & Koutalos Y (2001). Adaptation in vertebrate photoreceptors. *Physiol Rev* **81**, 117–151.

Fu Y, Kefalov V, Luo DG, Xue T & Yau KW (2008). Quantal noise from human red cone pigment. *Nat Neurosci* **11**, 565–571.

Gross OP, Pugh EN Jr & Burns ME (2012). Calcium feedback to cGMP synthesis strongly attenuates single-photon responses driven by long rhodopsin lifetimes. *Neuron* **76**, 370–382.

Gurevich VV, Hanson SM, Song X, Vishnivetskiy SA & Gurevich EV (2011). The functional cycle of visual arrestins in photoreceptor cells. *Prog Retin Eye Res* **30**, 405–430.

Hollinger S & Hepler JR (2002). Cellular regulation of RGS proteins: modulators and integrators of G protein signaling. *Pharmacol Rev* **54**, 527–559.

Kaupp UB & Seifert R (2002). Cyclic nucleotide-gated ion channels. *Physiol Rev* **82**, 769–824.

Kefalov V, Fu Y, Marsh-Armstrong N & Yau KW (2003). Role of visual pigment properties in rod and cone phototransduction. *Nature* **425**, 526–531.

Kefalov VJ, Estevez ME, Kono M, Goletz PW, Crouch RK, Cornwall MC & Yau KW (2005). Breaking the covalent bond – a pigment property that contributes to desensitization in cones. *Neuron* **46**, 879–890.

Korenbrot JI, Mehta M, Tserentsoodol N, Postlethwait JH & Rebrik TI (2013). EML1 (CNG-modulin) controls light sensitivity in darkness and under continuous illumination in zebrafish retinal cone photoreceptors. *J Neurosci* **33**, 17763–17776.

Kubo M, Hirano T & Kakinuma M (1991). Molecular cloning and sequence analysis of cDNA and genomic DNA for the human cone transducin α subunit. *FEBS Lett* **291**, 245–248.

Liu P, Osawa S & Weiss ER (2005). M opsin phosphorylation in intact mammalian retinas. *J Neurochem* **93**, 135–144.

Lobanova ES, Herrmann R, Finkelstein S, Reidel B, Skiba NP, Deng WT, Jo R, Weiss ER, Hauswirth WW & Arshavsky VY (2010). Mechanistic basis for the failure of cone transducin to translocate: why cones are never blinded by light. *J Neurosci* **30**, 6815–6824.

Lytton J (2007). Na^+/Ca^{2+} exchangers: three mammalian gene families control Ca^{2+} transport. *Biochem J* **406**, 365–382.

Lyubarsky AL, Chen C, Simon MI & Pugh EN Jr (2000). Mice lacking G-protein receptor kinase 1 have profoundly slowed recovery of cone-driven retinal responses. *J Neurosci* **20**, 2209–2217.

Ma J, Znoiko S, Othersen KL, Ryan JC, Das J, Isayama T, Kono M, Oprian DD, Corson DW, Cornwall MC, Cameron DA, Harosi FI, Makino CL & Crouch RK (2001). A visual pigment expressed in both rod and cone photoreceptors. *Neuron* **32**, 451–461.

Majumder A, Pahlberg J, Muradov H, Boyd KK, Sampath AP & Artemyev NO (2015). Exchange of cone for rod phosphodiesterase 6 catalytic subunits in rod photoreceptors mimics in part features of light adaptation. *J Neurosci* **35**, 9225–9235.

Mao W, Miyagishima KJ, Yao Y, Soreghan B, Sampath AP & Chen J (2013). Functional comparison of rod and cone $G\alpha_t$ on the regulation of light sensitivity. *J Biol Chem* **288**, 5257–5267.

Masland RH (2012). The neuronal organization of the retina. *Neuron* **76**, 266–280.

Matthews HR, Fain GL, Murphy RL & Lamb TD (1990). Light adaptation in cone photoreceptors of the salamander: a role for cytoplasmic calcium. *J Physiol* **420**, 447–469.

Matthews HR, Murphy RL, Fain GL & Lamb TD (1988). Photoreceptor light adaptation is mediated by cytoplasmic calcium concentration. *Nature* **334**, 67–69.

Mears AJ, Kondo M, Swain PK, Takada Y, Bush RA, Saunders TL, Sieving PA & Swaroop A (2001). Nrl is required for rod photoreceptor development. *Nat Genet* **29**, 447–452.

Morshedian A & Fain GL (2015). Single-photon sensitivity of lamprey rods with cone-like outer segments. *Curr Biol* **25**, 484–487.

Muradov H, Boyd KK, Kerov V & Artemyev NO (2007). PDE6 in lamprey *Petromyzon marinus*: implications for the evolution of the visual effector in vertebrates. *Biochemistry* **46**, 9992–10000.

Nakatani K, Tamura T & Yau KW (1991). Light adaptation in retinal rods of the rabbit and two other nonprimate mammals. *J Gen Physiol* **97**, 413–435.

Nakatani K & Yau KW (1988). Calcium and light adaptation in retinal rods and cones. *Nature* **334**, 69–71.

Nakatani K & Yau KW (1989). Sodium-dependent calcium extrusion and sensitivity regulation in retinal cones of the salamander. *J Physiol* **409**, 525–548.

Nickle B & Robinson PR (2007). The opsins of the vertebrate retina: insights from structural, biochemical, and evolutionary studies. *Cell Mol Life Sci* **64**, 2917–2932.

Nikonov S, Lamb TD & Pugh EN Jr (2000). The role of steady phosphodiesterase activity in the kinetics and sensitivity of the light-adapted salamander rod photoresponse. *J Gen Physiol* **116**, 795–824.

Nikonov SS, Brown BM, Davis JA, Zuniga FI, Bragin A, Pugh EN Jr & Craft CM (2008). Mouse cones require an arrestin for normal inactivation of phototransduction. *Neuron* **59**, 462–474.

Nikonov SS, Kholodenko R, Lem J & Pugh EN Jr (2006). Physiological features of the S- and M-cone photoreceptors of wild-type mice from single-cell recordings. *J Gen Physiol* **127**, 359–374.

Ong OC, Yamane HK, Phan KB, Fong HK, Bok D, Lee RH & Fung BK (1995). Molecular cloning and characterization of the G protein γ subunit of cone photoreceptors. *J Biol Chem* **270**, 8495–8500.

Picones A & Korenbrot JI (1992). Permeation and interaction of monovalent cations with the cGMP-gated channel of cone photoreceptors. *J Gen Physiol* **100**, 647–673.

Potter LR (2011). Guanylyl cyclase structure, function and regulation. *Cell Signal* **23**, 1921–1926.

Pugh EN Jr & Lamb TD (1993). Amplification and kinetics of the activation steps in phototransduction. *Biochim Biophys Acta* **1141**, 111–149.

Pugh EN Jr & Lamb TD (2000). Phototransduction in vertebrate rods and cones: molecular mechanism of amplification, recovery and light adaptation. In *Handbook of Biological Physics*, pp. 183–255. Elsevier, Amsterdam.

Rebrik TI, Botchkina I, Arshavsky VY, Craft CM & Korenbrot JI (2012). CNG-modulin: a novel Ca-dependent modulator of ligand sensitivity in cone photoreceptor cGMP-gated ion channels. *J Neurosci* **32**, 3142–3153.

Reingruber J, Holcman D & Fain GL (2015). How rods respond to single photons: Key adaptations of a G-protein cascade that enable vision at the physical limit of perception. *Bioessays* **37**, 1243–1252.

Rieke F & Baylor DA (1996). Molecular origin of continuous dark noise in rod photoreceptors. *Biophys J* **71**, 2553–2572.

Rieke F & Baylor DA (2000). Origin and functional impact of dark noise in retinal cones. *Neuron* **26**, 181–186.

Sakmar TP & Khorana HG (1988). Total synthesis and expression of a gene for the α-subunit of bovine rod outer segment guanine nucleotide-binding protein (transducin). *Nucleic Acids Res* **16**, 6361–6372.

Sakurai K, Chen J & Kefalov VJ (2011). Role of guanylyl cyclase modulation in mouse cone phototransduction. *J Neurosci* **31**, 7991–8000.

Sakurai K, Onishi A, Imai H, Chisaka O, Ueda Y, Usukura J, Nakatani K & Shichida Y (2007). Physiological properties of rod photoreceptor cells in green-sensitive cone pigment knock-in mice. *J Gen Physiol* **130**, 21–40.

Sampath AP & Baylor DA (2002). Molecular mechanism of spontaneous pigment activation in retinal cones. *Biophys J* **83**, 184–193.

Sampath AP, Matthews HR, Cornwall MC, Bandarchi J & Fain GL (1999). Light-dependent changes in outer segment free Ca^{2+} concentration in salamander cone photoreceptors. *J Gen Physiol* **113**, 267–277.

Sampath AP, Strissel KJ, Elias R, Arshavsky VY, McGinnis JF, Chen J, Kawamura S, Rieke F & Hurley JB (2005). Recoverin improves rod-mediated vision by enhancing signal transmission in the mouse retina. *Neuron* **46**, 413–420.

Schultze M (1866). Zur Anatomie und Physiologie der Retina. *Archiv für mikroskopische Anatomie* **2**, 175–286.

Shi G, Yau KW, Chen J & Kefalov VJ (2007). Signaling properties of a short-wave cone visual pigment and its role in phototransduction. *J Neurosci* **27**, 10084–10093.

Shichida Y & Matsuyama T (2009). Evolution of opsins and phototransduction. *Philos Trans R Soc Lond B Biol Sci* **364**, 2881–2895.

Shuart NG, Haitin Y, Camp SS, Black KD & Zagotta WN (2011). Molecular mechanism for 3:1 subunit stoichiometry of rod cyclic nucleotide-gated ion channels. *Nat Commun* **2**, 457.

Sokolov M, Lyubarsky AL, Strissel KJ, Savchenko AB, Govardovskii VI, Pugh EN Jr & Arshavsky VY (2002). Massive light-driven translocation of transducin between the two major compartments of rod cells: a novel mechanism of light adaptation. *Neuron* **34**, 95–106.

Tachibanaki S, Arinobu D, Shimauchi-Matsukawa Y, Tsushima S & Kawamura S (2005). Highly effective phosphorylation by G protein-coupled receptor kinase 7 of light-activated visual pigment in cones. *Proc Natl Acad Sci USA* **102**, 9329–9334.

Tachibanaki S, Tsushima S & Kawamura S (2001). Low amplification and fast visual pigment phosphorylation as mechanisms characterizing cone photoresponses. *Proc Natl Acad Sci USA* **98**, 14044–14049.

Takemoto N, Tachibanaki S & Kawamura S (2009). High cGMP synthetic activity in carp cones. *Proc Natl Acad Sci USA* **106**, 11788–11793.

Vinberg F, Wang T, Chen J & Kefalov V (2015). Na^{+}/Ca^{2+}, K^{+} exchangers 4 and 2 are required for the rapid light response recovery and normal light adaptation of cones. *Invest Ophthalmol Vis Sci* **56**, E-Abstract 1713.

Weiss ER, Ducceschi MH, Horner TJ, Li A, Craft CM & Osawa S (2001). Species-specific differences in expression of G-protein-coupled receptor kinase (GRK) 7 and GRK1 in mammalian cone photoreceptor cells: implications for cone cell phototransduction. *J Neurosci* **21**, 9175–9184.

Wen XH, Dizhoor AM & Makino CL (2014). Membrane guanylyl cyclase complexes shape the photoresponses of retinal rods and cones. *Front Mol Neurosci* **7**, 45.

Xu J, Morris L, Thapa A, Ma H, Michalakis S, Biel M, Baehr W, Peshenko IV, Dizhoor AM & Ding XQ (2013). cGMP accumulation causes photoreceptor degeneration in CNG channel deficiency: evidence of cGMP cytotoxicity independently of enhanced CNG channel function. *J Neurosci* **33**, 14939–14948.

Yee R & Liebman PA (1978). Light-activated phosphodiesterase of the rod outer segment. Kinetics and parameters of activation and deactivation. *J Biol Chem* **253**, 8902–8909.

Zhang X, Wensel TG & Kraft TW (2003). GTPase regulators and photoresponses in cones of the eastern chipmunk. *J Neurosci* **23**, 1287–1297.

Zhong H, Molday LL, Molday RS & Yau KW (2002). The heteromeric cyclic nucleotide-gated channel adopts a 3A:1B stoichiometry. *Nature* **420**, 193–198.

Additional information

Competing interests

None declared.

Funding

This work was supported by individual grants from the National Eye Institute of the NIH to G.L.F. (EY001844) and to A.P.S. (EY017606), as well as a core grant to the Jules Stein Eye Institute (EY000331).

Acknowledgements

We are grateful to past and present members of our laboratories for many useful discussions and for participating in some of the experiments we have described, and to Margery J. Fain for help with the figures.

APPENDIX B:

General Methods

Animals

Experiments were performed in accordance with the rules and regulations of the NIH guidelines for research animals, as approved by the institutional animal care and use committee of the University of California, Los Angeles, USA. Mice were kept under cyclic light (12-on/ 12-off) with adlib food and water in approved cages. After an over-night dark adaptation period, approximately equal numbers of male and female mice were sacrificed at 2-6 months of age. Immediately follow cervical dislocation, eyes were enucleated under infrared light.

Solutions

Bath solutions

The main perfusion solution was Ames' solution buffered with 1.9 g/L sodium bicarbonate and adjusted to 282-285 mOsm. Bath solution was continuously bubbled with 95% O_2/5% CO_2 to maintain pH between 7.3-7.4. When indicated, isradipine (10 μM; ISR; Sigma), niflumic acid (100-250 μM; NFA; Sigma), or tetraethylammonium (25 mM; TEA-Cl; Sigma) were added to Ames' solution to block L-type calcium channels, calcium-activated chloride, or potassium conductances, respectively. Slices were perfused at 2 ml/minute. Retinal slices were cut in HEPES buffered Ames' solution containing 2.38 g HEPES/L and balanced with 0.875 g NaCl per liter to give an osmolarity of 284 ± 1 mOsm (pH 7.35 ± 0.5). Ames'-HEPES was kept on ice and continuously bubbled with 100% O_2.

Pipette Solutions

Standard internal solution for recording pipets was a potassium aspartate (K-Asp) solution consisting of (in mM) 125 K-Asp, 10KCl, 10 HEPES, 5 *N*-methyl-D-glucamine (NMG)-HEDTA, 0.5 $CaCl_2$, 0.5 $MgCl_2$, 0.1 ATP-Mg, 0.5 GTP-TRIS, 2.5 NADPH (pH 7.3 ± 0.02 with NMG-OH; 280 ± 1 mOsm). All values have been corrected for liquid junction potentials, which were measured to be approximately 10 mV for K-Asp.

Whole-Cell Patch Clamp in Retinal Slices

Retinal Slices

Eyes were marked to indicate the dorsal-ventral pole before removal. Following enucleation, the anterior portion of the eye including the lens was removed, and the remaining eyecup was stored at 32 °C in a custom, light-tight storage container that allowed for the gassing of solutions. For each slice preparation, half the eyecup was isolated with a #10 scalpel, and the retina was gently separated from the RPE with fine tweezers. The isolated retinal piece was embedded in 3% of low-temperature gelling agar in Ames'-HEPES. Submerging the preparation in an ice-water bath for approximately 30 s accelerated the solidification process. In cold Ames'-HEPES, 200 µm thick slices were cut with a vibratome (Leica VT-1000S). The retina was cut vertically to maintain neural circuitry. Cut slices were either transferred to dishes for immediate recording or stored in the light-tight container with the remaining pieces of eyecups. When recording, slices were stabilized with handmade anchors, and the bath solution was maintained at 35 ± 1 °C.

Electrical Recording

Cones were identified from slices under infrared illumination (850- 950 nm LEDs) with a 60x water immersion lens (N/A 1.3; Nikon). No labels, markers, or tracers were needed, and standard microscopy (Nikon Eclipse E600FN) was used without DIC or phase contrast. Our method yielded a ~90% accurate indentification rate and could be applied across various photoreceptor genotypes. Cones were typically identified by their somata: A cone soma is slightly larger than rod soma and is more ellipsoid in shape. Cone somata are only located in the outmost layer of the ONL; many of them are found directly against the external limiting membrane (Applebury et al. 2000). However, the most distinguishing features were the patterns seen in the somata themselves. Under our optical conditions, healthy rod somata displayed a diffuse gradation throughout. Cone somata have instead distinct striping patterns. These patterns likely arise from differences in the chromatin packing structure reported in the nuclei of these photoreceptors (Solovei et al. 2009; Hughes et al. 2017).

Cones were patch-clamped in whole-cell configuration and could be recorded in voltage-clamp and current-clamp modes. During voltage clamp, cones were held at V_m = -50 mV and stimulated with 405 nm LEDs, unless otherwise indicated. Series resistance was compensated at 75-80% and did not produce ringing at these values. Data were filtered at 500 Hz (8-pole Bessel, Frequency Devices 900), sampled at 10kHz, and recorded in an open-source, Matlab-based program, Symphony Data Acquisition System (http://www.open-ephys.org/symphony/). Unless otherwise indicated, zero-current was injected in cones during current-clamp recordings, and these cells were used to determine resting membrane potentials.

Light responses from mouse cones in whole-cell configuration are generally stable for 5-10 minutes, with occasional cells lasting closer to 15 minutes. Run-down was typically manifested as a loss in response amplitude and a slowing of kinetics. Experiments were typically terminated when run-down was apparent. Interestingly, several ionic conductances (e.g. I_{ca}) remained stable and responsive to voltage stimulation even after the light response had run down.

Recording Pipets

Filamented borosilicate glass capillaries (BF120-69-10, Sutter Instruments) were pulled the day of the experiment with a P-97 Flaming/Brown micropipette puller (Sutter Instruments). Pipets used to record mouse photoreceptors generally had a resistance of 15-19 MOhms.

Light Stimuli

Light stimuli were either brief flashes or steady presentations of monochromatic light. Monochromatic light was provided by ultra-bright LEDs driven with a linear feedback driver (Opto-LED; Carin Research). LEDs emitting 365 nm and 505 nm light were used to test spectral sensitivity of individual cells and determine whether each cone was dominate for S, M, or a mixed of both pigments. After brief spectral testing, the subsequent illuminations were supplied by a 405 nm-emitting LED, as 405 nm is at approximately the isobestic point of S- and M- pigments in mouse and will stimulate either opsin type to the same degree.

Light intensities of individual LEDs were calibrated with a photodiode (Graseby Optronics 268R) and by the equation $E = h\nu$, to convert photovoltages into photons per second, where E is energy, h is Plank's constant (6.626×10^{-34} J*s), and ν is the frequency velocity of the monochromatic light. The measured photons per second was then converted to pigments bleached/s (P*/s) from the cone collecting areas determined as follows: Single-photon responses (SPRs) of rods were recorded from the same preparations as wildtype and *Cx36*$^{-/-}$ cones. By scaling the time-dependent variance to the mean SPRs in rods (Mendez et al. 2000; Cao et al. 2008; Okawa et al. 2010), we estimated the rod collecting area to be 0.2 rhodopsins activated (Rh*)/μm^2 in slices. This is close agreement with previous measurements made in retinal slice preparations (Cao et al. 2008; Okawa et al. 2010).

Two further adjustments were made to convert 0.2 Rh*/μm^2 into a cone collecting area. To account for the five-fold decrease in quantum efficiency and pigment activated by 405 nm compared to 505 nm, the collecting area was multiplied by 0.2 (Govardovskii et al. 2000). Due to the difference in outer segment volume, collecting area was multiplied by the ratio 14/38 (cone μm^3/rod μm^3; Nikonov et al. 2006). This yielded a final collecting area of 0.013 P*/μm^2 for cones stimulated with 405 nm light in 200 µm thick slices.

Analyses and Equations

General Analyses

Data traces were analyzed with custom scripts written in Matlab. Data was digitally filtered at 50 Hz unless otherwise indicated. Typically, data were baseline-subtracted to 0 by linear subtraction.

Sensitivity Measurements (Intensity-Response Relationships)

To derive sensitivities of response families, normalized photoresponses were plotted against the number of pigment molecules bleach and data were fit with the Michaelis-Menten relationship: $$R_x = \frac{I_x}{\left(I_x + I_{\frac{1}{2}}\right)}$$

where, R_x is the response at a given intensity, I_x; and $I_{1/2}$ is the intensity required to produce a half maximal response. $I_{1/2}$ was used as a sensitivity measure. Note here that this equation is the Hill equation with an exponent equal to 1.

General Statistical Methods

All averages are reported as mean ± SEM.

References

Applebury, M. L., M. P. Antoch, L. C. Baxter, L. L. Chun, J. D. Falk, F. Farhangfar, K. Kage, M. G. Krzystolik, L. A. Lyass and J. T. Robbins (2000). "The murine cone photoreceptor: a single cone type expresses both S and M opsins with retinal spatial patterning." Neuron **27**(3): 513-523.

Cao, Y., H. Song, H. Okawa, A. P. Sampath, M. Sokolov and K. A. Martemyanov (2008). "Targeting of RGS7/Gbeta5 to the dendritic tips of ON-bipolar cells is independent of its association with membrane anchor R7BP." J Neurosci **28**(41): 10443-10449.

Govardovskii, V. I., N. Fyhrquist, T. Reuter, D. G. Kuzmin and K. Donner (2000). "In search of the visual pigment template." Vis Neurosci **17**(4): 509-528.

Hughes, A. E., J. M. Enright, C. A. Myers, S. Q. Shen and J. C. Corbo (2017). "Cell Type-Specific Epigenomic Analysis Reveals a Uniquely Closed Chromatin Architecture in Mouse Rod Photoreceptors." Sci Rep **7**: 43184.

Mendez, A., M. E. Burns, A. Roca, J. Lem, L. W. Wu, M. I. Simon, D. A. Baylor and J. Chen (2000). "Rapid and reproducible deactivation of rhodopsin requires multiple phosphorylation sites." Neuron **28**(1): 153-164.

Nikonov, S. S., R. Kholodenko, J. Lem and E. N. Pugh, Jr. (2006). "Physiological features of the S- and M-cone photoreceptors of wild-type mice from single-cell recordings." J Gen Physiol **127**(4): 359-374.

Okawa, H., K. J. Miyagishima, A. C. Arman, J. B. Hurley, G. D. Field and A. P. Sampath (2010). "Optimal processing of photoreceptor signals is required to maximize behavioural sensitivity." J Physiol **588**(Pt 11): 1947-1960.

Solovei, I., M. Kreysing, C. Lanctot, S. Kosem, L. Peichl, T. Cremer, J. Guck and B. Joffe (2009). "Nuclear architecture of rod photoreceptor cells adapts to vision in mammalian evolution." Cell **137**(2): 356-368.